LEABHARLANN CHOLÁISTE NA TRÍONÓIDE, BAILE ÁTHA CLIATH | TRINITY COLLEGE LIBRARY DUBLIN
Ollscoil Átha Cliath | The University of Dublin

Terms and Conditions of Use of Digitised Theses from Trinity College Library Dublin

Copyright statement

All material supplied by Trinity College Library is protected by copyright (under the Copyright and Related Rights Act, 2000 as amended) and other relevant Intellectual Property Rights. By accessing and using a Digitised Thesis from Trinity College Library you acknowledge that all Intellectual Property Rights in any Works supplied are the sole and exclusive property of the copyright and/or other IPR holder. Specific copyright holders may not be explicitly identified. Use of materials from other sources within a thesis should not be construed as a claim over them.

A non-exclusive, non-transferable licence is hereby granted to those using or reproducing, in whole or in part, the material for valid purposes, providing the copyright owners are acknowledged using the normal conventions. Where specific permission to use material is required, this is identified and such permission must be sought from the copyright holder or agency cited.

Liability statement

By using a Digitised Thesis, I accept that Trinity College Dublin bears no legal responsibility for the accuracy, legality or comprehensiveness of materials contained within the thesis, and that Trinity College Dublin accepts no liability for indirect, consequential, or incidental, damages or losses arising from use of the thesis for whatever reason. Information located in a thesis may be subject to specific use constraints, details of which may not be explicitly described. It is the responsibility of potential and actual users to be aware of such constraints and to abide by them. By making use of material from a digitised thesis, you accept these copyright and disclaimer provisions. Where it is brought to the attention of Trinity College Library that there may be a breach of copyright or other restraint, it is the policy to withdraw or take down access to a thesis while the issue is being resolved.

Access Agreement

By using a Digitised Thesis from Trinity College Library you are bound by the following Terms & Conditions. Please read them carefully.

I have read and I understand the following statement: All material supplied via a Digitised Thesis from Trinity College Library is protected by copyright and other intellectual property rights, and duplication or sale of all or part of any of a thesis is not permitted, except that material may be duplicated by you for your research use or for educational purposes in electronic or print form providing the copyright owners are acknowledged using the normal conventions. You must obtain permission for any other use. Electronic or print copies may not be offered, whether for sale or otherwise to anyone. This copy has been supplied on the understanding that it is copyright material and that no quotation from the thesis may be published without proper acknowledgement.



Design & Performance of Deep Foundations in Ireland

A thesis submitted to The University of Dublin, Trinity College

for the degree of

Doctor of Philosophy in the Faculty of Engineering

2011

Andrew P. Galbraith

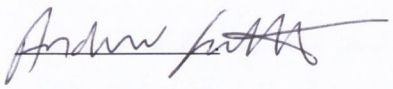
Baccalaureus in Arte & Baccalaureus in Arte Ingenaria 2007

TRINITY COLLEGE
2 0 JUL 2011
LIBRARY DUBLIN
THESIS
9099

Declaration

This thesis has not been submitted as an exercise for a degree before this time and except where referenced, is entirely the candidate's own work.

The candidate agrees that the Library may lend or copy this thesis.



Andrew Galbraith.

Summary

During the course of this study, a database of static load tests carried out on piles installed in varying ground conditions in Ireland, including fine and coarse grained soil and rock, was compiled. Site investigation data, including borehole logs and in-situ and laboratory test results pertaining to the soil at the various test sites, formed an essential part of the database.

This pile test database (PTD) was used to assess the methods by which the load resisting capacity of the ground against a pile (R_c) is estimated. Pile load tests carried out on instrumented piles were particularly useful and enabled the separation of the development of shaft and base resistances and also allowed the development of shaft stress along the length of the piles, to be estimated. This gave insight into the mechanism by which the applied load is shed from the pile into the adjacent soil for the different pile types.

The Author also installed and instrumented several piles throughout the course of the study, including two CFA piles toed in rock and several micro-piles which were used to investigate the methods by which the results of instrumented load tests are interpreted and also to consider the effect of spatial variation in the soil on R_c. It was found that the most convenient means of conversion of strain to force in the pile was by direct relationship at the pile head.

The PTD was also used to assess the variability associated with the expected values of R_c for the piles when estimated using ground test results and using the load test results themselves. Within-site variability was assessed in addition to the uncertainty associated with a single pile and this was done by statistical methods using ground test results and using groups of load tests carried out on *similar* piles, where *similar* was defined as piles of equal diameter and within 1m length of each other installed on the same site and in similar ground conditions.

Methods of estimation of R_c were assessed based on the results of pile load tests for which the piles were taken to failure. It was concluded, that, where piles were deflected to at least 5% of the pile diameter, extrapolation of load-deflection data assuming a hyperbolic relationship, as proposed by Chin (1970), to a pile head deflection equal to 10% of the pile diameter, denoted δ_f, yielded a good practical estimate of R_c, denoted $R_{c;chin}$.

The variation associated with the value of R_c, characterised by the coefficient of variation of the parameter, $V(R_c)$ for a single pile was found to reduce from around 0.40-0.10 where δ_{max}/D increased from 1-10% and this included an allowance for measurement error equivalent to a value of $V(R_{c;m})$ equal to 0.10, where $R_{c;m}$ is the measured value of R_c.

A simulation exercise was completed whereby all combinations of n load tests on similar piles, where n was between 2 and the maximum number of load tests in each group, were generated. This analysis was used to estimate the maximum expected value of $V(R_c)$ where a limited number of load tests are carried out, which is generally the case in practice. It was found, that, where two load tests are carried out, the expected value of $V(R_c)$ was around 0.38, and this reduced to 0.20 where at least 8 load tests are carried out.

Having characterised the uncertainty associated with R_c for a single pile and also the within-site variability representative of the test sites, the performance of the piles was assessed at the ULS and SLS with respect to single piles and for a pile design for a site. The performance was characterised using the reliability index β which may be related to the probability of a limit state occurring. Correlation factors and characteristic values were also evaluated using the load test and ground test results in the PTD.

Using the results of load tests on instrumented piles installed in DBC, together with ground test results carried out at the same sites, the factors used for calculation of R_c were interpreted. For CFA piles, it was found that the adhesion factor α reached values as high as 0.7 during the load tests, with a value of 0.8 predicted at δ_f. The base bearing factor N_c reached about 5 during the load tests and was predicted as 6.5 at δ_f with a predicted limiting value of around 9 had the pile been deflected further. In the case of driven piles in DBC, it was found that α was also around 0.8 with an indication that it could reach unity at higher deflections. The interpreted N_c value was around 10 times that for the CFA piles (65) at δ_f, with a limiting value approaching 90 on further deflection. The analysis was based on an estimate of the undrained shear strength of the soil s_u given by 5.5 times the N_{SPT}, verified using the results of triaxial tests on samples of DBC taken from various sites, along with the N_{SPT} recorded at several sites also comprising DBC.

Abstract

Pile foundations are critical to the construction industry, installed where the combination of loading and ground conditions is such that shallow foundations are impractical or unfeasible. The varying nature of the ground and diverse site locations in Ireland has led to the use of different types of piles, each requiring specialist installation equipment and considerable design and contracting experience to ensure adequate bearing capacity.

A single pile under load offers resistance on deflection through a complex pile-soil interaction that depends on the pile geometry, the strength properties of the ground and on the pile installation method. Bored and driven piles are both popular in Ireland and are known to shed load by two very distinct mechanisms, even where installed in similar soil.

In addition, precise estimation of the bearing capacity of a single pile is difficult, owing to spatial variation inherent to the soil, measurement errors in testing and variation due to pile installation effects. Recent application of reliability based design methods to geotechnical problems necessitates quantification of individual contributory sources of uncertainty, so that performance based design of foundations may be accomplished.

This thesis considers the results of over 170 static load tests carried out on piles installed across Ireland including bored, CFA and driven piles in fine and coarse grained material and also piles terminating in rock. These pile load test results were gathered together from various sources including Irish consultant engineers, contractors and from published literature on the topic.

The pile load test results are used together with ground test results to estimate the resistance of the piles at the ultimate and serviceability limit states and also to quantify the uncertainty associated with the expected value of the resistance of a single pile. Within-site variability is assessed by grouping the piles based on type, geometry and on the ground conditions in which they are installed. The levels of uncertainty calculated are used to assess the reliability of the piles that were tested, characterised using the reliability index, which may be related to the probability of failure of the foundation element.

Acknowledgements

This thesis is the result of a desk study by the Author, in combination with laboratory testing and field work by the Geotechnical Department at the University of Dublin, Trinity College, October 2007 – October 2010.

The research was carried out under the guidance and supervision of Dr Eric Farrell, Senior Lecturer in the Department of Civil, Structural and Environmental Engineering at Trinity College.

The technical staff in the Geotechnical Department of Trinity College, under the supervision of the Chief Technical Officer, Mr Chris O'Donovan, assisted the Author with laboratory testing and field work during the course of the study.

Field testing was carried out in conjunction with Byrne Looby Partners (BLP) and PJ Edwards Limited (PJE). Mr John Byrne – Director and co-founder of BLP and Mr Greg Edwards of PJE are acknowledged in particular.

Sponsorship for the research was provided by BLP and the Irish Research Council for Science, Engineering and Technology (IRCSET) under the enterprise partnership scheme. The Geotechnical Trust Fund of Engineers Ireland also made a contribution to the research. PJE kindly contributed the material and facilitated installation of the field testing carried out.

The Author's parents – Mr William Galbraith and Mrs Rebecca Galbraith are acknowledged for their continued encouragement and inspiration from early age.

Table of Contents

Declaration i

Summary ii

Abstract iv

Acknowledgements v

Table of Contents vi

Figures xi

Tables xxix

Nomenclature xxxi

1 Introduction 1

1.1 Background 1

2 Literature Review 4

2.1 Introduction 4

2.2 Pile Design Methods 4

2.2.1 Coarse grained soil 5

2.2.2 Fine grained soil 15

2.3 Pile Design and Testing in Ireland 22

2.3.1 Introduction 22

2.3.2 Driven Piles 24

2.3.3 CFA Piles 29

2.3.4 Piles in Rock 39

2.4 Estimating pile capacity from static load tests 41

2.4.1 Definition of Failure 42

2.4.2 Extrapolation to R_c 42

2.4.3 Comparison of methods 45

2.5 Reliability in pile design 47

2.5.1 Introduction 47

2.5.2 Target Reliability 48

2.6 Uncertainty in ground parameters 50

2.6.1 Inherent variability 51

2.6.2 Measurement error 56

2.6.3 Transformation error 58

2.6.4 Soil variability from in-situ test data 58

2.6.5 Load test results 59

2.6.6 Bayesian updating 61

2.7 Summary 62

3 Details of Pile Test Database 64

3.1 Introduction 64

3.2 Details of piles 64

3.3 Summary of PTD 75

3.4 Discussion 79

4 The ultimate capacity of a single pile 80

4.1 Assessment of extrapolation methods 80

4.2 Comparison of various failure criteria 87

4.3 Uncertainty in R_c for a single pile 92

4.4 Quantifying within-site variability 99

4.4.1 Case study – Malahide viaduct 99

4.5 Within-site variability: Ground test results 103

4.5.1 Quantifying variation in ground tests results 104

4.5.2 Spatial variation 108

4.5.3 Combining Uncertainty 110

4.6 Within-site variability: Load test results 111

4.7 Selection of an appropriate distribution 117

4.8 Conclusions 120

5 Piles in Glacial Till: Review and analysis 124

5.1 Undrained shear strength of DBC 124

5.2 CFA piles 127

5.3 Driven piles 131

5.4 Conclusions from instrumented tests 135

5.5 Appraisal of calculation factors 137

5.5.1 CFA piles in DBC 138

5.5.2 Driven piles in DBC 139

5.5.3 CFA piles in boulder clay other than DBC 140

5.5.4 Piles in Sand/Gravel 141

5.6 Conclusions 142

6 Instrumented piles toed in rock 144

6.1 Instrumented Pile Tests 144

6.1.1 Site Location 144

6.1.2 Pile Installation 144

6.1.3 Ground conditions 145
6.1.4 Load Test Arrangement 149
6.1.5 Instrumentation 149
6.2 Static load test results 150
6.2.1 Pile head load-deflection-time 150
6.2.2 Strain-depth measurements 152
6.2.3 Interpreted force-depth profile 154
6.2.4 Interpreted shaft resistance 160
6.2.5 Pile stiffness 161
6.3 Other instrumented tests on rock 165
6.3.1 Pile-Rock Interface Shear Stress 168
6.4 Discussion: Rock socketed piles 172
6.5 Conclusions 174
7 Reliability of Piles 178
7.1 Background 178
7.2 Reliability of a single pile 180
7.3 Reliability of a pile design – ULS 186
7.3.1 Using ground test results 186
7.3.2 Using load test results 190
7.4 Correlation factors 194
7.5 Reliability of a pile design – SLS 200
7.6 Characteristic values 201
7.6.1 Summary 208

8 Conclusions 212

Further Research 217

References 218

A. Ground Test Results 228

A.1 Introduction 228

B. Pile Load Tests 245

B.1 Introduction 245

C. Details of additional tests relating to instrumented piles 292

C.1 Introduction 292

a. Test pile logs 293

b. Instrumentation and data acquisition 295

i. Installation of strain gauges 295

ii. Data acquisition 297

c. Concrete cylinder tests 299

i. Loading arrangement and experimental setup 299

ii. Stress-strain results 301

iii. Interpreted stiffness-strain 303

d. Dummy pile test 304

i. Loading arrangement and experimental setup 304

ii. Stress-strain results 308

D. Reliability 310

D.1 Introduction 310

Figures

Figure 2.1 – Chart used to obtain N_q from ϕ' considering D_f/D (shown as D/B in Figure) (Berezantzev et al. 1961) 6

Figure 2.2 – Chart used to obtain N_q from ϕ' Berezantzev (Fleming et al. 2009) 7

Figure 2.3 – Chart used to obtain ϕ' from SPT (a) and CPT (b) results (Tomlinson 2001) . 7

Figure 2.4 - Definition of parameters for calculation of σ'_{rf} (Jardine et al. 2005) 11

Figure 2.5 - N_c for piles in clay after Skempton (1951) 16

Figure 2.6 – Correlation of s_u with SPT result (Stroud 1974) 17

Figure 2.7 - Suggested relationship between α and s_u for clay tills (Weltman and Healy 1978) 18

Figure 2.8 - Variation of α with strength ratio (Randolph and Murphy 1985) 19

Figure 2.9 – Ground conditions and N_{SPT} profile at Croke Park test site (Farrell et al. 1998) 27

Figure 2.10 – Development of base resistance with base deflection (Farrell et al. 1998) ... 28

Figure 2.11 – Shaft resistance profile at maximum load at the four load cycles (Farrell et al. 1998) 28

Figure 2.12 – Calculated s_u at SJH site (Farrell and Lawler 2008) 31

Figure 2.13 – Interpreted force-depth profile (a) Pile 450 (b) Pile 600 (Farrell and Lawler 2008) 32

Figure 2.14 – Mobilised adhesion factor, α vs. pile head deflection (interpreted from strain gauges in test pile) (Farrell and Lawler 2008) 33

Figure 2.15 – Pile 600: end bearing load against pile head/pile toe deflection (Farrell and Lawler 2008) 33

Figure 2.16 – Interpreted stratigraphy BB site (Gavin et al. 2008) 35

Figure 2.17 – Recorded N_{SPT} at BB site (Gavin et al. 2008) 35

Figure 2.18 – Pile head load-deflection (a) 450mm piles (b) 600mm piles (Farrell and Lawler 2008) 36

Figure 2.19 – Load-depth profile (a) TP1 (b) TP2 and (c) TP3 (Gavin et al. 2008) 37

Figure 2.20 – Mobilisation of (a) shaft resistance in TP1 and TP2 (b) shaft resistance in tension test (c) base resistance in TP1 (Gavin et al. 2008) 38

Figure 2.21 - α_{rock} values of Kulhawy and Phoon (1993) compared with trend for Irish rocks, (Long and Collins 1999) 40

Figure 2.22 - α_{rock} against RQD, (Long and Collins 1998) 40

Figure 2.23 - α_{rock} against FSI, (Long and Collins 1998) 41

Figure 2.24 – Load-deflection curve for a bored pile with R_c estimated by various means (Zhang and Tang 2001) 46

Figure 2.25 - Relationship between β and P_f (adapted from Table US Army Corps of Engineers 1997, Table B-1) (Phoon 2004) 50

Figure 2.26 – Inherent soil variability (Phoon and Kulhawy 1999) 52

Figure 2.27 – The data in the two charts share the same mean and variance, but display different patterns of spatial variation (Baecher and Christian 2003) 53

Figure 2.28 – Illustration of reduced variation in mean value over a finite failure domain given measured values of the soil parameter 'X' (Li and Lo 2006) 55

Figure 2.29 – Estimation of vertical scale of fluctuation reposted in Phoon and Kulhawy (1999) 56

Figure 3.1 – Location of sites in Dublin in which pile load tests were carried out 66

Figure 3.2 – Location of sites in which pile load tests were carried out 67

Figure 4.1 - Load-deflection data for Pile 26 82

Figure 4.2 – Linear plot by Chin for Pile 26 82

Figure 4.3 - Plot for assessment of Chin's method 83

Figure 4.4 - Plot for assessment of Decourt's method 84

Figure 4.5 – Linear plot by Decourt for Pile 26 85

Figure 4.6 – Comparison of Chin and Decourt methods 85

Figure 4.7 - Linear plot by Van der Veen for Pile 26 86

Figure 4.8 – Linear plot by Brinch-Hansen for Pile 26 86

Figure 4.9 – Pile 26: Comparison of estimated R_c by various methods 87

Figure 4.10 – Comparison of methods of estimation of R_c 88

Figure 4.11 - Comparison of methods of estimation of R_c 91

Figure 4.12 - $R_{c;chin}/R_{c;m}$ vs δ/δ_f with upper and lower bounds and mean trend 93

Figure 4.13 – Estimated $V(R_{c;chin})$ with varying δ_{max}/δ_f for a single pile under load 93

Figure 4.14 – Results of SPT and vane shear tests vs depth 100

Figure 4.15 – Interpreted Stratigraphy, (a) Pier 6-7 (b) Pier 10-11 (equal horizontal and vertical scales) 100

Figure 4.16 – Malahide: Measured pile head load-deflection data 102

Figure 4.17 – Malahide: Interpreted force-depth profile at 650-700 kN head load 103

Figure 4.18 - Regression analysis on raw N_{SPT} (a) and residuals from trend (b) for Site D 106

Figure 4.19 – Summary of within-site variation in N_{SPT} for various sites 108

Figure 4.20 – Plot of within-site variation versus number of pile load tests in each group 115

Figure 4.21 – Plot of within-site variation versus average normalised deflection of piles during load testing 116

Figure 4.22 – Plot of within-site variation versus pile diameter for pile groups 116

Figure 4.23 – Plot of within-site variation versus pile length for pile groups 117

Figure 4.24 – Plot of average within-site variation using all possible combinations of the load test data at n equal to 2 – 8 117

Figure 4.25 – Normal probability plot for Group 2, Group 14 and Group 15 119

Figure 4.26 – Lognormal probability plot for Group 2, Group 14 and Group 15 119

Figure 5.1 – Measurements of s_u in DBC 126

Figure 5.2 - s_u estimated for various sites 127

Figure 5.3 – N_{SPT} at SJH and BB sites including outliers and least squares regression lines 128

Figure 5.4 – Shaft stress against normalised pile head deflection 130

Figure 5.5 – Development of α against normalised pile head deflection 130

Figure 5.6 – Stress at base against normalised pile base deflection 131

Figure 5.7 – N_c against normalised pile base deflection 131

Figure 5.8 – N_{SPT} at Croke Park site with least squares regression line 133

Figure 5.9 – Croke Park: Shaft resistance against normalised pile head deflection 133

Figure 5.10 – Croke Park: Development of α against normalised pile head deflection 134

Figure 5.11 - Croke Park: Stress at base against normalised pile base deflection 134

Figure 5.12 – Croke Park: N_c against normalised pile base deflection 135

Figure 5.13 – Development of adhesion factor for CFA and driven piles 137

Figure 5.14 – Development of base bearing factor for CFA and driven piles 137

Figure 5.15 – Group 1: Histogram of $R_{c;cal}/R_{c;chin}$ 139

Figure 5.16 – Group 2: Histogram of $R_{c;cal}/R_{c;chin}$ 140

Figure 5.17 – Group 3: Histogram of $R_{c;cal}/R_{c;chin}$ 141

Figure 5.18 – Group 5: Histogram of $R_{c;cal}/R_{c;chin}$ 142

Figure 6.1 – Duleek: N_{SPT} (IGSL 2009) 146

Figure 6.2 – Stratigraphy in vicinity of P450 147

Figure 6.3 – Stratigraphy in vicinity of P640 148

Figure 6.4 – Legend for use with Figure 6.3 and Figure 6.2 148

Figure 6.5 – Test arrangement, P450 150

Figure 6.6 - Pile load-deflection data, (a) P450 (b) P640 151

Figure 6.7 – Load-time graphs for instrumented test piles 152

Figure 6.8 – Measured strain-depth P450 153

Figure 6.9 – Measured strain-depth P640 154

Figure 6.10 - Characteristic stress-strain behaviour of SCC with a thixotropic structure (Billberg 2006) 155

Figure 6.11 - Load-strain relationships, P450 and P640 157

Figure 6.12 – E_c values with depth (mean and best fit interpreted by Author (Ng et al. 2000) 159

Figure 6.13 – P450: Interpreted force-depth profile 159

Figure 6.14 – P640: Interpreted force-depth profile 160

Figure 6.15 – P450: Interpreted shaft resistance 161

Figure 6.16 – P640: Interpreted shaft resistance 161

Figure 6.17 – Secant/Tangent stiffness-strain relationship for P450 and P640 164

Figure 6.18 – Secant/Tangent stiffness-strain relationship for concrete cylinders 164

Figure 6.19 – P450: Equivalent Secant/Tangent pile stiffness-strain relationship using concrete stiffness-strain relationship from two concrete cylinders 165

Figure 6.20 – P450 and Dummy pile: Secant/Tangent pile stiffness-strain relationship .. 165

Figure 6.21 – JK11; Force-depth profile 166

Figure 6.22 – PTP1; Force-depth profile 167

Figure 6.23 – PTP2; Force-depth profile 167

Figure 6.24 – DC PTP1; Force-depth profile 168

Figure 6.25 – Shear stress development in rock 170

Figure 6.26 – $qs; rock$ vs. normalised deflection 171

Figure 6.27 – α vs. normalised deflection 171

Figure 6.28 – Stress on base vs. normalised base deflection 172

Figure 6.29 – Relationship between α and $q_c / 2p_a$ (Kulhawy and Phoon 1993) 173

Figure 6.30 – Relationship between α and RQD (Kulhawy and Phoon 1993) 173

Figure 6.31 – Relationship between q_s and FSI (Kulhawy and Phoon 1993) 174

Figure 7.1 - Variation of load and resistance (Zhang et al. 2005) 179

Figure 7.2 – CFA piles in DBC: Calculated β for a single pile 182

Figure 7.3 – Driven piles in DBC: Calculated β for a single pile 183

Figure 7.4 – CFA piles in boulder clay: Calculated β for a single pile 183

Figure 7.5 – Load-deflection compared 184

Figure 7.6 – Driven piles in boulder clay: Calculated β for a single pile 185

Figure 7.7 – CFA and bored piles in sand/gravel: Calculated β for a single pile 185

Figure 7.8 – CFA piles in rock: Calculated β for a single pile 186

Figure 7.9 – Effect of spatial averaging and pile length on calculated β 189

Figure 7.10 – CFA piles in DBC: Calculated β for a pile including within-site variation 191

Figure 7.11 – Driven piles in DBC: Calculated β for a pile including within-site variation 191

Figure 7.12 – CFA piles in boulder clay: Calculated β for a pile including within-site variation 192

Figure 7.13 – Driven piles in boulder clay: Calculated β for a pile including within-site variation 192

Figure 7.14 – CFA and bored piles in sand/gravel: Calculated β for a pile including within-site variation 193

Figure 7.15 – CFA piles in rock: Calculated β for a pile including within-site variation 193

Figure 7.16 – ξ_1 factors: for application to mean $R_{c;m}$ from a group of load tests 196

Figure 7.17 – ξ_2 factors: for application to minimum $R_{c;m}$ from a group of load tests.... 197

Figure 7.18 – ξ_3 factors: for application to mean $R_{c;cal}$ from ground test profiles..... 197

Figure 7.19 – ξ_4 factors: for application to minimum $R_{c;cal}$ from ground test profiles ... 198

Figure 7.20 – Comparison of calculated ξ_1 and ξ_3 factors 199

Figure 7.21 – Comparison of calculated ξ_2 and ξ_4 factors 200

Figure 7.22 – Calculated characteristic values by various methods applied to Site D data 204

Figure 7.23 – Plot showing variation in $R_{c;k}$ and $R_{c;P5}$ with $V(R_{c;chin})$ 207

Figure 7.24 – Comparing average β from load tests and that from ground tests at ULS . 210

Figure 7.25 – Comparing β_{ULS} with β_{SLS} 211

Figure A.1 - Site D N_{SPT} 228

Figure A.2 - Site F N_{SPT} 229

Figure A.3 - Site G N_{SPT} 229

Figure A.4 - Site J N_{SPT} (ground conditions mixed and with old foundations/rubble) 230

Figure A.5 – Site M N_{SPT} 230

Figure A.6 – Site N N_{SPT} 231

Figure A.7 – Site O N_{SPT} 231

Figure A.8 – Site Q N_{SPT} 232

Figure A.9 – Site R N_{SPT} 232

Figure A.10 – Site S N_{SPT} 233

Figure A.11 – Site T N_{SPT} 233

Figure A.12 – Site U N_{SPT} (ground conditions not known) 234

Figure A.13 – Site W N_{SPT} 234

Figure A.14 – Site X N_{SPT} 235

Figure A.15 – Site Y N_{SPT} 235

Figure A.16 – Site Z N_{SPT} 236

Figure A.17 – Site AA N_{SPT} 236

Figure A.18 – Site AB N_{SPT} 237

Figure A.19 – Site AH N_{SPT} 237

Figure A.20 – Site AG N_{SPT} 238

Figure A.21 – Site R: Water content, liquid and plastic limits (Farrell and Lawler 2008) 239

Figure A.22 – Site S: Water content, LL and PL: (Gavin et al. 2008) 239

Figure A.23 – Site W: Moisture Content 240

Figure A.24 – Site W: Plasticity Chart 240

Figure A.25 – Site Y: Plasticity Chart 241

Figure A.26 – Site AB: Rock cores 241

Figure A.27 – Site AH: Plasticity Chart 242

Figure A.28 – Site AH: Moisture Content 243

Figure A.29 – Site AG: Plasticity Chart 243

Figure A.30 – Site AG: Moisture Content 244

Figure B.1 – Pile 1 246

Figure B.2 – Pile 2 246

Figure B.3 – Pile 4 246

Figure B.4 – Pile 6 246

Figure B.5 – Pile 8 247

Figure B.6 – Pile 9 247

Figure B.7 – Pile 10 247

Figure B.8 – Pile11 247

Figure B.9 – Pile 12 248

Figure B.10 – Pile 13 248

Figure B.11 – Pile 15 248

Figure B.12 – Pile 16 248

Figure B.13 – Pile 18 249

Figure B.14 – Pile 19 249

Figure B.15 – Pile 20 249

Figure B.16 – Pile 21 249

Figure B.17 – Pile 22 250

Figure B.18 – Pile 23 250

Figure B.19 – Pile 24 250

Figure B.20 – Pile 25 250

Figure B.21 – Pile 26 251

Figure B.22 – Pile 27 251

Figure B.23 – Pile 28 251

Figure B.24 – Pile 30 251

Figure B.25 – Pile 31 252

Figure B.26 – Pile 32 252

Figure B.27 – Pile 34 252

Figure B.28 – Pile 35 (Tension)....252
Figure B.29 – Pile 36 (Tension)....253
Figure B.30 – Pile 37....253
Figure B.31 – Pile 38....253
Figure B.32 – Pile 39....253
Figure B.33 – Pile 40....254
Figure B.34 – Pile 41....254
Figure B.35 – Pile 42....254
Figure B.36 – Pile 43....254
Figure B.37 – Pile 44....255
Figure B.38 – Pile 46....255
Figure B.39 – Pile 47....255
Figure B.40 – Pile 48....255
Figure B.41 – Pile 49....256
Figure B.42 – Pile 50....256
Figure B.43 – Pile 51....256
Figure B.44 – Pile 52....256
Figure B.45 – Pile 53....257
Figure B.46 - Pile 54....257
Figure B.47 – Pile 55....257
Figure B.48 – Pile 56....257
Figure B.49 – Pile 57....258
Figure B.50 – Pile 58....258

Figure B.51 - Pile 59 258
Figure B.52 – Pile 60 258
Figure B.53 – Pile 61 259
Figure B.54 – Pile 62 259
Figure B.55 – Pile 63 259
Figure B.56 – Pile 64 259
Figure B.57 – Pile 65 260
Figure B.58 – Pile 66 260
Figure B.59 – Pile 67 260
Figure B.60 – Pile 68 260
Figure B.61 – Pile 69 261
Figure B.62 – Pile 70 261
Figure B.63 – Pile 71 261
Figure B.64 – Pile 72 261
Figure B.65 – Pile 73 262
Figure B.66 – Pile 74 (Tension) 262
Figure B.67 – Pile 75 262
Figure B.68 – Pile 76 262
Figure B.69 – Pile 77 263
Figure B.70 – Pile 78 (Tension) 263
Figure B.71 – Pile 79 (Tension) 263
Figure B.72 – Pile 80 (Tension) 263
Figure B.73 – Pile 81 (Tension) 264

Figure B.74 – Pile 82 264
Figure B.75 – Pile 83 264
Figure B.76 – Pile 84 264
Figure B.77 – Pile 85 265
Figure B.78 – Pile 87 265
Figure B.79 – Pile 88 265
Figure B.80 – Pile 89 265
Figure B.81 – Pile 90 266
Figure B.82 – Pile 91 266
Figure B.83 – Pile 93 266
Figure B.84 – Pile 94 266
Figure B.85 – Pile 95 267
Figure B.86 – Pile 96 267
Figure B.87 – Pile 97 267
Figure B.88 – Pile 98 267
Figure B.89 – Pile 99 268
Figure B.90 – Pile 100 268
Figure B.91 – Pile 102 268
Figure B.92 – Pile 103 268
Figure B.93 – Pile 104 269
Figure B.94 – Pile 107 269
Figure B.95 – Pile 108 269
Figure B.96 – Pile 109 269

Figure B.97 – Pile 110 270
Figure B.98 – Pile 111 270
Figure B.99 – Pile 112 270
Figure B.100 – Pile 113 270
Figure B.101 – Pile 114 271
Figure B.102 – Pile 115 271
Figure B.103 – Pile 116 271
Figure B.104 – Pile 117 271
Figure B.105 – Pile 118 272
Figure B.106 – Pile 119 272
Figure B.107 – Pile 120 272
Figure B.108 – Pile 121 272
Figure B.109 – Pile 122 273
Figure B.110 – Pile 123 273
Figure B.111 – Pile 124 273
Figure B.112 – Pile 125 273
Figure B.113 – Pile 126 274
Figure B.114 – Pile 128 274
Figure B.115 – Pile 129 274
Figure B.116 – Pile 130 274
Figure B.117 – Pile 131 275
Figure B.118 – Pile 132 275
Figure B.119 – Pile 133 275

Figure B.120 - Pile 134 275
Figure B.121 – Pile 135 276
Figure B.122 – Pile 136 276
Figure B.123 – Pile 137 276
Figure B.124 – Pile 138 (Tension) 276
Figure B.125 – Pile 139 (Tension) 277
Figure B.126 – Pile 140 (Tension) 277
Figure B.127 – Pile 141 (Tension) 277
Figure B.128 – Pile 142 277
Figure B.129 – Pile 143 278
Figure B.130 – Pile 145 278
Figure B.131 – Pile 147 278
Figure B.132 – Pile 148 278
Figure B.133 – Pile 151 279
Figure B.134 - Pile 156 279
Figure B.135 – Pile 159 279
Figure B.136 – Pile 162 279
Figure B.137 – Pile 163 280
Figure B.138 – Pile 164 280
Figure B.139 – Pile 165 280
Figure B.140 – Pile 166 280
Figure B.141 – Pile 167 281
Figure B.142 – Pile 168 281

Figure B.143 – Pile 169 281
Figure B.144 – Pile 171 281
Figure B.145 – Pile 172 282
Figure B.146 – Pile 173 282
Figure B.147 – Pile 174 282
Figure B.148 – Pile 175 282
Figure B.149 – Pile 177 283
Figure B.150 – Pile 178 283
Figure B.151 – Pile 180 283
Figure B.152 – Pile 181 283
Figure B.153 – Pile 182 284
Figure B.154 – Pile 183 284
Figure B.155 – Pile 184 284
Figure B.156 – Pile 185 284
Figure B.157 – Pile 186 285
Figure B.158 – Pile 187 285
Figure B.159 – Pile 188 285
Figure B.160 – Pile 189 285
Figure B.161 – Pile 190 286
Figure B.162 – Pile 191 286
Figure B.163 – Pile 192 286
Figure B.164 – Pile 193 286
Figure B.165 – Pile 194 287

Figure B.166 – Pile 195....287
Figure B.167 – Pile 196....287
Figure B.168 – Pile 197....287
Figure B.169 – Pile 198....288
Figure B.170 – Pile 199....288
Figure B.171 – Pile 200....288
Figure B.172 – Pile 201....288
Figure B.173 – Pile 202....289
Figure B.174 – Pile 203....289
Figure B.175 – Pile 204....289
Figure B.176 – Pile 205....289
Figure B.177 – Pile 206....290
Figure B.178 – Pile 207....290
Figure B.179 – Pile 208....290
Figure B.180 – Pile 209....290
Figure B.181 – Pile 210....291
Figure C.1 - Pile log, Pile 450....293
Figure C.2- Pile log, Pile 640....294
Figure C.3 - Coiled and colour coded cables on instrumented rebar....296
Figure C.4 - Strain gauge attachment and protective coat....296
Figure C.5–Strain gauges installed....297
Figure C.6 - Test arrangement with portable office....298
Figure C.7 - Inside portable office housing data acquisition equipment....299

Figure C.8 – Load test arrangement and instrumentation of concrete cylinders 300

Figure C.9 – Typical failure mechanism of concrete cylinder..... 301

Figure C.10 - Load-time graph for concrete cylinders..... 301

Figure C.11 – Measured stress-strain graphs for concrete cylinders 302

Figure C.12 – Measured stress-strain graphs for concrete cylinders for strain range observed in pile test..... 302

Figure C.13 – Stiffness degradation in concrete cylinders with increasing strain..... 303

Figure C.14 – Stiffness degradation in concrete cylinders with increasing strain for strain range observed in pile test 304

Figure C.15 – Dummy pile in test frame 305

Figure C.16 – Hydraulic ram in position for loading..... 306

Figure C.17 – End detail: Dummy pile contacting wooden shim..... 306

Figure C.18 - Location of surface strain gauges 307

Figure C.19 - Detail of surface strain gauges 307

Figure C.20 – Load-time graph for dummy pile..... 308

Figure C.21 – Average stress-strain curve for dummy pile..... 309

Figure D.1 – CFA piles in DBC: Calculated β for a single pile..... 311

Figure D.2 – Driven piles in DBC: Calculated β for a single pile..... 311

Figure D.3 – CFA piles in boulder clay: Calculated β for a single pile..... 312

Figure D.4 – Driven piles in boulder clay: Calculated β for a single pile 312

Figure D.5 – Bored and CFA piles in sand/gravel: Calculated β for a single pile 313

Figure D.6 – Bored and CFA piles in rock: Calculated β for a single pile 313

Figure D.7 – CFA piles in DBC: Calculated β for a pile design..... 314

Figure D.8 – Driven piles in DBC: Calculated β for a pile design..... 314

Figure D.9 – CFA piles in boulder clay: Calculated β for a pile design 315

Figure D.10 – Driven piles in boulder clay: Calculated β for a pile design 315

Figure D.11 – Bored and CFA piles in sand/gravel: Calculated β for a pile design.....316

Figure D.12 – Bored and CFA piles in rock: Calculated β for a pile design.....316

Tables

Table 2.1 – ICP procedures shaft capacity calculations in sand (Jardine et al. 2005) 10

Table 2.2(a) – Offshore CPT-based estimation of q_s and q_b for driven piles in siliceous sand (Schneider et al. 2008) 12

Table 2.3 – ICP procedures for long-term shaft capacity in clay (Jardine et al. 2005)..... 21

Table 2.4 – Typical q_s and q_b correlations with s_u in Ireland (Lehane 1997) 23

Table 2.5 – Suggested q_s for design, (Long and Collins 1999) 41

Table 2.6 – Commonly used pile failure criteria (Zhang et al. 2005) 46

Table 2.7 – Bias factors with respect to FHWA (Zhang et al. 2005) 46

Table 2.8 – Approximate guidelines for inherent soil variability (Phoon and Kulhawy 1999) 53

Table 2.9 – Summary of variability of geotechnical properties and resistances (Becker 1996) 54

Table 2.10 – Independent assessments of ICP methods for total capcity: R_c/R_m ranges (Jardine et al. 2005) 54

Table 2.11 – Summary of total measurement error of some laboratory tests (Phoon and Kulhawy 1999) 57

Table 2.12 – Summary of measurement error of in situ tests (Phoon and Kulhawy 1999) 58

Table 2.13 – Within-site variability of the capacity of driven piles at eight test sites (Zhang 2008) 61

Table 3.1(a) – Summary of site locations and pile details for sites in the PTD 68

Table 3.2(a) – Summary of pile load test results 70

Table 3.3 – Summary of material properties of DBC (Long and Menkiti 2007) 75

Table 3.4 – Summary of PTD grouped according to pile type and ground conditions..... 78

Table 4.1 – Piles loaded to failure 83

Table 4.2 – Group 1: CFA piles in DBC 94

Table 4.3 – Group 2: Driven piles in DBC 95

Table 4.4 – Group 3: CFA piles in boulder clay 95

Table 4.5 – Group 4: Driven piles in boulder clay 96

Table 4.6 – Group 5: Bored and CFA piles in sand and gravel 96

Table 4.7 – Group 6: Piles toed in rock 97

Table 4.8 – Group 7: Piles in mixed soil conditions 98

Table 4.9 – Group 9: Piles for which the ground conditions are unknown 98

Table 4.10 – Summary of estimated $V(R_c)$ for each group of piles 99

Table 4.11 – Summary of N_{SPT} and associated uncertainty at test sites 107

Table 4.12 – $V(N_{SPT})$ assuming values of Θ_z 110

Table 4.13 – Details of groups of similar piles on various sites and estimate of $R_{c;chin}$ for each individual pile 114

Table 4.14 – Within-site variability of $R_{c;chin}$ of similar piles installed in various sites 115

Table 6.1 – Summary of q_u statistics on rock at Duleek test site (a) from UCS tests and (b) and (c) from point load tests 149

Table 6.2 – Strain gauge arrangement 150

Table 6.3 – Pile details: instrumented tests on piles toed in rock 166

Table 7.1 – Summary of calculated pile design reliabilities: SLS 201

Table 7.2 – Interpreted values of $R_{c;k}$ by different methods 206

Table 7.3 – ULS: Summary of β calculated from static load test results 209

Table 7.4 – ULS: Summary of β calculated from ground test results 209

Table A.1 – Site AB: Rock core test results 242

Nomenclature

A_b	the area of the base of a pile
A_c	the cross-sectional area of a pile comprised of concrete
A_G	the gross cross-sectional area of a pile
A_s	the surface area of the shaft of a pile
A_{steel}	the cross-sectional area of a pile comprised of steel
CPT	the cone penetration test
D	the diameter of the pile
$E_{c;secant}$	the secant modulus of concrete
$E_{c;tangent}$	the tangent modulus of concrete
$E_{G;secant}$	the gross secant modulus of a pile
$E_{G;tangent}$	the gross tangent modulus a pile
E_s	the modulus a steel
f_c	the unconfined compressive strength of concrete measured using a cylinder test
f_1	the multiplication correlation factor to estimate s_u from the N_{SPT}
F_k	the characteristic load applied to a pile
FSI	Fracture Spacing Index of a rock core
L	the length of the pile
L_f	the assumed/estimated length of a geotechnical failure surface
n	the number of pile load tests in a site/group
$N_{c;B}$	the value of N_c for a bored pile

$N_{c;D}$	the value of N_c for a driven pile
N_q	the bearing capacity factor accounting for any surcharge pressure
N_γ	the bearing capacity factor accounting for the weight of soil below foundation level
N_{SPT}	the blow count for 300mm penetration of the SPT rod through the soil
$N_{SPT;base}$	the value of the N_{SPT} representative of the soil at the base of a pile
$N_{SPT;shaft}$	the value of the N_{SPT} representative of the soil along the shaft of a pile
OFS	the traditional overall factor of safety against failure
p_a	atmospheric pressure
PTD	Pile test database
q_b	the average stress developed at the base of the pile at δ_f
$q_{b;rock}$	the value of q_b for a pile bearing on rock
q_c	the tip resistance measured during the CPT
q_s	the average stress developed along the shaft of the pile at δ_f
$q_{s;rock}$	the value of q_s for a pile with a rock socket
Q_T	the maximum load applied to a pile under static loading
R_b	the base resistance of the pile
$R_{b;cal}$	the calculated value of R_b at δ_f
R_c	the compressive resistance of the ground against a pile at δ_f
$R_{c;avg}$	the estimated average value of R_c
$R_{c;Brinch-Hansen}$	the estimate of ultimate value of R_c by Brinch-Hansen
$R_{c;cal}$	the calculated value of R_c from ground test results

$R_{c;chin}$	estimate of value of R_c at δ_f by Chin's extrapolation
$R_{c;chin;ult}$	estimate of ultimate value of R_c by Chin's extrapolation
$R_{c;Davisson}$	estimate of ultimate value of R_c by Davisson
$R_{c;decourt}$	estimate of value of R_c at δ_f by Decourt's extrapolation
$R_{c;decourt;ult}$	estimate of ultimate value of R_c by Decourt's extrapolation
$R_{c;k}$	the characteristic value of R_c
$R_{c;m}$	the measured value of R_c from pile load test(s) at δ_f
$R_{c;Vander-Veen}$	estimate of ultimate value of R_c by Van der Veen
$R_{c;10}$	the resistance of the pile corresponding to 10mm displacement at the pile head
R_s	the shaft resistance of the pile
$R_{s;cal}$	the calculated value of R_s at δ_f
RQD	Rock Quality Designation
SPT	Standard Penetration Test
s_u	the undrained shear strength of a fine grained soil
$s(X)$	the sample standard deviation of a parameter 'X' about its mean value
SLS	the serviceability limit state
ULS	the ultimate limit state
$V(X)$	the coefficient of variation of a parameter 'X'
W	the equivalent weight of a pile in concrete
α	the adhesion factor for piles

α_{rock}	the reduction factor for piles socketed in rock
β	the reliability index
β_{rock}	a factor allowing for rock fracture spacing
γ	the unit weight of the soil
γ_Q	the partial factor applied to the effects (loads)
γ_R	the partial factor applied to the resistances
δ	the measured pile head deflections during a pile load test
δ_b	the deflection at the pile base
δ_f	the deflection at the pile head defining failure of the pile (equal to ten percent of the pile diameter)
δ_{max}	the maximum deflection measured at the pile head during a pile load test
ε	the strain measured during a pile load test
$\mu(X)$	the mean value of a parameter 'X'
ξ_1	the correlation factor applied to the mean $R_{c;m}$ to derive $R_{c;k}$
ξ_2	the correlation factor applied to the minimum $R_{c;m}$ to derive $R_{c;k}$
ξ_3	the correlation factor applied to the mean $R_{c;cal}$ to derive $R_{c;k}$
ξ_4	the correlation factor applied to the minimum $R_{c;cal}$ to derive $R_{c;k}$
σ'_{vb}	the mean vertical effective stress at the base of a pile
σ'_{vs}	the mean vertical effective stress over the length of the shaft of a pile
ϕ'	the internal angle of friction of a soil
ϕ'_{cv}	the constant volume angle of friction of a soil
Γ^2	the variance reduction factor
Θ_z	the vertical scale of fluctuation of a soil parameter

1 Introduction

1.1 Background

Piles form an integral part of many structures and are required to satisfy similar reliability criteria as other elements. Piles, however, differ from other components in that their performance is governed by complex interaction of a structural element with the ground, and this performance is a function of the type of pile and of its method of installation. A reliable pile design approach, therefore, requires not only a sound theoretical background but confidence in the application of these theoretical methods in practice. Such an approach must necessarily include an appreciation of the inherent uncertainty and in methods of mitigating such uncertainty. This would be in line with the approach taken to pile design in the recently introduced Eurocode 7.

In Ireland, many projects were completed for which pile foundations were the obvious geotechnical solution. The uncertainty associated with the mechanisms that govern the bearing capacity of a pile in the highly variable glacial deposits and gravels typical of Irish cities has led to a wealth of full-scale static load testing in industry and through dedicated research programmes at Irish universities. Moving forward, it is essential that this information is well documented, correctly interpreted and further developed in order to facilitate efficient pile design for future projects in which economics will have an increasing effect on design in an uncertain financial age.

This study comprises a literature review on the practice in pile design and performance with the main focus on the national practice in Ireland. Reference is made to bored, CFA and driven piles, in a variety of Irish soils, through review of useful case histories often involving high quality instrumented pile test programmes.

An assessment of the current design practice in Ireland was carried out by compilation and examination of a pile test database (PTD) which comprised the results of over 170 static load tests carried out on piles installed across the country. The pile load test results were collated from a variety of sources from the piling industry in Ireland and also from various technical papers. The PTD demonstrates the assortment of pile types installed in Ireland and is also evidence of the broad range of ground conditions that exist on the island.

More often than not, pile load tests are carried out to a pre-determined maximum test load, rather than to failure. This means that where piles exhibit small deflection under load, the ultimate compressive resistance of the pile (R_c) remains unknown and the pile design may be highly conservative considering the characteristic load (F_k) that it will likely be subjected to under working conditions and the true factor of safety remains unknown.

To address this, various methods of extrapolation of measured load-deflection data were assessed by application to those pile load test results for which a failure load was actually reached, where failure was defined as the load corresponding to a deflection at the pile head equal to ten percent of the pile diameter. Results of the analysis were used to ensure reasonable extrapolation of limited load-deflection data for estimation of R_c of other piles that were not taken to failure.

An understanding of the mechanism of load transfer from the pile into the surrounding soil requires that the development of the two major components of resistance be considered separately. The PTD contained the results of load tests carried out on several piles that were instrumented, such that the shaft and base resistances contributing to R_c could be evaluated individually. These load test results were examined alongside the measured ground properties in the vicinity of each instrumented pile and the results were used to back-calculate the parameters commonly used to estimate R_c from ground test results.

The recent introduction of pile design using partial factors, through the adoption of Eurocode 7, the new geotechnical standard in Europe, emphasises the shift from traditional design methods to reliability based design (RBD) methods, which aim to provide a more consistent level of safety in geotechnical design. These RBD methods rely on quantification of the uncertainty associated with estimated loads and resistances, which, in turn, require that the uncertainty associated with the ground and with pile installation techniques also be quantified. In light of this, the uncertainty in R_c for a single pile is assessed by application of statistical methods to the load test results gathered together in the PTD.

In Ireland, a pile design is generally specified for a site, or for an area within a site over which the ground conditions are considered similar, and thus, accurate characterisation of the within-site variability is critical to RBD of pile foundations in this country. To characterise this within-site variability, the results of pile load tests carried out on *similar* piles within sites of relatively *uniform* ground conditions, were identified and grouped

together. The within-site variability was then calculated based on the estimated values of R_c from each of the load tests and was characterised using the coefficient of variation in the parameter, denoted $V(R_c)$. The value of $V(R_c)$ was also calculated using the measured ground test results at the various sites in which piles were installed.

The PTD is ultimately used to assess the reliability of pile foundations that has been achieved in Ireland to date. Reliability is characterised using the reliability index (β) which may be related to the probability of failure of the foundation and may be assessed at the ultimate and serviceability limit states.

During the course of the study, a full-scale instrumented pile test programme was designed to investigate the effects of spatial variation in the ground and also to investigate the variability due to installation effects. Four instrumented micro piles were installed on a single site in two sets of two piles. Micro piles in the same set were installed close to each other, while the two sets of pile tests were located at distance. The load-deflection and strain-depth profiles measured show how spatial variation can affect the behaviour of piles installed on the same site, over which, only one pile design may be specified.

Following this, the research also included full-scale load tests on instrumented CFA piles toed in rock to evaluate methods of interpretation of measured strain-depth profiles in instrumented piles to produce force-depth profiles and from this to interpret shaft and base resistance development with pile deflection. The instrumentation installed in these piles was varied to compare measurements of strain in the different elements comprising the pile cross-section and to validate the common assumption that the strain induced by loading is uniform over the entire pile cross-section.

2 Literature Review

2.1 Introduction

Piles form an essential part of many structures and pile performance is a function of the pile geometry, the method of installation and of the properties of the ground in which the pile is installed. Recently, pile performance has been assessed using reliability based methods which require an estimate of the expected resistance of the pile from ground test results or from full-scale load test results.

Pile design methods, therefore, form the basis of this literature review and are related to various ground conditions and also to the type of pile, characterised by the method of installation. Particular reference to the design approaches used in Ireland is made. Furthermore, static load tests on piles are usually carried out to achieve a maximum test load, to prove a pile adequate. Often, the corresponding pile head deflections are small, implying that the ultimate pile capacity is greater than the test load. Consequently, techniques by which limited load-deflection data may be interpreted to achieve an estimation of the pile capacity at failure are also reviewed.

Reliability based methods necessarily require an understanding of the uncertainty associated with the expected pile capacity, by whatever means, and of the effect of within-site variability on this value. This total variability comprises inherent soil variability, measurement error and transformation error, with additional sources of uncertainty arising due to pile installation methods. Accordingly, quantification of these uncertainties is reviewed based on the results of ground tests and of static load tests presented in the literature.

2.2 Pile Design Methods

A pile subjected to a uniaxial compressive load develops resistance on deflection by two mechanisms – end bearing pressure acting normal to the pile toe denoted R_b and shaft resistance over the surface area of the pile shaft denoted R_s. The ultimate bearing capacity of the pile R_c is given by the sum of these two components, as shown in Equation 2.1.

$$R_c = R_b + R_s = A_b q_b + A_s q_s \qquad 2.1$$

where A_b is the area of the pile base over which the average end bearing pressure, q_b acts and A_s is the surface area of the shaft, over which the shaft friction between the pile shaft and the soil, q_s acts.

This section discusses the methods of determination of q_b and q_s in the case of bored/CFA and driven piles installed in coarse and fine grained soils. Traditional methods of estimation of R_c are discussed alongside more recent analytical methods, generally developed using the results of high quality instrumented pile load tests.

2.2.1 Coarse grained soil

End bearing pressure

The value of q_b is generally estimated from bearing-capacity theory using (Terazaghi 1943) and extended for use with deep foundations as in Equation 2.2 by Tomlinson (2001)

$$q_b = cN_c s_c d_c b_c + \sigma_v N_q s_q d_q b_q + 0.5\gamma D N_\gamma s_\gamma d_\gamma b_\gamma \qquad 2.2$$

where c is the cohesion of the soil, σ_v is the vertical total stress at the pile toe, γ is the unit weight of the soil, D is the diameter of the pile and N_c, N_q and N_γ are bearing capacity factors that are based on the internal friction angle of the soil, the compressibility of the soil and the pile geometry, s_c, s_q and s_γ are shape factors, d_c, d_q and d_γ are depth factors and b_c, b_q and b_γ are base inclination factor.

If the undrained or short-term bearing capacity is to be calculated then parameters appropriate to undrained conditions should be substituted into Equation 2.2 along with σ_v – the total stress, as shown here. If the long-term (drained) bearing capacity is required then effective stress parameters should be substituted into Equation 2.2 with the effective stress in the soil denoted σ'_v.

In coarse grained soil, Equation 2.2 is usually reduced to Equation 2.3 – the product of the effective vertical stress at the pile toe σ'_v and the bearing capacity factor N_q, as c is taken to be zero and the term $0.5\gamma D N_\gamma$ is small, when compared with $\sigma'_v N_q$. The weight of the pile should be accounted for where a substantial portion of the pile extends above the ground as is the case in a marine environment or where the soil is light (for example in peat).

$$q_b = \sigma'_v N_q \qquad 2.3$$

Values of N_q routinely used are those calculated by Berezantsev et al. (1961) though it has been suggested these are conservative (Cheng 2004). The value of N_q depends on the ratio of the depth of the foundation to the diameter of the pile, D_f/D and on the angle of shearing resistance, ϕ' as shown in Figure 2.1. Figure 2.1 is often reduced to Figure 2.2 if the effect of D_f/D is assumed small. The value of ϕ' may be measured by laboratory test but is more frequently estimated by correlation with standard penetration test (SPT) or cone penetration test (CPT) results using Figure 2.3 (a) and (b) respectively.

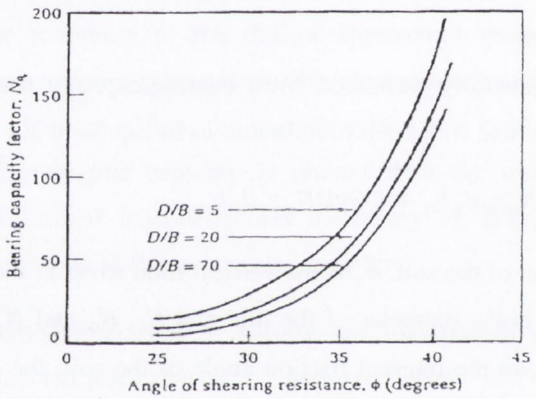


Figure 2.1 – Chart used to obtain N_q from ϕ' considering D_f/D (shown as D/B in Figure) (Berezantzev et al. 1961)

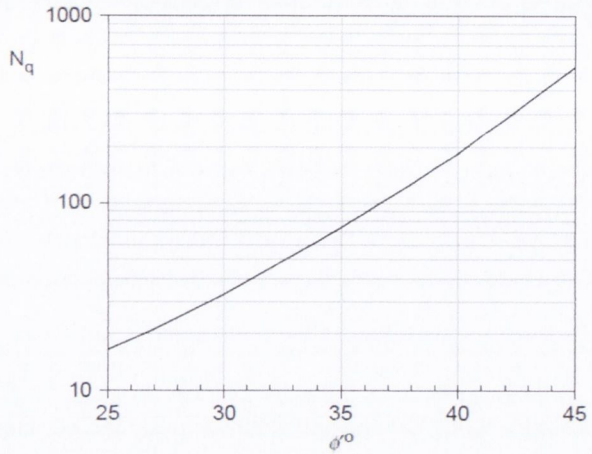


Figure 2.2 – Chart used to obtain N_q from ϕ' Berezantzev (Fleming et al. 2009)

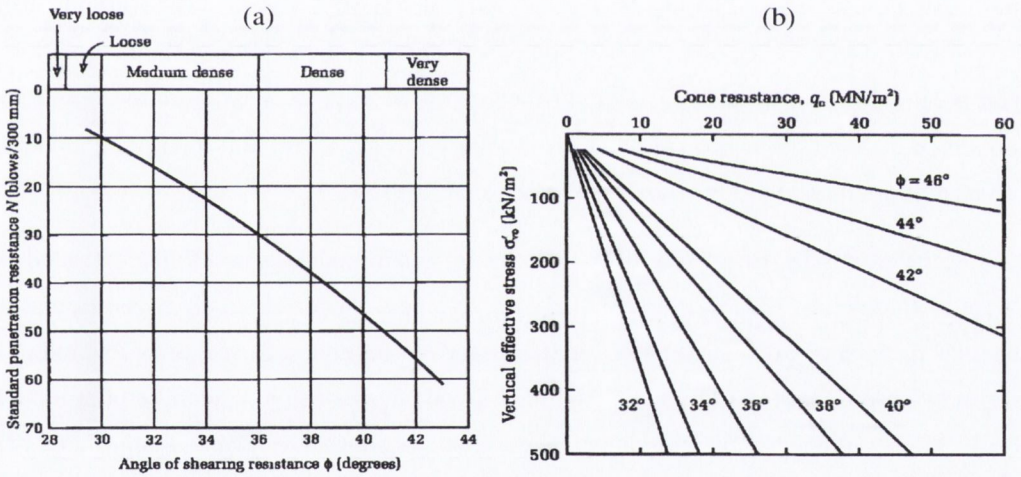


Figure 2.3 – Chart used to obtain ϕ' from SPT (a) and CPT (b) results (Tomlinson 2001)

Equation 2.4 to Equation 2.6 may be used iteratively with Figure 2.1 or Figure 2.2 until a constant value of N_q is obtained (Cheng 2004).

$$\phi' = \phi'_{cv} + 3I_R \qquad 2.4$$

$$I_R = I_D \left[5.4 - ln\left(\frac{p'}{p_a}\right)\right] - 1 \qquad 2.5$$

$$p' \sim \sqrt{N_q}\sigma_v' \qquad 2.6$$

where ϕ_{cv}' is the critical state friction angle (the angle of friction during shearing with no change in volume), I_R is the corrected relative density of the soil, I_D is the uncorrected relative density of the soil and p' is the ambient vertical effective stress.

Recognising that the Cone Penetration Test (CPT) bears similarity to the behaviour of a driven pile, many Researchers have attempted to provide direct correlation between q_b and the CPT cone tip resistance, q_c (Nordlund 1963; Bustamante and Gianeselli 1982; Fleming and Thorburn 1983; Kraft 1990; DeNicola and Randolph 1993; Jardine and Chow 1996; Lee and Salgado 1999; API 2000; Lehane and Randolph 2002; Clausen et al. 2005; Kolk et al. 2005).

These methods outline adjustment of the measured q_c to estimate q_b. This is necessary due to differences in scale of the cone used in the CPT and the piles themselves and also due to the fact that pile deflection must be limited under working conditions. The methods differ in that they apply to different types of pile (open and closed ended) in different conditions (onshore and offshore) and the method of averaging of the q_c values close to the pile toe, on which q_b is based, varies. The Reader is referred to Lehane et al. (2005) and Schneider (2008) for comparison of the most frequently used methods.

Given the extensive use of the SPT (in Ireland), Gavin and Lehane (1998) extended the work of Jardine and Chow (1996) on the CPT, to propose a correlation between q_b and the results of the standard penetration test (SPT) for closed ended driven piles in sand. The relationship proposed is shown in Equation 2.7 and was based on a database of around 16 static load test results on piles installed in sand. It should be noted, that, where base bearing was not fully mobilised during the load tests, then the load-deflection data recorded was extrapolated using Chin's method (Chin 1970).

$$q_{b;0.1} = 0.8N_{SPT}(D/D_{50})^{-0.15}(\sigma_v'/p_a)^{-0.33} \qquad 2.7$$

where $q_{b;0.1}$ is the end bearing stress at a deflection equal to the diameter of the pile D divided by 10, N_{SPT} is the measured values of the SPT, averaged over three diameters above and below the pile toe and corrected for fines content using Equation 2.8 (Terazaghi and Peck 1967), D_{50} is the mean particle size of the sand, σ_v' is the vertical effective stress at the pile toe and p_a is atmospheric pressure equal to 100kPa.

$$N = 15 + 0.5(N - 15) \quad 2.8$$

Shaft resistance

The traditional approach used to calculate shaft resistance in coarse grained soil is to relate the shaft stress to the pile-soil interface friction angle (δ) using Equation 2.9

$$q_s = \sigma_n' \tan\delta = K\sigma_v' \tan\delta \quad 2.9$$

where σ_n' is the normal effective stress on the pile shaft and K is the coefficient of earth pressure equal to the ratio σ_v'/σ_n'.

The parameter K is not constant over the length of the pile and depends on the relative density of the soil (Jardine and Chow 1996), the method of installation of the pile and on the in-situ coefficient of earth pressure, K_0 (Tomlinson 2001). Equation 2.10 and Equation 2.11 may be used to calculate K_0 for normally consolidated and over consolidated soil respectively (Mayne and Kulhawy 1982).

$$K_0 = 1 - sin\phi' \quad 2.10$$

$$K_0 = 1 - sin\phi' OCR^{sin\phi'} \quad 2.11$$

Where measurements of δ are not available, then, assuming there is no dilation of the material being sheared as the pile is loaded, δ may be replaced with the critical state friction angle, ϕ_{cv}' (the angle of shearing resistance with no change in volume) (Fleming et al. 2009). The value of δ may be related to the value of ϕ' of the soil in which the pile is installed depending on the surface roughness of the pile surface (Kishida and Uesugi 1987).

Work carried out by Imperial College London (ICP) in which piles were instrumented to measure radial effective stress, σ_r' during loading, led to a new method of estimation of q_s (Jardine et al. 2005) for driven piles known as the ICP method. The steps required to perform the ICP estimate of shaft resistance for piles in sand are shown in Table 2.1, while the parameters required for this design method are defined in Figure 2.4.

Table 2.1 – ICP procedures shaft capacity calculations in sand (Jardine et al. 2005)

A	**SHAFT CAPACITY OF CLOSED-ENDED CYLINDRICAL PILES**	
A1	$Q_s = \pi D \int \tau_f \, dz$	**Shaft capacity** Integral of the local shear stresses along the embedded shaft length
A2	$\tau_f = \sigma'_{rf} \tan \delta_{cv}$ $\sigma'_{rf} = (\sigma'_{rc} + \Delta\sigma'_{rd})$	**Local shear stress** Coulomb failure criterion
A3	$\sigma'_{rc} = 0.029 \, q_c \, (\sigma'_{v0}/P_a)^{0.13} \, (h/R)^{-0.38}$	**Local radial effective stress** Function of CPT resistance, free-field vertical effective stress σ'_{v0} (normalised by absolute atmospheric pressure, P_a = 100 kPa) and h/R; q_c is measured (not corrected for OCR) and h/R is limited to a minimum value of 8.
A4	$\Delta\sigma'_{rd} = 2G \, \Delta r / R$ $G = q_c \, [A + B\eta - C\eta^2]^{-1}$ where $\eta = q_c \, (P_a \, \sigma'_{v0})^{-0.5}$ $A = 0.0203$ $B = 0.00125$ $C = 1.216e\text{-}6$	**Dilatant increase in local radial effective stress during pile loading** Related to sand shear stiffness, pile roughness R_{cla} and radius. G taken from Baldi et al.'s (1989) correlation with CPT q_c. $\Delta r = 2R_{cla} = 0.02$ mm for lightly rusted steel piles.
A5	δ_{cv} Measure directly in tests. If not feasible estimate from Figure 5	**Interface angle of friction at failure** Equal to constant volume value from interface shear tests, depends on pile roughness and other factors.
A6	$\tau_f = (0.8\sigma'_{rc} + \Delta\sigma'_{rd}) \tan \delta_{cv}$	In **tension loading** Equation A6 should be used in place of Equation A2.
B	**SHAFT CAPACITY OF OPEN-ENDED TUBULAR PILES**	
B3	$\sigma'_{rc} = 0.029 \, q_c \, (\sigma'_{v0}/P_a)^{0.13} \, (h/R^*)^{-0.38}$ $R^* = (R^2_{outer} - R^2_{inner})^{0.5}$ **In tension** $\tau_f = 0.9(0.8\sigma'_{rc} + \Delta\sigma') \tan \delta_{cv}$	**Modified radius, R*** Substituted into Equation A3 to give B3. $h/R^* \geq 8$. Shear stresses in tension reduced by a further 10%

Note: Above recommendations apply to (i) silica sands, (ii) piles with circular cross-sections (iii) capacities available in 'first-time' slow maintained loading tests conducted around ten days after driving.

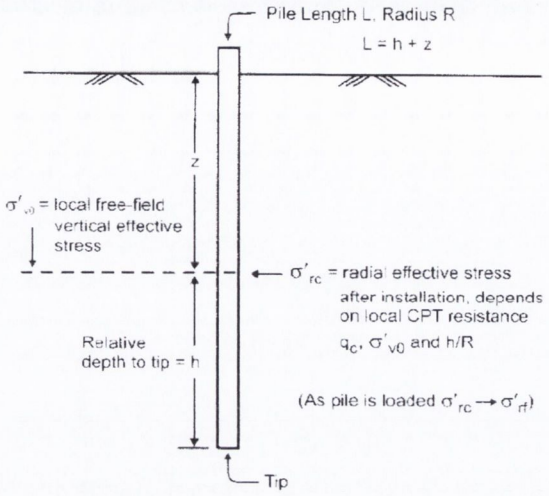


Figure 2.4 - Definition of parameters for calculation of σ'_{rf} (Jardine et al. 2005)

In practice, it is difficult to obtain representative samples for laboratory testing to provide many of the parameters used in estimation of q_b and q_s, thus, correlations that exist between the results of in situ tests (mainly the N_{SPT} and q_c with q_s and q_b) remain popular. Gavin (2009), based on the results of load testing of two instrumented CFA piles in glacial sand in Ireland, concluded that the in situ tests of the SPT and CPT captured the effect of sand density on the mobilised q_s.

Schneider et al. (2008), used a database of 77 static load test results on driven piles in siliceous sands for which adjacent CPT profiles existed, to evaluate the various methods of design based on the results of the CPT. Due to the distinct lack of CPT results available in Ireland, mainly owing to the nature of the ground and presence of boulders, the various methods of design using the results of the CPT are not reported on in detail, but those methods deemed most useful are summarised in Table 2.2 for estimation of q_s and q_b, (Schneider et al. 2008). For a more detailed appraisal of 15 different methods of design of displacement piles using the results of the CPT, predominantly in coarse grained material (sand) the Reader is referred to Schneider (2007).

Table 2.2(a) – Offshore CPT-based estimation of q_s and q_b for driven piles in siliceous sand (Schneider et al. 2008)

Methods	Design equations	
Fugro-05[a]	$\tau_f = 0.08 q_c \left(\frac{\sigma'_{v0}}{p_{ref}}\right)^{0.05} \left(\frac{h}{R^*}\right)^{-0.90}$	(compression loading for $h/R^* \geq 4$)
	$\tau_f = 0.08 q_c \left(\frac{\sigma'_{v0}}{p_{ref}}\right)^{0.05} (4)^{-0.90} \left(\frac{h}{4R^*}\right)$	(compression loading for $h/R^* \leq 4$)
	$\tau_f = 0.045 q_c \left(\frac{\sigma'_{v0}}{p_{ref}}\right)^{0.15} \left[\max\left(\frac{h}{R^*}, 4\right)\right]^{-0.85}$	(tension loading)
ICP-05	$\tau_f = a\left[0.029 b q_c \left(\frac{\sigma'_{v0}}{p_{ref}}\right)^{0.13} \left[\max\left(\frac{h}{R^*}, 8\right)\right]^{-0.38} + \Delta\sigma'_{rd}\right] \tan\delta_f$ a=0.9 for open-ended piles in tension and 1.0 for all other cases b=0.8 for piles in tension and 1.0 for piles in compression	
NGI-05	$\tau_f = z / L p_{ref} F_{D_r} F_{sig} F_{tip} F_{load} F_{mat} \geq \tau_{min}$ $F_{D_r} = 2.1(D_r - 0.1)^{1.7}$ $D_r = 0.4 \ln(q_{c1N}/22)$ $F_{sig} = (\sigma'_{v0}/p_{p_a})^{0.25}$ F_{tip}=1.0 for driven open ended and 1.6 for driven closed ended F_{load}=1.0 for tension and 1.3 for compression F_{mat}=1.0 for steel and 1.2 for concrete $\tau_{min} = 0.1\sigma'_{v0}$	[nominal relative density (which may be greater than 1.0)]

Table 2.2(b) – Offshore CPT-based estimation of q_s and q_b for driven piles in siliceous sand (Schneider et al. 2008)

Methods	Design equations
UWA-05	$\tau_f = \frac{f_t}{f_c}\left[0.03 q_c A_{rs,eff}^{0.3}\left[\max\left(\frac{h}{D}, 2\right)^{-0.5}\right] + \Delta\sigma'_{rd}\right]\tan\delta_f$ $A_{rs,eff}$(effective area ratio)$= 1 - \text{IFR}(D_i/D)^2$ A_r(area ratio)$= 1 - (D_i/D)^2$ IFR$(=\Delta L_p/\Delta z)$. When IFR is not measured, average IFR $= \min[1, (D_i(\text{m})/1.5)^{0.2}]$ f_t/f_c=ratio of tension to compression capacity (equal to 1 for compression and 0.75 in tension)

Note: τ_f=local ultimate shaft friction; δ_f=interface friction angle; p_{ref}=100 kPa=reference stress; L=pile length; z=element depth; h=height above pile tip; R^*=equivalent pile radius$=(R^2 - R_i^2)^{0.5}$ where R_i=internal pile radius$=D_i/2$. For noncircular piles, an equivalent circular area is used to assess R^* and D. $\Delta\sigma'_{rd} \approx 4G\Delta y/D$=change in radial stress during pile loading; $G \approx 185 q_c q_{c1N}^{-0.7}$=operational level of shear modulus; see Eq. (8*b*) for calculation of q_{c1N}; $\Delta y \approx 2R_a \approx 0.02$ mm=radial displacement during pile loading; and R_a=average roughness of the pile.

[a]The format of the equation for compression shaft friction within $4R^*$ of the pile tip differs slightly from Kolk et al. (2005a) due to a typing error in that paper.

Table 2.2(c) – Offshore CPT-based estimation of q_s and q_b for driven piles in siliceous sand (Schneider et al. 2008)

Methods	End condition	Design equations
Fugro-05	Closed and open ended	$q_{b0.1}/q_{c,avg}=8.5(p_{ref}/q_{c,avg})^{0.5}A_r^{0.25}$
ICP-05	Closed ended	$q_{b0.1}/q_{c,avg}=$maximum $[1-0.5\log(D/D_{CPT}),0.3]$
	Open ended	if $D_i \geq 2.0(D_r-0.3)$ or $D_i \geq 0.083q_{c,avg}/p_{ref}D_{CPT}$, D_i in meters, then the pile is "unplugged," and $q_{b0.1}/q_{c,avg}=A_r$ if not, the pile is "plugged," and $q_{b0.1}/q_{c,avg}=$maximum $[0.5-0.25\log(D/D_{CPT}),0.15,A_r]$
NGI-05	Closed ended	$q_{b0.1}/q_{c,tip}=F_{D_r}=0.8/(1+D_r^2)$
	Open ended	$q_{b0.1}=$minimum [plugged $q_{b0.1}$, unplugged $q_{b0.1}$] the plugged $q_{b0.1}$ value is calculated as: $q_{b0.1}/q_{c,tip}=F_{D_r}=0.7/(1+3D_r^2)$ the unplugged $q_{b0.1}$ is calculated as: $q_{b0.1}=q_{b,ann}A_r+q_{b,plug}(1-A_r)$; $q_{b,ann}=q_{c,tip}$, and $q_{b,plug}=12\tau_{f,avg}L/(\pi D_i)$ $\tau_{f,avg}$: averaged external skin friction (Clausen et al. 2005); L: pile embedment depth
UWA-05	Closed and open ended	$q_{b0.1}/q_{c,avg}=0.15+0.45A_{rb,eff}$

Notes: D: pile outer diameter; D_i: pile inner diameter; $p_{ref}=100$ kPa; $D_{CPT}=0.036$ m; A_r (area ratio) $=1-(D_i/D)^2$; $A_{rb,eff}$ (effective area ratio) $=1-FFR(D_i/D)^2$; FFR: IFR $(=\Delta L_p/\Delta z)$ averaged over last $3D$ of the pile penetration; $q_{c,avg}=q_c$ averaged $\pm 1.5D$ over pile tip level for Fugro-05 and ICP-05 methods; $q_{c,avg}=q_c$ averaged using Dutch averaging technique for UWA-05 method; $D_r=0.4\ln(q_{c1N}/22)$; as decimal, nominal relative density which may be greater than 1.0 for NGI method.

2.2.2 Fine grained soil

End bearing pressure

In the case of undrained soil conditions at the pile toe, $N_q = 1$, $N_\gamma = 0$ and also, for piles where the base diameter is not enlarged, the overburden is approximately equal to the weight of the pile – so Equation 2.2 reduces to Equation 2.12 and it is usual to calculate q_b where piles are toed in clay by Equation 2.12, applicable to both bored and driven piles (Poulos and Davis 1980).

$$q_b = s_{u;b} N_c \qquad 2.12$$

where $s_{u;b}$ is the undrained shear strength of the soil at the toe of the pile.

In the case of bored piles, N_c is generally taken as equal to 9, interpreted by Skempton (1951) from the results of numerous load tests on bored piles and from plate loading tests carried out in boreholes (Skempton 1951; Skempton 1959). The results are shown in Figure 2.5 where Meyerhof (1951) used plastic theory to show that limiting values of N_c for bored piles are equal to 9.3 where the shaft friction q_s is zero and 9.7 where q_s equals $s_{u;b}$ (Meyerhof 1951; Meyerhof and Murdock 1953). Values in the range 7.4 – 9.3 were computed by Ladanyi (1963) from cavity expansion analysis in a soil mass. Where a pile toe just penetrates a stiff layer underlying a soft layer it is suggested N_c be reduced to reflect this (Fleming et al. 2009).

In the case of a driven pile, N_c may be considerably larger. A value of over 50 was interpreted for a driven pile installed in Croke Park in the Dublin boulder clay deposit, thought to be as a result of stresses induced during installation (Farrell et al. 1998). St John (1980) showed that, in reality, N_c increases with overconsolidation ratio and reported values of as high as 30.

Shaft resistance

The shaft resistance developed along the length of a pile in fine grained material is traditionally estimated using Equation 2.13 – the product of an adhesion factor α and the average undrained shear strength of the soil over the length of the pile shaft $\bar{s}_u$.

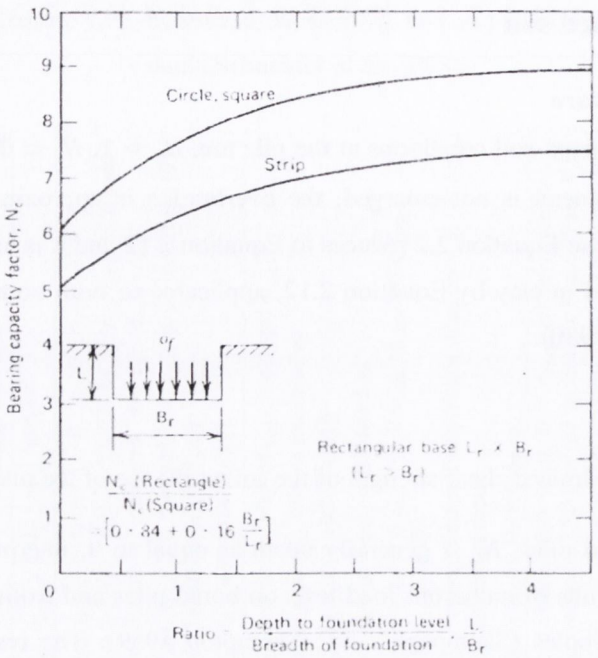


Figure 2.5 - N_c for piles in clay after Skempton (1951)

$$q_s = \alpha \bar{s}_u \qquad 2.13$$

The value of s_u may be estimated from in-situ or laboratory tests (CPT, SPT, pressuremeter and triaxial tests) though it is recognised that there is substantial variation in the interpreted values of s_u from each of these tests, (Kulhawy and Mayne 1990). The interpretation of the value of s_u from the SPT for example, is by empirical correlation to shear strength measurements made on tests deemed more to yield a more reliable estimate of the parameter.

The relationship between the N_{SPT} value and s_u proposed by Stroud (1974), which depends on the plasticity index of the clay, is frequently used in practice and is shown in Figure 2.6 (where s_u is referred to as c_u in Figure 2.6) for different clays. The value of s_u/N_{SPT} is generally denoted f_1 and is referred to as the N_{SPT} to s_u multiplication correlation factor.

The value of α depends on the stress history of the soil in which the pile is installed, on the method of installation of the pile, and also on the rate of loading during testing. Various researchers have attempted to provide a means of calculation of the α value for use in

Equation 2.13, usually from databases containing pile load tests from which α values are back calculated.

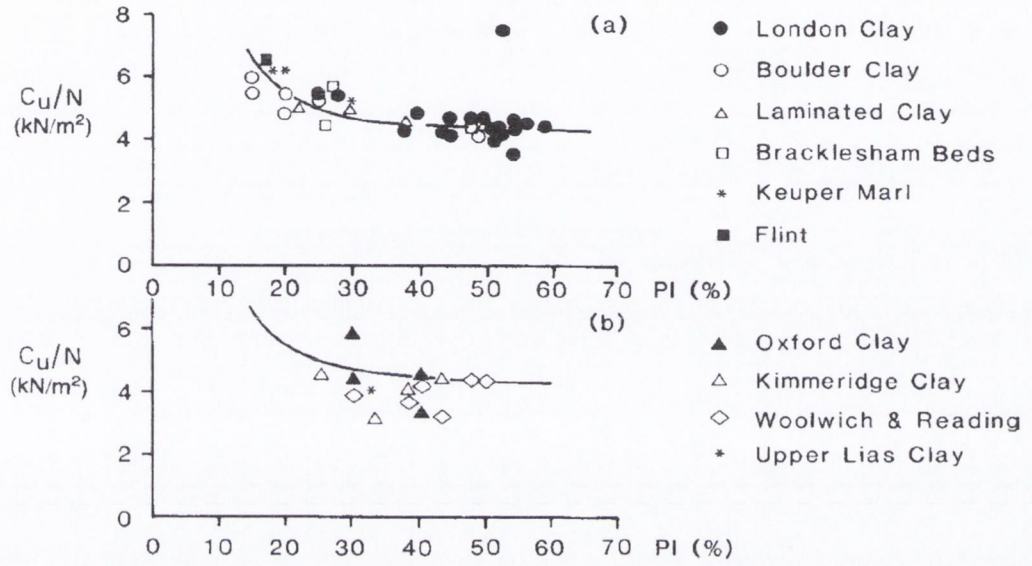


Figure 2.6 – Correlation of s_u with SPT result (Stroud 1974)

Skempton (1959) presented the results of 34 pile load tests on bored piles in London clay for which he back calculated α values in the range 0.21-0.61 with an average value of 0.45 and suggested this average value be used in design with a lower limit of 0.3, however, it should be noted some of these piles were installed by hand.

Figure 2.7 suggests typical relationships between α and s_u for various types of pile (Trenter 1999) based on work by Weltman and Healy (1978) considering piles tested in glacial till. Short comings in the analysis are highlighted, in that, not all the piles tested were taken to failure and differences between fissured and intact tills were not considered. Figure 2.7 shows a downward trend in α from 1.0 to 0.45 with increasing s_u from 80-200kPa in the case of driven piles. A similar relationship is shown for bored piles where the α values are reduced by about 20% compared to those values suggested for driven piles.

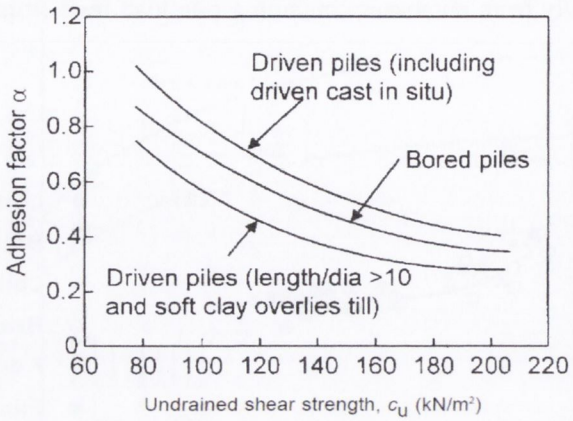


Figure 2.7 - Suggested relationship between α and s_u for clay tills (Weltman and Healy 1978)

Randolph and Murphy (1985) related the value of α to the strength ratio of the soil $\bar{s}_u/\sigma'_v$ (where σ'_v is the vertical effective stress) using the results of pile load tests. The results are shown in Figure 2.8. The α values are seen to reduce from above 1 to about 0.3 with increasing $\bar{s}_u/\sigma'_v$.

The value of α may be calculated by Equation 2.14 and Equation 2.15 if it is assumed equal to one for normally consolidated clay (Fleming et al. 2009).

$$\alpha = (s_u/\sigma'_v)_{nc}^{0.5}(s_u/\sigma'_v)^{-0.5} \qquad s_u/\sigma'_v \leq 1 \qquad 2.14$$

$$\alpha = (s_u/\sigma'_v)_{nc}^{0.5}(s_u/\sigma'_v)^{-0.25} \qquad s_u/\sigma'_v > 1 \qquad 2.15$$

Kulhawy and Jackson (1989), using a database containing 106 pile tests on bored piles, back calculated α values and a subsequent best fit when plotted against s_u/p_a is shown by Equation 2.16. It should be noted that over half, (65) of these piles were tested in tension. It has been observed that the shaft resistance in tension may be less than that in compression (Lehane and Jardine 1994; Farrell et al. 1998). The tensile resistance of a pile may be less than that in compression due to the effect of Poisson's ratio (DeNicola and Randolph 1993).

$$\alpha = 0.21 + 0.26/(s_u/p_a) \qquad 2.16$$

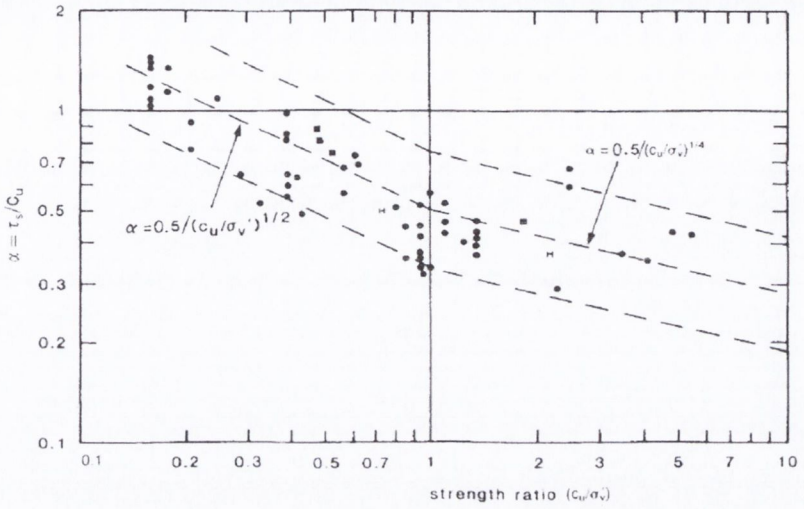


Figure 2.8 - Variation of α with strength ratio (Randolph and Murphy 1985)

This work was improved upon by Chen and Kulhawy (1994) by applying a regression analysis to the results of a database of 127 pile load tests and, in this case, the estimates of s_u were made consistent i.e. converted such that the bias in measurement due to measurement technique was removed, and the relationship shown in Equation 2.17 was suggested. Goh et al. (2005) report $s_{u;CIUC}$ is the estimate of s_u converted so that the result comes from a consistent test type - a consolidated isotropic undrained compression (CIUC) test, where the relationships between s_u from various means of measurement were taken from Kulhawy and Mayne (1990).

$$\alpha_{CIUC} = 0.31 + 0.17/(s_{u;CIUC}/p_a) \qquad 2.17$$

O'Neill and Reese (1999) estimated α using the databases of Chen and Kulhawy (1994), Davidson et al. (1994) and Reese and O'Neill (1988), but only considered piles of diameter within the range 0.70 to 1.83m and where $s_u \geq$ 50kPa at the site of the test. The relationships in Equation 2.18 and Equation 2.19 were suggested for calculation of α, but it was also concluded that site specific estimation of α based on load testing is the best means of determination of the parameter (O'Neill and Reese 1999).

$$\alpha = 0.55 \qquad s_u/p_a \leq 1.5 \qquad 2.18$$

$$\alpha = 0.55 - 0.1\,(s_u/p_a - 1.5) \qquad 1.5 \leq s_u/p_a \leq 2.5 \qquad 2.19$$

Jardine et al. (2005), consider that, the α method is *fundamentally flawed* and claimed that failure of soil along the pile shaft is not governed by s_u but as previously described for coarse grained material, assuming a solely frictional relationship between the pile shaft and the soil, therefore, q_s may be calculated using Equation 2.9.

In the case of piles driven in clay, installation effects can lead to a reduction in the s_u value at the pile-soil interface. This means δ_f is not as for the intact soil and s_u is also modified in this interface zone. The α value therefore varies depending on soil type and position on the shaft.

During installation of driven piles in clay, excess pore water pressures are often developed and as a result the available shaft capacity Q_s varies until these excess pore water pressures are dissipated. This period is known as the equalisation period. As excess pore water pressure dissipates, σ_r' varies, and this is reflected in changes in Q_s (Jardine et al, 2005).

The ICP method (shown in Table 2.3 for driven piles in clay) was applied to concrete piles driven in Mexico City clay and was also applied to a database of test piles compiled from various locations around the same city (Saldivar and Jardine 2005). It was concluded that this method led to more reliable estimates of Q_s than the α method (the method of design traditionally used in Mexico City). It should be noted that the parameters on which the ICP method relies to estimate Q_s are highly variable and thus uncertain (for example the pile-soil interface friction angle, δ depends on the plasticity index (PI) of the material which is highly variable.

The effective stress relationship displayed in Equation 2.9 may be used to calculate q_s for bored piles in fine grained material. Where the pile is installed soon after the excavation is created, then, K in Equation 2.9, may be taken as equal to K_0 as little change in the initial stress state in the soil should occur.

A recent assessment of the estimation of K_0 in overconsolidated clays was presented by Sivakumar et al. (2009) from tests on both reconstituted and undisturbed samples of several types of clays including London clay and Belfast clay. Where the clay is normally

Table 2.3 – ICP procedures for long-term shaft capacity in clay (Jardine et al. 2005)

E	SHAFT CAPACITY OF CLOSED-ENDED PILES	
E1	$Q_s = \pi D \int \tau_f \, dz$	**Shaft capacity** is found by integrating local shear stresses along the embedded shaft length.
E2	$\tau_f = \sigma'_{rf} \tan \delta_f = (K_f/K_c)\, \sigma'_{rc} \tan \delta_f$	**Local shear stress** is expressed using the Coulomb failure criterion, expanded in terms of loading factor, K_f/K_c and σ'_{rc} the local radial effective stress after equalisation.
E3	$\sigma'_{rc} = K_c\, \sigma'_{v0}$ $K_c = [2.2 + 0.016\, YSR - 0.870\, \Delta I_{vy}] YSR^{0.42}\, (h/R)^{-0.20}$ and $\Delta I_{vy} = \log_{10} S_t$ or: $K_c = [2 - 0.625\, \Delta I_{v0}]\, YSR^{0.42}\, (h/R)^{-0.20}$	**Local radial effective stress after equalisation** σ'_{rc} is found from K_c and σ'_{v0}; K_c depends on Yield Stress Ratio (YSR), normalised distance from the pile tip (h/R) and sensitivity S_t expressed by ΔI_{vy} The alternative ΔI_{v0} expression is marginally less conservative. h/R is limited to a minimum of 8.
E4	$K_f/K_c = 0.8$	The **Loading Factor** is constant regardless of the direction of loading or drainage conditions.
E5	δ_f between δ_{peak} and $\delta_{ultimate}$	The **peak and ultimate interface angles of friction** are measured in interface ring shear tests as specified in Appendix A. The operational value depends on the degree of progressive failure, pile roughness, clay type and shearing history.
F	**SHAFT CAPACITY OF OPEN-ENDED PILES**	
F3	$K_c = f(h/R^*)$ where $R^* = (R^2_{outer} - R^2_{inner})^{0.5}$	K_c can be taken from either of the expressions in Step E3, with the substitution of the **equivalent radius, R^***, in the h/R term. A lower limit of $h/R^* = 8$ applies.

consolidated, K_0 may be found using an empirical relationship of which there are many reported in the literature. These are listed by Sivakumar et al. (2009) and include estimates proposed by (Jaky 1948; Brooker and Ireland 1965; Abdelhamid and Krizek 1976; Bolton 1991; Simpson 1992).

Where K_0 is large, in heavily over-consolidated clays, a reduction to K_0 should be applied, suggested as 20% (Fleming et al. 2009) as some relaxation of the soil around the shaft is

likely. Delays in pouring concrete are likely to adversely affect the in-situ horizontal effective stress in the soil surrounding the pile shaft (Ng et al. 2000; Mandolini et al. 2005).

The value of δ is also required – if it is assumed the surface of a bored pile is sufficiently rough so that the failure plane along the length of the pile occurs within the soil close to the pile shaft surface then the critical state friction angle ϕ'_{cv} may be used.

If the profile of K_0 with depth is not known, which is generally the case for over-consolidated clays; then, total stress methods (the α method) may be used to estimate the shaft resistance. Figure 2.7 displays the suggested relationship between α and s_u for bored piles based on static pile load tests carried out in glacial tills (Weltman and Healy 1978). The α values for bored piles are around 0.8 times those suggested for driven piles. However, there is substantial scatter in the results on which these curves are based.

2.3 Pile Design and Testing in Ireland

2.3.1 Introduction

Pile design in Ireland is principally based on the experience of the piling contractor who generally specifies the pile dimensions required for a particular specified working load (SWL). This may be based on the results of preliminary static load tests carried out on the site or on other sites with similar ground conditions (Lehane 1997).

More recently, with the introduction of the new geotechnical design standard for Europe – Eurocode 7, pile design will be carried out using partial factors which may be applied to the soil parameters measured by in-situ or laboratory tests, or alternatively to the results of static or dynamic load tests carried out on a pile or piles installed at a site.

On large piling contracts, where 250 or more piles are required, preliminary load tests are usually carried out on approximately 1% of the total number of piles, with a further 1% proof load tests on working piles. Medium sized contracts, involving pile numbers in the range 50-250, rely on proof tests on working piles alone, usually loaded to 1.5 times the SWL. On smaller projects static load tests are rarely carried out but piles are designed more conservatively, based on the ground conditions alone, or in combination with dynamic testing (Lehane 1997).

The results of static load tests may be used for pile design by examination of the measured load-deflection curve of the pile(s) tested. The allowable pile head deflection is traditionally limited to 10mm for single piles and it is usual to check that pile recovery on unloading at least equals the estimated elastic shortening of the pile (Lehane 1997). In the case of pile groups, it may be acceptable for the deflection of any single pile in the group to exceed the allowable 10mm.

In fine grained soil, pile design from site investigation in Ireland relies on correlations between q_s and q_b with s_u for estimation of R_s and R_b respectively. Typical values used in practice, suggested by Lehane (1997), are shown in Table 2.4 (where q_s, q_b and s_u are written f_s, f_b and c_u respectively). The value of s_u may be obtained from unconsolidated undrained (UU) triaxial tests, however, this is rarely the case due to the difficulties in obtaining suitable samples for laboratory testing (Farrell and Wall 1990; Farrell et al. 1998; Gavin et al. 2008) and s_u is more likely estimated by correlation with the results of the SPT.

Collins and Mitchell (1990) back-figured shaft and base resistances from the results of over sixty static load tests carried out on piles installed on twenty-four separate sites across Ireland. This database comprised bored, precast concrete and steel H-piles in gravels and glacial tills. The results give typical values of the shaft and base resistances observed in practice mainly in Dublin and in Cork. This work is also referred to in this Section.

The uncertainty in the methods of design and the appropriateness of correlation factors has led to research programmes in Ireland whereby high quality instrumented tests have been installed in an attempt to quantify the development of q_s and q_b with pile head deflection. Instrumented test results published in the literature are reviewed in this Section, also included are case studies of other relevant pile observations reported in Ireland.

Table 2.4 – Typical q_s and q_b correlations with s_u in Ireland (Lehane 1997)

	Bored/CFA pile	Driven piles
f_s	$\approx 0.5\ c_{u0}$	$\approx 0.4\ c_{u0}$ for $c_{u0} > 100$ kPa $\approx 1.0\ c_{u0}$ for $c_{u0} < 30$ kPa
f_b	$\approx 9\ c_{u0}$	$\approx 9\ c_{u0}$ in alluvium $\approx 20\ c_{u0}$ in glacial till

As already mentioned, the high stone content of Irish glacial tills means that it is usually difficult to obtain representative undisturbed samples, at least routinely, for laboratory testing to obtain the soil parameters to be used for design purposes. This has led to the extensive use of in-situ tests, most frequently, the standard penetration test, although the presence of large gravel and boulders can distort the results. The results of the SPT may be empirically correlated with s_u for use in design.

Traditionally, total stress methods in the form of the α method, described previously, have been used to estimate R_c when designing piles in these boulder clays, whose behaviour is generally dictated by the fine grained material contained within. Despite the known limitations (Jardine and Chow 1996; Farrell et al. 1998) this method is typically used at present.

This section reviews the published results of six high quality pile load tests on instrumented piles installed in Dublin boulder clays. Three of these tests were carried out by Farrell et al (1998; 2008), one on a closed ended driven pile at Croke Park, North Dublin and the others on CFA piles installed at Saint James Hospital. Gavin et al. (2008) presented the results of three other load tests on instrumented CFA piles at Ballsbridge, south Dublin with one pile loaded in tension. The results of all six tests are discussed.

Rock socketed piles are also widely used in Ireland, footed in the commonly found fresh, meaning not weathered, Carboniferous limestone underlying Dublin, Limerick and Cork – three of Ireland's major cities (Long and Collins 1999). Long and Collins (1999) presented the back analysis of the results of thirty pile tests located across the island of Ireland and used these to suggest a new design method for rock socketed piles that introduced the effects of pile shaft roughness. The findings are reviewed in this section.

2.3.2 Driven Piles

This sub-section reviews the results of static load tests carried out on driven piles in Ireland which were carried out to investigate the development of shaft and base resistance with deflection and also to investigate the effects of installation methods on pile capacity.

Farrell et al. (1998) installed a close-ended tubular steel pile of 273 mm outer diameter and 7.5 m in length at Croke Park, North Dublin which was instrumented close to the pile head and over the lower 3.5m with vibrating wire strain gauges and pore pressure probes. This

test pile was loaded in compression in three load cycles, 2.4 hours, 1.8 days and 17 days after installation before a tension pull out test was carried out 24 days after installation.

Ground conditions at the site, shown in Figure 2.9, comprised approximately 2m depth of made ground, over 2m Dublin brown boulder clay, over Dublin black boulder clay which was proved to 10m depth. SPT results yielded values of N_{SPT} mostly in the range 30-80 in the boulder clay layers with many refusals reported even at shallow depth – the N_{SPT} recorded at the various depths are also shown in Figure 2.9.

Using an undrained bearing capacity analysis, as shown in Equation 2.12, the value of N_c for this driven steel pile was estimated as 55, likely due to an increase in the mean effective stress at the pile toe during pile driving (Farrell et al. 1998). Development of the base resistance is plotted against the base deflection in Figure 2.10, the interpreted value of q_b reached during the load test was about 14MPa and that predicted as ultimate was about 25MPa.

Figure 2.11 shows the interpreted shaft resistance for each of the loading cycles. During the first load cycle, α was interpreted as 0.22 when excess pore pressures were still high, rising to 0.55 for the third load cycle (had the pile been taken to failure) where dissipation of excess pore water pressures had likely taken place.

Farrell et al. (1998) concluded that the shaft resistance profile is inconsistent with the α method, in that, it is clearly increasing with decreasing distance from the pile toe, consistent with the ICP design method described earlier in Section 2.2.2.

Armishaw (1987), reported on the results of several load tests carried out on precast driven piles at a town centre development in Tallaght, South Dublin. Site investigation, comprising 18 boreholes and around 50 trial pits, revealed a mixed upper layer of grey/brown glacial till overlying stiff Dublin black boulder clay at a depth varying between 3.1 and 4.3m below the ground level.

Grading tests on the DBC at the site gave a fines (silt/clay) content in the range 23-43% and both the deposits plotted in the CL region of Casagrandes classification Chart (see Figure A.27 of Appendix A). It is reported that, under inspection by electron microscope, the fines in the DBC were comprised of finely ground quartz and not clay minerals (Armishaw 1987) and thus it was not clear whether the till would exhibit drained or

undrained behaviour in the short term. There were no piezometers installed on the piles with which to assess the behaviour of the soil in which the piles were installed.

Significant problems were reported during pile installation, in that, some of the piles had suffered deterioration in set on re-driving and a substantial increase in penetration was needed to achieve the required set a second time.

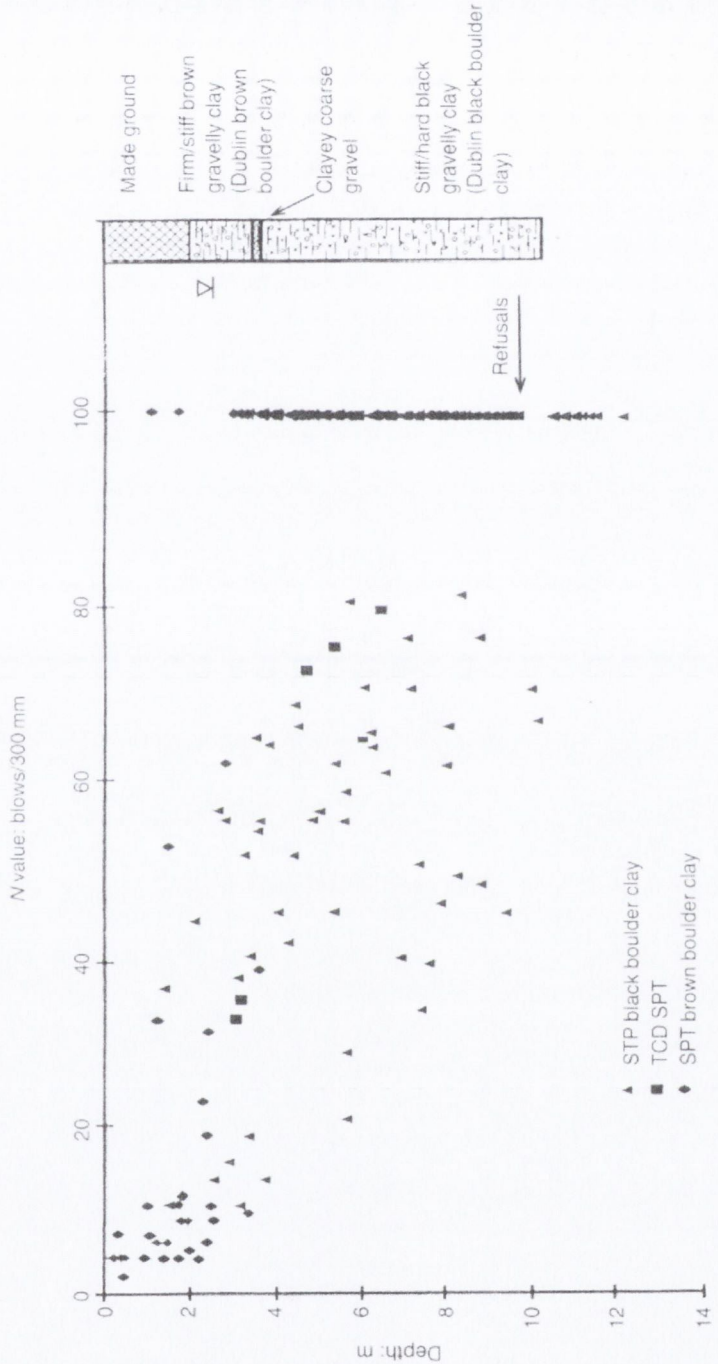


Figure 2.9 – Ground conditions and N_{SPT} profile at Croke Park test site (Farrell et al. 1998)

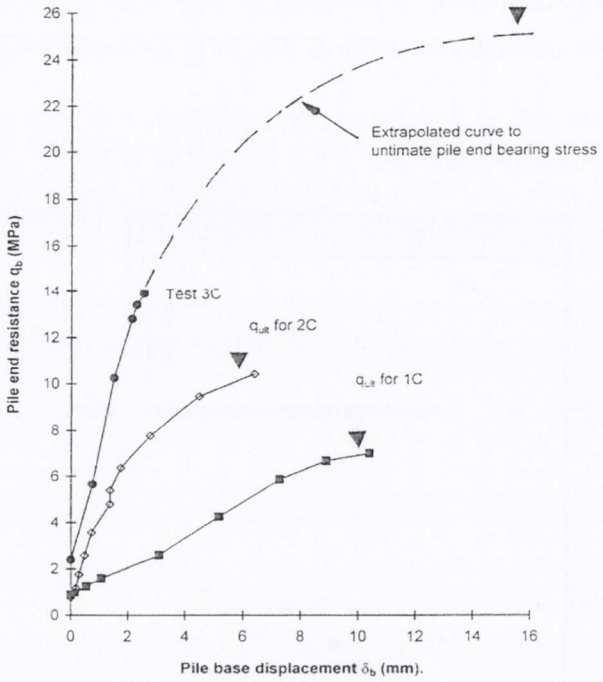


Figure 2.10 – Development of base resistance with base deflection (Farrell et al. 1998)

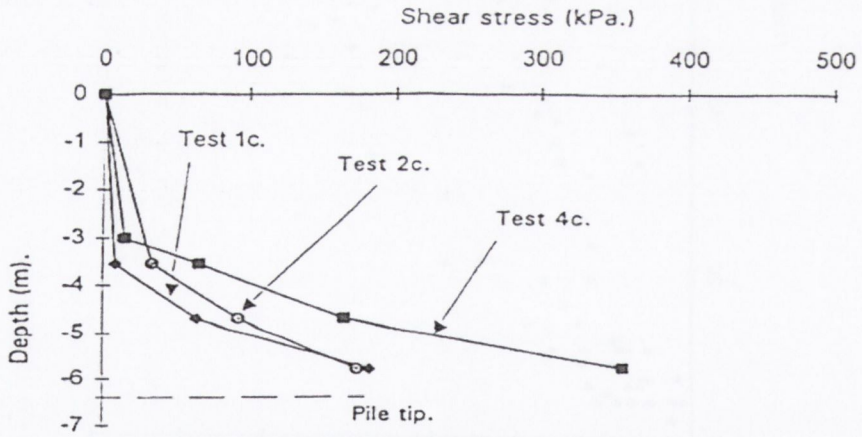


Figure 2.11 – Shaft resistance profile at maximum load at the four load cycles (Farrell et al. 1998)

Armishaw (1987), concluded that the reasons, though unclear, are considered to be due to relaxation of the soil in the highly stressed regions along the shaft and beneath the toe, induced during installation. Armishaw pointed out, that, although small pore pressure changes were likely to have developed on pile driving, this would only account for slight deterioration of set and that it was more likely that creep occurred due to crushing of particles in the highly stressed zones adjacent to the piles, causing the deterioration in set.

Gavin and O'Kelly (2007) installed 4 No. instrumented stainless-steel, tubular, closed-ended piles, 73mm in diameter, in heavily over-consolidated, glacially derived, very dense fine sand in Blessington, about 25km southwest of Dublin. The focus of the study was to investigate the mechanism of friction fatigue in displacement piles by subjecting the same size piles, in similar ground, to various load cycles during installation and then load testing these statically and cyclically.

The piles were instrumented, each with pore pressure transducers and earth pressure cells, placed at three levels within 1.7m of the pile toe. It was found that the effective stress mechanism controlling shaft friction depended on the in situ state of the sand, characterised here using CPT results.

It was concluded that the shaft resistance for the monotonically installed or *jacked-in-place* piles (installed at a constant rate), was initially substantially greater than that for the cyclic installation which involved installation by driving using hammer blows to the pile head, however, a very small amount of load cycles negated any improvement. Very high shaft resistance was developed close to the pile toe and reduced with distance from the pile toe (Gavin 2010). The base resistance was reported to be unaffected by the installation method.

2.3.3 CFA Piles

This section presents the results of static load tests on CFA piles installed in DBC. The piles were instrumented to enable separate estimation of the shaft and base resistance development with pile deflection.

Farrell and Lawler (2008) presented the results of six CFA piles installed in DBC on the site of Saint James Hospital (SJH) in Dublin. These were statically load tested in compression and two of these were instrumented with strain gauges, each at seven levels,

to estimate the distribution of load from the pile to the soil. The two instrumented piles, Pile 450 and Pile 600, were 450 and 600mm in diameter, 12.3 and 11m in length and were loaded to 3.15MN and 4.50MN respectively.

Ground conditions at the SJH site, shown in Figure 2.12, comprised about 2–3m of made ground/silty clay over a lodgement till, overlying limestone bedrock at about 15m below ground level. The water table (observed in standpipes) was about 2–3m below ground level. The lodgement till comprised an upper 2m weathered zone of firm/stiff brown sandy gravelly clay over very stiff/hard black sandy gravelly clay. These layers are locally referred to as Dublin brown boulder clay and Dublin black boulder clay respectively.

Estimates of the undrained shear strength, s_u of these layers are also shown in Figure 2.12 and these were calculated based on SPT's carried out at the site (by multiplication of N_{SPT} by 6). The calculated values of s_u were mostly in the range 200-500kPa indicating values of N_{SPT} in the range 30-80 between depths of 2 and 10m below ground level, these values are similar to those recorded at the Croke Park site described previously in Figure 2.9.

The interpreted force-depth profiles for the instrumented tests are shown in Figure 2.13. Using these, the average shaft resistance developed for Pile 450 and Pile 600 (at the maximum applied load) was estimated (by Farrell and Lawler) as 230 and 270kPa respectively. Collins and Mitchell (1990) reported comparable values of q_s calculated from static load test results on bored piles also installed in glacial till in Dublin, in the range 130 - 540kPa, with an average value of 250kPa for the 10 piles tested.

The q_s values calculated here correspond to an estimate of the mobilised α in the range 0.65 – 0.75, much greater than that suggested in Figure 2.7 for this glacial till with a high value of s_u – assumed equal to 360kPa (Farrell and Lawler 2008). The development of α is plotted against pile head deflection for the two instrumented piles in Figure 2.14.

It is apparent from Figure 2.13 that the majority of the pile capacity in the case of both piles was derived from shaft resistance with little base bearing resistance being mobilised at the applied head loads. The development of end bearing resistance for Pile 600 is shown in Figure 2.15 and this interpretation includes the region of the pile below the lowermost ring of strain gauges, which was located 0.4m above the pile toe in the case of Pile 600. Indeed, the reason for not including the same interpretation for Pile 450 was that the lowermost ring of gauges was too far from the pile toe - 1.35m above it.

It was concluded, that, when using an undrained bearing capacity analysis (Equation 2.12), the interpreted value of N_c for this pile in the DBC was 7. This is slightly less than the value of 9, suggested by Skempton (1951) and substantially less than that of 55 which was the case for the driven pile in Croke Park discussed in Section 2.3.2.

It is, however, acknowledged by Farrell and Lawler, that there may be significant uncertainty associated with this value, as the value of $s_{u;b}$ for use with Equation 2.12, was estimated using recorded N_{SPT} at the test site and also the pile was not loaded to failure.

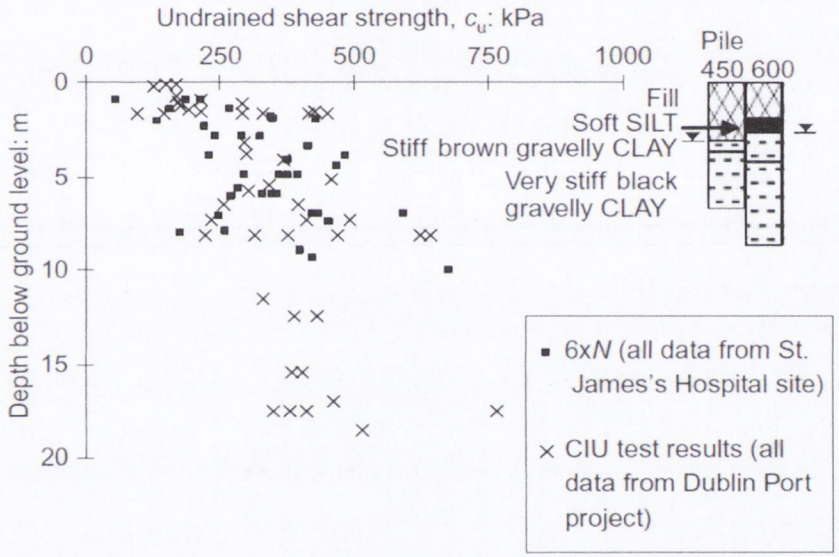


Figure 2.12 – Calculated s_u at SJH site (Farrell and Lawler 2008)

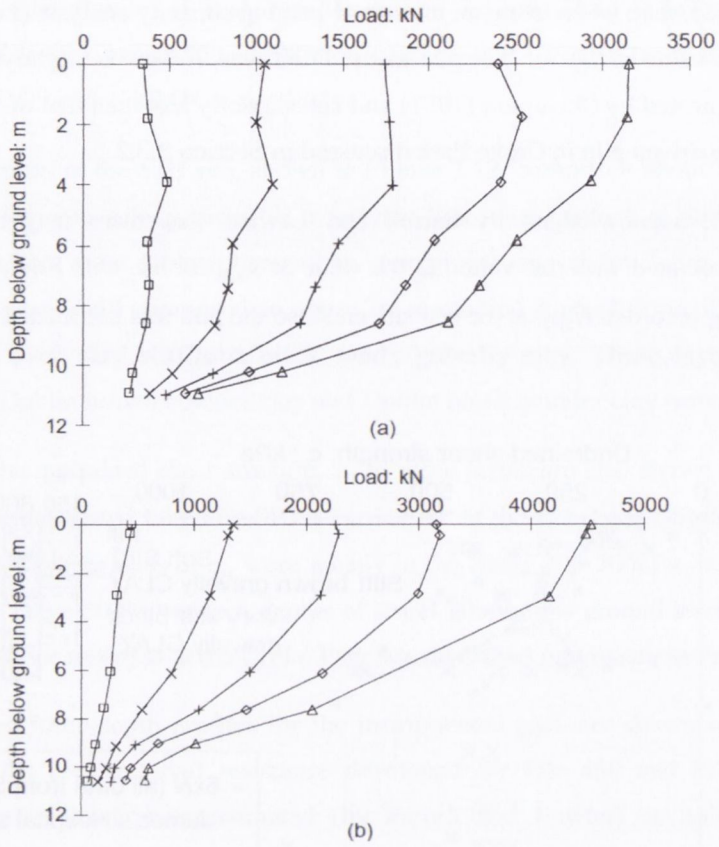


Figure 2.13 – Interpreted force-depth profile (a) Pile 450 (b) Pile 600 (Farrell and Lawler 2008)

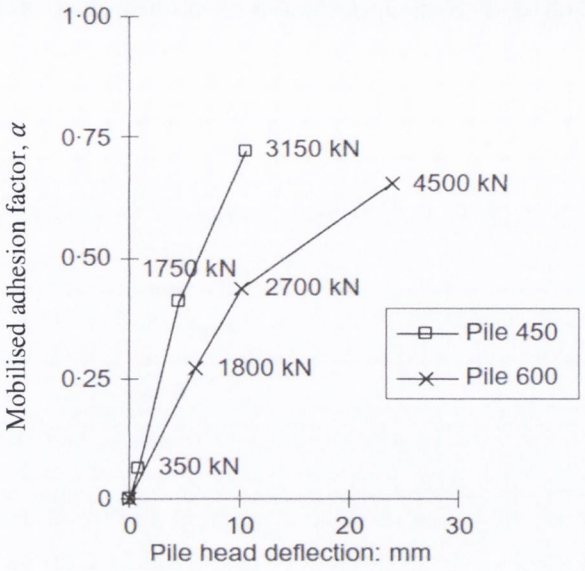


Figure 2.14 – Mobilised adhesion factor, α vs. pile head deflection (interpreted from strain gauges in test pile) (Farrell and Lawler 2008)

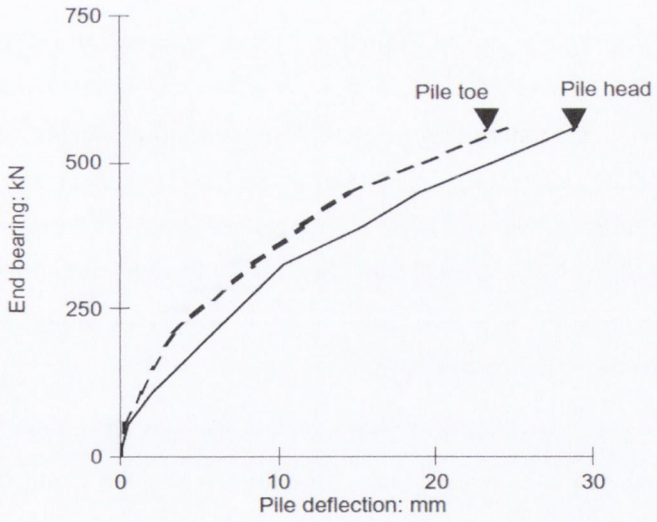


Figure 2.15 – Pile 600: end bearing load against pile head/pile toe deflection (Farrell and Lawler 2008)

As mentioned previously, proof tests on identical (same size) piles, of diameter 450 and 600 and length 12.3 and 11.0m respectively were also carried out at the same site after the

instrumented tests. The load-deflection response at the pile head, shown in Figure 2.18, was seen to be significantly different for the instrumented tests than for the proof tests. The instrumented piles were loaded 3-5 days after installation whereas the proof piles were loaded within the period 22-28 days subsequent to installation.

Despite recognising that the concrete stiffness would be reduced for those piles tested early, Farrell and Lawler suggest that some of the reduction in performance of those piles tested earlier is due to installation effects. Possible excess pore water pressures developed during installation of the piles would dissipate with time after installation and could lead to increased performance.

Gavin (2008) presented the results of static load tests carried out on three instrumented CFA piles installed on a site in Ballsbridge, about 2 km South of Dublin City Centre. The piles, TP1 TP2 and TP3, were 762 mm in diameter and of length 12, 13.8 and 11m respectively. Piles TP1 and TP2 were loaded in compression to a maximum of 3750kN (2.5 times the design load). TP3 was the only one to encounter rock and was toed in fractured limestone by 1.35m and this pile was loaded in tension to 3000kN. The interpreted force-depth profiles for the three piles are shown in Figure 2.19.

Ground conditions at the site shown in Figure 2.16, comprised 2-4m of fill material, over 2-4m of alluvial gravels over Dublin boulder clay which was typically encountered at 6m below ground level. The boulder clay layer consisted of approximately 1m brown boulder clay over the black boulder clay. A V-shaped ancient river channel was identified at the site which had become infilled with DBC (as shown in Figure 2.16) thus, in some areas the depth to rock was estimated as greater than 20m. SPT's carried out at the site yielded N_{SPT} values in the range 40-80 in the DBC, again similar to those reported on other sites such as Croke Park and SJH described previously.

Similar to those results recorded by Farrell and Lawler at SJH, the majority of the pile capacity is derived from shaft resistance, with little resistance being mobilised in end bearing. The shaft resistance was observed to increase with pile head deflection with values in the range 150 – 300kPa interpreted for the Dublin boulder clay, while 850kPa was developed in the highly fractured limestone near the toe of TP3 (see Figure 2.20).

The base resistance was interpreted for TP1 (assuming the shaft friction below the lowermost ring of strain gauges followed the same trend as that immediately above) and is estimated to rise to 1.75MPa at the maximum load application (Figure 2.20). Both the

interpreted shaft and base resistances developed appear to be increasing up to the maximum load application, suggesting the piles have extra capacity over and above that mobilised during the load tests, as was the case for the piles tested by Farrell and Lawler at SJH.

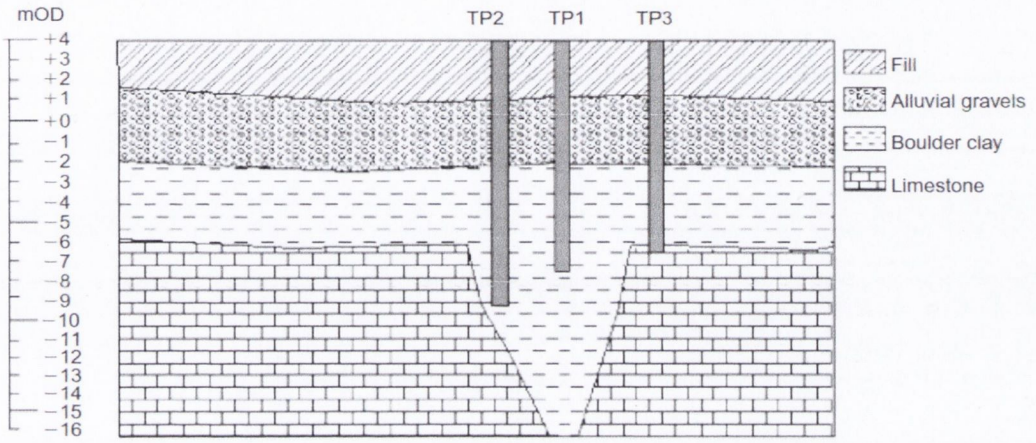


Figure 2.16 – Interpreted stratigraphy BB site (Gavin et al. 2008)

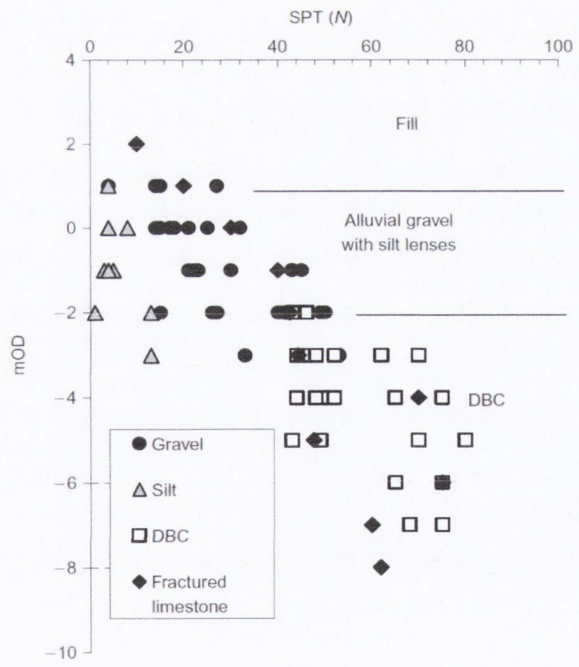


Figure 2.17 – Recorded N_{SPT} at BB site (Gavin et al. 2008)

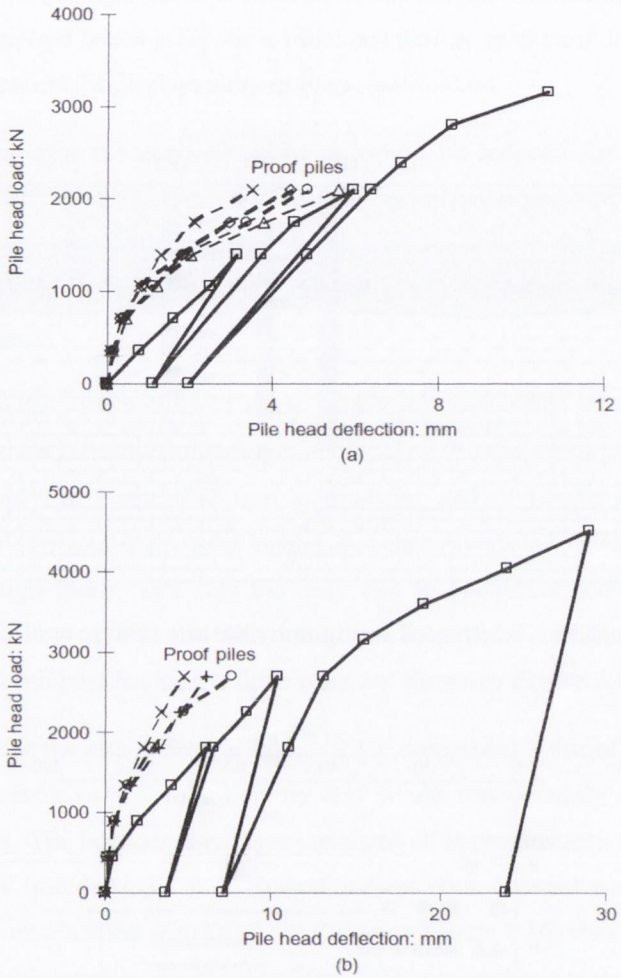


Figure 2.18 – Pile head load-deflection (a) 450mm piles (b) 600mm piles (Farrell and Lawler 2008)

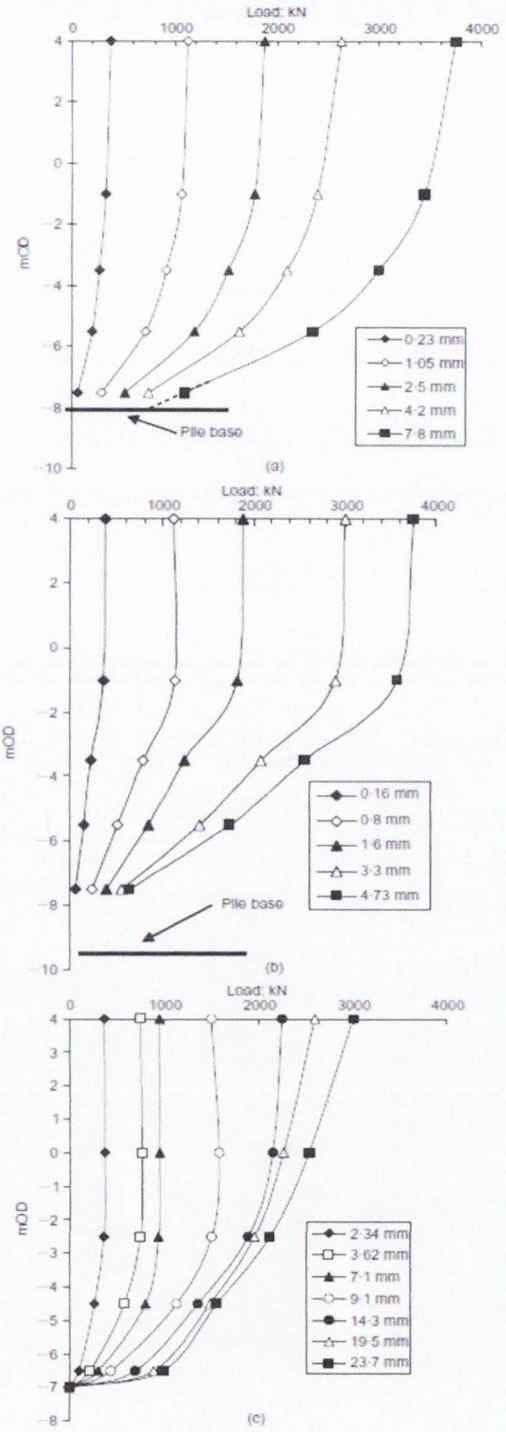


Figure 2.19 – Load-depth profile (a) TP1 (b) TP2 and (c) TP3 (Gavin et al. 2008)

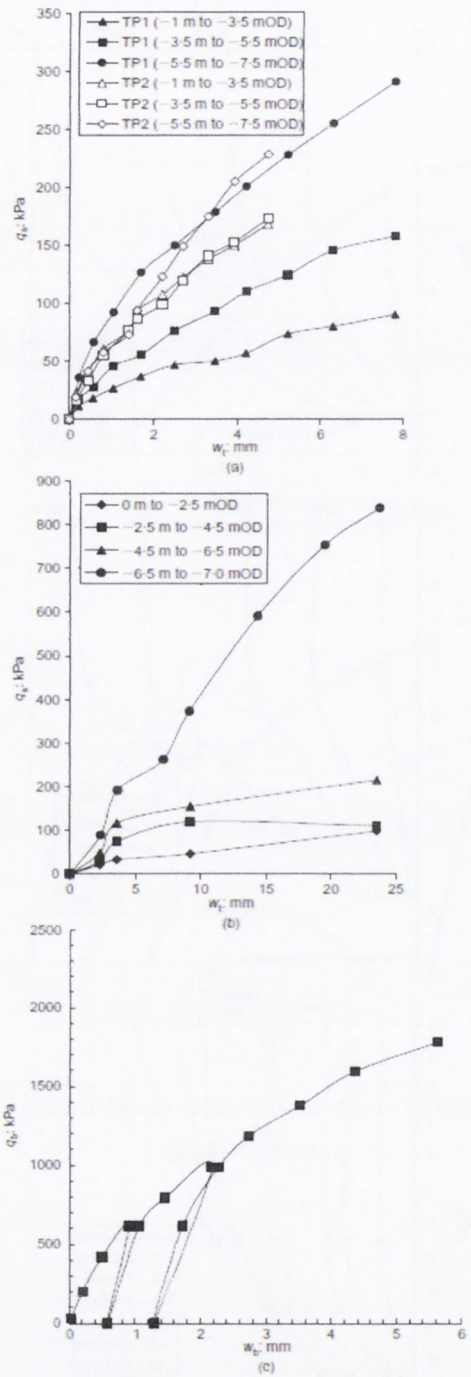


Figure 2.20 – Mobilisation of (a) shaft resistance in TP1 and TP2 (b) shaft resistance in tension test (c) base resistance in TP1 (Gavin et al. 2008)

2.3.4 Piles in Rock

Long (1999) compiled a database of 30 pile load tests carried out across Ireland, for which, there was geotechnical information which included the results of rock coring and where load tests were carried out to a particular specification. The piles involved in the study ranged in diameter from 0.17-0.8m, in length from 3.0-19m and with rock sockets between 0.2-3.3m.

The design of rock socketed piles in Ireland is generally required to limit the concrete/grout strength to 25% of its characteristic strength and to limit the deflection to 10mm under application of the SWL (Long and Collins 1999). The bearing capacity is then given by the sum of the shaft and base capacities which are calculated as in Equation 2.20 or Equation 2.21 and Equation 2.22 respectively.

$$R_s = q_s A_s \qquad 2.20$$

$$R_s = \alpha_{rock} \beta_{rock} q_u \qquad 2.21$$

$$R_b = q_b A_b \qquad 2.22$$

where q_s is the stress on the shaft having typical design values of 500-750kPa (Long and Collins 1999), α_{rock} is an adhesion factor related to the unconfined compressive strength of the rock (q_u), β_{rock} is a factor allowing for rock fracture spacing and q_b is the average stress on the pile toe.

According to Long (1999), q_b is usually chosen between 5-20MPa in Ireland, justified from experience. The α_{rock} and β_{rock} factors are based on work by Williams and Pells (1981) on weak sandstones, mudstones and shales in Australia and Long suggests these are unrepresentative of the strong limestone and granite characteristic of Ireland.

Long compared α_{rock} values calculated for the pile tests in Irish rocks with those of Kulhawy and Phoon (1993) shown in Figure 2.21 and has shown these are not applicable to Irish rock. It is suggested by Long, that this may be due to the generally higher strength of the rock found in Ireland. Long (1998) concludes that rock quality is what governs the development of shaft resistance of rock socketed piles here and parameters suggestive of rock quality, such as rock quality designation (RQD) and the fracture spacing index (FSI) are better indicators of q_s than q_u. Relationships between α_{rock} and RQD and FSI are

shown in Figure 2.22 and Figure 2.23 respectively and both indicate that the more fractured the rock the higher the available shaft resistance.

Long suggests the values of q_s shown in Table 2.5 for use with Equation 2.20, established on the results of the analysis of the piles in the database. Values of q_b are also suggested within the range 7.5-20MPa in limestone, with as high as 50MPa suggested for Irish granites, in particular those of Galway.

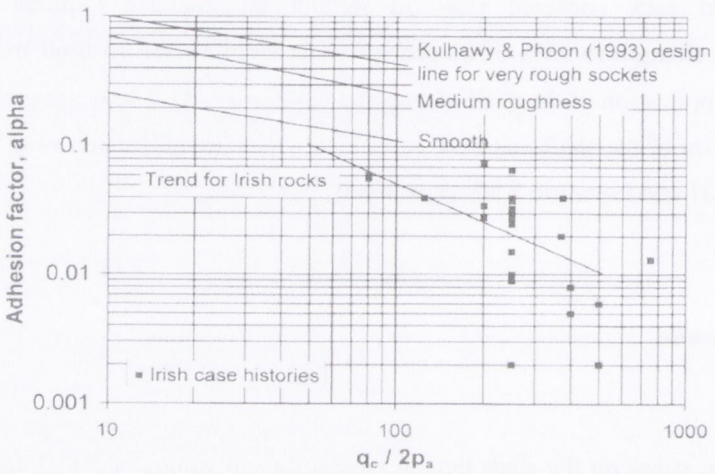


Figure 2.21 - α_{rock} values of Kulhawy and Phoon (1993) compared with trend for Irish rocks, (Long and Collins 1999)

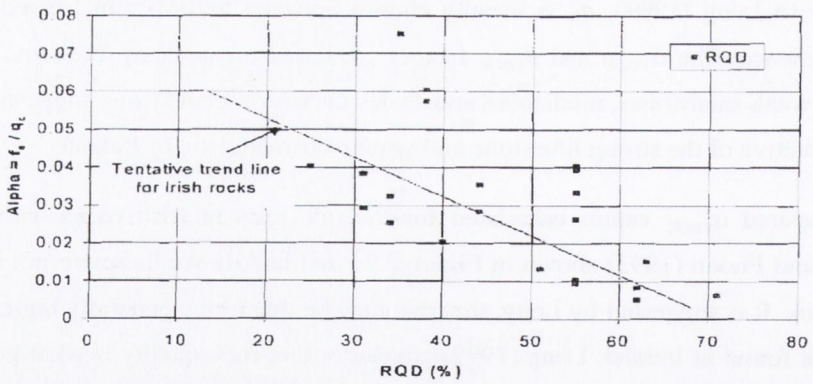


Figure 2.22 - α_{rock} against RQD, (Long and Collins 1998)

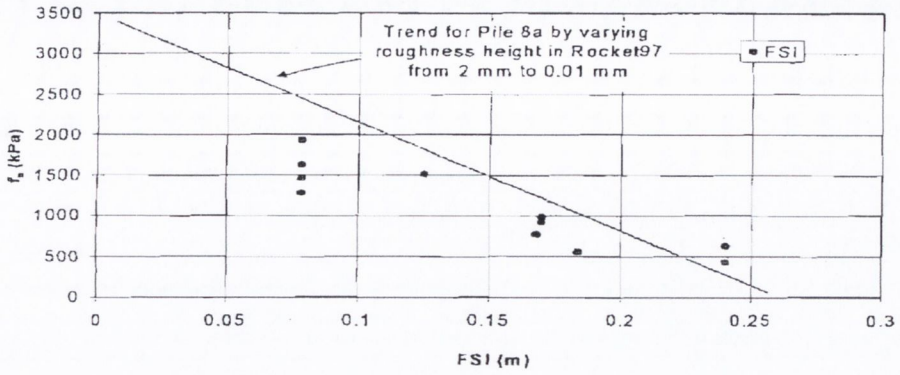


Figure 2.23 - α_{rock} against FSI, (Long and Collins 1998)

Location / rock type	TCR / RQD (%)	f_s (kN/m^2)
Dublin limestone	≥ 80 / ≥ 30	1,500 - 2,000
Limerick limestone	As above	1,200
South Dublin granite	As above	1,500
Galway granite	As above	3,000

Table 2.5 – Suggested q_s for design, (Long and Collins 1999)

2.4 Estimating pile capacity from static load tests

Static load tests on piles are generally carried out to achieve a maximum test load, which, is applied incrementally over two or three load cycles while the deflection at the pile head is measured. Frequently, small deflections are measured, and as pile failure is often defined as a limiting deflection, at both ultimate and serviceability limit states, pile failure is generally not reached during the course of a static load test, thus, the ultimate capacity of the pile remains unknown.

As a result, various methods of estimation of the ultimate compressive resistance of a pile, from the limited load-deflection data observed during a pile load test, have been developed and these methods are reviewed in this section.

2.4.1 Definition of Failure

The various definition of pile failure, that have been proposed, can be separated into those that refer to the rate of deflection, those that refer to a fixed deflection and those that define R_c in terms of a deflection that is related to pile dimension.

Where piles are not tested to failure, the available load-deflection data is often used to estimate R_c or to predict the deflection that would occur at a particular load in excess of the test load. Several mathematical and graphical techniques exist for application to load-deflection data in an attempt to identify the load at failure; these are discussed.

2.4.2 Extrapolation to R_c

Hansen (1963) suggested that the pile capacity, denoted $R_{c;BH}$ be taken as the load resulting in a deflection at the pile head equal to four times that obtained for 80% of that load (Hansen 1963) or the load resulting in a deflection at the pile head equal to two times that obtained for 90% of that load. The basic assumption of the method is that failure occurs when 'plunging' of the pile takes place and the method outlines the criteria for plunging. This value may be identified directly on inspection of a load-deflection curve but may be calculated more accurately as follows.

1) Plot the square root of each deflection divided by its corresponding load value against the deflection itself.
2) Use Equation 2.23 to compute $R_{c;BH}$ (the corresponding deflection δ_{BH} may be calculated using Equation 2.24).

$$R_{c;BH} = \frac{1}{2\sqrt{mc}} \qquad 2.23$$

$$\delta_{BH} = \frac{c}{m} \qquad 2.24$$

where m and c are the slope and y axis intercept of the plot of the square root of each deflection divided by its corresponding load value against the deflection, (over the portion of the graph for which this is a relatively constant value).

An idealised load-deflection curve may be computed on the basis of this relationship by substituting values of the deflection at the pile head, δ into Equation 2.25.

$$Q = R = \frac{\delta}{m\delta + c} \qquad 2.25$$

It is then required to confirm that the point $0.8R_{c;BH}/0.25\delta_{BH}$ or the point $0.9R_{c;BH}/0.5\delta_{BH}$ does indeed lie on or near to the measured load-deflection curve.

A limitation of this method is that, if mc is negative, then the solution is a (non-sensical) imaginary root. Abdelrahman et al (2003), in their analysis of a database of 64 CFA piles statically load tested across Eqypt, could only apply the method successfully to the load-deflection data for little over half the piles tested (55%).

Chin (1970) suggested a method of extrapolation of limited load-deflection data based on the assumption that the load and deflection data follow a hyperbolic relationship; in this case, the estimated failure load is approached asymptotically. The goodness-of-fit of the hyperbola determined may be assessed by means of a plot of each deflection divided by its corresponding load against the deflection, which should form a straight line for which the regression coefficients may be calculated and the inverse gradient m of this line provides an estimate of the ultimate resistance of the pile denoted $R_{c;chin;ult}$ as shown in Equation 2.26. Similar to the Brinch-Hansen method, a smoothed load-deflection curve may also be approximated using Equation 2.25.

$$R_{c;chin;ult} = \frac{1}{m} \qquad 2.26$$

Using Chin, the higher the test load, the higher the estimation of the ultimate load, and it is suggested that at pile head displacements in excess of 5% of the pile diameter, sufficient mobilisation of the base capacity has transpired so as to permit fair extrapolation of the measured load-deflection data by Chin's method (NeSmith and Siegel 2009).

Fellenius (2001) points out the advantage of observing the development of Chin's straight line plot during a load test – if there is a kink in the plot this may indicate a weakness in the pile-soil system. In agreement with NeSmith and Siegel (2009), it is also highlighted that Chin's method should not be applied too early in the test as it can take some time for the 'true' gradient of the Chin plot to materialise, (Fellenius 1980).

Borel et al. (2004) also carried out an appraisal of Chin's method using the results of 50 static load test results carried out to failure. Assessment of extrapolation of limited load-deflection data by Chin's method to a pile head deflection equal to 10% of the pile diameter was carried out. It was found, that, where the pile head deflection exceeds 3% and 5% of the pile diameter, R_c was predicted within the range 1-25% and 1-17% respectively, of the actual measured value.

The Davisson offset limit was developed considering wave equation analysis and static load testing of driven piles (Davisson 1972). It defines the ultimate resistance of the pile as the intersection of the measured load-deflection curve with an offset elastic load-deflection line for the pile if it were a free standing column (Davisson 1972; Fellenius 1980; NeSmith and Siegel 2009).

This offset is equal to 4mm plus the soil quake, which is equal to the deflection of the pile toe required to mobilise the strength of the soil below it. The soil quake may be approximated as the diameter of the pile divided by 120 (NeSmith and Siegel 2009).

It is suggested that the assumptions forming the basis of this method do not hold for bored piles, with the result that it leads to a lower estimate of R_c and, in turn, to over conservative design in the case of bored piles (NeSmith and Siegel 2009).

Decourt (1999) divides each measured load by the corresponding head deflection and plots the result against the corresponding load. Similar to Chin, the resulting data is approximated by a straight line for which the regression coefficients may be calculated (Decourt 1999). Decourt's estimate of the ultimate capacity of the pile, $R_{c;decourt;ult}$ may be calculated as the ratio of the y axis intercept and the slope of the Decourt straight line plot as in Equation 2.27.

$$R_{c;decourt;ult} = \frac{c}{m} \qquad 2.27$$

Again, an idealised load-deflection curve may be computed based on the relationship by substituting values of δ into Equation 2.28.

$$Q = R = \frac{c\delta}{1 - m\delta} \qquad 2.28$$

Van der Veen (1953) presented a method of identification of the ultimate pile capacity, denoted $R_{c;vv;ult}$, whereby a plot of $\ln(1 - Q \,/\, R_{c;vv;ult})$ against the corresponding δ was

constructed for chosen values of $R_{c;vv;ult}$. When this plot approximated a straight line, then the correct value of $R_{c;vv;ult}$ had been chosen.

2.4.3 Comparison of methods

Various Authors have assessed the methods of estimation of the ultimate capacity of a single pile by the various means described in this Section (Fellenius 1980; Fellenius 2001; Zhang and Tang 2001; Abdelrahman et al. 2003). The potential differences in the various methods of assessment of R_c for a single bored pile of diameter 0.79m and length 6.2m are illustrated by Zhang and Tang (2001) shown in Figure 2.24 and are considerable.

Zhang et al. (2005) identified various failure criteria, outlined in Table 2.6, and quantified the mean bias λ_F (calculated by Equation 2.29) and the corresponding variation in the bias COV_F, in each, with respect to the Federal Highway Administration (FHWA) criterion of a downward deflection at the pile head equal to 5% of the pile diameter.

Zhang also included a model error (that error associated with the predicted R_c by calculation) described by the bias in the model λ_M and its coefficient of variation COV_M. The two sources of bias are combined to give the values of λ_R and COV_R in Table 2.7 where $\lambda_M = 1.0$ (assuming no bias in the model) and $COV_M = 0.13$ were assumed.

$$\lambda_F = \frac{R_{c;FHWA}}{R_{c;x}} \qquad 2.29$$

where $R_{c;FHWA}$ is the value of R_c computed using the FHWA failure criterion and $R_{c;x}$ the value of R_c computed using the 'x' failure criterion, where 'x' represents the other failure criteria investigated.

Interpreted, the results showed that the Davisson criterion is most conservative, predicting a value of R_c 40% less than the FHWA criterion on average. The Florida Department of Transportation (FDOT) and the Standards Association of Australia (AS-2159) criteria were on average 16 and 11% less than the FHWA criterion and the Ministry of Construction, Beijing (JGJ 94-94) and International Society for Soil Mechanics and Foundation Engineering (ISSMFE) predicted greater values of R_c than the FHWA criterion by an average of 7 and 20% respectively.

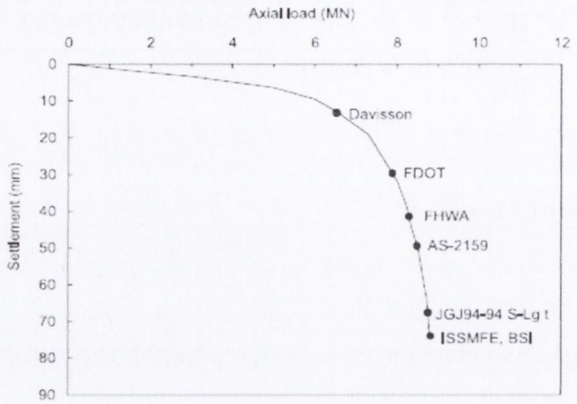


Figure 2.24 – Load-deflection curve for a bored pile with R_c estimated by various means (Zhang and Tang 2001)

Table 2.6 – Commonly used pile failure criteria (Zhang et al. 2005)

Failure criterion	Displacement at failure
AS-2159 (SAA 1995)	S = 50 mm at 1.5 times design load and 30 mm upon unloading; S = 15 mm at serviceability load and 7 mm upon unloading
Davisson's criterion (Davisson 1972)	$S = \frac{PL}{AE} + \frac{D}{120} + 4$(mm)
FDOT criterion (FDOT 1999)	$S = \frac{PL}{AE} + \frac{D}{30}$ for piles with D > 0.61 m (2 feet)
FHWA criterion (Reese and O'Neill 1988)	$S = 5\%D$
ISSMFE criterion (ISSMFE 1985) and BS 8004 criterion (BSI 1986)	$S = 10\%D$
JGJ 94-94 S-Lg t criterion (MOC 1995; Zhang et al. 2003)	The displacement at failure is determined based on characteristics of pile displacement development with time at each load increment. As shown in Fig. 1, the ultimate load (P_3) is defined as the load beyond which the displacement will not converge.

Note: S, settlement at failure; L, pile length; E, Young modulus; P, failure load; A, cross-sectional area; D, pile diameter.

Table 2.7 – Bias factors with respect to FHWA (Zhang et al. 2005)

	Davisson	FDOT	AS-2159	FHWA	JGJ 94-94	ISSMFE
Number of cases	97	98	97	98	8	97
λ_F (Failure criterion)	1.39	1.16	1.11	1.00	0.93	0.82
COV_F (Failure criterion)	0.21	0.18	0.14	0	0.11	0.14
λ_R (Combined)	1.39	1.16	1.11	1.00	0.93	0.82
COV_R (Combined)	0.29	0.27	0.24	0.13	0.23	0.24

Fellenius (1980) recommended three of the methods reviewed, namely, Davisson due to the fact that it allows pre-determination of the maximum allowable movement for a given load based on only the pile dimensions, Chin's method, due to its insensitivity to imprecise measurements and the fact that it may be used during the load test to highlight

imperfections and the Brinch-Hansen 80% criterion, as it results in an R_c value close to that subjectively viewed (by Fellenius) as the true value.

More recently, Abdelrahman et al (2003) analysed several of these methods; Davisson, Brinch-Hansen, Chin and Decourt, using a database of 64 CFA piles statically load tested across Egypt. The extrapolation methods led to nonsensical solutions when applied to the load-deflection data for some of the piles and in some cases the linear relationship on which the method of extrapolation was based was not apparent. For these reasons the methods were applicable to the load-deflection data of 6.3, 55, 100 and 100% of the piles respectively.

It was concluded that Davisson's criterion tended to be conservative and not applicable to pile load tests involving load-unload cycles. The conservatism of Davisson is consistent with the findings of NeSmith and Siegel (2009) who propose that it be modified for use with bored piles.

The Brinch-Hansen method led to a value of R_c, regarded subjectively by Fellenius, to be the true value when considering load test results. The Chin and Decourt methods are considered similar by Abdelrahman et al. to over predict the value of R_c, who suggested R_c estimated by either of these methods, be divided by a factor between 1.16 and 1.20, as is the case when estimating R_c from limited load-deflection data in the Egyptian code.

2.5 Reliability in pile design

2.5.1 Introduction

Limit state design methods are becoming increasingly popular in geotechnical engineering. The first steps toward rationalising foundation design are generally attributed to Hansen (1965) who suggested separate verification of ultimate and serviceability limit states and also that partial factors be applied to loads and to soil parameters as opposed to a 'lumped' overall factor of safety (OFS) as in classic deterministic design (Phoon 2004).

The load applied to a pile and the resistance developed due to the application of this load, both have an associated uncertainty that may be quantified, in a consistent manner, using reliability based design (RBD) methods.

Recently, load resistance factor design (LRFD), is being considered worldwide alongside existing allowable stress design (ASD) methods and RBD methods have been implemented in the United States (FHwA 2001), Canada (National Building Code of Canada NRC 1995), Australia (AS-2159 1995), Europe (CEN 2001) and in Japan (Architectural Institute of Japan, AIJ 2000), (Haldar and Babu 2008).

These RBD methods are based on the concept of achieving an acceptable level of performance in the foundation, defined using the reliability index β, which is related to the probability of failure of the foundation under load.

Well established techniques used to estimate the value of β and to estimate the probability of failure of a system involving loads and resistances already exist and these may be applied to geotechnical problems. The various reliability methods include the first-order, second-moment approach (FOSM), first and second-order reliability methods (FORM and SORM) and Monte Carlo simulation. The Reader is referred to Nadim (2007) for a detailed summary of the methods listed.

2.5.2 Target Reliability

The target reliability index β_T in RBD is an important parameter and should be selected primarily taking into account the uncertainties associated with the load and resistance, but also the level of safety required and the overall cost of the foundation. Paikowsky (2004) outlined the main methods of determination of the probability of an event occurring, which include the use of historical data and mathematical modelling stemming from probability theory.

A β_T value for piles, equal to 3.00, is recommended by Paikowsky (2004) based on a coefficient of variation in pile resistance in the range 0.3-0.4. This value of β_T is recommended for non-redundant piles, defined as where there are 4 or less piles per pile cap. In the case of redundant piles, defined as where there exist 5 or more piles per pile cap, the recommended value of β_T is reduced to 2.33.

The resistance factors put forward for use in the National Building Code of Canada to ensure the occurrence of the ULS is sufficiently unlikely for shallow and deep foundations resulted in a β value between 3.0 - 3.5 (Becker 1996). The factors were derived based on calibration using traditional ASD methods in combination with RBD methods.

Figure 2.25, from Phoon (2004) suggests that β between 2.5 and 3.0 corresponds to a probability of failure that is below average to above average.

Structural design to Eurocode suggests a value of β_T of 3.80 for the design life of a structure which takes into account the complexity of the design and the risk to property and life (CEN 2001). Three geotechnical categories are outlined in Eurocode 7 depending on the complexity of the geotechnical design and the associated ricks. Geotechnical category 2 includes structures and foundations *with no exceptional risk or difficult soil or loading conditions*. Most pile foundations would be deemed to fall under this category and thus a β_T value of 3.80 may be adopted to ensure ultimate failure is sufficiently unlikely. This is higher than the values suggested previously.

To enable calculation of β the uncertainty in the resistance and in the applied load must be quantified. It is, therefore, necessary to know or assume a value for dead and live loads depending on the loading situation. Generally the uncertainty associated with the applied load will be less than that associated with the resistances, thus β is affected more by $V(R_c)$ than $V(Q_c)$.

The value of $V(R_c)$ may be determined by calculation model using the results of ground tests on the material in which the foundation is to be installed or, perhaps better, by full-scale testing of the foundation under study installed on a site specific basis.

Foye et al. (2006) outlines a simple framework for the determination of uncertainty in the bearing capacity of footings on clay, but the basic principles may be applied to any geotechnical design scenario. The procedure is as follows:

1) Identify the limit state Equation
2) Identify the component variables
3) Identify the geotechnical test associated with each variable
4) Identify the components of uncertainty for each variable including transformations
5) Evaluate the composite uncertainties and select probability distribution functions for reliability analysis.

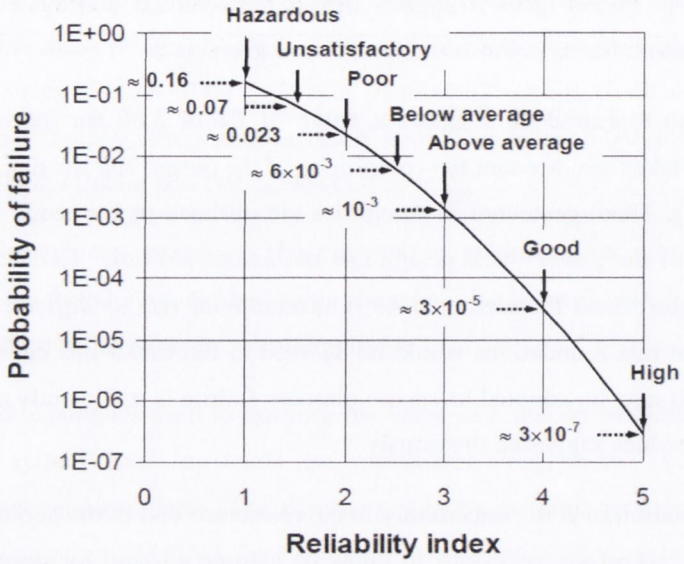


Figure 2.25 - Relationship between β and P_f (adapted from Table US Army Corps of Engineers 1997, Table B-1) (Phoon 2004)

2.6 Uncertainty in ground parameters

The uncertainty in the ultimate capacity of a single pile, R_c estimated by calculation from ground test results, depends on the level of uncertainty associated with the various parameters used to predict it. Inherent variability of the soil, that exists due to the complex processes that led to its formation and also variability due to the subsequent stress-strain cycles to which it may or may not have been subjected, are the main contributory factors.

In addition, calculation of R_c summarised in Section 2.1, generally involves many parameters, which are often empirically generated and transformed in some way for use in design. Thus, variation due to measurement, procedure, interpretation and transformation of these parameters contribute to the uncertainty in the prediction of R_c.

If these uncertainties can be correctly identified and accurately quantified then piles may be designed such that a level of safety is achieved to ensure the occurrence of under performance of the foundation is sufficiently unlikely with respect to both collapse and serviceability. This section reviews the different sources of uncertainty and the procedures used to quantify those relevant to geotechnical design with particular reference to piles.

The primary sources of geotechnical uncertainty comprise inherent soil variability, measurement errors and transformation uncertainties (Phoon and Kulhawy 2002) and these are discussed in this section.

2.6.1 Inherent variability

Inherent soil variability is due to spatial uncertainty in the soil mass, mainly due to the complex processes that led to the formation of the soil. As a result, soil properties in a mass of material can be expected to vary horizontally and vertically. This spatial variation is described by Phoon and Kulhawy (1999) using Equation 2.30.

$$\xi(z) = t(z) + w(z) \qquad 2.30$$

where $\xi(z)$ is the in-situ soil property at depth z, made up of a smoothly varying trend function, $t(z)$ and a fluctuating component equal to the inherent soil variability, $w(z)$. This concept is illustrated in Figure 2.26 where a measured parameter depth profile is shown alongside a fitted trend line. The measured data are seen to vary about the trend.

Figure 2.27 considers (artificial) measurements of a soil parameter made at the same horizon and in eleven consecutive boreholes along a line. The data have the same mean and standard deviation but the first dataset clearly displays a horizontal trend – this trend may be characterised deterministically using an equation, generally fitted by least squares regression analysis of the data. The variability about this trend is described by the residuals which usually have mean equal to zero, and some non-zero variance.

Phoon and Kulhawy (2002) summarised the results of an extensive literature review aimed at estimating inherent soil variability. The results are shown in Table 2.8 and are presented for various test types by a range of the coefficient of variation, V (COV in Table 2.8) given for each parameter. A range of mean values of each parameter is also given, within which the results are applicable.

Becker (1996) also conducted an extensive literature review, which summarised the variability of geotechnical properties and resistances, including R_c. The results are shown in Table 2.9, the variability in R_c by calculation from ground parameters, characterised by the coefficient of variation in the parameter, was found to be in the range 0.17 – 0.50 and

was slightly lower when based on pile load test results, between 0.08 and 0.30 with an average value of 0.25.

Independent assessments of the variability of the ICP method used to calculate R_c are presented in Table 2.10. The statistic used to assess the calculation method is the calculated value of the pile resistance (calculated by the ICP method) divided by that of the measured value of the pile resistance from a static load test. The coefficient of variation of this ratio was calculated in the range 0.23 – 0.34 where four different databases of pile load tests were used.

In soils, it is generally the case that the residual values off the mean trend are not probabilistically independent, but show strong correlation over some distance. This feature of inherent soil variability requires an additional parameter to represent the separation distance over which significant correlation of the measured parameter exists and may be accounted for using the scale of fluctuation, which can be quantified in both the vertical and horizontal planes. The vertical and horizontal scales of fluctuation are denoted Θ_z and Θ_h respectively. The value of Θ_z may be used to calculate a variance reduction factor, Γ^2 for application to the observed sample variance of the soil measurements, s^2 to estimate the variance of the mean value of the parameter over the failure domain. This principle is illustrated in Figure 2.28.

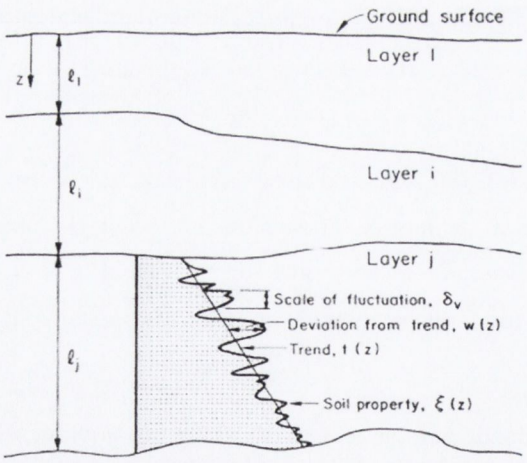


Figure 2.26 – Inherent soil variability (Phoon and Kulhawy 1999)

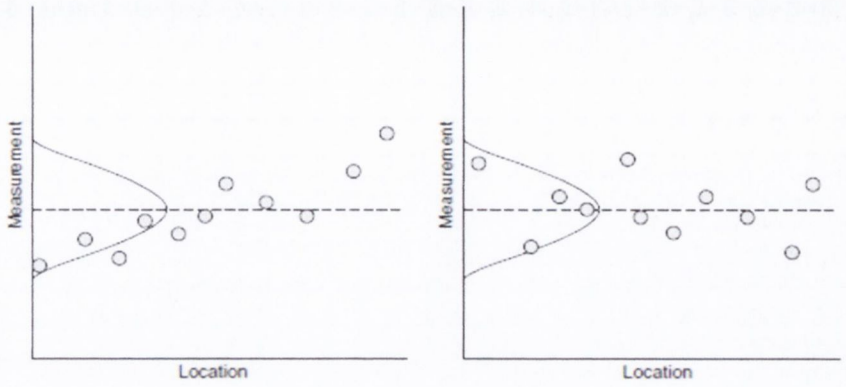


Figure 2.27 – The data in the two charts share the same mean and variance, but display different patterns of spatial variation (Baecher and Christian 2003)

Table 2.8 – Approximate guidelines for inherent soil variability (Phoon and Kulhawy 1999)

Test type	Property	Soil type	Mean	COV(%)
Lab strength	s_u(UC)	Clay	10–400 kN/m^2	20–55
	s_u(UU)	Clay	10–350 kN/m^2	10–30
	s_u(CIUC)	Clay	150–700 kN/m^2	20–40
	$\overline{\phi}$	Clay and sand	20–40°	5–15
CPT	q_T	Clay	0.5–2.5 MN/m^2	<20
	q_c	Clay	0.5–2.0 MN/m^2	20–40
	q_c	Sand	0.5–30.0 MN/m^2	20–60
VST	s_u(VST)	Clay	5–400 kN/m^2	10–40
SPT	N	Clay and sand	10–70 blows/ft	25–50
DMT	A	Clay	100–450 kN/m^2	10–35
	A	Sand	60–1300 kN/m^2	20–50
	B	Clay	500–880 kN/m^2	10–35
	B	Sand	350–2400 kN/m^2	20–50
	I_D	Sand	1–8	20–60
	K_D	Sand	2–30	20–60
	E_D	Sand	10–50 MN/m^2	15–65
PMT	p_L	Clay	400–2800 kN/m^2	10–35
	p_L	Sand	1600–3500 kN/m^2	20–50
	E_{PMT}	Sand	5–15 MN/m^2	15–65
Lab index	w_n	Clay and silt	13–100%	8–30
	w_L	Clay and silt	30–90%	6–30
	w_p	Clay and silt	15–25%	6–30
	PI	Clay and silt	10–40%	—[a]
	LI	Clay and silt	10%	—[a]
	γ, γ_d	Clay and silt	13–20 kN/m^3	<10
	D_r	Sand	30–70%	10–40; 50–70[b]

[a]COV = (3–12%)/mean.
[b]The first range of values gives the total variability for the direct method of determination, and the second range of values the total variability for the indirect determination using SPT values.

Table 2.9 – Summary of variability of geotechnical properties and resistances (Becker 1996)

Geotechnical characteristics	V_R[a]	References
Index properties		
Natural variability	0.05–0.15	Kay 1993
Natural water content	(18)	Kulhawy 1992; Phoon et al. 1993
Liquid and plastic limits	(0.11)	Kulhawy 1992; Phoon et al. 1993
Unit weight	0.04–0.16 (0.07)	Cherubini et al. 1993; Kulhawy 1992
Initial void ratio	(0.20)	Kulhawy 1992
SPT N penetration resistance	0.15–0.50	Barker et al. 1991; Meyerhof 1993, 1995
CPT qc tip resistance	0.15–0.37	Barker et al. 1991; Meyerhof 1993, 1995
Strength		
Angle of internal friction		
From laboratory tests	0.05–0.25 (0.13)	Cherubini et al. 1993; Meyerhof 1993, 1995; Kulhawy 1992; Manoliu and Marcu 1993
From CPT correlations for sand	0.15–0.25	Barker et al. 1991
Undrained shear strength	0.12–0.85 (0.34)	Meyerhof 1993, 1995; Cherubini et al. 1993; Kulhawy 1992
Deformation		
Elastic modulus	0.2–0.5	Meyerhof 1993, 1995
Modulus of deformation	0.2–0.4	Meyerhof 1993, 1995
Compression index, Cc	0.17–0.55 (0.37)	Cherubini et al. 1993; Meyerhof 1993, 1995; Kulhawy 1992
Resistance models		
Bearing capacity		
Shallow foundations		
From SPT/CPT correlations	0.5	Barker et al. 1991
From theory	0.25–0.30	Barker et al. 1991; Meyerhof 1993, 1995
Pile capacity: from theory		
α, λ method	0.17–0.41	Barker et al. 1991
β method	0.21	Barker et al. 1991
SPT correlations	0.50	Barker et al. 1991
CPT correlations	0.36	Barker et al. 1991
Drilled shafts	0.15–0.46	Barker et al. 1991
Pile load tests	0.08–0.30 (0.25)	Kay 1993; Hettler 1993; Matsumoto et al. 1993; Okahara et al. 1993
Earth pressure	0.15–0.20	Barker et al. 1991; Meyerhof 1993, 1995
K_A, K_0	0.20	Barker et al. 1991
Embankment stability	0.14–0.32	Kay 1993
Design model uncertainty	0.05–0.25	Kay 1993
Design decision uncertainty	0.15–0.45	Kay 1993
Construction variability	0.05–0.15	Kay 1993

[a]Mean value for V_R provided in parentheses when sufficient information provided by reference sources.

Table 2.10 – Independent assessments of ICP methods for total capcity: R_c/R_m ranges (Jardine et al. 2005)

Case	Number of piles in database	Mean (μ)	Standard deviation (s)	Coefficient of Variation (COV)
Clausen and Aas (2001) 'Super piles' in sand	34	0.93	0.21	0.23
CUR (2001) Open and closed-ended piles in sand All with CPT data	19	0.89	0.24	0.27
Fugro (2004) Open-ended piles in sand All with CPT data	12	0.94	0.23	0.24
Clausen and Aas (2001) 'Super piles' in clay NB Few site specific δ_r measurements	43	0.81	0.28	0.34

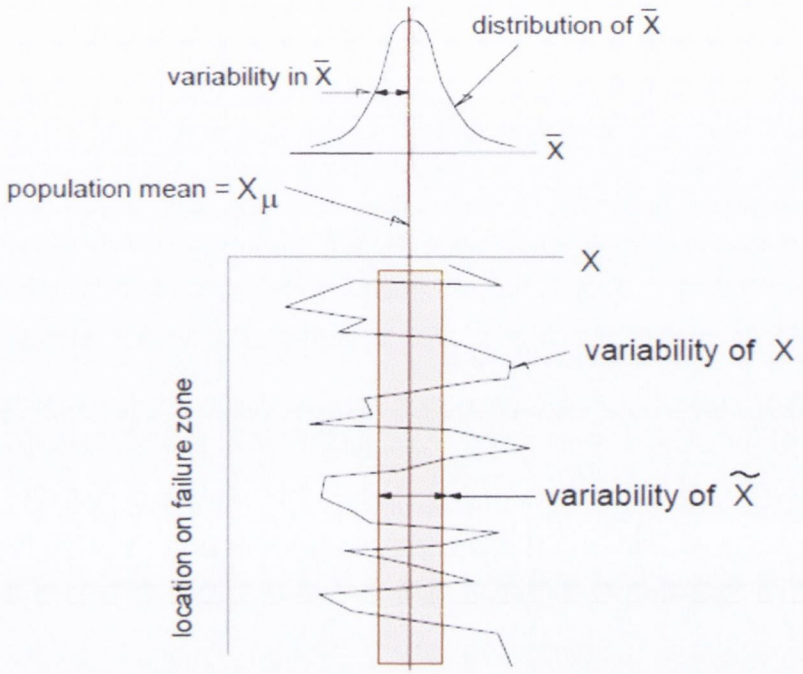


Figure 2.28 – Illustration of reduced variation in mean value over a finite failure domain given measured values of the soil parameter 'X' (Li and Lo 2006)

The value of Γ^2 may be calculated using Equation 2.31, given by Haldar and Babu (2009) and attributed to Vanmarke (1983) or by the simplified Equation 2.32 and Equation 2.33 presented by Cherubini and Vessia (2007), also attributed to Vanmarke (1983) and this value may be applied to s^2 to estimate σ^2 using Equation 2.34.

$$\Gamma^2(L_f) = 2\left(\frac{\Theta_z}{2L_f}\right)^2\left(\frac{2L_f}{\Theta_z} - 1 + e^{-2L_f/\Theta_z}\right) \quad 2.31$$

$$\Gamma^2(L_f) = 1 \qquad L_f = \Theta_z \quad 2.32$$

$$\Gamma^2(L_f) = \frac{\Theta_z}{L_f} \qquad L_f > \Theta_z \quad 2.33$$

$$\sigma^2 = \Gamma^2 s^2 \quad 2.34$$

where Θ_z is the vertical scale of fluctuation and L_f the length of the averaging interval. In the case of a pile, L_f may be approximated as equal to the length of the pile itself (Cherubini and Vessia 2007) – the length of the failure plane over which the soil property is averaged.

The effect of the choice of the value of Θ_z on the calculated reliability can be substantial, as shown by Pula (2007), who varied the value between 0.6 and 1.0 in a design example for laterally loaded rigid piles and showed that the influence of spatial averaging on the β values was high. Also, the β values were significantly increased when spatial averaging was applied, compared to the situation where no spatial averaging was applied.

A simplified method for the estimation of Θ_z was presented by Spry et al. (1988), shown in Figure 2.29. A mean trend line is fitted to the parameter measured at various locations down a borehole, then, by observation, the number of times the measured value crosses the trend line is noted. The average depth over which crossing of the trend line occurs is calculated and multiplied by 0.8 to provide an estimate of Θ_z (denoted δ_v in Figure 2.29).

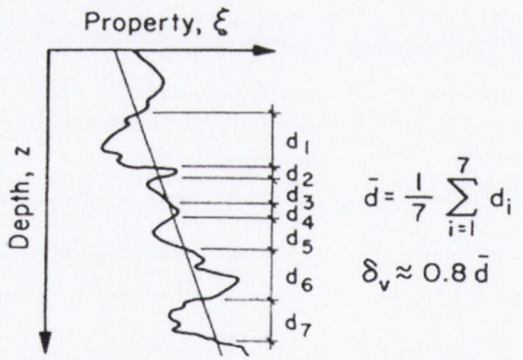


Figure 2.29 – Estimation of vertical scale of fluctuation reposted in Phoon and Kulhawy (1999)

2.6.2 Measurement error

Soil properties must be measured in some way and the measurement procedure leads to additional uncertainty in the measured parameter, arising from inaccuracies in the equipment being used. Also in soils, inaccuracies due to variations in the geometry of

measuring equipment or the type of test carried out lead to uncertainty in the measured parameter (Rahardjo 2001; Goh et al. 2005). Tests that are operator dependent, or complicated to carry out, generally increase the magnitude of the measurement error.

There will also be some random testing error, that is, any remaining variability that may not be attributed to testing method, equipment, the operator or to the inherent soil variability, (Phoon and Kulhawy 1999).

The total variability of a measured soil parameter, ξ_m may be described by Equation 2.35 (Phoon and Kulhawy 1999).

$$\xi_m(z) = \xi(z) + e(z) = t(z) + w(z) + e(z) \qquad 2.35$$

where $e(z)$ is the measurement error at depth z.

The summary of Phoon and Kulhawy (1999) of the total measurement errors associated with various soil parameters obtained from laboratory tests and from in-situ test measurements is seen in Table 2.11 and Table 2.12. It should be noted that, in the case of the field testing data, only the total variability was obtained as it was too difficult to separate the contributions from the inherent and measurement variability.

Table 2.11 – Summary of total measurement error of some laboratory tests (Phoon and Kulhawy 1999)

Property[a]	Soil type	No. of data groups	No. of tests per group		Property value		Property COV (%)	
			Range	Mean	Range	Mean	Range	Mean
s_u(TC) (kN/m^2)	Clay, silt	11	—	13	7–407	125	8–38	19
s_u(DS) (kN/m^2)	Clay, silt	2	13–17	15	108–130	119	19–20	20
s_u(LV) (kN/m^2)	Clay	15	—	—	4–123	29	5–37	13
$\bar{\phi}$ (TC) (°)	Clay, silt	4	9–13	10	2–27	19.1	7–56	24
$\bar{\phi}$ (DS) (°)	Clay, silt	5	9–13	11	24–40	33.3	3–29	13
$\bar{\phi}$ (DS) (°)	Sand	2	26	26	30–35	32.7	13–14	14
tan $\bar{\phi}$ (TC)	Sand, silt	6	—	—	—	—	2–22	8
tan $\bar{\phi}$ (DS)	Clay	2	—	—	—	—	6–22	14
w_n (%)	Fine grained	3	82–88	85	16–21	18	6–12	8
w_l (%)	Fine grained	26	41–89	64	17–113	36	3–11	7
w_p (%)	Fine grained	26	41–89	62	12–35	21	7–18	10
PI (%)	Fine grained	10	41–89	61	4–44	23	5–51	24
γ (kN/m^3)	Fine grained	3	82–88	85	16–17	17.0	1–2	1

[a]LV, laboratory vane shear test.

Table 2.12 – Summary of measurement error of in situ tests (Phoon and Kulhawy 1999)

Test	Coefficient of variation, COV (%)				
	Equipment	Procedure	Random	Total[a]	Range[b]
Standard penetration test (SPT)	5–75[c]	5–75[c]	12–15	14–100[c]	15–45
Mechanical cone penetration test (MCPT)	5	10–15[d]	10–15[d]	15–22[d]	15–25
Electric cone penetration test (ECPT)	3	5	5–10[d]	7–12[d]	5–15
Vane shear test (VST)	5	8	10	14	10–20
Dilatometer test (DMT)	5	5	8	11	5–15
Pressuremeter test, prebored (PMT)	5	12	10	16	10–20[e]
Self-boring pressuremeter test (SBPMT)	8	15	8	19	15–25[e]

[a]COV(Total) = [COV(Equipment)^2 + COV(Procedure)^2 + COV(Random)^2]$^{0.5}$.
[b]Because of limited data and judgment involved in estimating COVs, ranges represent probable magnitudes of field test measurement error.
[c]Best to worst case scenarios, respectively, for SPT.
[d]Tip and side resistances, respectively, for CPT.
[e]It is likely that results may differ for p_o, p_f, and p_L, but the data are insufficient to clarify this issue.

2.6.3 Transformation error

Transformation errors arise from the need to convert measured test results to a desired soil property – measurements from tests are often not directly applied to a design, for example, the correlation factor used to transform the result of the standard penetration test (SPT), to undrained shear strength, s_u can introduce a transformation error which may vary with different soil types. The precision of the correlation model used to transform the measured value to the desired design parameter governs the magnitude of the transformation error.

2.6.4 Soil variability from in-situ test data

The SPT is the most popular means of ground investigation by in-situ test in Ireland. The result of the SPT is characterised by the N_{SPT} – the number of blows required to move forward a cone vertically through the ground by 300mm. This is not the standard test, although it is used in Ireland because of gravels – a split-spoon sampler is used normally (Rahardjo 2001). Due to its simplicity, N_{SPT}-depth profiles are often produced and may be used directly or indirectly to estimate the resistance of a pile installed in the soil.

Phoon and Kulhawy (1999) estimated the uncertainty associated with the N_{SPT} in clay and sand (shown previously in Table 2.8). The range of variability of the N_{SPT} is seen to be very large, equivalent to a coefficient of variation in the parameter quoted as 25-50%, where the mean value ranged from 10-70 blows. Becker (1996) reported similar values of $V(N_{SPT})$ in the range 15-50%.

Oka and Tanaka (2009) characterised the variability of the results of SPT and CPT measurements taken in various sites in Japan. The slopes of the trend line resulting from

the SPT and from the CPT, carried out on the same site, were compared and demonstrated good relation. Furthermore, the variation in the residuals from the SPT and the CPT were seen to correlate well – when the variation was large for the SPT it was also large for the CPT and the Author's pointed out that this indicates that the main source of variation in the computed trend line comes from heterogeneity of the soil and not from measurement error.

Oka and Tanaka (2009) also observed, that, the statistical distribution of the residuals of both the SPT and CPT followed a normal distribution at most of the sites, with those measured at three sites that comprised granular material, following a Beta distribution.

Paikowsky (2004) recommends that within-site variability should be considered in three simple steps. Firstly, for each significant load resisting layer, assess the average parameter used for strength analysis (generally the N_{SPT} in Ireland). Secondly, compute the coefficient of variation V between the average value and that measured at each borehole in which test results were obtained and, thirdly, categorise the site variability as low, medium or high where V is less than 25%, between 25% and 40% or greater than 40% respectively.

2.6.5 Load test results

As seen previously, in Section 2.6.1 to Section 2.6.4, the quantification of uncertainty in R_c from ground test results is challenging, as it includes variation from several sources that are hard to separate. An alternative means by which to quantify the uncertainty in R_c is to take measurements of R_c through static load testing of piles installed on a site. The results of load tests provide a more realistic value of R_c as it is actually observed and the uncertainty in R_c is also reduced as the errors in load testing are much smaller than those resulting from calculation models based on ground test results (Zhang 2004).

The load test approach means that the serviceability requirements of the pile foundation may also be assessed, as deflections are measured, and this method has the added advantage that it includes uncertainty due to installation techniques, as well as encompassing the various sources of uncertainty associated with the ground, discussed earlier. Furthermore, model errors and model bias are eliminated.

Static load tests, known as proof load tests, are often carried out on piles to validate a particular pile design. In Ireland, these proof piles are generally loaded to 1.5 times the characteristic load of the pile, rather than being conducted to failure. The value of R_c of

these test piles often remains unknown (though it is known to be greater than the test load) thus leading to difficulty in the quantification of the variability of the measured value of the resistance of the pile.

Zhang (2004) developed a systematic approach to include the results of such proof load tests, not loaded to failure. In the assessment of the reliability of the pile under study, Zhang attempted to verify RBD methods using the results of proof load tests with Bayesian analysis to systematically update the design of the pile calculated using ground test results and using the site specific information gained in carrying out the load tests (Zhang 2004; Zhang 2008).

Measurements of the within-site variability of the capacity of driven piles load tested in eight different sites in southern Italy are presented in Table 2.13. The average value of $V(R_c)$ was 0.2, or 20%, and this value was adopted by Zhang for subsequent analysis of the reliability of the piles. A value of $V(R_c)$ from load test results was taken as 25% for purposes of calculation of partial factors during development of the National Building Code of Canada (Becker 1996). Baguelin (1990) in studying the influence of the number of pile load tests on safety factors used a value of $V(R_c)$ equal to 20% but suggested this may increase to 30% in exceptional circumstances.

The within-site variability computed in this way is particular to a site, given its geological characteristics, and is also particular to the method of installation and type of pile used at the site. This within-site variability cannot be reduced by spatial averaging or by increasing the number of load tests carried out.

Table 2.13 – Within-site variability of the capacity of driven piles at eight test sites (Zhang 2008)

Site	*Number of piles*	*Diameter (m)*	*Length (m)*	*Soil*	*COV*	*References*
Ashdod, Israel	12	–	–	Sand	0.22	Kay 1976
Bremerhaven, Germany	9	–	–	Sand	0.28	Kay 1976
San Francisco, USA	5	–	–	Sand and clay	0.27	Kay 1976
Southern Italy	12	0.40	8.0	Sand and gravel	0.25	Evangelista *et al.*, 1977
Southern Italy	4	0.40	12.0	Sand and gravel	0.12	Evangelista *et al.*, 1977
Southern Italy	17	0.52	18.0	Sand and gravel	0.19	Evangelista *et al.*, 1977
Southern Italy	3	0.36	7.3	Sand and gravel	0.12	Evangelista *et al.*, 1977
Southern Italy	4	0.46	7.0	Sand and gravel	0.14	Evangelista *et al.*, 1977
Southern Italy	16	0.50	15.0	Clay, sand and gravel	0.20	Evangelista *et al.*, 1977

2.6.6 Bayesian updating

In certain scenarios, such as the effects of wave motion on offshore structures or ground movements due to the occurrence of earthquakes, the uncertainty predicted by reliability analysis may be too large and is, therefore, of little use to the geotechnical engineer when making decisions with regard to design (Wu 2009). In these cases Peck's observational approach may be used to iteratively modify the design based on any new information, (Peck 1969).

In the case where this approach is adopted, an important philosophy is that of Bayesian statistics, whereby information from various sources, such as site investigation, full-scale load testing or past experience may be combined using Bayes' theorem shown in Equation 2.36.

$$P(A|B) = \frac{P(B|A)P(A)}{P(B)} \qquad 2.36$$

where $P(A)$ is the prior probability of A, $P(A|B)$ is 'the probability of A given B' and is called the posterior probability, $P(B|A)$ is the probability of B given A and $P(B)$ is probability of B.

Bayes theorem may be extended for use with continuous distributions, such as the Normal distribution, in which case, the probabilities in Equation 2.36 are replaced with probability densities. Bayesian statistical methods have been proposed in geotechnical engineering for some time, and specifically, for the combination of prior knowledge of pile capacity with the results of pile load tests, (Kay 1976; Kay 1977; Baecher and Rackwitz 1982).

A key feature of Bayesian analysis is that new information may be added sequentially as and when it becomes available. For example, the ultimate capacity of a pile may be calculated based on ground investigation at a site (yielding a prior distribution for the capacity), then a preliminary test pile may be installed and tested giving further information on the ultimate capacity of the pile under design. Bayesian analysis may be used to combine what is known from the ground tests and what was observed during the pile load test to give a posterior distribution for R_c thus combining statistically what is known.

Ching et al (2009) took a database of 57 load tests of bored piles in Taipei City and used incomplete load test results (from piles not loaded to failure) to calibrate resistance factors for the region. Bayesian analysis was used to update probability density functions using the results of static load tests on the 57 piles to make decisions about the design of the next pile in the region.

Predictions about future observations may be made from the posterior distribution. The Bayesian confidence interval (called the credible interval) actually relates to the probability that the parameter is within the interval as opposed to the Frequentist confidence interval which is defined as the interval within which the statistic will be a particular percentage of the time.

2.7 Summary

This section summarises the various research areas of interest reviewed in this Chapter. The literature review began by outlining popular pile design methods in coarse and fine grained soils and design methods for piles installed in rock. Various types of piles were considered including driven, bored and CFA piles. Total and effective stress methods used to predict pile shaft resistance and base resistance from measured or interpreted ground

parameters were reviewed and also design methods by direct correlation with in-situ ground tests such as the CPT or the SPT.

Following this, a review of the research relating to piles that has been carried out in Ireland, was presented. This included static load tests carried out on driven and CFA piles installed mostly in the Dublin area. Some of the piles that were load tested were instrumented with strain gauges at various levels to enable the separation of shaft and base resistances and also to relate the development of these resistances with pile deflection in different soils.

Methods of extrapolation of limited load-deflection data resulting from static load tests carried out on piles have long been used to predict the ultimate capacity of the pile under test and, in turn, of other similar piles installed on the same site or in similar ground conditions. These methods of extrapolation were presented and reviewed.

Many modern geotechnical design codes rely on performance or reliability based design methods to ensure a minimum level of safety against failure is achieved and these methods are based on levels of uncertainty associated with measured soil parameters or with the results of static or dynamic load tests carried out on piles. Reliability based design methods attempt to mitigate the risk associated with a geotechnical design and thus accurate quantification of the uncertainty associated with the resistance of a pile, determined by whatever means, is critical to reliability based design methods.

The main sources of uncertainty contributing to the overall uncertainty were also reviewed in this chapter and these comprise inherent variability, measurement errors and transformation errors. Inherent variability is associated with the soil, due to the complex mechanisms by which it was formed and due to its subsequent stress history. Measurement errors are associated with the testing of materials, due to variations in measuring technique, equipment and operational errors. Transformation errors, introduced in transforming measured parameters to those useful for design, can also contribute to the overall uncertainty associated with the predicted resistance of a pile and these are also noted in this section.

3 Details of Pile Test Database

3.1 Introduction

Static pile load tests are a valuable source of information and many preliminary and proof static load tests are invested in by industry. During the course of this study, as many of these relatively expensive tests carried out within Ireland as was possible were collated by the Author to form a pile test database (PTD) in a bid to critically review current practice with respect to pile design and installation in Ireland.

Various research programmes involving high quality instrumented load tests on full-scale piles or model piles have also been carried out in Ireland over the years to investigate a range of aspects of pile resistance to loading, in a variety of ground conditions and for different pile types.

This Chapter lists the main details of the piles comprising the PTD and outlines the locations of the sites in which pile tests were carried out. Details of the ground conditions at the various test sites are also summarised alongside the results of the static load tests.

3.2 Details of piles

The PTD comprises 180 pile load tests over 33 different sites on the island of Ireland. The majority of the sites, 19 in number, were located in the greater Dublin area where most of development requiring deep foundations occurs. The precise location of each of these sites is indicated on Figure 3.1. Other sites locations included Arklow, Cork, Limerick, Londonderry, Monaghan, Mullingar, Portlaoise and Waterford. The location of these test sites are indicated on Figure 3.2.

Table 3.1(a) and (b) indicate the location of the site for each of the site references mapped on Figure 3.1 and Figure 3.2. The source of the information of the pile test results is also shown in Table 3.1(a) and (b) for each site alongside the number of tests carried out on the site and also the range of pile diameter and pile length of the piles tested.

The pile load test results were gathered together from the following sources: AGL Consulting, Byrne Looby Partners, Murphy International Limited, from various technical

publications (Armishaw 1987; Farrell et al. 1998; Farrell and Lawler 2008; Gavin et al. 2008; Gavin et al. 2009) and from the Author's own tests.

Table 3.2 comprises a list of the main details relating to each of the pile load test results comprising the PTD. Each site may be identified by its unique letter and each pile by its individual pile reference number. The principal load resisting stratum has also been identified for each pile – it should be noted that where a pile is toed in rock, then the rock is taken as the principal load resisting stratum for that pile by default. Thus, two piles on the same site may have a different principal load resisting stratum depending on whether or not they penetrate the rock layer.

The pile type, bored, CFA or driven, denoted B, CFA and D respectively, is noted alongside the pile diameter and the pile length for each pile. The load test results for each pile are summarised as the maximum test load and the corresponding deflection measured for each of the piles under test. The maximum deflection δ_{max} normalised by the failure deflection, δ_f, defined as a deflection at the pile head equal to 10% of the pile diameter, is also shown in Table 3.2 expressed as a percentage.

The characteristic value of the applied load, F_k to which each pile would most likely be subjected, is included in Table 3.2. These values are equivalent to the minimum load the piles should resist under working conditions, while satisfying the serviceability and ultimate limit state requirements.

Piles that were loaded in tension are listed within Table 3.2 and may be identified by the symbol ^{T}. Piles loaded to failure, where failure is defined as loading of the pile causing a downward deflection at the pile head equal to 10% of the pile diameter (or upward for piles loaded in tension) is highlighted by the symbol ^{F}.

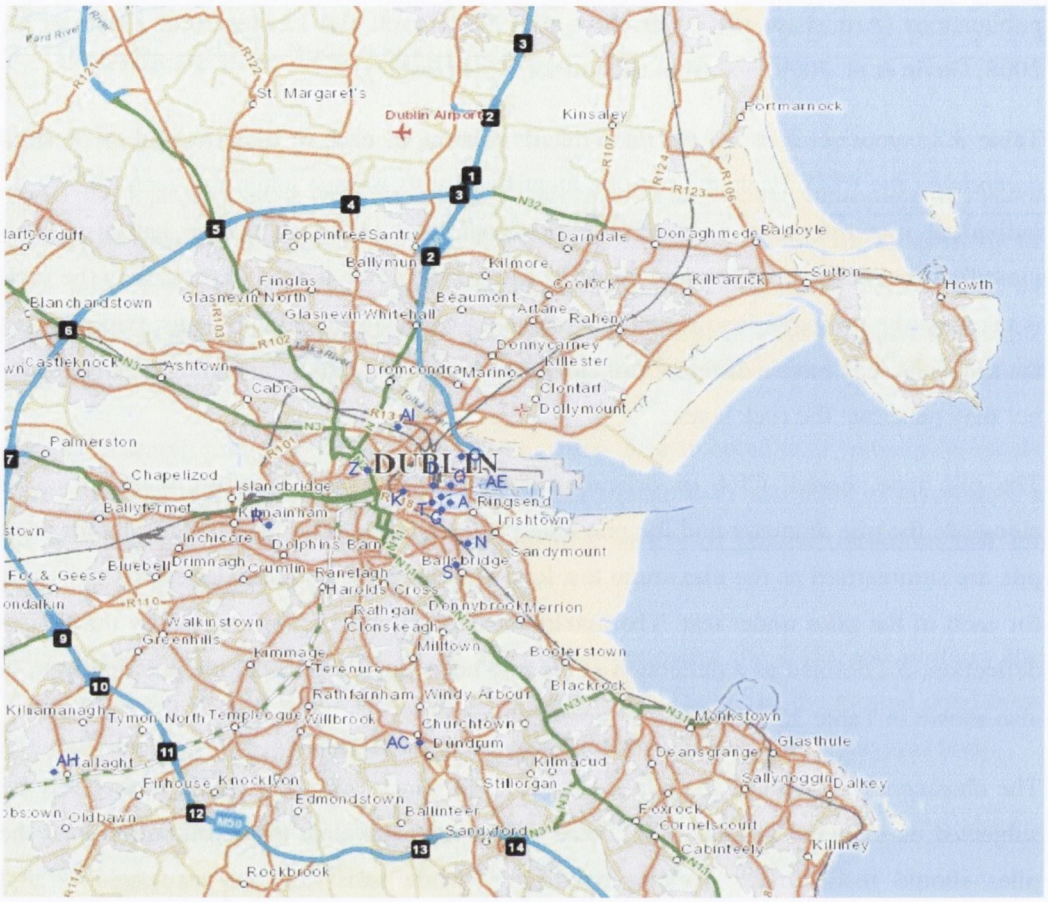


Figure 3.1 – Location of sites in Dublin in which pile load tests were carried out



Figure 3.2 – Location of sites in which pile load tests were carried out

Table 3.1(a) – Summary of site locations and pile details for sites in the PTD

Site Ref	County	Area	Source of Information	No. Piles tested	Range of Pile Diameter	Range of Pile Length
				n [_]	D [mm]	L [m]
A	Dublin	Hanover Quay	BLP100.42	6	450	6.0-10.0
B	Limerick	Bishops Quay	BLP100.65	1	600	11.5
C	Dublin	Riverside	BLP100136	3	450	11.0
D	Dublin	Spencer Dock	BLP100.140/BLP100.251	13	600-1200	9.5-13.6
E	Limerick	Two Mile Inn	BLP100.148	1	450	16.5
F	Arklow	Bridgewater	BLP100.167	4	350-900	12.0-16.0
G	Dublin	Charlotte Quay	BLP100.172	4	600	15.0
H	Kerry	Tralee	BLP100.178	1	600	3.0
I	Mayo	Corrib	BLP100.185	2	305-450	10.5-13.0
J	Limerick	Georges Quay	BLP100186	2	900	2.1-2.5
K	Dublin	City Quay	BLP100.207	1	450	10.3
L	Dublin	Transit House	BLP100.242	1	600	24.0
M	Wexford	Tesco	BLP100.246	1	600	17.0
N	Dublin	Lansdowne Road	BLP100.256	13	350-750	6.0-10.0
O	Dublin	East Road	BLP100.261	2	600	12.0-13.0
P	Monaghan	Clones Library	BLP100.267	1	450	9.2
Q	Dublin	North Wall Quay	BLP100.269	6	900	10.0-12.1
R	Dublin	Saint James Hospital	Farrell and Lawler (2008)	6	450	11-12.3
S	Dublin	Ballsbridge	Gavin, Cadogan and Twomey (2008)	2	762	12-13.8
T	Dublin	Grand Canal	BLP100.293	8	600	11.0
U	Dublin	Stockyard	BLP100.329	1	600	16.0

Table 3.1(b) – Summary of site locations and pile details for sites in the PTD

Site Ref	County	Area	Source of Information	No. Piles tested	Range of Pile Diameter	Range of Pile Length
				n [_]	D [mm]	L [m]
V	Dublin	Wyattville Junction	BLP100.1	1	600	32.0
W	Mullingar	Bennetts Mullingar	BLP100.265	6	900	10.6-18.0
X	Cork	UCC IT Building	AGL Consulting	4	880	10.0-16.1
Y	Waterford	Waterford A	AGL Consulting	19	450-600	11.5-24.5
Z	Dublin	O'Connell Street	AGL Consulting	1	1080	24.3
AA	Londonderry	Coolkeragh	AGL Consulting	11	450	8.3-12.0
AB	Meath	Duleek	Authors own	2	450-640	9.3-13.3
AC	Dublin	Dundrum	AGL Consulting	4	900	18.2-27.0
AD	Dublin	Cherrywood	BLP	1	600	8.2
AE	Dublin	St John Rodgers Quay	BLP	1	1000	13.5
AF	Portlaoise	M7/M8 Motorway	Murphy International	18	-	3.6-21.3
AG	Waterford	Waterford B	AGL Consulting	5	322	15.0-20.2
AH	Dublin	Tallaght	Armishaw (1987)	11	339*	5.9-9.6
AI	Dublin	Croke Park	AGL Consulting	11	339*	5.7-10.5

*indicates equivalent diameter in case the of square pile

BLP - Byrne Looby Partners

AGL - Advanced Geotechnics Limited

Table 3.2(a) – Summary of pile load test results

Site Ref	Principal Load Resisting Stratum	Pile Type	Pile Ref	Pile Diameter	Pile Length	Characteristic Load	Max Test Load	Max Def	
				D [mm]	L [m]	F_k [kN]	G_T [kN]	δ_{max} [mm]	δ_{max}/δ_f [%]
A	-	CFA	1	450	10.0	1000	1500	31.4	70
A	-	CFA	2	450	11.4	1000	3000	11.9	26
A	-	CFA	4	450	7.5	1000	2500	23.6	52
A	-	CFA	6	450	6.0	1000	2000	16.6	37
A	-	CFA	8	450	6.5	1000	1500	16.3	36
A	-	CFA	9	450	7.5	1000	1500	16.6	37
B	-	B	10	600	11.5	3000	7500	29.2	49
C	DBC	CFA	11	450	11.0	1000	2500	34.6	77
C	DBC	CFA	12	450	11.0	1000	2000	47.8 [F]	106
C	DBC	CFA	13	450	11.0	1000	2000	26.7	59
D	DBC	CFA	15	900	10.0	3000	7500	35.5	39
D	DBC	CFA	16	900	10.0	3000	7500	26.3	29
D	DBC	CFA	18	900	10.0	3000	4500	12.3	14
D	DBC	CFA	19	900	10.0	3000	4500	12.7	14
D	DBC	CFA	20	900	10.0	3000	4500	9.6	11
D	DBC	CFA	21	900	9.7	3000	4500	8.7	10
D	DBC	CFA	22	900	9.8	3000	4500	17.4	19
D	DBC	CFA	23	900	9.5	3000	4500	5.1	6
E	Limestone	CFA	24	450	16.5	1300	1950	29.4	65
F	Mix	CFA	25	350	12.0	600	900	48.4 [F]	138
F	Mix	CFA	26	450	15.0	1000	2500	53.2 [F]	118
F	Mix	CFA	27	600	15.0	2000	2000	42.8	71
F	Mix	CFA	28	900	16.0	3000	5250	48.4	54
G	DBC	CFA	30	600	15.0	2000	5000	25.0	42
G	DBC	CFA	31	600	15.0	2000	3000	15.2	25
G	DBC	CFA	32	600	15.0	2000	3000	12.8	21
H	-	CFA	34	600	3.0	1800	2700	59.8	100
I	Micaceous Schist	CFA	35	450	13.0	450	1350 [T]	31.1	69
I	Micaceous Schist	CFA	36	305	10.5	450	1350 [T]	19.6	64
J	Mix	CFA	37	900	2.5	2000	3000	29.0	32
J	Mix	CFA	38	900	2.1	2000	3000	62.3	69
K	Limestone	CFA	39	450	10.3	1000	1500	14.1	31
L	Mix	CFA	40	600	24.0	2200	5500	17.1	28
M	Mudstone	CFA	41	600	17.0	2000	4000	34.3	57

Table 3.2(b) – Summary of pile load test results

Site Ref	Principal Load Resisting Stratum	Pile Type	Pile Ref	Pile Diameter	Pile Length	Characteristic Load	Max Test Load	Max Def	
				D	L	F_k	G_T	δ_{max}	δ_{max}/δ_f
				[mm]	[m]	[kN]	[kN]	[mm]	[%]
D	DBC	CFA	42	1200	13.6	10500	15757	13.7	11
D	DBC	CFA	43	1050	13.5	6000	9000	4.1	4
D	DBC	CFA	44	900	15.2	3500	5250	5.6	6
D	DBC	CFA	46	600	12.0	1800	2700	8.8	15
D	DBC	CFA	47	900	12.0	3500	5250	5.0	6
N	Mix	CFA	48	750	10.0	4000	6000	16.6	22
N	Mix	CFA	49	600	6.5	2500	3750	13.2	22
N	Mix	CFA	50	750	10.0	4000	6000	22.1	29
N	Mix	CFA	52	450	10.0	1500	2250	6.2	14
N	Mix	CFA	54	600	6.0	2500	3750	12.1	20
N	Mix	CFA	55	450	CFA	1500	2250	12.2	27
N	Mix	CFA	56	600	8.9	2500	3750	5.3	9
N	Mix	CFA	57	600	6.7	2500	3750	14.5	24
N	Mix	CFA	59	350	6.6	750	1125	16.8	48
O	Sand & Gravel	CFA	61	600	13.0	1600	1600	6.6	11
O	Sand & Gravel	CFA	62	600	12.0	1600	1600	7.8	13
P	-	CFA	63	450	9.2	1000	1000	8.4	19
Q	DBC	CFA	64	900	10.0	3500	5250	10.1	11
Q	DBC	CFA	65	900	10.0	3500	5250	6.9	8
R	DBC	CFA	66	450	12.3	1400	3150	10.6	24
R	DBC	CFA	67	450	12.3	1400	2100	5.6	12
R	DBC	CFA	68	450	12.3	1400	2100	3.5	8
R	DBC	CFA	69	600	11.0	1800	4490	29.0	48
R	DBC	CFA	70	600	11.0	1800	2700	4.8	8
R	DBC	CFA	71	600	11.0	1800	2700	6.1	10
S	DBC	CFA	72	762	12.0	1400	3820	7.9	10
S	DBC	CFA	73	762	13.8	1400	3790	4.8	6
S	Limestone	CFA	74	762	11.0	1500	3000 [T]	23.7	31
Q	DBC	CFA	75	900	10.0	3500	5250	6.6	7
Q	DBC	CFA	76	900	10.0	3500	8750	9.2	10
Q	DBC	CFA	77	900	10.0	3500	5250	6.9	8
Q	Limestone	CFA	78	900	13.5	1100	1635 [T]	163.0 [F]	181
Q	Limestone	CFA	79	900	13.3	1100	1635 [T]	204.0 [F]	227
Q	Limestone	CFA	80	900	13.5	1100	1635 [T]	134.0 [F]	149

Table 3.2(c) – Summary of pile load test results

Site Ref	Principal Load Resisting Stratum	Pile Type	Pile Ref	Pile Diameter	Pile Length	Characteristic Load	Max Test Load	Max Def	
				D	L	F_k	G_T	δ_{max}	δ_{max}/δ_f
				[mm]	[m]	[kN]	[kN]	[mm]	[%]
Q	Limestone	CFA	81	900	13.3	1100	1635 [T]	121.0 [F]	134
T	Limestone	CFA	82	600	7.6	1000	2500	20.8	35
T	Limestone	CFA	83	600	7.0	1000	2500	48.9	81
T	Limestone	CFA	84	600	9.2	1000	2500	34.6	58
T	Limestone	CFA	85	600	11.0	1000	2000	47.8	80
T	Limestone	CFA	87	600	11.0	1000	2500	35.6	59
T	Limestone	CFA	88	600	11.0	1000	1500	9.3	16
T	Limestone	CFA	89	600	11.0	1000	1500	8.0	13
U	-	CFA	90	600	16.0	2000	5000	23.8	40
Q	Limestone	CFA	91	900	12.1	3500	8750	12.4	14
V	-	B	93	600	32.0	2666	3930	23.2	39
W	Gravel	CFA	94	900	10.6	3000	2942	39.3	44
W	Gravel	CFA	95	900	11.7	3000	4413	16.7	19
W	Gravel	CFA	96	900	10.8	3000	4413	68.1	76
W	Gravel	CFA	97	900	18.0	3000	3000	23.7	26
W	Gravel	CFA	98	900	18.0	3000	3000	21.8	24
W	Gravel	CFA	99	900	18.0	3000	4500	5.8	6
X	Sand & Gravel	B	100	880	12.0	3200	4807	47.7	54
X	Sand & Gravel	B	102	880	10.8	3200	4806	69.2	79
X	Sand & Gravel	B	103	880	10.0	3200	4803	27.6	31
X	Sand & Gravel	B	104	880	16.1	3200	6404	23.7	27
Y	Boulder Clay	CFA	107	600	18.0	1401	1600	84.6 [F]	141
Y	Shale	CFA	108	600	19.0	1400	1051	4.8	8
Y	Boulder Clay	CFA	109	600	18.0	1400	1236	53.5	89
Y	Boulder Clay	CFA	110	600	18.0	1400	1030	45.5	76
Y	Boulder Clay	CFA	111	450	18.0	900	1350	50.7 [F]	113
Y	Boulder Clay	CFA	112	450	18.0	900	630	11.5	26
Y	Boulder Clay	CFA	113	450	21.5	900	1350	72.8 [F]	162
Y	Shale	CFA	114	600	24.5	1400	2100	7.3	12
Y	Boulder Clay	CFA	115	600	22.9	1400	2100	53.9	90
Y	Shale	CFA	116	450	19.9	900	1350	6.5	14
Y	Shale	CFA	117	450	19.0	900	1324	8.9	20
Y	Shale	CFA	118	450	18.0	900	1324	8.3	18
Y	Boulder Clay	CFA	119	450	17.0	900	883	28.7	64
Y	Shale	CFA	120	600	14.5	900	2060	6.0	10
Y	Shale	CFA	121	600	11.5	900	2060	2.8	5
Y	Boulder Clay	CFA	122	450	18.0	900	1148	51.0 [F]	113

Table 3.2(d) – Summary of pile load test results

Site Ref	Principal Load Resisting Stratum	Pile Type	Pile Ref	Pile Diameter	Pile Length	Characteristic Load	Max Test Load	Max Def	
				D	L	F_k	G_T	δ_{max}	δ_{max}/δ_f
				[mm]	[m]	[kN]	[kN]	[mm]	[%]
Y	Boulder Clay	CFA	123	600	18.0	900	2060	47.2	79
Y	Shale	CFA	124	450	22.4	900	1324	6.8	15
Y	Boulder Clay	CFA	125	450	18.0	900	1351	68.7 F	153
Z	Limestone	B	126	1080	24.3	6000	12018	13.7	13
AA	Sandstone	CFA	129	450	11.0	1100	2728	31.5	70
AA	Sandstone	CFA	130	450	10.0	1000	1500	5.5	12
AA	Sandstone	CFA	131	450	12.0	1100	2748	11.6	26
AA	Mudstone	CFA	132	450	11.0	1000	1500	16.2	36
AA	Weathered Rock	CFA	133	450	11.0	1000	1499	5.1	11
AA	Till	CFA	134	450	8.3	1050	1575	50.0 F	111
AA	Siltstone	CFA	135	450	9.0	700	1049	34.8	77
AA	Siltstone	CFA	136	450	12.0	700	2688	30.1	67
AA	Siltstone	CFA	137	450	9.0	700	1577	18.9	42
AA	Weathered Rock	CFA	138	600	9.0	475	713 T	6.6	11
AA	Weathered Rock	CFA	139	450	8.5	270	675 T	5.9	13
AA	Weathered Rock	CFA	140	600	9.0	475	712 T	6.5	11
AA	Weathered Rock	CFA	141	450	8.0	200	300 T	2.3	5
AA	Weathered Rock	CFA	142	450	12.0	1100	2750	30.2	67
AA	Weathered Rock	CFA	143	450	11.5	1100	2698	18.2	40
AB	Limestone	CFA	145	640	9.3	2000	5000	11.0	17
AB	Limestone	CFA	147	450	13.3	1000	2500	5.2	11
AC	Granite	B	148	900	18.7	9000	15000	10.8	12
AC	Granite	B	151	900	18.2	6000	18008	94.8 F	105
AC	Granite	B	156	900	23.8	6000	18006	20.0	22
AC	Granite	B	159	900	27.0	6000	18002	17.1	19
AD	-	CFA	162	600	8.2	1600	2400	5.3	9
AE	-	CFA	163	1000	13.5	3500	8750	19.9	20
AF	Boulder Clay	D	164	394	7.1	1000	1499	6.5	16
AF	Boulder Clay	D	165	395	4.0	1100	1650	7.1	18
AF	Boulder Clay	D	166	395	10.6	1350	2024	11.3	29
AF	-	D	167	344	15.7	700	1059	2.5	7
AF	Limestone	D	168	344	10.2	700	1049	3.1	9
AF	Limestone	D	169	344	21.3	1350	2024	10.9	32
AF	-	D	171	395	10.2	1350	2024	13.6	34
AF	Boulder Clay	D	172	395	9.2	770	1153	11.3	28
AF	Boulder Clay	D	173	339	7.0	440	659	4.3	13
AF	-	D	174	344	14.5	1500	2249	9.5	27

Table 3.2(e) – Summary of pile load test results

Site Ref	Principal Load Resisting Stratum	Pile Type	Pile Ref	Pile Diameter	Pile Length	Characteristic Load	Max Test Load	Max Def	
				D	L	F_k	G_T	δ_{max}	δ_{max}/δ_f
				[mm]	[m]	[kN]	[kN]	[mm]	[%]
AF	Boulder Clay	D	175	344	9.0	1500	2252	5.7	17
AF	Boulder Clay	D	177	395	9.9	920	1379	11.3	29
AF	-	D	178	395	11.2	960	1439	6.4	16
AF	Boulder Clay	CFA	180	900	9.1	3000	4499	5.9	7
AF	-	D	181	395	3.6	1500	2249	5.6	14
AF	Mix	CFA	182	600	21.0	900	1353	3.4	6
AF	Mix	CFA	183	600	19.0	1250	1874	3.0	5
AF	Boulder Clay	CFA	184	900	11.9	1900	2851	1.5	2
AG	Boulder Clay	D	185	322	20.2	850	1700	23.4	73
AG	Boulder Clay	D	186	322	17.3	850	1060	14.3	45
AG	Boulder Clay	D	187	322	15.0	600	750	48.0 [F]	149
AG	Boulder Clay	D	188	322	15.0	440	1095	23.4	73
AG	Boulder Clay	D	189	322	15.0	440	383	15.1	47
AH	DBC	D	190	339	7.0	1000	2158	17.5	52
AH	DBC	D	191	339	5.7	1000	2354	33.3	98
AH	DBC	D	192	339	8.5	1000	2207	36.1 [F]	107
AH	DBC	D	193	282	9.4	550	1373	5.4	19
AH	DBC	D	194	282	7.0	550	1059	5.1	18
AH	DBC	D	195	339	6.0	1000	2143	9.0	26
AH	DBC	D	196	339	5.9	1000	1717	29.7	88
AH	DBC	D	197	339	5.8	1000	1962	9.4	28
AH	DBC	D	198	339	5.7	1000	1962	10.9	32
AH	DBC	D	199	339	9.6	1000	1884	11.3	33
AH	DBC	D	200	339	5.9	1000	1933	8.9	26
AI	DBC	D	201	339	6.4	800	750	2.5	7
AI	DBC	D	202	339	6.7	800	2000	11.7	35
AI	DBC	D	203	339	10.5	800	2000	5.5	16
AI	DBC	D	204	339	4.9	800	1200	5.8	17
AI	DBC	D	205	339	6.0	800	1200	4.3	13
AI	DBC	D	206	339	8.1	800	1200	4.4	13
AI	DBC	D	207	339	5.7	800	1200	4.8	14
AI	DBC	D	208	339	5.9	800	1200	4.7	14
AI	DBC	D	209	339	5.8	800	450	1.9	6
AI	DBC	D	210	339	8.0	800	1200	4.2	13
AI	DBC	D	211	273	6.4	800	1400	24.8	91

[T] indicates tension load test

[F] indicates loaded to failure

The DBC in Table 3.2 refers to the superficial deposit that underlies the majority of the greater Dublin area and is described in detail by Lehane and Simpson (2000) and more recently by Skipper et al. (2005) and by Long and Menkiti (2007) who identified four distinct formations within the deposit. The engineering characteristics of the four sub units are summarised in Table 3.3 and are seen to be similar. The values shown in brackets are the those reported by Lehane and Simpson (2000).

The four sub units are all highly overconsolidated with low plasticity indexes in the range 10-15% (Farrell and Wall 1990) and low field permeability in the range 10^{-9} to 10^{-11} m/s (Long and Menkiti 2007). The constant volume friction angle, ϕ'_{cv} was measured (in tension and in compression) as 36° with a high peak friction angle, ϕ'_p of 44° (measured under mean consolidation stresses in the range 50-150kPa) with an effective cohesion c' close to zero (Long and Menkiti 2007). Though referred to as boulder clay, the deposit contains little clay minerals and the fines (clay/silt) content is comprised of mainly rock (quartz) flour (Armishaw 1987).

Table 3.3 – Summary of material properties of DBC (Long and Menkiti 2007)

	UBrBC	UBkBC	LBrBC	LBkBC
Moisture content: %	13·1	9·7 (11±3)	11·5	11·3
Bulk density: Mg/m^3	2·228	2·337	2·283	2·284
Liquid limit: %	29·3	28·3 (25±4)	30·0	29·5
Plastic limit: %	15·9	15·1	14·9	17·8
Plasticity index: %	13·4	13·2 (11±2)	15·1	11·8
Clay content: %	11·7	14·8 (15±5)	17·8	17·5
Silt content: %	17·0	24·7	28·3	30·5
Sand content: %	25·0	24·7	25·7	34·0
Gravel content: %	46·3	35·8 (30±5)	28·0	35·5

3.3 Summary of PTD

Details of the PTD are summarised in Table 3.4. The characteristics of each pile are summarised on the basis of pile type and also on the basis of the type of ground in which the piles are installed. Of the 174 piles in the database, 134 were bored, mostly by CFA methods and these ranged from 2.1-32m in length with an average length of 12.5m and

from 305-1200mm in diameter with around 40 piles of diameter 450, 600 and 900mm each. The remaining 40 piles were driven, mainly precast concrete with a few steel H-piles and ranged in length from 3.6-21.3m with an average length of about 9m. Eleven of the piles were loaded in tension and these were all installed by boring by CFA methods and were all toed in rock.

The piles loaded in compression were loaded to deflections in the range 0.2-15% of the diameter (or equivalent diameter for non-circular piles) with an average deflection of around 4% of the diameter. The average deflection of the tension piles was greater, around 8% of the pile diameter.

The results of ground tests carried out at the sites in the PTD are given in Appendix A. Ground investigation at each of the sites generally consisted of boreholes with the results of the SPT. In addition to the SPT-depth profiles, the results of other tests for classification purposes are presented, generally in the form of plasticity charts. Appendix B presents the individual load-deflection plots for each of the pile tests in the PTD.

Of the total number of piles, 82 were installed on sites where the principal load resisting strata comprised boulder clay and 54 of these piles were installed on sites where the principal load resisting strata comprised Dublin boulder clay (DBC). Of those piles installed in the DBC, 32 were bored and 22 were driven. The other sites comprising boulder clay, of which there were three, were located in two separate developments outside of Dublin.

There were three separate sites where the soil was classified as gravel or as a combination of sand and gravel, located in Cork, Dublin and Mullingar. These sites collectively contained 12 of the pile tests loaded in compression, again each of the piles terminated in the sand/gravel layer. The piles at the Cork site were bored cast-in-situ while the rest were installed by CFA methods.

Not including the piles loaded in tension, 38 of the remaining piles were toed in rock, (only 2 of these were driven piles under the site reference AF). The rock ranged from competent limestone to weathered granite, weathered sandstone/mudstone, siltstone and shale.

Of the total number of piles, 16 were installed on sites where the ground conditions could only be described as mixed, 8 of these are located on a single site in Dublin referenced 'N'.

The ground conditions for 18 of the pile load tests in the database could not be determined to the Author's satisfaction, generally due to a lack of site investigation information, however, these load test results were retained as the load-deflection data recorded was useful in assessment of extrapolation methods for the determination of the ultimate capacity of single piles.

Table 3.4 – Summary of PTD grouped according to pile type and ground conditions

Pile Group	Ground Type	Pile Type	Number Piles	Pile Diameter		Pile Length		Max Def/ Failure Def		Max Test Load	
Pile Group	Ground Type	Pile Type	n	D [mm]		L [m]		δ_{max}/δ_f [%]		Q [kN]	
				μ	Range	μ	Range	μ	Range	μ	Range
1	DBC	CFA	32	755	450 - 1200	12	9 - 15	21	4 - 106	4752	2000 - 15757
2	DBC	Driven	22	330	273 - 339	7	5 - 11	35	6 - 107	1571	450 - 2354
3	Boulder Clay	CFA	13	577	450 - 900	17	9 - 23	86	2 - 162	1699	630 - 4499
4	Boulder Clay	Driven	12	355	322 - 395	12	4 - 20	45	13 - 149	1300	383 - 2252
5	Sand/Gravel	Bored/CFA	12	843	600 - 900	13	10 - 18	34	6 - 79	3857	1600 - 6404
6	Rock	Bored (2 Driven)	38	573	344 - 1080	14	7 - 27	34	5 - 105	4109	1049 - 18008
7	Mixed	Bored/CFA	16	625	350 - 900	10	2 - 21	43	5 - 138	3141	900 - 6000
8	Rock (Tension)	Bored/CFA	11	656	305 - 900	11	8 - 13	81	5 - 227	1331	300 - 3000
9	Unknown	Bored (4 Driven)	18	515	344 - 1000	11	3 - 32	35	7 - 100	3086	1000 - 8750
		Total Bored -	134								
		Total Driven -	40								

3.4 Discussion

A PTD has been developed by collation of the results of 174 static load tests carried out on piles installed in a variety of soils and rock in Ireland. Details including the pile dimensions, ground conditions and the load test results are listed in Table 3.2 and are described in more detail in Appendix A and in Appendix B.

Table 3.4 summarised the details of the PTD where piles were grouped together based on pile type and on ground conditions and is indicative of the wide range civil engineering projects carried out in Ireland. The pile dimensions ranged in diameter from 270 to 1200mm and in length from 3 to 32m and the extent of the range of loading was from 450-18000kN.

From Table 3.4, the average and range of the maximum pile head deflections normalised by the failure deflection, are rather low. Considering group 1 and group 2 in the DBC, δ_{max}/δ_f was equal to 21 and 35% on average where load tests are generally conducted to 1.5 or 2.5 times F_k for the pile. The actual average δ_{max} was 14 and 11mm for group 1 and group 2 respectively.

Where the ULS is defined as deflection of the pile head equal to 10% of the pile diameter, this implies that both bored and driven piles in DBC have greater capacity than that observed from the pile load tests. Considering the SLS, which is generally defined as a pile head deflection of 10mm, on average, the piles in the DBC exceeded this limit for both bored and driven piles but at loads in the range 1.5 – 3.0 times F_k, indicating the SLS is generally not reached in practice under F_k.

With the exception of group 3 and group 8, piles in the remaining groups averaged values of δ_{max}/δ_f of around 40% again indicating that the ULS is not nearly approached. The average value of δ_{max}/δ_f for group 3 was 85% where most of the piles were installed on a single site – the load tests on this site are particularly useful as the piles were loaded to δ_f in several cases. Group 8 contains the results of piles loaded in tension.

Despite the fact that the average values of δ_{max}/δ_f were low, at least one pile in each group was loaded to δ_f apart from group 5 (containing piles in sand/gravel) where the maximum value of δ_{max}/δ_f was around 80%.

4 The ultimate capacity of a single pile

Taking the total resistance of the pile as the load corresponding to a deflection at the pile head equal to 10% of the pile diameter, then only 12 No. piles of the 176 No. comprising the PTD, satisfied this criterion. It is, therefore, necessary to investigate a means by which R_c can by reliably predicted for those piles not loaded to δ_f from the limited load-deflection data recorded during a pile load test.

This section compares various methods of extrapolation of limited load-deflection data, which were reviewed in Section 2.4.2, including methods proposed by Brinch-Hansen, Chin, Davisson, Decourt and Van der Veen. The validity of each method is assessed by comparison of the predicted values of R_c to those measured using the load tests that reached δ_f, denoted $R_{c;m}$.

The load-deflection data recorded for the piles loaded to δ_f are also used to assess the uncertainty associated with application of the extrapolation methods to limited load-deflection data.

The analysis is then extended to estimate the uncertainty associated with R_c, characterised by the coefficient of variation in the parameter, $V(R_c)$ for similar piles installed within-sites of relatively uniform ground conditions. Within-site variability is also quantified on the basis of the N_{SPT} measured at each of the test sites.

4.1 Assessment of extrapolation methods

Chin's method was applied to the load-deflection data from each pile load test in a systematic way, described here, and illustrated using the load-deflection response from one of the piles – Pile 26. The results are shown for this pile as δ_f was achieved and all the methods of extrapolation of the data were applicable to the load-deflection response for this pile.

1) The raw load-deflection data were plotted (as in Figure 4.1(a) for Pile 26).
2) These raw data were reduced by removal of data from any unload cycles. Also, where there were several readings of the deflection at a particular load, the maximum one was taken in every case. For example, at load 2250kN in Figure 4.1(a) there were many readings of deflection noted for the duration of this load

application, the largest was taken for use in the reduced load-deflection data of Figure 4.1(b). This ensures that the effects of creep are taken into account in the estimation of the value of R_c – the effects of creep lead to a lower estimate of the value of R_c for a particular pile. As apparent in Figure 4.1, the effects of load-unload cycles applied to the piles does not much affect the estimation of the value of R_c as the load-deflection data on reloading tends to reach the virgin load-deflection curve and continue on further loading without any obvious change to the original load-deflection trend for the pile.

3) The reduced load-deflection data of Figure 4.1(b) was used to produce the plot of deflection divided by load against deflection (providing the basis for the Chin hyperbolic fit and is shown in Figure 4.2 for Pile 26).
4) The initial non-linear points on this plot were removed, if present, along with any obvious anomalies and a least squares regression line was fitted to the remaining data. As a measure of the 'goodness of fit' of the regression line to the actual data points, the R-squared value for the regression line was calculated in the case of each pile.

Having reduced the raw data, as described, for each of the piles to that to which Chin's method could be applied, any piles deflected downward at the pile head by an amount greater than or equal to δ_f were identified (shown in Table 4.1). A minimum limit of R-squared equal to 0.9 was required to qualify the load-deflection data for use in assessing Chin's method and all the ten piles also satisfied this requirement (shown for Pile 26 in Figure 4.2). This minimum limit ensures that only the data that are approximated well by a straight line are used; Chin's method depends on the gradient of this line and thus the resulting R_c is compromised if the line does not fit the data well. Limited portions of the reduced load-deflection data for these piles were then used to estimate $R_{c;m}$, this estimated resistance is denoted $R_{c;m;est}$. The ratio $R_{c;m;est}/R_{c;m}$ was then plotted against the corresponding deflection normalised by δ_f, the results are shown in Figure 4.3.

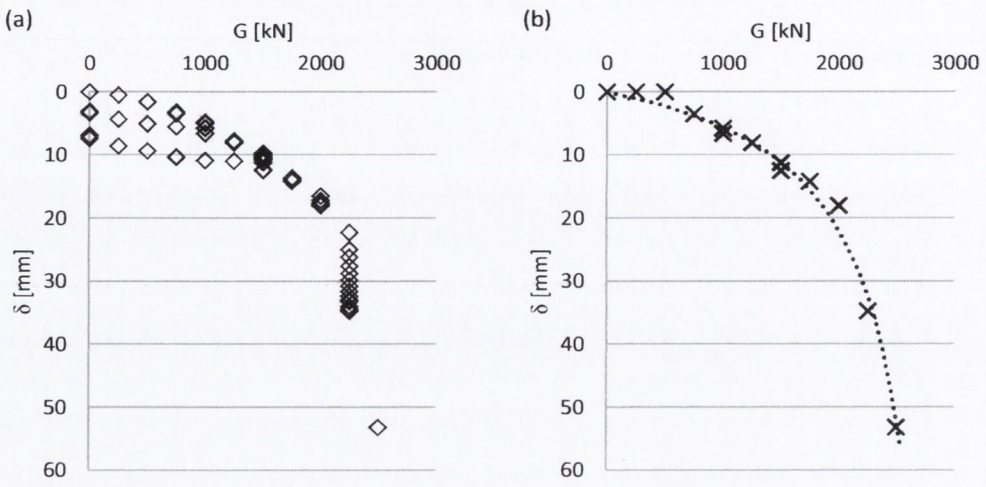


Figure 4.1 - Load-deflection data for Pile 26

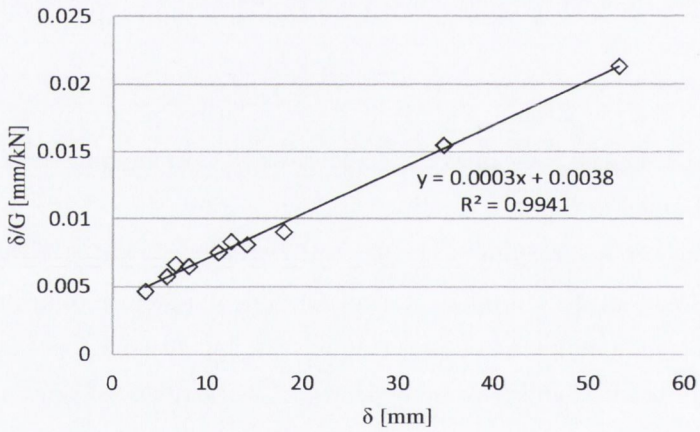


Figure 4.2 – Linear plot by Chin for Pile 26

Table 4.1 – Piles loaded to failure

Site Ref	Pile Type	Pile Ref	Pile Diameter	Pile Length	Characteristic Load	Max Test Load	Max Def			
			D	L	F_k	G_T	δ_{max}	δ_{max}/δ_f	R-sq	$R_{c;chin}$
			[mm]	[m]	[kN]	[kN]	[mm]	[%]	[_]	[kN]
C	CFA	12	450	11.0	1000	2000	47.8	106	0.95	1890
F	CFA	25	350	12.0	600	900	48.4	138	1.00	867
F	CFA	26	450	15.0	1000	2500	53.2	118	0.98	2393
Y	CFA	107	600	18.0	1401	1600	84.6	141	0.99	1488
Y	CFA	111	450	18.0	900	1350	50.7	113	0.99	1337
Y	CFA	113	450	21.5	900	1350	72.8	162	0.99	1143
Y	CFA	122	450	18.0	900	1148	51.0	113	0.99	1110
Y	CFA	125	450	18.0	900	1351	68.7	153	0.98	1253
AA	CFA	134	450	8.3	1050	1575	50.0	111	0.99	1555
AC	B	151	900	18.2	6000	18008	94.8	105	0.99	17523
AG	D	187	322	15.0	600	750	48.0	149	1.00	699
AH	D	192	339	8.5	1000	2207	36.1	107	1.00	2200

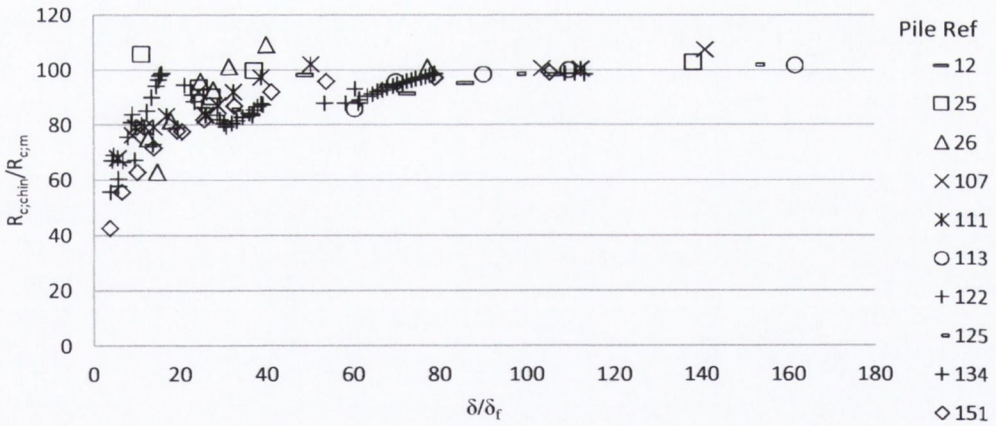


Figure 4.3 - Plot for assessment of Chin's method

Interpreted, Figure 4.3 shows that, for the ten piles considered, with load-deflection data up to a deflection greater than or equal to 50% of δ_f, $R_{c;chin}$ was within the range 85-100% of $R_{c;m}$ and for a deflection greater than or equal to 30% of δ_f, $R_{c;chin}$ was within the range 80-100% of $R_{c;m}$.

It is also noted that where load-deflection data was limited to $< 0.3\delta_f$ the value of R_c was generally under predicted. Also, where piles were deflected over and above δ_f the value of R_c was not over predicted, thus yielding confidence in the method of analysis.

This would indicate that where limited load-deflection data is available, which is often the case with pile load tests, one can have reasonable confidence in predicting R_c conservatively if the pile is deflected to around 50% of δ_f, equivalent to 5% of the pile diameter.

The results of a similar analysis carried out using Decourt's method are shown in Figure 4.4. Comparing these with Chin, in Figure 4.6, it is seen that both methods predict similar values of $R_{c;m;est}$ but Chin's method exhibits less scatter than the Decourt method.

This is also reflected in the reduced R-squared values in the Decourt plots of load divided by deflection against load, i.e. the linear trend on which the Decourt parabolic load-deflection relationship is based, does not fit the data as well as that linear trend underlying the Chin hyperbola, and therefore, results are more variable when Decourt is used.

For these reasons, and because the variability one can expect when applying Chin's method to limited load-deflection data below δ_f has been quantified, Chin's method is used where required for further analysis of load-deflection data.

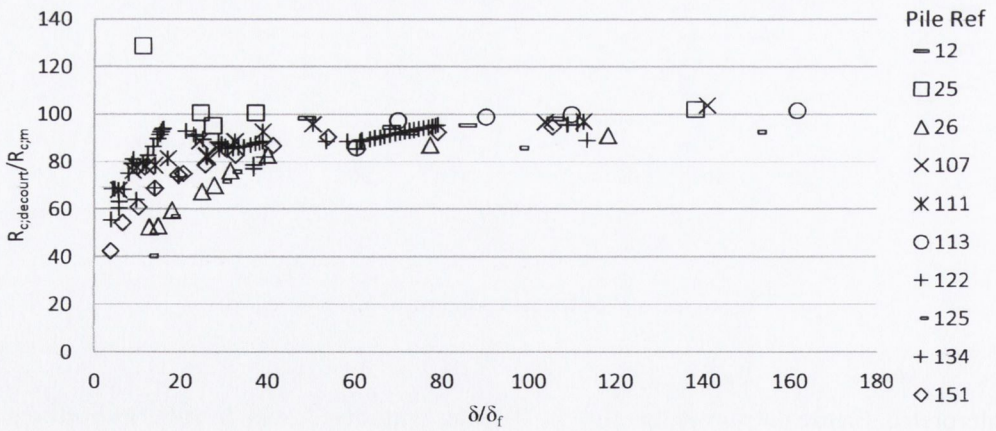


Figure 4.4 - Plot for assessment of Decourt's method

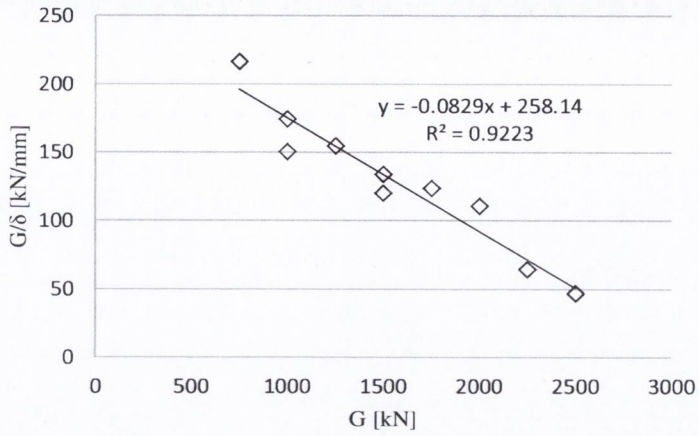


Figure 4.5 – Linear plot by Decourt for Pile 26

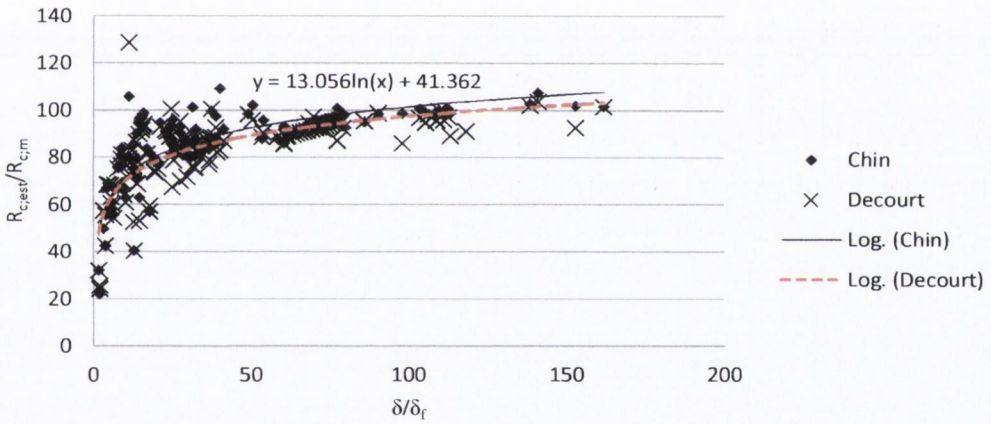


Figure 4.6 – Comparison of Chin and Decourt methods

Alternative methods, discussed in Section 2.4, were also used to estimate R_c and the Charts involved in the plots are shown for Pile 26 as an example in Figure 4.7 and Figure 4.8. Figure 4.7 shows the plot required for Van der Veen's method, in this example the points are fairly well approximated by the linear regression shown, on which, the estimate of R_c is based.

Figure 4.8 shows the plot required for Brinch-Hansen's method, there are only four points shown as this plot is generally highly non-linear at the beginning of the load test, thus, the

Brinch-Hansen estimate is usually based on the results of the load test at higher loads only, as a result it may not be possible to apply this method to piles only deflected by a small amount. This method was applicable to just 80 of the 174 static load test results in the PTD.

Figure 4.9 shows predicted value of R_c for Pile 26, as an example, computed by the various methods, plotted at a head deflection of 10% of the pile diameter (45mm). In the case of this pile, the predicted value of R_c ranged between 1800 and 2900kN. The methods are compared for all the piles in the next Section 4.2, to make a more representative comparison.

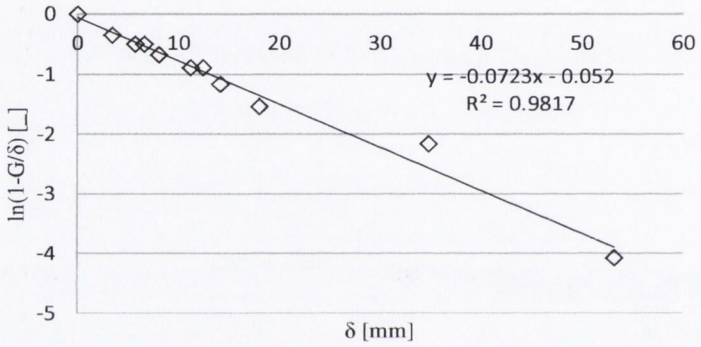


Figure 4.7 - Linear plot by Van der Veen for Pile 26

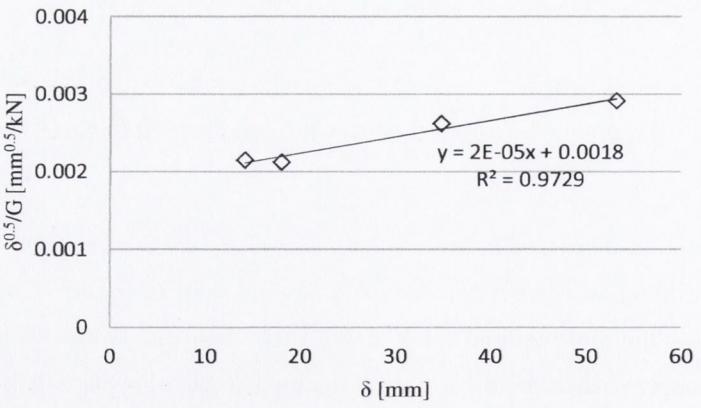


Figure 4.8 – Linear plot by Brinch-Hansen for Pile 26

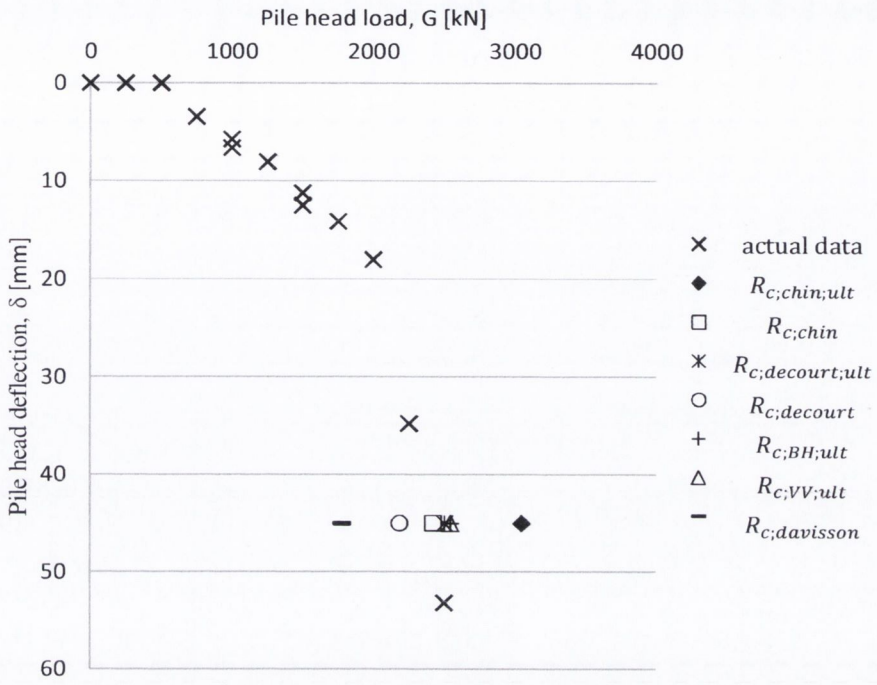


Figure 4.9 – Pile 26: Comparison of estimated R_c by various methods

4.2 Comparison of various failure criteria

The load-deflection response for each pile was used to estimate R_c by the methods described in Section 2.4.2 and implemented for Pile 26 in Section 4.1. These methods are compared in this section.

Each method of estimation of R_c was applied to those piles loaded to δ_f shown in Table 4.1 and the resulting estimates of R_c were then normalised by the measured value of R_c, $R_{c;m}$. It should be noted that all the methods were not applicable to the load-deflection data for one of these piles (as the linear relationship on which the extrapolation method was based was not apparent) and so this pile test result was not used in the assessment bringing the total number of piles with which to assess the methods to 9.

The normalised R_c values are presented in the form of histograms in Figure 4.10 which display the average normalised value and give an indication of the spread of each prediction about the measured value, $R_{c;m}$.

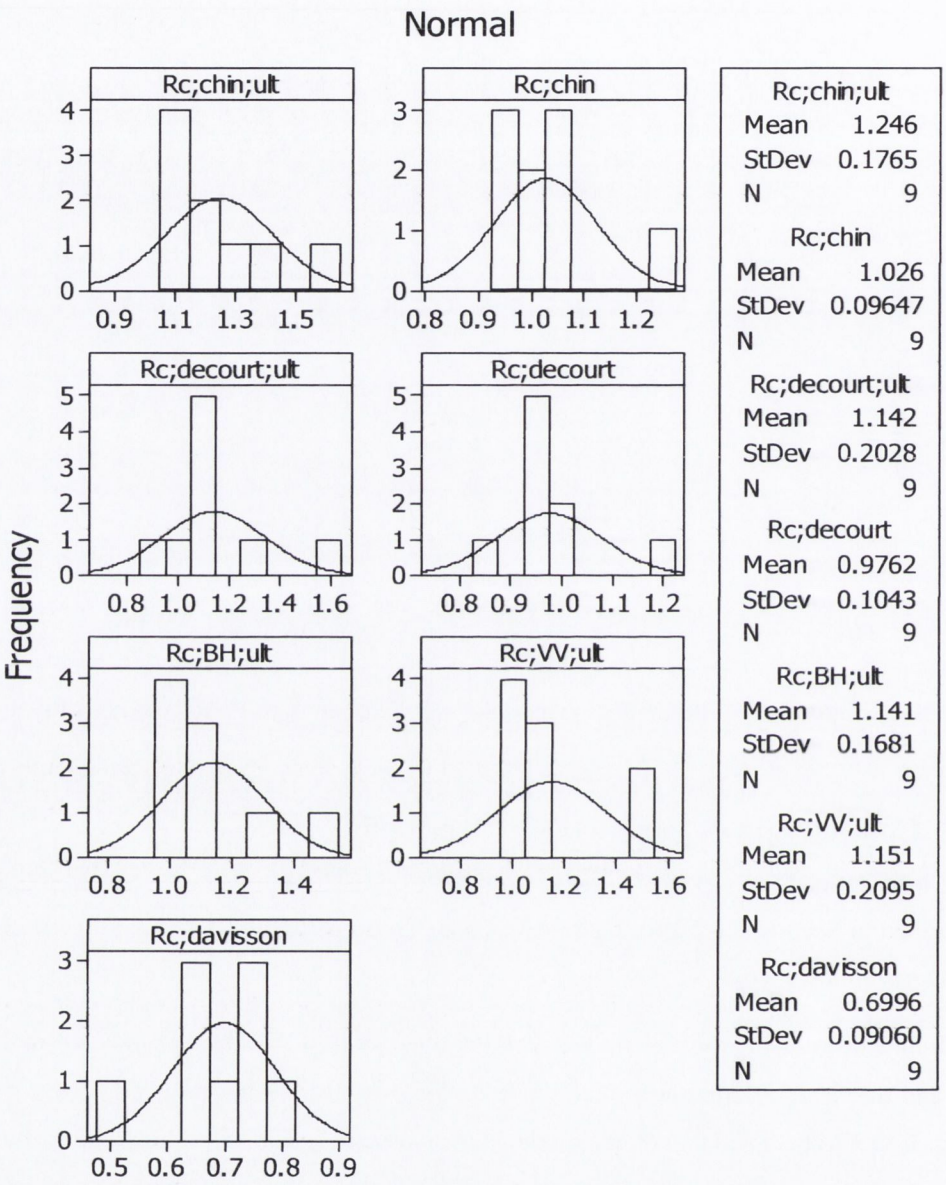


Figure 4.10 – Comparison of methods of estimation of R_c

Interpreting Figure 4.10, the following may be deduced on average:

1) The $R_{c;chin;ult}$ estimate of R_c is around 25% above $R_{c;m}$ and with a standard deviation of 18%.

2) $R_{c;chin}$ was close to $R_{c;m}$ at around 103% $R_{c;m}$ with a standard deviation of 10%.
3) $R_{c;decourt;ult}$ leads to an estimate of R_c, on average, 14% greater than $R_{c;m}$, however, the standard deviation is 20%, more than that for $R_{c;chin;ult}$ indicating that the spread of $R_{c;decourt;ult}$ is greater than that of $R_{c;chin;ult}$.
4) $R_{c;decourt}$ is comparable to that of $R_{c;chin}$, estimating R_c at 98% of $R_{c;m}$, but again, with a slightly larger spread than that of $R_{c;chin}$.
5) $R_{c;BH;ult}$ led to an estimate of R_c of 14% above $R_{c;m}$ and with a standard deviation of 17%,
6) $R_{c;vv;ult}$ was on average 15% greater than $R_{c;m}$ with a large standard deviation of 21%, this method led to more variable results.
7) $R_{c;davisson}$ was much lower than the other methods assessed, estimated at about 70% of $R_{c;m}$, in agreement with NeSmith and Siegel (2009) who suggested that the assumptions forming the basis of this method do not hold for bored piles, with the result that it leads to a lower ultimate resistance (all the piles used in this assessment were bored).

As the number of piles with which to assess the methods of extrapolation of the load-deflection data was limited, due to the fact many piles were not loaded to failure, those piles loaded to at least 50% δ_f were also used to compare the methods. It was shown in Section 4.1 that load-deflection data to at least 50% δ_f led to a reasonable estimate of R_c.

The static load test results in the PTD were filtered in order as follows:

1) Piles loaded in tension were removed leaving only those loaded in compression.
2) Piles not deflected downward at the pile head by at least 5% of the pile diameter were removed.
3) Piles with an R-squared value of the regression in Chin's plot of deflection divided by load against deflection were removed if this value was less than 0.9.
4) Piles where any one of the methods under study was not applicable were removed.

This left 25 piles of the 174 and over 13 sites, with which to assess the methods of determination of R_c. An average value for all the estimates denoted $R_{c;avg}$ was computed in the case of each pile and this was used to normalise each prediction of R_c so that each method could be related to each other, in the absence of $R_{c;m}$.

Figure 4.11 may be used to compare the various methods. Details of the statistics of each are shown in the legend in Figure 4.11. Interpreting Figure 4.11, the following may be deduced on average:

1) The $R_{c;chin;ult}$ estimate of R_c is around 15% above $R_{c;avg}$ and with a standard deviation of 10%.
2) $R_{c;chin}$ was closest to $R_{c;avg}$ at around 95% $R_{c;avg}$ with a standard deviation of 8%.
3) $R_{c;decourt;ult}$ leads to an estimate of R_c, on average, 7% greater than $R_{c;avg}$, however, the standard deviation is 13%, slightly more than that for $R_{c;chin;ult}$ indicating that the spread of $R_{c;decourt;ult}$ is greater than that of $R_{c;chin;ult}$ when this method is applied to limited load-deflection data.
4) $R_{c;decourt}$ is comparable to that of $R_{c;chin}$, estimating R_c at 90% of $R_{c;avg}$, but again, with a slightly larger spread than that of $R_{c;chin}$.
5) $R_{c;BH;ult}$ led to the greatest estimate of R_c, almost 25% above $R_{c;avg}$ and with a very large standard deviation of 35%, indicating that this method is highly variable in its estimation of R_c when load-deflection data is limited, tending to over-predict R_c when compared with the other methods.
6) $R_{c;vv;ult}$ was almost identical to $R_{c;decourt;ult}$ when compared with $R_{c;avg}$.
7) $R_{c;davisson}$ was again much lower than the other methods assessed, estimated at about 60% of $R_{c;avg}$. (It is suggested this method underestimates R_c in bored piles and 25 of the 30 piles used in this assessment were bored).

Chin's method of extrapolation to δ_f yielding the value $R_{c;chin}$ is considered the most consistent estimate, on average, of the value of R_c, with a relatively small spread and is compared with the measured $R_{c;m}$ for those piles that were deflected to a minimum of δ_f using the ratio $R_{c;chin}/R_{c;m}$. Of the 25 piles used in the analysis, 10 were deflected by this amount and the average ratio $R_{c;chin}/R_{c;m}$ was equal to 0.99 with a standard deviation of 0.1, indicating that $R_{c;chin}$ matches $R_{c;m}$ extremely well, for the piles under study.

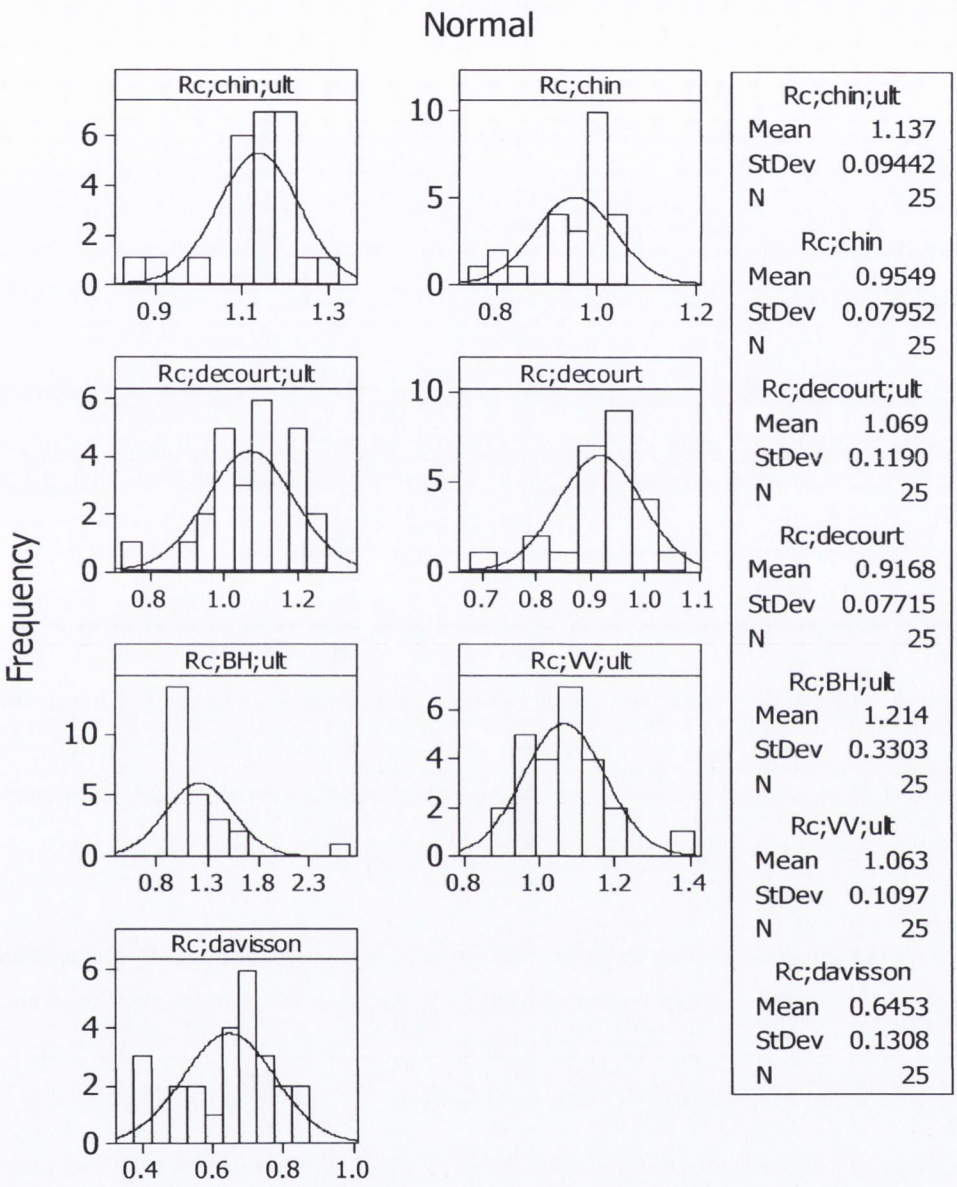


Figure 4.11 - Comparison of methods of estimation of R_c

4.3 Uncertainty in R_c for a single pile

The most consistent means of extrapolation is considered to be $R_{c;chin}$ as presented in Section 4.1. A method of quantification of the uncertainty associated with $R_{c;chin}$ from limited load-deflection data is presented in this section.

Adapting Figure 4.6, and assuming that the bulk of the estimates of R_c lie within about two standard deviations of the mean (corresponding to the 95% confidence limits) then the standard deviation of R_c at pile head deflections less than δ_f may be quantified. The lower and upper bound to the mean trend line are shown in Figure 4.12 and these were used to back-calculate $s(R_c)$ for various proportions of δ_f. The value of $V(R_c)$ was then calculated in the usual way. Any outliers would lie outside the bounds given by three standard deviations from the mean, it is clear from Figure 4.12 that no point would lie outside these limits.

Figure 4.12 implies, that, if a pile is deflected to δ_f, then the corresponding load is equal to $R_{c;m}$ with no associated uncertainty, this is obviously not the case as measurement error in the applied load and the corresponding deflection will contribute some level of uncertainty to $R_{c;m}$. There are also issues with the time increment at which loads are applied – too quickly and creep in the pile-soil system may not have fully occurred leading to measured deflections lower than those under actual loading conditions (which are generally very slow).

The coefficient of variation due to these measurement and procedural errors was assumed to equal 10%, therefore, where a pile is loaded to δ_f the uncertainty in the measured value will be a value of $V(R_c)$ equal to 10%, which seems a reasonable level of uncertainty in measurements during load testing, (Fenton and Griffiths 2003; Fenton and Griffiths 2007).

Figure 4.13 shows how the computed $V(R_{c;chin})$ varies with δ/δ_f. Where the pile is deflected to only 10% δ_f, then $V(R_{c;chin})$ is equal to 30% reducing to 10% where the pile is loaded to δ_f. Figure 4.13 highlights the benefit of carrying out pile load tests to cause deflections as close to δ_f as possible. With increased deflection, comes increased confidence in the true value of R_c and as a result, higher levels of reliability in the foundation may be achieved.

Applying the relationship shown in Figure 4.13, to each pile in the PTD and grouping the piles based on pile type and on the ground conditions, details of the estimated $R_{c;chin}$ are shown in Table 4.2 to Table 4.9. The measured or calculated pile resistance corresponding to a pile head deflection of 10mm, denoted $R_{c;10}$ is also shown for each pile for use later in relation to serviceability requirements. The average and range of the uncertainty in $V(R_{c;chin})$ for each of the groups, is shown in Table 4.10. The average $V(R_{c;chin})$ values are in the range 0.14-0.27 indicating that, on average, piles are not loaded close to δ_f.

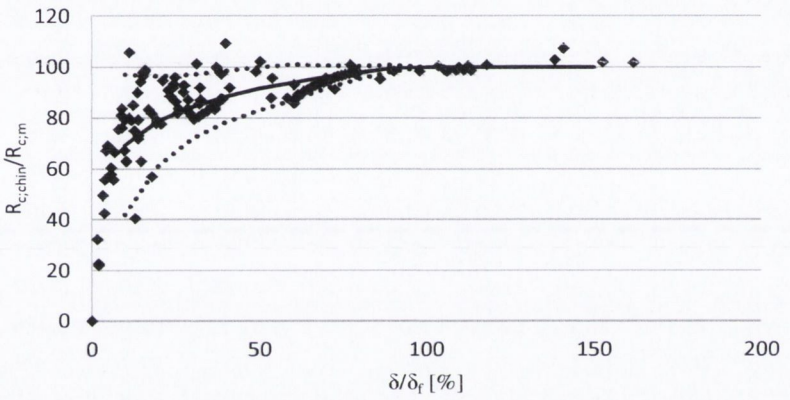


Figure 4.12 - $R_{c;chin}/R_{c;m}$ vs δ/δ_f with upper and lower bounds and mean trend

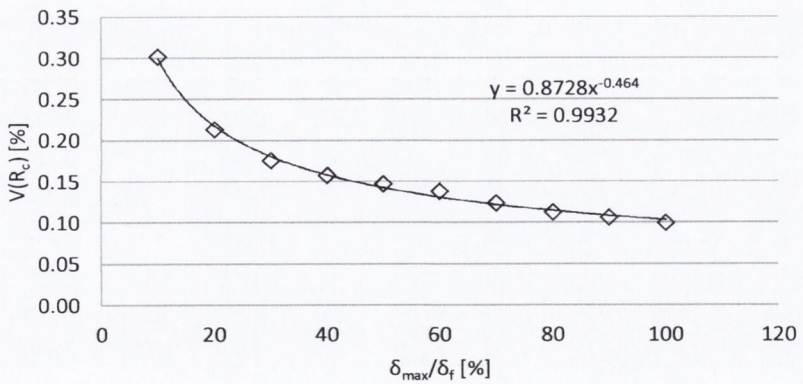


Figure 4.13 – Estimated $V(R_{c;chin})$ with varying δ_{max}/δ_f for a single pile under load

Table 4.2 – Group 1: CFA piles in DBC

Site Ref	Pile Ref	D [mm]	L [m]	F_k [kN]	G_T [kN]	δ_{max}/δ_f [%]	R-sq [_]	$R_{c;chin}$ [kN]	$V(R_{c;chin})$ [_]	$R_{c;10}$ [kN]
C	11	450	11.0	1000	2500	77	0.89	2998	0.117	994
C	12	450	11.0	1000	2000	106	0.95	1890	0.100	671
C	13	450	11.0	1000	2000	59	0.95	2327	0.131	1317
D	15	900	10.0	3000	7500	39	0.95	9023	0.159	3651
D	16	900	10.0	3000	7500	29	0.95	9862	0.183	4373
D	18	900	10.0	3000	4500	14	0.90	6649	0.260	3811
D	19	900	10.0	3000	4500	14	0.93	5838	0.256	3781
D	20	900	10.0	3000	4500	11	0.96	6642	0.291	4301
D	21	900	9.7	3000	4500	10	0.93	6695	0.305	4482
D	22	900	9.8	3000	4500	19	0.94	5945	0.221	3349
D	23	900	9.5	3000	4500	6	0.94	5821	0.392	4940
G	30	600	15.0	2000	5000	42	0.97	6474	0.155	3037
G	31	600	15.0	2000	3000	25	0.98	4068	0.195	2450
G	32	600	15.0	2000	3000	21	0.99	4403	0.211	2640
D	42	1200	13.6	10500	15757	11	0.98	25996	0.282	13152
D	43	1050	13.5	6000	9000	4	0.95	18398	0.466	12978
D	44	900	15.2	3500	5250	6	0.93	8761	0.376	6204
D	46	600	12.0	1800	2700	15	0.93	4005	0.251	2694
D	47	900	12.0	3500	5250	6	0.98	16322	0.393	8126
Q	64	900	10.0	3500	5250	11	0.91	8643	0.285	4961
Q	65	900	10.0	3500	5250	8	0.99	12085	0.340	6429
R	66	450	12.3	1400	3150	24	0.91	5977	0.202	3039
R	67	450	12.3	1400	2100	12	0.99	2492	0.271	2236
R	68	450	12.3	1400	2100	8	0.98	2544	0.337	2371
R	69	600	11.0	1800	4490	48	0.91	4931	0.145	2655
R	70	600	11.0	1800	2700	8	0.97	3294	0.333	2934
R	71	600	11.0	1800	2700	10	0.96	3057	0.298	2722
S	72	762	12.0	1400	3820	10	0.96	5606	0.295	3996
S	73	762	13.8	1400	3790	6	0.94	6671	0.372	4906
Q	75	900	10.0	3500	5250	7	0.93	9377	0.346	6159
Q	76	900	10.0	3500	8750	10	0.97	10312	0.298	7133
Q	77	900	10.0	3500	5250	8	0.99	12067	0.340	6426

Table 4.3 – Group 2: Driven piles in DBC

Site Ref	Pile Ref	D [mm]	L [m]	F_k [kN]	G_T [kN]	δ_{max}/δ_f [%]	R-sq [_]	$R_{c;chin}$ [kN]	$V(R_{c;chin})$ [_]	$R_{c;10}$ [kN]
AH	190	339	7.0	1000	2158	52	1.00	2384	0.140	1913
AH	191	339	5.7	1000	2354	98	1.00	2391	0.104	1589
AH	192	339	8.5	1000	2207	107	1.00	2200	0.100	1422
AH	193	282	9.4	550	1373	19	0.96	2953	0.221	1948
AH	194	282	7.0	550	1059	18	0.99	1963	0.228	1476
AH	195	339	6.0	1000	2143	26	0.92	4095	0.191	2301
AH	196	339	5.9	1000	1717	88	1.00	1782	0.110	1093
AH	197	339	5.8	1000	1962	28	0.97	3840	0.187	2062
AH	198	339	5.7	1000	1962	32	0.94	3824	0.174	1919
AH	199	339	9.6	1000	1884	33	0.55	-	-	1884
AH	200	339	5.9	1000	1933	26	0.90	3938	0.191	2133
AI	201	339	6.4	800	750	7	0.98	2091	0.347	1573
AI	202	339	6.7	800	2000	35	0.98	2828	0.169	1753
AI	203	339	10.5	800	2000	16	0.99	3896	0.240	2777
AI	204	339	4.9	800	1200	17	0.96	2455	0.234	1629
AI	205	339	6.0	800	1200	13	0.99	1925	0.270	1584
AI	206	339	8.1	800	1200	13	0.85	1961	0.267	1546
AI	207	339	5.7	800	1200	14	0.88	1736	0.254	1412
AI	208	339	5.9	800	1200	14	0.99	2841	0.257	1876
AI	209	339	5.8	800	450	6	1.00	2557	0.394	1544
AI	210	339	8.0	800	1200	13	0.98	1913	0.270	1434
AI	211	273	6.4	800	1400	91	0.58	1534	0.108	520

Table 4.4 – Group 3: CFA piles in boulder clay

Site Ref	Pile Ref	D [mm]	L [m]	F_k [kN]	G_T [kN]	δ_{max}/δ_f [%]	R-sq [_]	$R_{c;chin}$ [kN]	$V(R_{c;chin})$ [_]	$R_{c;10}$ [kN]
Y	107	600	18.0	1401	1600	141	0.99	1488	0.100	953
Y	109	600	18.0	1400	1236	89	0.98	1195	0.109	879
Y	110	600	18.0	1400	1030	76	0.99	1060	0.117	666
Y	111	450	18.0	900	1350	113	0.99	1337	0.100	927
Y	112	450	18.0	900	630	26	0.96	950	0.194	601
Y	113	450	21.5	900	1350	162	0.99	1143	0.100	495
Y	115	600	22.9	1400	2100	90	0.97	2132	0.108	743
Y	119	450	17.0	900	883	64	1.00	952	0.127	689
Y	122	450	18.0	900	1148	113	0.99	1110	0.100	855
Y	123	600	18.0	900	2060	79	0.98	2070	0.115	1303
Y	125	450	18.0	900	1351	153	0.98	1253	0.100	789
AF	180	900	9.1	3000	4499	7	-	-	-	-
AF	184	900	11.9	1900	2851	2	-	-	-	-

Table 4.5 – Group 4: Driven piles in boulder clay

Site Ref	Pile Ref	D [mm]	L [m]	F_k [kN]	G_T [kN]	δ_{max}/δ_f [%]	R-sq [_]	$R_{c;chin}$ [kN]	$V(R_{c;chin})$ [_]	$R_{c;10}$ [kN]
AF	164	394	7.1	1000	1499	16	0.85	3132	0.239	1870
AF	165	395	4.0	1100	1650	18	0.34	6941	0.229	2258
AF	166	395	10.6	1350	2024	29	0.91	3088	0.184	1799
AF	172	395	9.2	770	1153	28	0.10	3141	0.185	965
AF	173	339	7.0	440	659	13	0.44	-	-	-
AF	175	344	9.0	1500	2252	17	0.97	8814	0.237	3690
AF	177	395	9.9	920	1379	29	1.00	2148	0.185	1293
AG	185	322	20.2	850	1700	73	0.90	2182	0.120	886
AG	186	322	17.3	850	1060	45	0.40	2497	0.150	718
AG	187	322	15.0	600	750	149	1.00	699	0.100	502
AG	188	322	15.0	440	1095	73	0.99	1224	0.120	752
AG	189	322	15.0	440	383	47	0.99	460	0.147	342

Table 4.6 – Group 5: Bored and CFA piles in sand and gravel

Site Ref	Pile Ref	D [mm]	L [m]	F_k [kN]	G_T [kN]	δ_{max}/δ_f [%]	R-sq [_]	$R_{c;chin}$ [kN]	$V(R_{c;chin})$ [_]	$R_{c;10}$ [kN]
O	61	600	13.0	1600	1600	11	0.98	2900	0.287	1918
O	62	600	12.0	1600	1600	13	1.00	2297	0.266	1720
W	94	900	10.6	3000	2942	44	0.95	2983	0.152	1881
W	95	900	11.7	3000	4413	19	0.94	5097	0.225	3465
W	96	900	10.8	3000	4413	76	0.99	4428	0.117	2561
W	97	900	18.0	3000	3000	26	0.99	3610	0.192	2261
W	98	900	18.0	3000	3000	24	0.97	3427	0.199	2358
W	99	900	18.0	3000	4500	6	0.95	5378	0.367	4631
X	100	880	12.0	3200	4807	54	0.95	4945	0.137	2399
X	102	880	10.8	3200	4806	79	0.95	4781	0.115	1670
X	103	880	10.0	3200	4803	31	0.96	6419	0.177	2626
X	104	880	16.1	3200	6404	27	0.99	9680	0.190	3831

Table 4.7 – Group 6: Piles toed in rock

Site Ref	Pile Ref	D [mm]	L [m]	F_k [kN]	G_T [kN]	δ_{max}/δ_f [%]	R-sq [_]	$R_{c;chin}$ [kN]	$V(R_{c;chin})$ [_]	$R_{c;10}$ [kN]
E	24	450	16.5	1300	1950	65	0.96	1982	0.126	1324
K	39	450	10.3	1000	1500	31	0.95	1808	0.177	1262
M	41	600	17.0	2000	4000	57	0.98	4264	0.134	2639
T	82	600	7.6	1000	2500	35	0.98	2794	0.169	1855
T	83	600	7.0	1000	2500	81	0.99	2626	0.114	1189
T	84	600	9.2	1000	2500	58	0.89	3503	0.133	994
T	85	600	11.0	1000	2000	80	0.95	2131	0.115	702
T	87	600	11.0	1000	2500	59	0.98	2793	0.132	1338
T	88	600	11.0	1000	1500	16	0.52	4504	0.245	1595
T	89	600	11.0	1000	1500	13	0.94	2921	0.262	1674
Q	91	900	12.1	3500	8750	14	0.94	15610	0.259	7761
Y	108	600	19.0	1400	1051	8	0.98	1683	0.334	1320
Y	114	600	24.5	1400	2100	12	0.98	2142	0.274	1722
Y	116	450	19.9	900	1350	14	0.97	1899	0.253	1519
Y	117	450	19.0	900	1324	20	0.98	2025	0.219	1373
Y	118	450	18.0	900	1324	18	0.98	1952	0.226	1410
Y	120	600	14.5	900	2060	10	0.02	-	-	-
Y	121	600	11.5	900	2060	5	0.16	-	-	-
Y	124	450	22.4	900	1324	15	0.90	2324	0.248	1587
Z	126	1080	24.3	6000	12018	13	0.96	37218	0.269	9607
AA	129	450	11.0	1100	2728	70	0.90	4321	0.122	2088
AA	130	450	10.0	1000	1500	12	0.86	2713	0.273	1927
AA	131	450	12.0	1100	2748	26	0.74	6524	0.194	2508
AA	132	450	11.0	1000	1500	36	0.93	1872	0.166	1247
AA	133	450	11.0	1000	1499	11	0.95	2220	0.283	1810
AA	135	450	9.0	700	1049	77	0.80	926	0.116	627
AA	136	450	12.0	700	2688	67	1.00	2819	0.124	2000
AA	137	450	9.0	700	1577	42	0.98	1722	0.155	1438
AA	142	450	12.0	1100	2750	67	0.98	2893	0.124	2111
AA	143	450	11.5	1100	2698	40	0.91	3674	0.157	2030
AB	145	640	9.3	2000	5000	17	0.95	8965	0.234	4581
AB	147	450	13.3	1000	2500	11	0.96	4643	0.282	3279
AC	148	900	18.7	9000	15000	12	0.92	35972	0.276	13850
AC	151	900	18.2	6000	18008	105	0.99	17523	0.101	6574
AC	156	900	23.8	6000	18006	22	0.98	31039	0.208	11430
AC	159	900	27.0	6000	18002	19	0.95	39285	0.223	11968
AF	168	344	10.2	700	1049	9	0.57	5944	0.314	2826
AF	169	344	21.3	1350	2024	32	0.51	4147	0.176	1855

Table 4.8 – Group 7: Piles in mixed soil conditions

Site Ref	Pile Ref	D [mm]	L [m]	F_k [kN]	G_T [kN]	δ_{max}/δ_f [%]	R-sq [_]	$R_{c;chin}$ [kN]	$V(R_{c;chin})$ [_]	$R_{c;10}$ [kN]
F	25	350	12.0	600	900	138	1.00	867	0.100	663
F	26	450	15.0	1000	2500	118	0.98	2393	0.100	1479
F	27	600	15.0	2000	2000	71	1.00	2189	0.121	1037
F	28	900	16.0	3000	5250	54	0.91	5408	0.138	2199
J	37	900	2.5	2000	3000	32	0.96	3685	0.174	1742
J	38	900	2.1	2000	3000	69	0.93	2909	0.122	1289
N	48	750	10.0	4000	6000	22	0.97	8222	0.208	4628
N	49	600	6.5	2500	3750	22	0.33	-	-	-
N	50	750	10.0	4000	6000	29	0.93	9464	0.182	3506
N	52	450	10.0	1500	2250	14	0.83	3488	0.259	2562
N	54	600	6.0	2500	3750	20	0.93	5052	0.217	3275
N	56	600	8.9	2500	3750	9	0.95	6304	0.317	4584
N	57	600	6.7	2500	3750	24	0.91	5459	0.199	2908
N	59	350	6.6	750	1125	48	0.97	1214	0.145	936
AF	182	600	21.0	900	1353	6	0.15	-	-	-
AF	183	600	19.0	1250	1874	5	0.12	-	-	-

Table 4.9 – Group 9: Piles for which the ground conditions are unknown

Site Ref	Pile Ref	D [mm]	L [m]	F_k [kN]	G_T [kN]	δ_{max}/δ_f [%]	R-sq [_]	$R_{c;chin}$ [kN]	$V(R_{c;chin})$ [_]	$R_{c;10}$ [kN]
A	1	450	10.0	1000	1500	70	0.96	1483	0.122	1031
A	2	450	11.4	1000	3000	26	0.96	5364	0.192	2734
A	4	450	7.5	1000	2500	52	0.92	3544	0.139	1299
A	6	450	6.0	1000	2000	37	0.92	2981	0.164	1602
A	8	450	6.5	1000	1500	36	0.92	1631	0.165	1131
A	9	450	7.5	1000	1500	37	0.92	1828	0.164	1118
B	10	600	11.5	3000	7500	49	0.97	10006	0.144	3746
H	34	600	3.0	1800	2700	100	0.93	2519	0.103	879
L	40	600	24.0	2200	5500	28	0.92	8794	0.185	3949
P	63	450	9.2	1000	1000	19	0.98	1692	0.224	1188
U	90	600	16.0	2000	5000	40	0.94	6104	0.158	2369
V	93	600	32.0	2666	3930	39	0.98	4399	0.160	2400
AD	162	600	8.2	1600	2400	9	0.95	5574	0.318	3420
AE	163	1000	13.5	3500	8750	20	0.79	12052	0.218	5282
AF	167	344	15.7	700	1059	7	0.78	3843	0.351	2584
AF	171	395	10.2	1350	2024	34	0.52	4040	0.169	1529
AF	174	344	14.5	1500	2249	27	0.98	3907	0.188	2359
AF	178	395	11.2	960	1439	16	0.98	2210	0.240	1659
AF	181	395	3.6	1500	2249	14	0.93	6518	0.256	3354

Table 4.10 – Summary of estimated $V(R_c)$ for each group of piles

Group	$V(R_{c;chin})$		
	μ	min	max
1	0.27	0.10 -	0.47
2	0.22	0.10 -	0.39
3	0.12	0.10 -	0.19
4	0.16	0.10 -	0.24
5	0.20	0.12 -	0.37
6	0.20	0.10 -	0.33
7	0.17	0.10 -	0.32
8	0.21	0.10 -	0.41
9	0.18	0.10 -	0.32

4.4 Quantifying within-site variability

The uncertainty associated with individual piles is of limited use, applying only to the pile that is actually tested in the exact location of that pile having been installed in the precise manner of that pile. If a pile design is to be proposed for installation of many similar piles across a site, then, in addition to the uncertainty associated with the resistance of a single pile, information on the effect of within-site variation on $V(R_c)$ is required.

4.4.1 Case study – Malahide viaduct

This point was demonstrated by the Author at a test site about 15km North of Dublin, at the Malahide Railway Viaduct. Two sets of two piles were installed and load tested, where piles within a set were installed close to each other, about 3m apart, but where the distance between the two sets of piles was about 50m. All the piles were installed in the same manner using the same piling rig and the same materials.

The results of in-situ testing carried out at the site in the form of N_{SPT} from the SPT and s_u measured using shear vane tests are shown in Figure 4.14(a) and in Figure 4.14(b) respectively. The interpreted stratigraphy at the site in each of the two test locations is shown for Pile 1 & Pile 2 in Figure 4.15(a) and for Pile 3 & Pile 4 in Figure 4.15(b). The stratigraphy in each location indicates about 5-6m crushed rock, over about 3-5m of

alluvial material, over glacial till underlain by limestone bedrock well below the founding level of the piles.

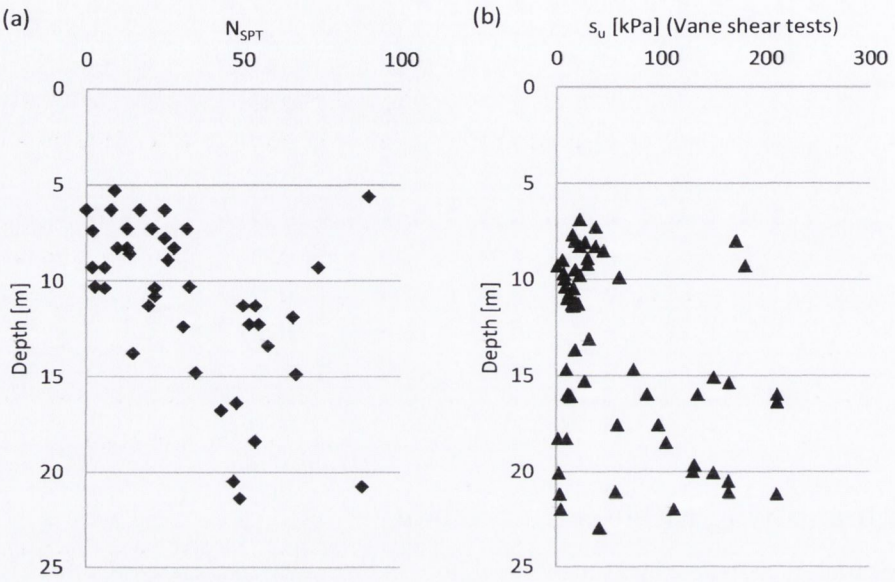


Figure 4.14 – Results of SPT and vane shear tests vs depth

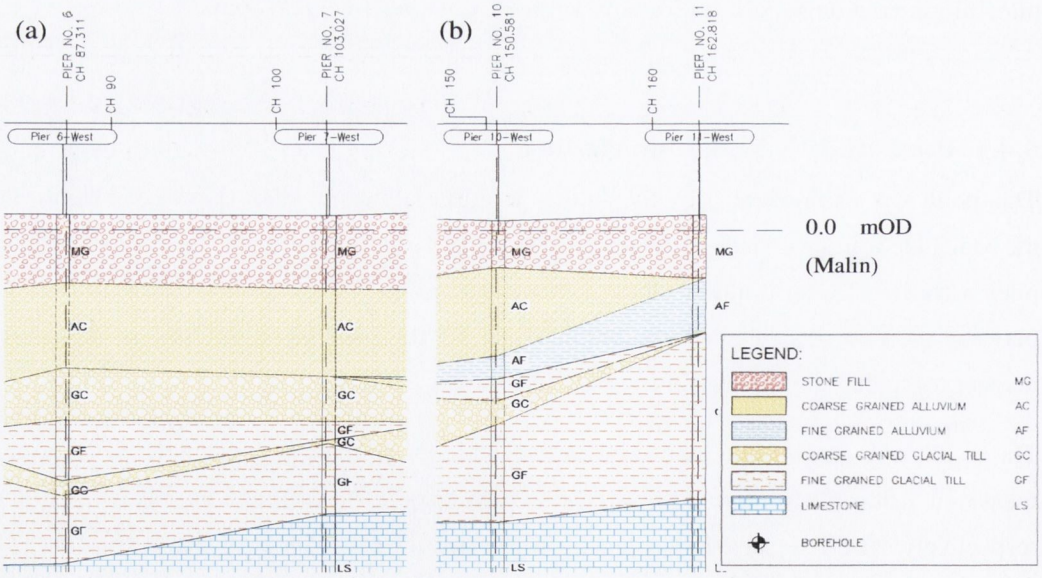


Figure 4.15 – Interpreted Stratigraphy, (a) Pier 6-7 (b) Pier 10-11 (equal horizontal and vertical scales)

The four piles were intended to be 15m in length, but the actual pile lengths varied between 13.5-15.0m due to variations in the ground and installation limitations. Differences in the pile length of this order are typical where piles are installed across a site.

To minimise inconsistency in the methods of testing and measurement, the two piles in each set were loaded at the same time using a single test frame, identical jacking systems and the pile head deflections were measured at the same time for each of the piles using a single precise level.

The aim of the experiment was to demonstrate the effects of spatial variability on the interpreted R_c value, for similar piles installed in a single site that is deemed to have fairly uniform soil conditions. It should be noted that this test also includes variability due to installation of the piles. The measured pile head load-deflection results are shown in Figure 4.16 alongside smoothed hyperbolic extrapolations for each. Set 1 comprised Pile 1 and Pile 2 while Set 2 comprised Pile 3 and Pile 4.

Piles within sets are seen to exhibit a very similar response with respect to load-deflection behaviour at the pile head, while the load-deflection response between sets is seen to be quite different. It is the magnitude of this difference in the load-deflection response of similar piles installed on a single site that must be quantified to accurately assess the reliability of a particular pile design for a given site.

The fact that piles within the same set, for both the sets, yielded almost identical results, would indicate that the method of installation of the piles was fairly repeatable and contributed little to the overall variation in R_c. This implies that the variation in response between sets is primarily due to variation in the ground.

At δ_f, equal to 14mm for these 140mm diameter micropiles, the interpreted value of R_c would be about 640 and 1160kN for piles in Set 1 and Set 2 respectively, which equates to a rather high value of $V(R_c)$ equal to 0.42, calculated by dividing the standard deviation in R_c, $s(R_c)$ by the mean value of R_c, $\mu(R_c)$.

Figure 4.17 shows the interpreted force-depth profiles for each of the piles; calculated using the strain gauge readings at each depth. Again, piles within sets are seen to exhibit more similar behaviour than piles between sets. The shaft resistance developed during loading of the piles was not quantified as it is difficult to assess accurately the actual diameter of the piles due to the installation method. However, the gradient of the graphs in

Figure 4.17 give an indication of the shaft resistance developed along the pile shafts – there is substantial shaft resistance developed in the uppermost 5m in the crushed rock layer with virtually zero shaft resistance developed in the alluvial layers. Towards the toe of the piles shaft resistance was also developed in the glacial till layers with almost zero load on the pile toes in general.

It is, therefore, imperative that within-site variation be appreciated and approximated accurately where a pile design is proposed for a site. This can be done using ground test results from site investigation and/or from load test results carried out on preliminary piles installed prior to installation of the working piles.

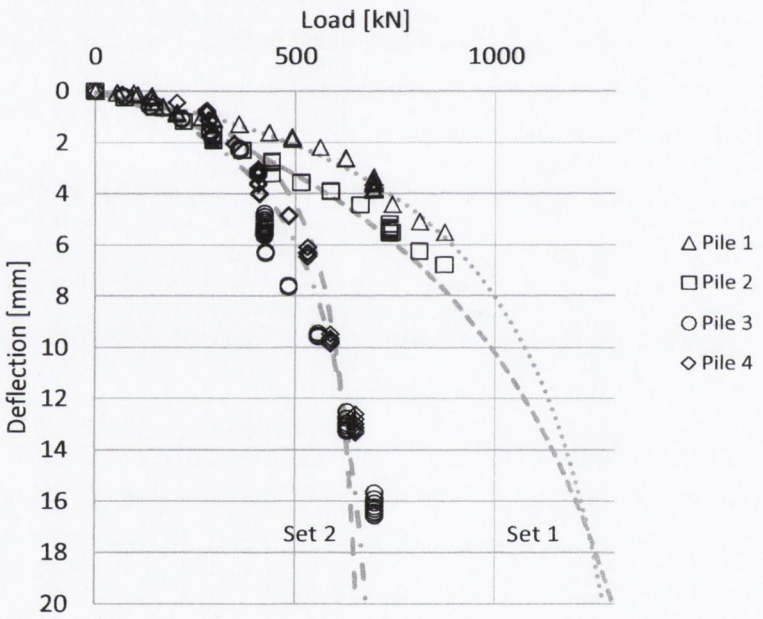


Figure 4.16 – Malahide: Measured pile head load-deflection data

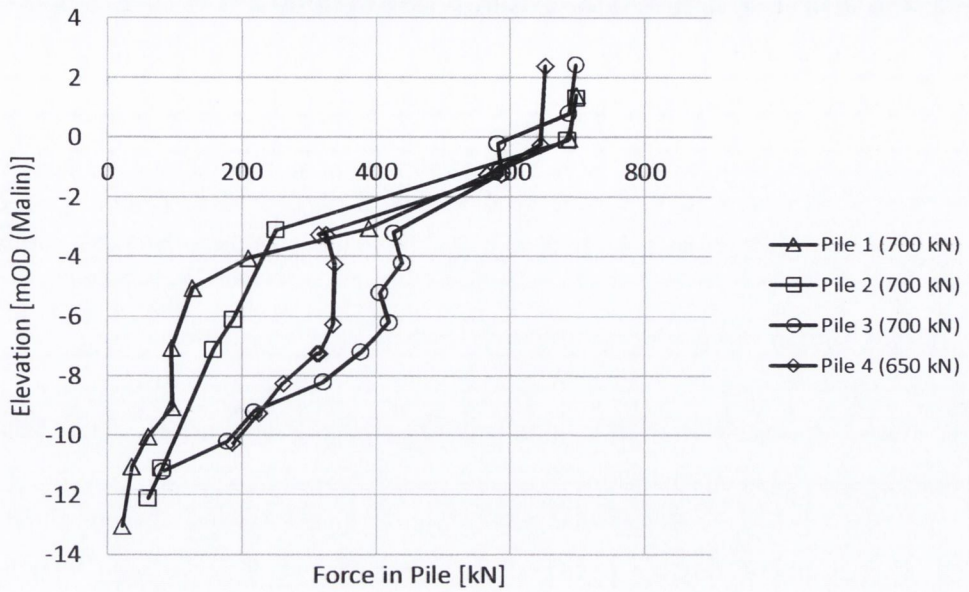


Figure 4.17 – Malahide: Interpreted force-depth profile at 650-700 kN head load

4.5 Within-site variability: Ground test results

Quantification of the variation in the soil properties used in design is critical to reliability-based design (RBD) methods for deep foundations. For this reason, realistic assessment of measured site investigation data is necessary if RBD methods are to be successfully applied to geotechnical design.

In Ireland, ground conditions on a site are generally characterised using boreholes in which SPT's are carried out. It is common practice to then correlate the recorded N_{SPT} empirically with s_u and ϕ' in the case of fine and coarse grained soils respectively and to estimate R_c using these parameters.

Of the 32 different sites listed in the PTD, 20 had ground test results (available to the Author) from the SPT and these were analysed statistically in an attempt to characterise the within-site variability, ultimately with a view to computing the value of $V(R_c)$ for a particular size pile installed on a particular site.

4.5.1 Quantifying variation in ground tests results

An N_{SPT}/depth regression analysis showed that there was a statistically significant increase in N_{SPT} with depth on 16 of the 20 sites investigated.

The procedure in carrying out the regression analysis on the raw data was as follows:

1) The raw N_{SPT} values measured in various boreholes within a particular site were grouped together.
2) Any refusals noted were removed from each dataset.
3) A regression analysis was then applied to the remaining dataset using N_{SPT} as the response variable and z as the predictor (the statistical software package – Minitab 15 was used to assess the results).
4) The regression coefficients and their respective standard errors were computed and an analysis of variance (ANOVA) on the regressed data was used to indicate whether or not there was a statistically significant increase in N_{SPT} with z.
5) If there appeared to be an increase in N_{SPT} with z, then any results deemed erroneous were flagged (based on standardised deleted residuals) and removed from the dataset. This step acts to remove unusually high or low measured N_{SPT} values, perhaps due to thin layers of weaker material or lines of cobbles, which are often present within the bulk material, but generally having little effect on the response of the bulk material globally.
6) Steps 3 – 5 were then repeated, where necessary, a maximum of three times (so that there remained few or no results being deemed erroneous) and the calculated regression coefficients were taken as the best estimate of the relationship between N_{SPT} and z.

In the case that the N_{SPT} value increased with depth a linear trend was assumed and the results for each site were divided into two component parts: the linear trend function, $[t(z_1 \ldots \ldots \ldots z_n)]$ and the residuals, $[\xi(z_1 \ldots \ldots \ldots z_n)]$ (the difference between each individual measurement and the trend function). The N_{SPT} value may be written as Equation 4.1 and the trend function as Equation 4.2.

$$N_{SPT} = N_{SPT}(t) + N_{SPT}(\xi) \qquad 4.1$$

$$N_{SPT}(t) = a + bz \qquad 4.2$$

where $N_{SPT}(t)$ is assumed to increase linearly with depth and a and b are the regression coefficients of the plot of depth, z against the measured N_{SPT}.

The results of this analysis are presented in Figure 4.18 with the raw data for one of the test sites as an example. In Figure 4.18(a) one can observe the general increase in N_{SPT} from around 30-70 with depth increasing from 2-9m. From a soil mechanics perspective this may be due to increasing stress level in the ground with increasing depth. Also shown in Figure 4.1(a) are those values of N_{SPT} deemed erroneous from the results of the regression analysis. Figure 4.18(b) displays the residuals, and these are seen to be more or less uniformly distributed with depth and with a mean equal to zero.

In the case where the N_{SPT} results showed no statistically significant increase with depth an average value for the results was computed and assumed constant with depth. The minimum R-squared value of the trend function, which is a measure of the strength of correlation between the N_{SPT} and the depth was equal to 0.2, while the maximum was equal to 0.6 with an average R-squared value for all the sites equal to 0.4.

The results for all the test sites are summarised in Table 4.11 which also shows the number of data points, n on which each analysis was based and the minimum and maximum depth over which SPT's were carried out at each test site. The calculated $V(N_{SPT})$ are shown graphically in Figure 4.19.

The notation $'s'$ is used for standard deviation as it refers to the standard deviation of a sample of data, according to probability theory, this value equates to the expected (mean) value of the population standard deviation of the same variable, σ which is an unknown.

It is thought that the residuals are comprised of two sources of variation, namely, measurement error and heterogeneity of the soil under study (Oka and Tanaka 2009). Here, the residuals are shown to be constant with depth, and because N_{SPT} is shown to increase with depth, this would indicate that the residuals are independent of the magnitude of the measured N_{SPT}.

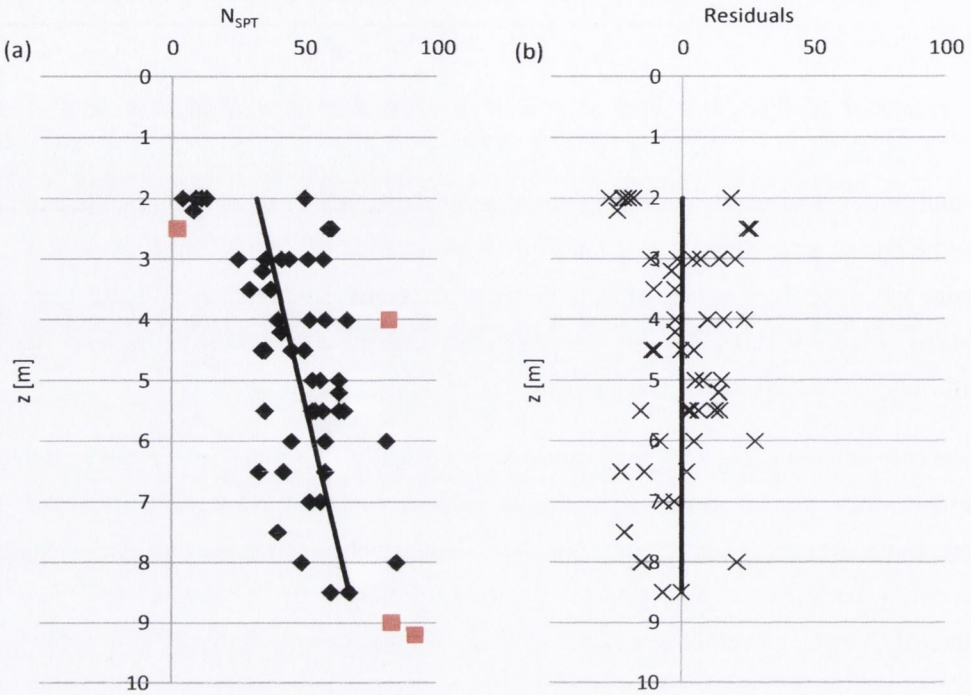


Figure 4.18 - Regression analysis on raw N_{SPT} (a) and residuals from trend (b) for Site D

Table 4.11 – Summary of N_{SPT} and associated uncertainty at test sites

Site Ref	n	a	b	$s(N_{SPT})$	d_{min} [m]	d_{max} [m]	$N_{SPT;min}$	$N_{SPT;max}$	$N_{SPT;avg}$	$V(N_{SPT})$
A	-	-	-	-	-	-	-	-	-	-
B	-	-	-	-	-	-	-	-	-	-
C	-	-	-	-	-	-	-	-	-	-
D	51	20.7	5.5	14.6	2.0	8.5	32	67	46	0.32
E	-	-	-	-	-	-	-	-	-	-
F	156	-	-	17.1	0.3	19.3	-	-	30	0.56
G	17	18.8	5.5	10.7	0.5	6.0	22	52	37	0.29
H	-	-	-	-	-	-	-	-	-	-
I	-	-	-	-	-	-	-	-	-	-
J	15	1.0	3.2	3.0	1.2	14.6	5	47	18	0.17
K	-	-	-	-	-	-	-	-	-	-
L	-	-	-	-	-	-	-	-	-	-
M	17	-	-	6.0	1.0	18.0	-	-	34	0.17
N	210	-	-	12.2	1.2	9.2	-	-	20	0.62
O	45	-	-	17.9	1.2	19.2	-	-	32	0.56
P	-	-	-	-	-	-	-	-	-	-
Q	59	-3.3	3.6	8.3	0.5	12.5	0	42	41	0.20
R	31	37.9	3.4	12.5	0.9	9.4	41	70	53	0.23
S	56	-8.1	7.7	10.6	2.0	11.0	7	76	41	0.26
T	21	19.9	4.4	9.4	1.0	8.0	24	55	36	0.26
U	24	29.3	1.4	11.9	1.0	15.0	31	50	39	0.30
V	-	-	-	-	-	-	-	-	-	-
W	153	15.6	0.8	10.0	0.5	21.0	16	32	23	0.44
X	127	15.3	1.5	9.5	1.3	15.0	17	38	26	0.37
Y	81	-70.9	5.6	9.0	14.9	22.9	13	58	35	0.25
Z	84	8.9	4.6	16.0	1.0	14.0	13	73	38	0.42
AA	52	14.5	5.5	19.2	1.3	13.0	21	86	49	0.39
AB	31	13.6	1.3	1.6	0.5	5.2	14	20	17	0.09
AC	-	-	-	-	-	-	-	-	-	-
AD	-	-	-	-	-	-	-	-	-	-
AE	-	-	-	-	-	-	-	-	-	-
AF	-	-	-	-	-	-	-	-	-	-
AG	-	-	-	-	-	-	-	-	-	-
AH	75	24.3	3.9	15.0	1	9.1	28	60	42	0.36
AI	56	18.3	5.7	17.7	2.3	10.2	31	76	37	0.48

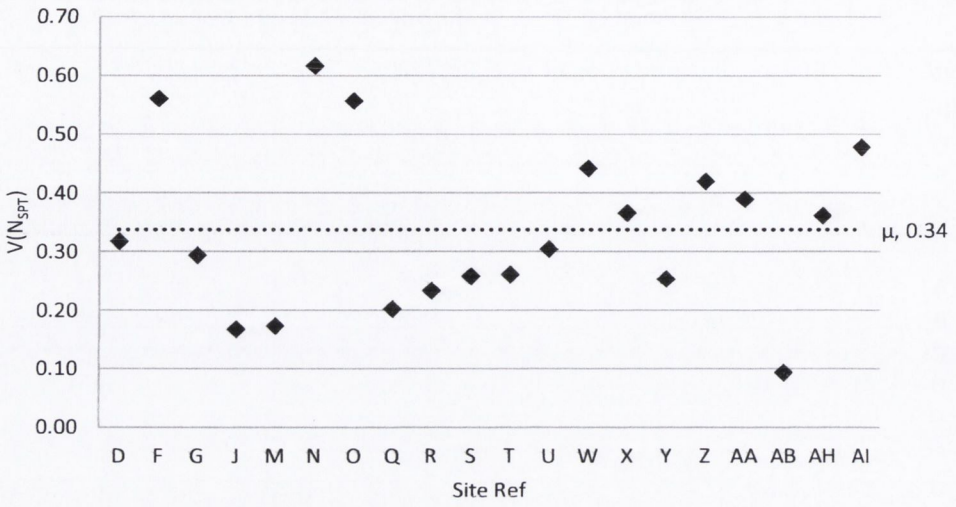


Figure 4.19 – Summary of within-site variation in N_{SPT} for various sites

4.5.2 Spatial variation

The concept of spatial averaging, stemming from the observation that soil properties measured closer to each other exhibit a stronger correlation than those measured further away, was applied to the N_{SPT} results from each of the sites listed in Table 4.11.

Different values of the vertical scale of fluctuation Θ_z were assumed, in the range 1–6m and were used to calculate variance reduction factors Γ^2, by Vanmarke (1983) using Equation 2.31 for application to the observed variance of the measured N_{SPT}.

The average length of a pile in the PTD was 10m, recognising that the top 2m of ground generally contributes little to the shaft resistance of the pile, the length over which spatial averaging was applied for comparison of its effect on the observed variation in the N_{SPT} was 8m. The results are displayed in Table 4.12.

The value of Γ^2 varied from 0.1 to 1.0 where Θ_z was assumed equal to 1 and 6 respectively. Where Θ_z is greater than or equal to 8m, this is equivalent to no reduction in the observed variance of the measured N_{SPT} (i.e no spatial variation) – this case is shown in Table 4.12 also. The range of the observed $V(N_{SPT})$ where no spatial averaging was applied (Θ_z= L–2 = 8m), was 0.09-0.62 with an average value of 0.34. The variability itself varies over a wide range due to the fact there are several contributory factors that combine to yield the overall variability.

Four different values of Θ_z, equal to 1, 2, 4 and 6m, considered to range from a low value of the parameter to a high value, were assumed and were used to compute Γ^2 which was then applied to $V(N_{SPT})$. The average $V(N_{SPT})$ reduced from 0.34 to 0.22, 0.19, 0.15 and 0.11 where Θ_z was assumed equal to 6, 4, 2 and 1m respectively.

It is clear that the value of Θ_z has a significant effect on the variability in the ground over a particular failure surface. The observed variation in N_{SPT} reduced three-fold where a low value of Θ_z was assumed and where L_f was assumed equal to the average pile length of those piles in the PTD minus 2m.

Spatial averaging is only effective when L_f is large when compared to Θ_z. It should be noted that the values in Table 4.12 are representative of the *average* pile length in the PTD, which was 10m, as already stated. The length over which spatial averaging was applied was then reduced to 8m. Where piles are longer than 10m, spatial averaging will result in a greater reduction in $V(N_{SPT})$ than that shown in Table 4.12 and for piles shorter than 10m the opposite would be true.

Spatial averaging can result in reduced values of $V(R_s)$, when computed based on ground test results leading to reduced values of $V(R_c)$. Longer piles will benefit more from spatial averaging than shorter ones in similar ground conditions.

Spatial averaging is not applied to $V(R_b)$ as the failure surface typical at the pile toe is of relatively limited extent and the observed value of $V(N_{SPT})$ without any spatial averaging is recommended for computation of $V(R_b)$ (Fenton and Griffiths 2003; Fenton and Griffiths 2007).

Table 4.12 – $V(N_{SPT})$ assuming values of Θ_z

Site	Θ_z	1	2	4	6	$\geq L_f$
Ref	Γ^2	0.12	0.22	0.38	0.49	1.00
D		0.11	0.15	0.19	0.22	0.32
F		0.19	0.26	0.34	0.39	0.56
G		0.10	0.14	0.18	0.21	0.29
J		0.06	0.08	0.10	0.12	0.17
M		0.06	0.08	0.11	0.12	0.17
N		0.21	0.29	0.38	0.43	0.62
O		0.19	0.26	0.34	0.39	0.56
Q		0.07	0.09	0.12	0.14	0.20
R		0.08	0.11	0.14	0.16	0.23
S		0.09	0.12	0.16	0.18	0.26
T		0.09	0.12	0.16	0.18	0.26
U		0.10	0.14	0.19	0.21	0.30
W		0.15	0.21	0.27	0.31	0.44
X		0.13	0.17	0.23	0.26	0.37
Y		0.09	0.12	0.16	0.18	0.25
Z		0.14	0.20	0.26	0.29	0.42
AA		0.13	0.18	0.24	0.27	0.39
AB		0.03	0.04	0.06	0.07	0.09
AH		0.12	0.17	0.22	0.25	0.36
AI		0.16	0.22	0.29	0.33	0.48
mean		0.12	0.16	0.21	0.24	0.34

4.5.3 Combining Uncertainty

The variation in the measured N_{SPT} may be used to calculate the uncertainty associated with the calculated values of R_s and R_b characterised using the coefficient of variation in each of the parameters, denoted $V(R_s)$ and $V(R_b)$ respectively, which may be combined to estimate $V(R_c)$.

Uncertainty in the various parameters in the calculation model may be combined using the rules shown in Equations 4.3 to 4.5.

$$f^n = aA \qquad \sigma_f^2 = a^2\sigma_A^2 \qquad 4.3$$

where a is a constant (precisely known) and A is a variable having standard deviation σ_A

$$f^n = AB \dots N \qquad (V_f)^2 = (V_A)^2 + (V_B)^2 + \cdots + (V_N)^2 \qquad 4.4$$

$$f^n = A + B + \cdots + N \qquad (V_f)^2 = \frac{A(V_A)^2 + B(V_B)^2 + \cdots + N(V_N)^2}{f} \qquad 4.5$$

where $A, B \dots N$ are uncorrelated variables having coefficient of variation $V_A, V_B \dots V_N$ respectively.

Using the relations shown in Equations 4.3 to 4.5, $s(R_s)$ and $s(R_b)$ may be expressed as shown in Equation 4.6 and Equation 4.7 respectively assuming A_s & A_b to be known and f_1 & N_{SPT} as independent random variables. These may be combined to calculate $V(R_c)$ using Equation 4.8.

$$s(R_s) = A_s \alpha f_1 N_{SPT} \sqrt{{V_{f_1}}^2 + {V_{N_{SPT}}}^2} \qquad 4.6$$

$$s(R_b) = A_b N_c f_1 N_{SPT} \sqrt{{V_{f_1}}^2 + {V_{N_{SPT}}}^2} \qquad 4.7$$

$$V(R_c) = \frac{R_b V(R_b) + R_s V(R_b)}{R_c} \qquad 4.8$$

The estimation of R_c and $V(R_c)$ enables an assessment of the reliability of the pile foundation if the characteristic load of the pile is known and a reasonable value of the uncertainty in this load is assumed.

4.6 Within-site variability: Load test results

Within-site variability may also be assessed based on the results from pile load tests carried out on similar sized piles on a single site. This method of estimation of $V(R_c)$ will include all sources of uncertainty as the piles are actually installed and tested and a direct measurement of R_c is made (if the piles are loaded to δ_f) so, in addition to the ground variability within a site, characterised in Section 4.5, estimating the uncertainty in this way will include the uncertainty due to installation effects.

Based on the results of load tests on driven piles from eight different sites, listed in Table 2.13 of this thesis, Zhang (2008) calculated the within-site variability of R_c - $V(R_c)$ to be equal to 20%.

Groups of similar piles in the PTD, where piles in each in group were installed on the same site, were identified and the calculated $R_{c;chin}$ was used to assess $V(R_c)$ within the sites. The 15 groups of similar piles identified are detailed in Table 4.13 which shows the site reference, the number of piles in each group, the dimensions of the piles and the value of $R_{c;chin}$ for each of the piles in the various groups.

The variability of the similar piles within each site is characterised by the coefficient of variation of $R_{c;chin}$ denoted $V(R_{c;chin})$ in Table 4.14. The values of $V(R_{c;chin})$ range between 15 and 37% (neglecting one very low and one very high result calculated for groups 12 and 13 respectively) and the average value is equal to 28% (regardless of whether or not the lowest and highest result is included, as these two values also average 28%). All the groups involved CFA piles except the last two, 14 and 15 which comprised driven precast concrete piles.

The value of $V(R_{c;chin})$ was then assessed from all combinations of n load tests using the groups of data in Table 4.13 where n ranged from 2 to 8. The following steps were carried out:

1) All possible combinations of n load tests from each group (containing similar piles) were generated, (for example Group 1 containing a total of 4 load test results has 6, 4 and 1 combination of 2, 3 and 4 load test results respectively).
2) The maximum value of $V(R_{c;chin})$ was noted at each n for each group of load tests.
3) A representative value of $V(R_{c;chin})$ for each n was calculated by averaging the maximum $V(R_{c;chin})$ at each n over all the groups (this means the worst case scenario for each test site was identified at each n and an average was taken to yield the expected worst case scenario, given data from a new site).

The values of $V(R_{c;chin})$ from this analysis are superimposed on the calculated results from the actual data and are shown by the dashed line in Figure 4.20.

A plot of $V(R_{c;chin})$ against the average normalised deflection during load testing for each pile group, $\mu(\delta_{max}/\delta_f)$, shown in Figure 4.21, reveals no real relationship between the two and thus indicates that the uncertainty in the estimation of R_c by Chin does not have

much of an effect on the calculated within-site variability for each individual group of piles. Most of the $V(R_{c;chin})$ values lie within the range 25-30%.

Figure 4.20, Figure 4.22 and Figure 4.23 show plots of $V(R_{c;chin})$ versus the number of piles in each group, the pile diameter and the pile length respectively. There appears to be a reduction in $V(R_{c;chin})$ with increased number of load tests (though there are some departures from the suggested trend in Figure 4.20) and also with increasing pile diameter for the CFA piles (Figure 4.22). There appears to be no effect on $V(R_{c;chin})$ with pile length, as shown in Figure 4.23.

The two groups comprising similar driven piles seem to fit with the data for the CFA piles. It should be noted that an equivalent diameter based on equal area was used for the driven piles which had a square section.

The expected true long-run value of $V(R_{c;chin})$, which is deemed to represent the within-site variability, may also be estimated using the results of this analysis. Previously, where the average maximum value of $V(R_{c;chin})$ was identified for each combination of n load test results using the different groups, here the average value for each combination is selected at each n to provide an estimate of the expected within-site variability.

The results are shown in Figure 4.24 and are very similar for CFA and driven piles. The average value of $V(R_{c;chin})$ is 25% which is slightly larger than that of 20% proposed by Zhang (2008). It should be noted that the average number of load tests in each of the groups identified by the Author was 4, compared with 9 for those groups presented by Zhang. On inspection of Figure 4.20 the *best fit* line to the observed data appears to tend to 20% and may reach this value if groups containing the results of more load tests were available. The results are in agreement with the values of $V(R_c)$ taken by others (Baguelin 1990; Becker 1996).

The pile-soil interaction, depending on the complex processes leading to the formation of the soil, its stress history, and on the method of installation of the piles, among other factors, mean that it is likely that the within-site variability will not reduce much less than this with respect to piles. Within-site variability may reduce slightly where the site in which piles are installed is extremely uniform with respect to the ground conditions and also where the method of installation of the piles is extremely repeatable.

The fact that the estimated long-run expected within-site variation calculated, for sites where CFA or driven piles were installed, were very similar, suggests that the main source of variation is that inherent to the ground and that the method of installation does not have much of an effect, however, more test sites with pile load tests carried out on similar piles, are required if attempts are to be made at separating the inherent soil variability and the variability due to installation effects for piles.

Table 4.13 – Details of groups of similar piles on various sites and estimate of $R_{c;chin}$ for each individual pile

Group [_]	Site Ref	n [_]	L [m]	D [mm]		$R_{c;1}$ [kN]	$R_{c;2}$ [kN]	$R_{c;3}$ [kN]	$R_{c;4}$ [kN]	$R_{c;5}$ [kN]	$R_{c;6}$ [kN]	$R_{c;7}$ [kN]	$R_{c;8}$ [kN]
1	A	4	6.9	450		3544	2981	1631	1828	-	-	-	-
2	D	8	9.9	900		9023	9862	6649	5838	6642	6695	5945	5821
3	G	3	15.0	600		6474	4068	4403	-	-	-	-	-
4	Q	5	10.0	900		8643	12085	9377	10312	12067	-	-	-
5	V	3	11.1	900		2983	5097	4428	-	-	-	-	-
6	V	3	18.0	900		3610	3427	5378	-	-	-	-	-
7	Y	5	18.0	450		1337	950	1952	1110	1253	-	-	-
8	Y	4	18.0	600		1488	1195	1060	2070	-	-	-	-
9	AA	3	11.2	450		1872	2220	3674	-	-	-	-	-
10	AA	3	8.8	450		1555	926	1722	-	-	-	-	-
11	AA	2	12.0	450		2819	2893	-	-	-	-	-	-
12	R	3	12.3	450		5977	2492	2544	-	-	-	-	-
13	R	3	11.0	600		4931	3294	3057	-	-	-	-	-
14	AH	6	5.8	339	*	2391	4095	1782	3840	3824	3938	-	-
15	AI	7	6.1	339	*	2091	2828	1925	1736	2841	2557	1534	-

indicates equivalent D *

Table 4.14 – Within-site variability of $R_{c;chin}$ of similar piles installed in various sites

Group [_]	Site Ref	n [_]	L [m]	D [mm]	$\mu(R_{c;chin})$ [kN]	$s(R_{c;chin})$ [kN]	$V(R_{c;chin})$ [%]
1	A	4	6.9	450	2496	918	37
2	D	8	9.9	900	7059	1533	22
3	G	3	15.0	600	4982	1303	26
4	Q	5	10.0	900	10497	1558	15
5	V	3	11.1	900	4169	1080	26
6	V	3	18.0	900	4139	1077	26
7	Y	5	18.0	450	1320	382	29
8	Y	4	18.0	600	1453	448	31
9	AA	3	11.2	450	2589	956	37
10	AA	3	8.8	450	1401	420	30
11	AA	2	12.0	450	2856	52	2
12	R	3	12.3	450	3671	1997	54
13	R	3	11.0	600	3761	1021	27
14	AH	6	5.8	339	3312	973	29
15	AI	7	6.1	339	2216	529	24

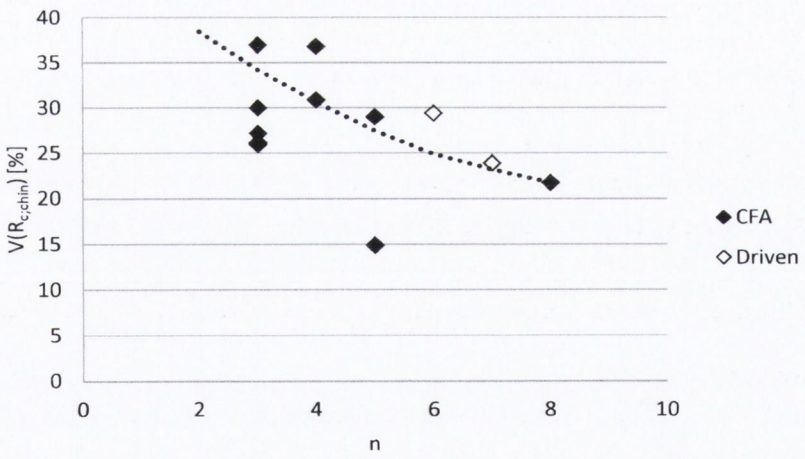


Figure 4.20 – Plot of within-site variation versus number of pile load tests in each group

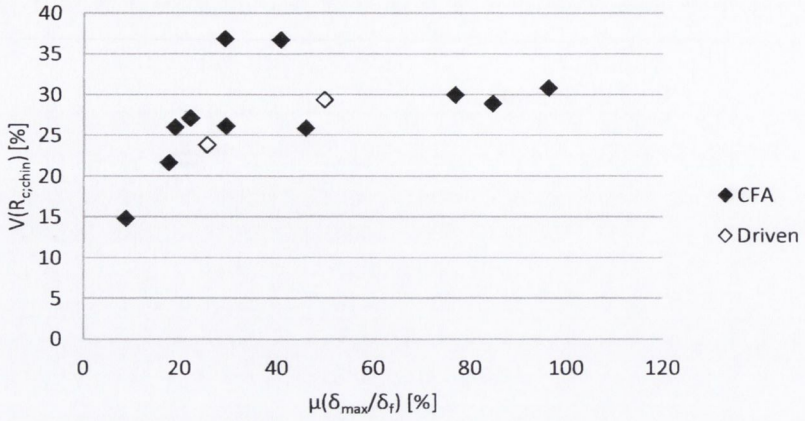


Figure 4.21 – Plot of within-site variation versus average normalised deflection of piles during load testing

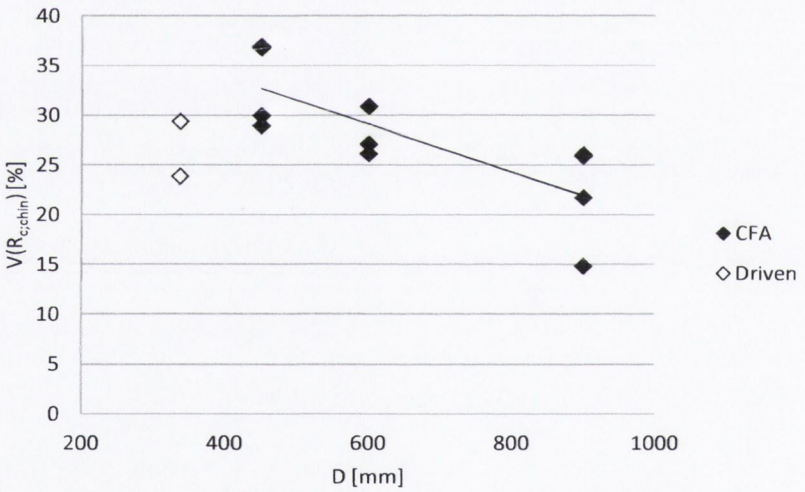


Figure 4.22 – Plot of within-site variation versus pile diameter for pile groups

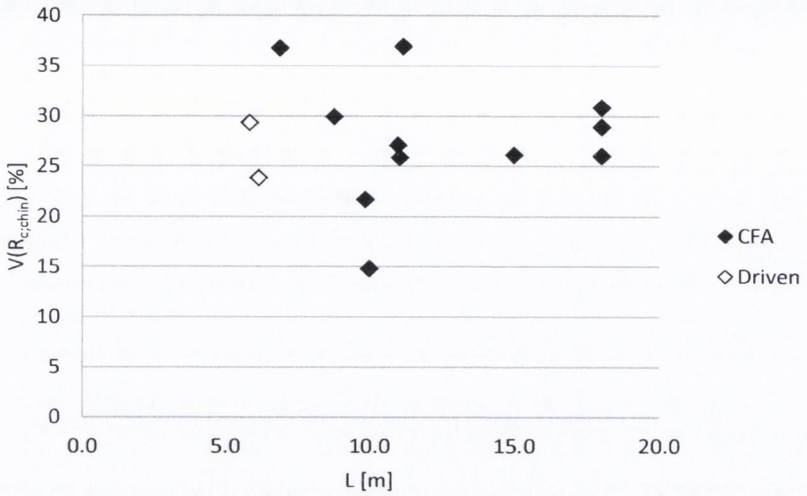


Figure 4.23 – Plot of within-site variation versus pile length for pile groups

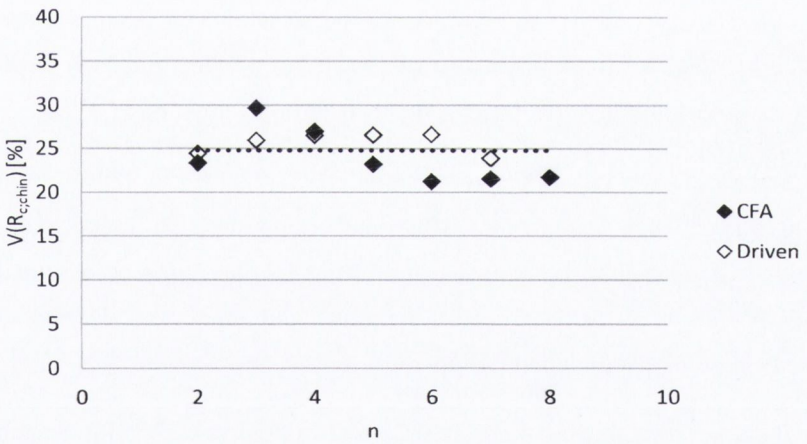


Figure 4.24 – Plot of average within-site variation using all possible combinations of the load test data at n equal to 2 – 8

4.7 Selection of an appropriate distribution

The selection of an appropriate probabilistic distribution as a model for the measured values of R_c from load test results can have an effect on the calculated reliability of a particular foundation.

Zhang (2008) took the measured data from pile load tests carried out on 16 similar piles installed on one site and assessed the statistical distribution with which to represent $R_{c;m}$. The values of $R_{c;m}$ at this particular site did not fit either the normal or lognormal distributions particularly well, however, Zhang outlined that the data did not exceed the 5% critical values (having applied a statistical goodness-of-fit test to the data) and proceeded to use the lognormal distribution for purposes of analysis, adding that this was mathematically convenient to do so and also yielded results on the conservative side.

Figure 4.25 and Figure 4.26 show the results of probability plots used to assess the goodness-of-fit of the normal and lognormal distributions respectively to the observed data for three of the sites identified in this study in which similar piles were installed (Table 4.14). Groups 2, 14 and 15 were selected, as these contained the greatest number of similar piles with which to assess the applicability of the distributions.

The Anderson-Darling test was used to assess the goodness-of-fit of the statistical model to the measured (or extrapolated) values of R_c in the case of each of the three pile groupings. The Anderson-Darling test yields a p-value on the basis of which the assumption of data normality or log-data normality may be assessed. If the p-value is greater than or equal to 0.05 then the assumption that the data fits the distribution cannot be rejected.

The p-values for Groups 2, 14 and 15 are 0.017, 0.033 and 0.461 for the normal distribution respectively and 0.036, 0.026 and 0.544 for the lognormal distribution respectively, indicating that the results from Group 15 only, may be assumed normal or lognormal, the p-values indicate both the normal and lognormal distributions may be rejected in the case of Group 2 and Group 14.

The 95% limits are also shown in Figure 4.25 and in Figure 4.26 and it is seen that in the case of each of the three groups of similar piles, the measured values do not exceed these limits, and so, by the same logic as Zhang (2008) and for mathematical convenience, the lognormal distribution is the assumed distribution hereafter.

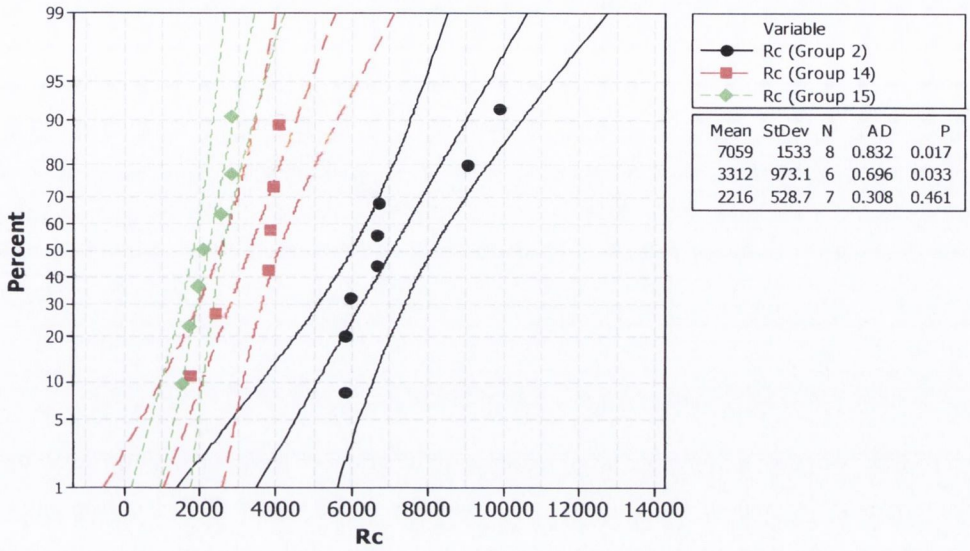


Figure 4.25 – Normal probability plot for Group 2, Group 14 and Group 15

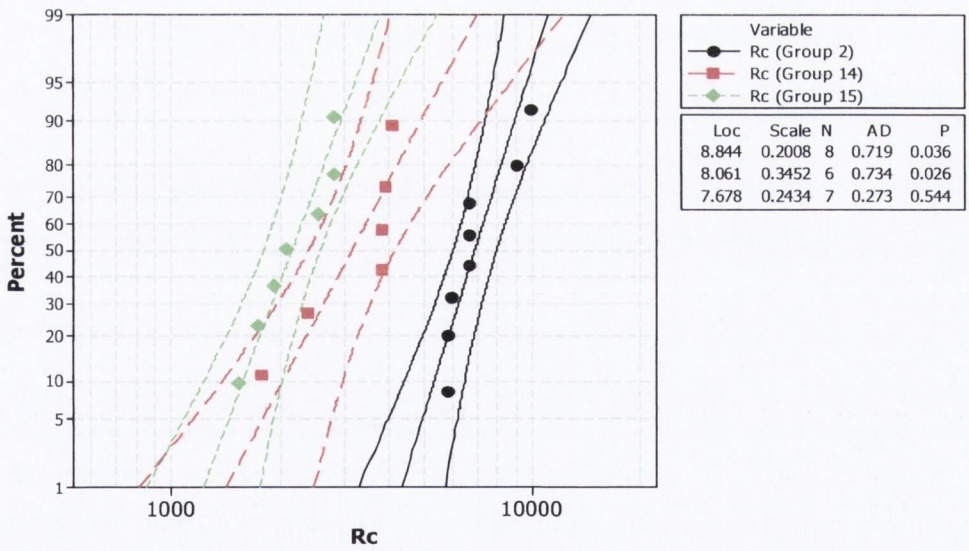


Figure 4.26 – Lognormal probability plot for Group 2, Group 14 and Group 15

4.8 Conclusions

Using the results of nine compressive pile load tests, which were each deflected to δ_f and for which all the methods of estimation of R_c were applicable to the load-deflection data recorded, the various methods of estimation of R_c were assessed and it was found that the method proposed by Chin (1970) to estimate R_c at δ_f matched $R_{c;m}$ well.

Using the results of twenty-five compressive pile load tests which were each deflected to at least 5% of the pile diameter and for which all the methods of estimation of R_c were applicable to the limited load-deflection data recorded, the methods of estimation of R_c from limited load-deflection data were assessed and the results are summarised.

1) The value of $R_{c;chin;ult}$ is considered a high estimate of R_c, on average 15% higher than $R_{c;avg}$ calculated using all the methods under study. Chin's extrapolation of load-deflection data to δ_f, denoted $R_{c;chin}$ was closest to $R_{c;avg}$ (~0.95 $R_{c;avg}$) and is considered a good practical estimate of R_c.
2) The value of $R_{c;decourt;ult}$ and $R_{c;decourt}$ were, on average, 7% above and 10% below $R_{c;avg}$ but with greater variation than the Chin equivalents and for this reason Chin is considered a more reliable estimate of R_c. The value of $R_{c;vv;ult}$ was almost identical to $R_{c;decourt;ult}$ when compared with $R_{c;avg}$.
3) The value of $R_{c;BH;ult}$ led to the greatest estimate of R_c almost 25% above $R_{c;avg}$ and with a very large standard deviation of 35%, indicating that this method is highly variable in its estimation of R_c and tends to over-predict it when compared with the other methods. The range of $R_{c;BH;ult}$ was extremely large, between 50-250% of $R_{c;avg}$ and thus, this method is not recommended by the Author.
4) The value of $R_{c;davisson}$ was considerably less than the other methods assessed and was about 60% of $R_{c;avg}$, in agreement with NeSmith and Siegel (2009) who suggested that the assumptions forming the basis of this method do not hold for bored piles with the result that it leads to a lower ultimate resistance and to conservative design with respect to bored piles (the piles used in this assessment were CFA).

The application of Chin's method to limited pile load test data was assessed using the load-deflection results of ten pile tests in which the piles were loaded to at least δ_f. It is shown that, with load-deflection data up to a deflection greater than or equal to 50% of δ_f, $R_{c;chin}$

was within the range 85-100% of $R_{c;m}$ and for a deflection greater than or equal to 30% of δ_f, $R_{c;chin}$ was within the range 80-100% of $R_{c;m}$.

It is therefore concluded that, where pile load tests are conducted to 50% of δ_f equivalent to 5% of the diameter of the pile, that R_c can be reasonably well predicted using Chin's method. Where load-deflection data was limited further (to less than a deflection of 30% of δ_f) the value of R_c was generally under predicted, though it is not recommended that a value of R_c be estimated from such limited data in practice.

The uncertainty associated with the estimated value of R_c is critical to the design of safe foundations and this section also quantified the uncertainty in R_c, characterised using the coefficient of variation in the parameter, $V(R_c)$.

An initial estimate of R_c, prior to pile load testing, is generally provided using the results of the SPT carried out at the site, reported as the N_{SPT}. The N_{SPT} were reported for 20 sites where pile load tests were carried out and these measured values were filtered as described in Section 4.5.1 and regressed with depth. The values of $V(N_{SPT})$ were seen to range from 0.1 to 0.6 with an average value of 0.35.

Assuming several different values of the vertical scale of fluctuation Θ_z considered to be in the range low to high, variance reduction factors Γ^2 were calculated using Vanmarke (1983) for application to the observed $V(N_{SPT})$. The average $V(N_{SPT})$ reduced from 0.35 to 0.11 where Θ_z was equal to 1.0m and where the length over which spatial averaging was applied was assumed equal to 8m, (the average length of the piles tested in the pile test database minus 2m).

It is clear that an appropriate value of Θ_z is required to ensure the variation in measured ground parameters is characterised correctly for use in reliability analyses when designing piled foundations using ground tests results. More work is required in this area internationally and in Irish soil.

The Author has defined failure as the load corresponding to a deflection at the pile head equal to 10% of the pile diameter, denoted δ_f. Only ten piles of 174 in the pile test database were loaded to δ_f, highlighting that, even where piles are loaded statically, the value of R_c is not directly measured in most cases. The uncertainty in the estimation of R_c

due to limited load-deflection data recorded during a pile load test was quantified by the Author in Section 4.3.

An allowance for operative errors in applying the load and measuring the deflection during a pile load test was made by assuming these errors resulted in a value of $V(R_c)$ equal to 10%, so that, where a pile is actually loaded to δ_f the uncertainty associated with $V(R_{c;m})$ is equal to 10%.

Where piles were loaded to less than δ_f, the error in the estimate of R_c was characterised using values of $R_{c;chin}$ computed based on limited portions of the load-deflection data recorded for those piles where a value of $R_{c;m}$ was available (i.e. those piles loaded to δ_f). Including the allowance for operative errors, this resulted in an estimation of the value of $V(R_c)$ for a single pile from load test results reducing from 30% where piles were loaded to just 10% of δ_f to 10% where $R_{c;m}$ was observed.

Though quantifying the uncertainty relating to the estimation of R_c for a single pile, either estimated using ground test results or load test results, is important, a pile design in Ireland is generally specified for a site or an area within a site over which ground conditions are considered similar, thus, the within-site variability must also be considered. Within-site variability was assessed using the SPT results carried out across the site and also from pile load test results carried out on similar piles on the same site.

Section 4.6 listed 15 separate groups of similar piles from the pile test database on sites in Ireland and quantifies the within-site variation in pile capacity, again this is characterised by the parameter $V(R_c)$. Values of $V(R_c)$ ranged from about 15-40% across the different sites with an average of 28%.

The maximum value of $V(R_c)$ at each n for each group of similar piles was computed where all combinations of n load tests on each site were generated (where n is the number of load test results). An average value of the maximum $V(R_c)$ at each n over all the sites was then calculated.

This value of $V(R_c)$ at each n is considered representative of the average worst-case within-site variation and was seen to reduce from 40% where n equalled one, to 20% where n equalled 8. The Author considers 20% to be a reasonable and representative lower bound to the within-site variation in R_c for a particular pile design on a particular site and at least this level of within-site variation should be accounted for when designing piled

foundations and this value is in agreement with other Author's (Baguelin 1990; Becker 1996; Zhang 2008).

5 Piles in Glacial Till: Review and analysis

The results of the instrumented load tests on CFA piles presented by Farrell and Lawler (2008) and Gavin et al. (2008) and also the driven pile of Farrell et al. (1998) reviewed in Section 2.3 are re-examined by the Author in this section. The load-deflection response and force-depth profiles presented are used to draw conclusions about the development of shaft resistance and end bearing of piles installed in DBC.

Firstly, an analysis of the measured values of s_u in DBC, reported in the literature, is carried out and used to verify the relationship between the measured N_{SPT} and s_u on the sites where the pile load tests were carried out.

The value of s_u interpreted from the N_{SPT} on each site is then used to compute the adhesion factor α and the base bearing factor N_c from the instrumented pile load test results. Extrapolation of the load test data recorded was then carried out to estimate limiting values for each of the factors for the two types of pile.

5.1 Undrained shear strength of DBC

Various measurements of the undrained shear strength s_u reported in the literature are presented in Figure 5.1 from different DBC sites. The data below a depth equal to 3m were treated as a single data set and regressed with depth.

It is recognised that it may not be strictly true that the upper 3m of material comprises UBrBC in all cases as is indicated in Figure 5.1, however, this boundary has been chosen such that the effects of weathering of the soil close to the surface on the shear strength of the material does not corrupt the regression analysis – Farrell et al. (1995) concluded that the UBrBC was a weathered version of the UBkBC and that the depth of this weathered zone is generally limited to about 3m.

It is shown that there is a statistically significant increase in s_u with depth, though the correlation between the two parameters is weak, with a low R-Squared value equal to 0.3, (R-Squared equal to 0 indicates no correlation and 1 indicates a perfect correlation). There is significant scatter in the results with several very high and several very low values which is typical of this spatially varying glacially derived soil mass.

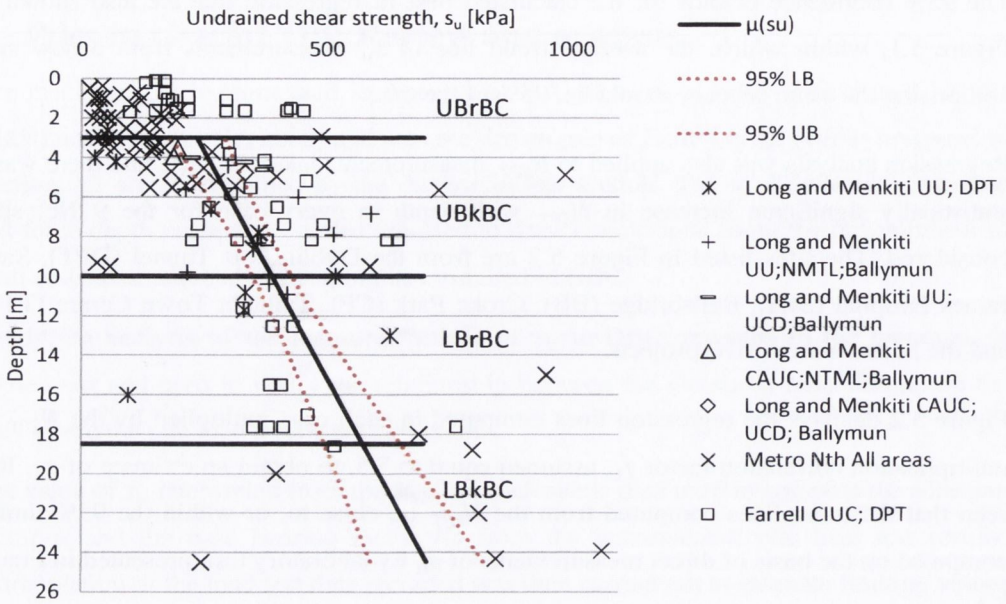
The 95% confidence bounds for the calculated best fit regression line are also shown in Figure 5.1, within which, the average trend line of s_u measurements from a new site, comprising the same deposit, should lie, 95% of the time.

Regression analysis was also applied to N_{SPT} measurements taken in DBC and there was a statistically significant increase in N_{SPT} with depth in every case for the 9 No. sites considered. The sites listed in Figure 5.2 are from the Dublin Port Tunnel (DPT), Saint James Hospital (SJH), Ballsbridge (BB), Croke Park (CP), Tallaght Town Centre (TTC) and the Metro North (MN) projects.

Figure 5.2 displays the regression lines computed in each case multiplied by the N_{SPT}-s_u multiplication correlation factor f_1, assumed equal to 5.5, to obtain an estimate of s_u. It is seen that the trend lines computed from the N_{SPT} lie close to, or within the 95% limits, computed on the basis of direct measurements of s_u by laboratory test, presented in Figure 5.1.

Where the SPT is carried out at depths greater than about 12m, the maximum N_{SPT} can be limited by the operator during the test, often to 50 blows if 300mm penetration is not reached before this. This was the case for the DPT and MN7 sites and for these two sites the correlated N_{SPT} are seen to compare well with the measured s_u to a depth of 8-10m. Below this depth, the N_{SPT} values were limited by the test operator and are, therefore, not representative of increasing shear strength of the soil with depth below this level. The average values of the N_{SPT} below 10 and 8m for the DPT and MN7 sites are included for the Readers information and are seen to be close to 275kPa (5.5 times 50).

Figure 5.2 shows the best fit regression lines fitted to the N_{SPT} after multiplication by f_1 (taken equal to 5.5). This is shown to yield a reasonable estimate of s_u in this deposit where N_{SPT} is not limited by the operator when it potentially exceeds a value of 50. This f_1 value equal to 5.5 is slightly less than that equal to 6, suggested in the literature for low plasticity boulder clays in general (Stroud 1989) and also from literature pertaining to the DBC directly (Farrell and Wall 1990; Farrell and Lawler 2008; Gavin et al. 2008).



UU - idicates result from unconsolidated undrained test; CAUC - indicates result from consolidated anisotropically undrained compression test; CIUC - indicates result from consolidated isotropically undrained compression test; UCD - indicates test carried out by University College Dublin laboratory; NTML - indicates test carried out by the National Materials Testing Laboratory

Figure 5.1 – Measurements of s_u in DBC

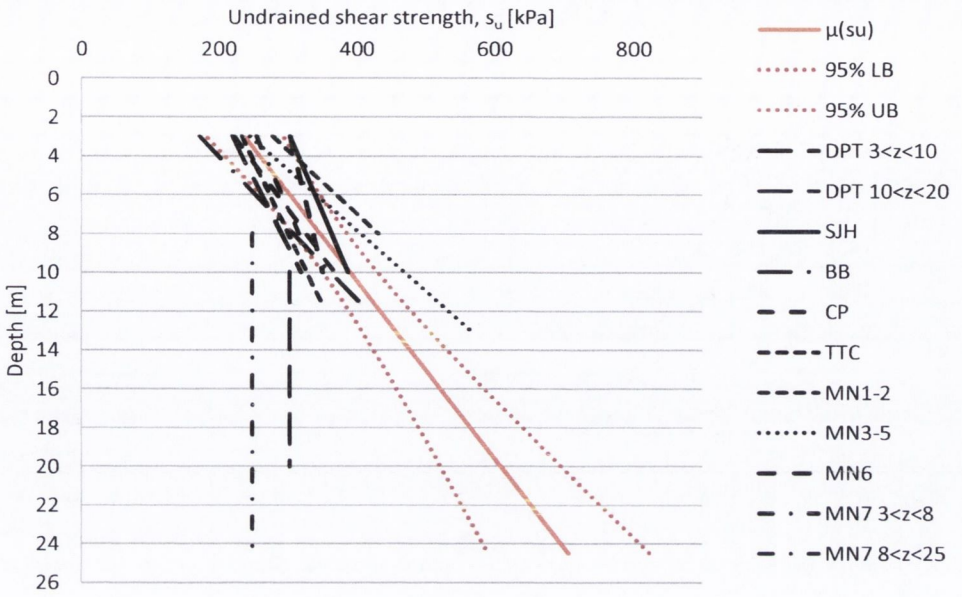


Figure 5.2 - s_u estimated for various sites

5.2 CFA piles

In all, four instrumented piles were installed by CFA methods and statically load tested by the maintained load method under uniaxial compression. SPT's were carried out on both the sites and these are compared in Figure 5.3. It should be noted that on the BB site there was a gravel layer overlying the DBC, shown in Figure 2.16; the shaft resistance developed in this layer could be separated from that developed in the DBC layer using the force-depth profile for the pile, so that analysis of the development of load resistance in the DBC layer only, could be investigated.

The square symbols on Figure 5.3 represent those N_{SPT} considered to be erroneous results, based on standardised deleted residuals identified through regression of N_{SPT} with depth for each of the two sites and, therefore, these results are not considered when the best fit regression line is computed and are only shown as outliers for the Reader's information.

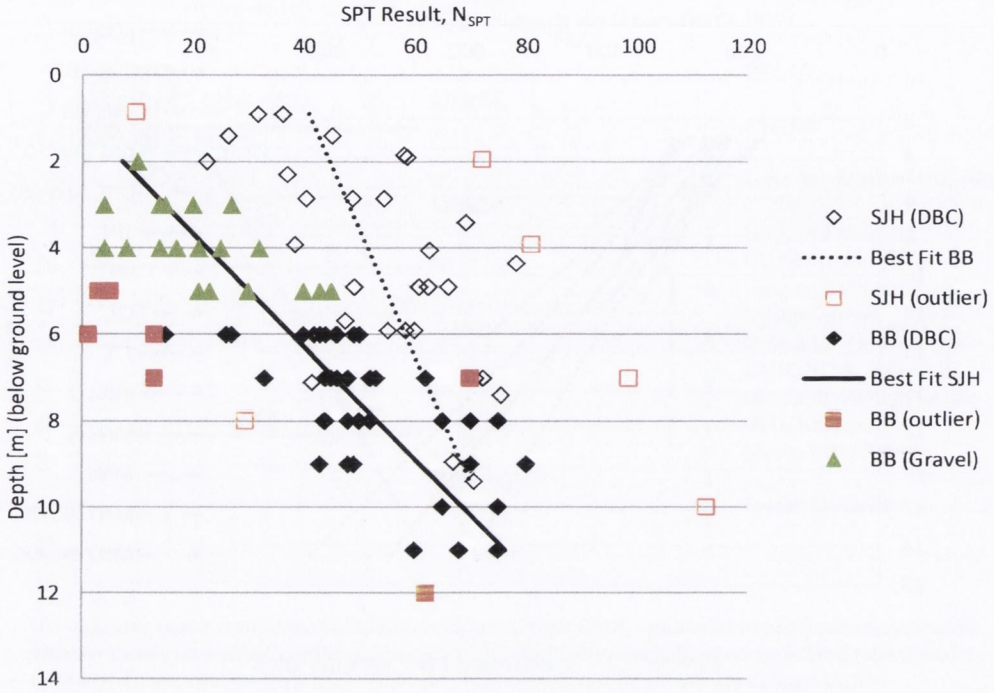


Figure 5.3 – N_{SPT} at SJH and BB sites including outliers and least squares regression lines

The shaft and base resistances are estimated from the N_{SPT} using total stress methods in this fine grained soil, as described in Section 2.2.2, therefore, it is required to estimate the adhesion factor α, the base bearing factor N_c and also the undrained shear strength of the soil s_u. The value of s_u was estimated by multiplication of the N_{SPT} by a correlation factor f_1 taken as 5.5 (see Section 5.1).

Accurate separation of R_s and R_b, using the force-depth profile, requires that the lowest strain measurement be as close to the pile toe as is possible. In the case of TP1 and P600 the strain gauges were placed sufficiently close to the bottom of the piles to enable reasonably accurate separation of R_s and R_b, however, this was not considered to be the case for the TP2 or P450 where the lowest strain gauge reading was 2.30 and 1.35m from the base of each pile respectively and so the data from these piles were not used.

The CFA piles were not loaded to failure, therefore, the relationship between R_s and δ, was assumed hyperbolic and was extrapolated to failure for each of the two piles: TP1 and P600. The shaft friction q_s was calculated by Q_s/A_s and this is plotted against the head

deflection normalised by the pile diameter, δ/D in Figure 5.4. In the short region of the shaft between the lowest strain reading and the base of the pile, q_s was assumed equal to that computed just above the bottom level of strain gauges.

The estimated value of α, calculated by dividing the average q_s by the average s_u is plotted against δ/D in Figure 5.5 where f_1 was taken as equal to 5.5 (see Section 5.1). At δ_f the value of α is coincident for the two piles, marked on Figure 5.5, at around 0.8. The fact that the extrapolated curve for TP1 leads to a lower α value than that for P600 (if extrapolated further), despite the fact that it exhibited a stiffer shaft resistant response, albeit at low deflections, reveals a limitation of Chin's method of extrapolation. This is consistent with Figure 4.3 which showed that where load-deflection data is limited then the value of R_c can be under estimated.

Similarly, due to the piles not being loaded to failure, a hyperbolic relationship was assumed to exist between Q_b and the base deflection δ_b (calculated as δ minus the elastic shortening of the pile) and the stress beneath the pile toe q_b was calculated using Q_b/A_b. The computed curves are shown in Figure 5.6.

The value of q_b was divided by s_u to estimate the value of N_c, this is plotted against δ_b/D in Figure 5.7. It is estimated that N_c values equal to 5.1 and 4.7 were developed in the case of TP1 and P600 respectively during the load tests. On extrapolation of the data, it is estimated that, at δ_b/D equal to 10%, N_c was about 7 on average and tends toward a limiting value just short of 9 on further deflection, this compares with the limiting value of N_c equal to 9 suggested by Skempton (1951) and others for bored piles in clay.

It is recognised the load test results are rather heavily extrapolated – piles TP1 and P600 were loaded to only 1.0 and 4.8% of their diameters. As shown in Section 4.3, this can lead to uncertainty in extrapolated values. P600, however, loaded to almost 5% of the diameter should lead to values at the failure condition within the range 85-100% of the values had the pile been loaded to at least δ_f, this, combined with the fact that extrapolated values applied to the load-deflection data of the other piles compares well, yields some confidence in the extrapolation of this limited load-deflection data.

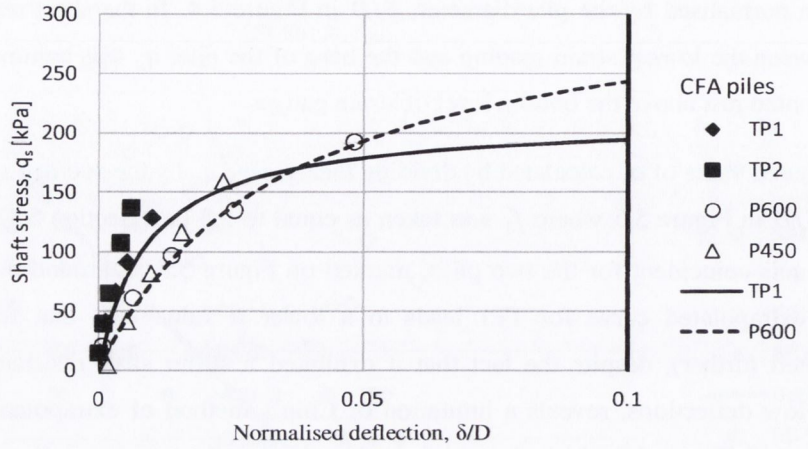


Figure 5.4 – Shaft stress against normalised pile head deflection

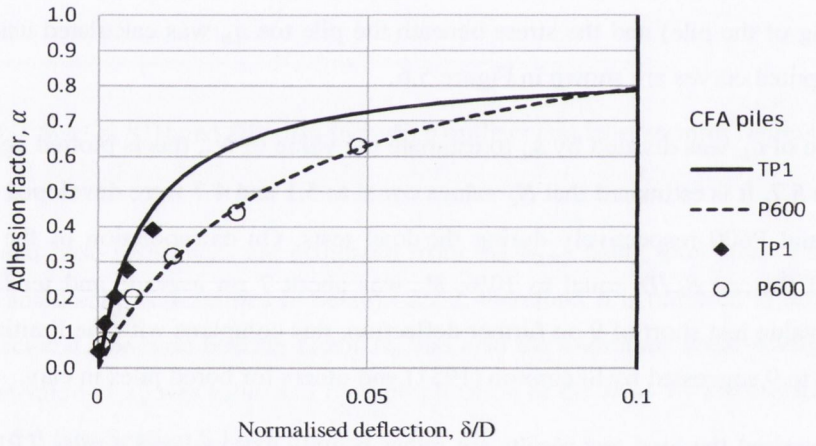


Figure 5.5 – Development of α against normalised pile head deflection

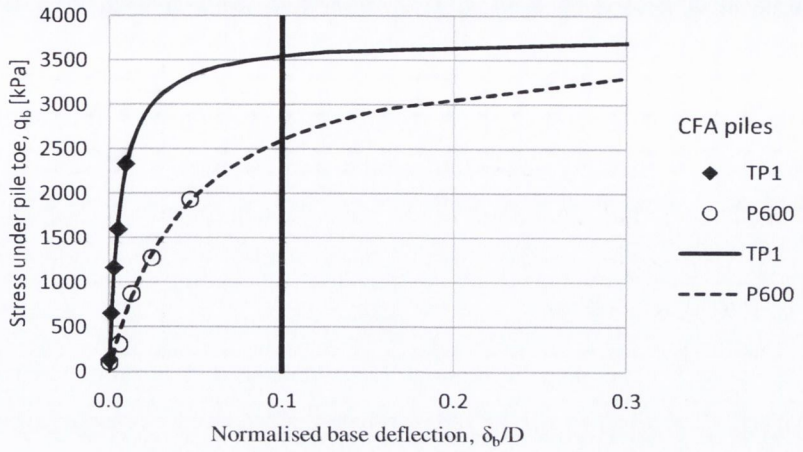


Figure 5.6 – Stress at base against normalised pile base deflection

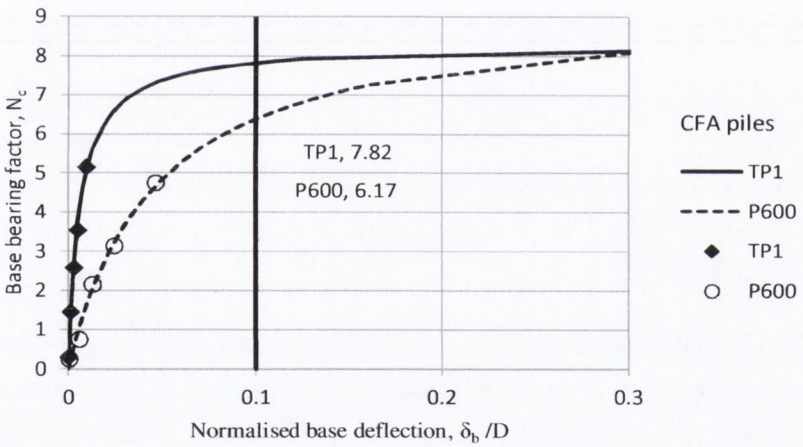


Figure 5.7 – N_c against normalised pile base deflection

5.3 Driven piles

The same method of analysis as that presented in Section 5.2 was applied to the data measured on the instrumented closed-ended steel pile of Farrell (1998) driven at Croke Park, also installed in the DBC. The top three metres of fill were assumed to contribute nothing to the shaft resistance developed as was assumed initially by Farrell et al. (1998).

The measured N_{SPT} are shown in Figure 5.8 where they are regressed with depth – there were no outliers in the case of this data.

The average shaft resistance developed is plotted against the normalised head deflection in Figure 5.9 for the three compression load cycles. It is estimated that around 150kPa was developed at the maximum applied load and hyperbolic extrapolation of the data predicts a limiting shaft resistance of around 230kPa. These values are almost identical to those computed by Farrell et al. (1998).

Taking f_1 equal to 5.5 (justified in Section 5.1) mobilised and extrapolated values of the adhesion factor α, calculated by q_s/s_u are estimated as 0.64 and 1.0 respectively as shown in Figure 5.10, for load cycle 3. At a pile head deflection equal to δ_f, it is estimated that around 80% of the available shaft resistance had developed. It should be noted that the Author's calculated and extrapolated α values are significantly larger than those computed by Farrell et al. (1998) which was based on s_u equal to 450kPa, rather than 5.5 times N_{SPT}.

It should also be noted that, during load cycles 1 and 2, carried out within 2 days of installation of the pile, the interpreted shaft stress and corresponding adhesion factor (shown in Figure 5.9 and in Figure 5.10 respectively) were considerably lower than those for load cycle 3. This is thought to be due to the dissipation of pore pressures built up during pile installation with increasing time after installation resulting in an enhancement of the shaft resistance.

Unlike with CFA piles where the shaft resistance developed on loading remains relatively constant with depth, in the case of driven piles, the shaft resistance increases towards the pile toe (see Figure 2.11). For this reason, the application of an adhesion factor, which relates to the average shaft resistance developed along the pile shaft, may be of limited use in the design of driven piles.

The average stress on the base of the pile, q_b for the three load cycles, is shown in Figure 5.11. The calculated maximum q_b mobilised was about 16MPa with hyperbolic extrapolation suggesting a limiting value of about 26MPa, again in agreement with Farrell et al. (1998). This corresponds to an N_c value of 55 actually developed during the load tests and an estimated limiting value of 90 predicted by hyperbolic extrapolation. At a pile head deflection equal to δ_f it is estimated that around 70% of the limiting stress on the base was mobilised.

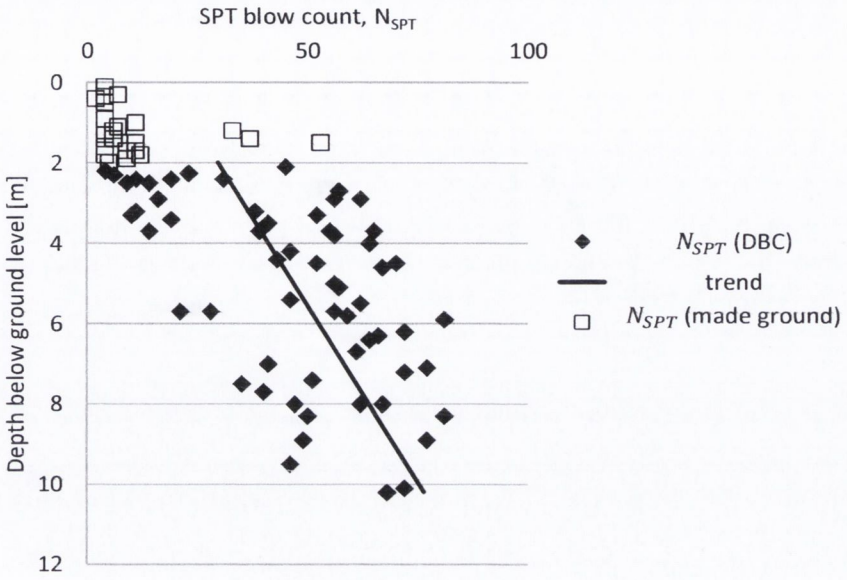


Figure 5.8 – N_{SPT} at Croke Park site with least squares regression line

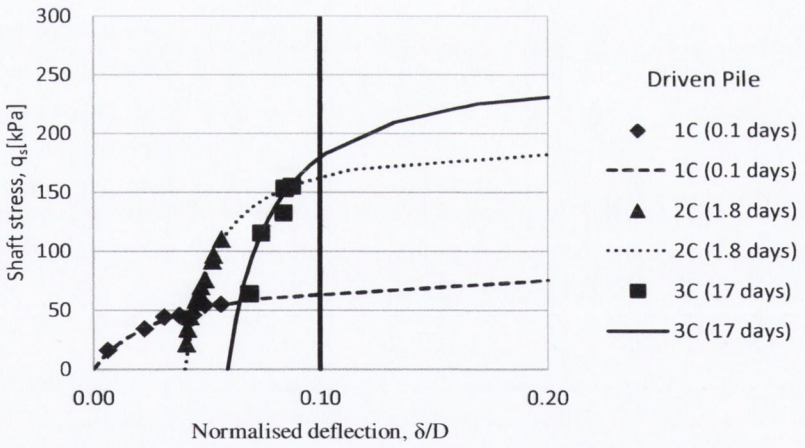


Figure 5.9 – Croke Park: Shaft resistance against normalised pile head deflection

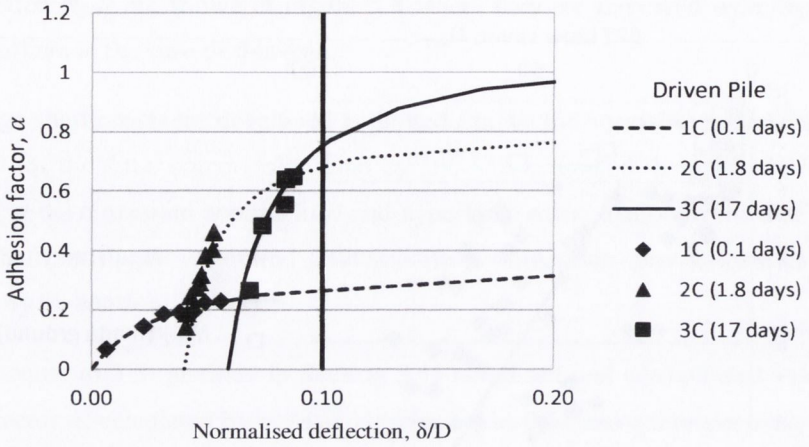


Figure 5.10 – Croke Park: Development of α against normalised pile head deflection

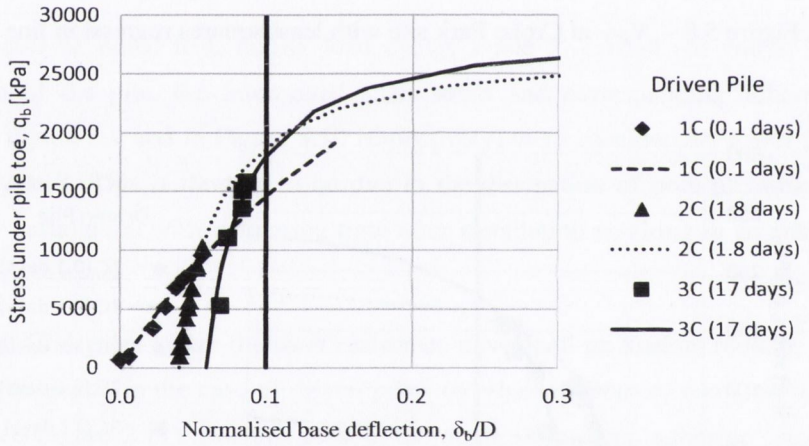


Figure 5.11 - Croke Park: Stress at base against normalised pile base deflection

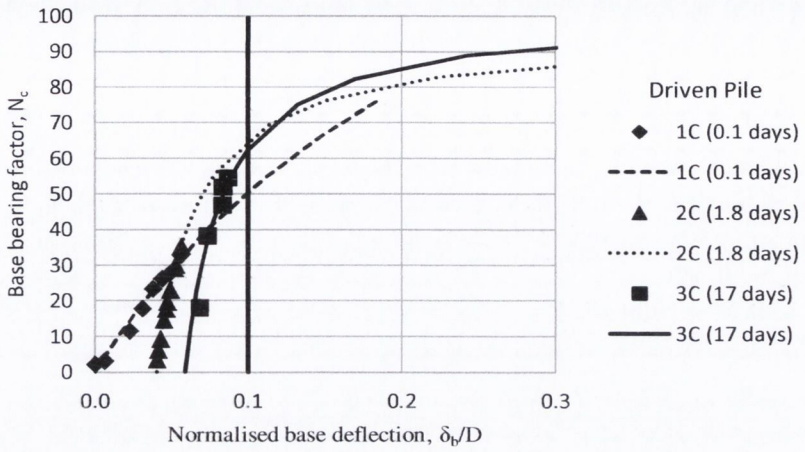


Figure 5.12 – Croke Park: N_c against normalised pile base deflection

5.4 Conclusions from instrumented tests

If the undrained shear strength of the soil s_u is assumed to be a multiple of the N_{SPT} then it is shown to increase linearly with depth for the three sites where the instrumented pile load tests were carried out. Using a multiple of f_1 equal to 5.5, the best fit regression line for the N_{SPT} was converted to s_u and the calculated shaft friction q_s (interpreted from load-depth profile from measured strain) was divided by the relationship to estimate the adhesion factor, α. The α value represents the proportion of s_u mobilised on deflecting the pile by loading.

The computed α values are plotted against the pile head deflection normalised by the respective pile diameters in Figure 5.13. It is estimated that the α value for the two CFA piles is around 0.8 at δ_f and the limiting value is about 0.9. The same is true for the driven steel pile also installed in the DBC, however, given the stress distribution over the length of the driven pile, which is clearly increasing with depth, the α method may not be applicable.

The interpreted α value of around 0.8 at δ_f for both types of pile, is in excess of that typically used in design in Ireland and also of that generally suggested for piles installed in over-consolidated clays, however, is in agreement with values interpreted by Bond and Jardine (1991) where values of α between 0.8 and 1.0 were interpreted for piles driven or piles which were jacked quickly, with an average value of 0.9 soon after installation. These

results were interpreted from load tests carried out on high quality instrumented closed-ended steel piles installed in heavily over-consolidated London clay and are, therefore, considered reliable and relevant.

An auger-bored, 900mm diameter pile, installed in the Lambeth Clay in Canary Wharf, London is reported on by Hight et al. (2004). Interpretation of the instrumentation in the pile during load testing indicated an α value of 0.8 achieved in the Lambeth Clay layer through which the pile penetrated. It is acknowledged that the back calculated α values are highly dependent on the chosen value of s_u as was indicated by the Author in the case of the interpreted α value for the driven pile installed at Croke Park.

A weakness in the analysis is that shaft and base capacities were extrapolated to estimate ultimate values as the piles were not loaded to failure on testing. It was estimated that an α value equal to 0.7 was actually developed for one of the CFA piles and an N_c value of around 5, on extrapolation, the limiting values of these factors for the CFA piles were estimated as 0.9 and 9 respectively (Figure 5.13 and Figure 5.14).

It is clear that there is an increase in the shaft capacity of the driven pile on retesting (see Figure 5.9 and Figure 5.10) thought to de due to the fact that excess pore pressures developed during installation had dissipated (pore pressures were also measured and were seen to dissipate with time) (Farrell et al. 1998).

In the case of the driven pile the α value was estimated as 0.7 and N_c reached 55, the limiting values on extrapolation were estimated as 1.0 and 90 respectively.

Development of the α and N_c factors with pile head and base deflection respectively, are summarised in Figure 5.13 and Figure 5.14 for the CFA and driven piles considered, where s_u is estimated by 5.5 times the N_{SPT}.

Figure 5.13 predicts that α values between 0.8 and unity may be developed with increased deflection in the case of each of the piles. This suggests that potentially the full s_u of the soil may be realised in shaft resistance for both CFA piles and driven piles in some cases. Comparing the lower curve in Figure 5.13, corresponding to the load cycle applied to the driven pile very shortly after installation, with those curves 2 and 17 days after installation, shows that the capacity of the driven pile increases with time after installation, possibly up until excess pore pressures developed during installation are dissipated.

Figure 5.14 suggests that CFA piles develop much lower base resistances than driven piles in the same material. In this particular example the potential base resistance is estimated to be about ten times less for each of the CFA piles than for that of the driven pile.

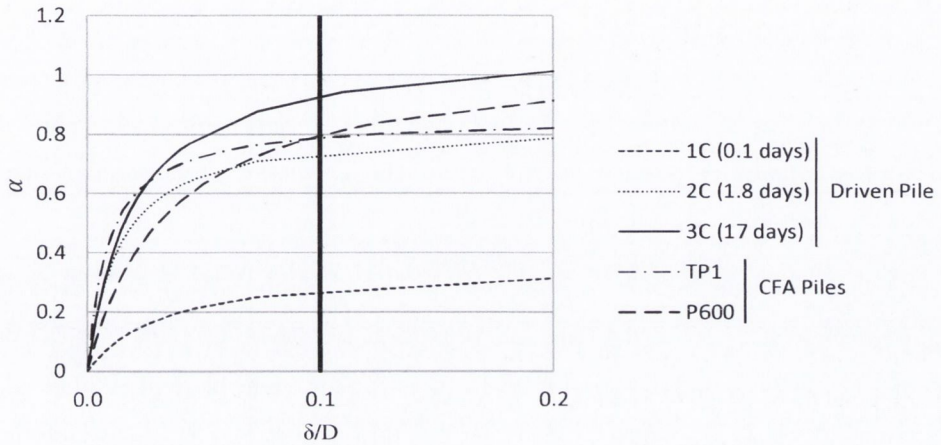


Figure 5.13 – Development of adhesion factor for CFA and driven piles

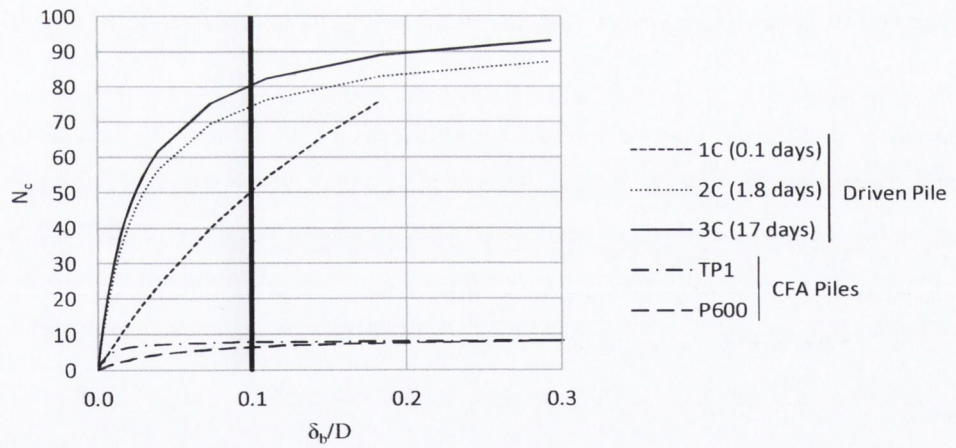


Figure 5.14 – Development of base bearing factor for CFA and driven piles

5.5 Appraisal of calculation factors

This Section is used to make an appraisal of the factors calculated from the instrumented tests presented in Sections 5.2 to 5.4. The calculated factors are applied to the ground test

results from the different sites to estimate the pile resistance and this is compared with that estimated using the pile load test results on the same site.

5.5.1 CFA piles in DBC

The relevant CFA piles, 32 in number, are shown in Table 4.2. Two sites were excluded, Site C as no N_{SPT} were available and Site Q as many N_{SPT} were limited to a value of 50 and are not considered representative of the soil. This brought the total number of piles with which to assess the calculated parameters to 24.

The calculated value of the pile resistance using the α method, $R_{c;cal}$ were divided by $R_{c;chin}$ for each of the piles in the DBC and the results are shown in Table 4.2. The mean value of $R_{c;cal}/R_{c;chin}$ was 1.2 for these CFA piles, which implies that $R_{c;cal}$ overestimates R_c or $R_{c;chin}$ underestimates it. The spread of $R_{c;cal}/R_{c;chin}$ is quite large, and this could be down to errors in the estimate of both $R_{c;cal}$ or $R_{c;chin}$, it is not possible to tell.

Using the calculation model $R_{b;cal}$ is in the range 10-30% of $R_{c;cal}$and is equal to 20% on average and so 80% of $R_{c;cal}$ is, on average, made up by shaft resistance in the case of the CFA piles.

The ratio $R_{c;cal}/R_{c;chin}$ may be thought of as a measure of the bias of the calculation model, (though it is recognised that the value of $R_{c;chin}$ may not be absolutely accurate). A histogram of the bias for the CFA piles in the DBC is shown in Figure 5.15. The average bias is equal to 1.2 suggesting that, on average, $R_{c;cal}$ is an overestimate of R_c where α was taken as 0.8, N_c as 7.0 and f_1 equal to 5.5. Alternatively, $R_{c;chin}$ is an underestimate of R_c, as stated earlier.

The standard deviation of the bias is very large (equal to 0.41), suggesting that it is difficult to estimate R_c with much accuracy. These large deviations are thought to be due to the relatively large variation in the recorded N_{SPT} and also due to limited load-deflection data recorded during the pile load tests. The need for loading closer to δ_f is once again highlighted.

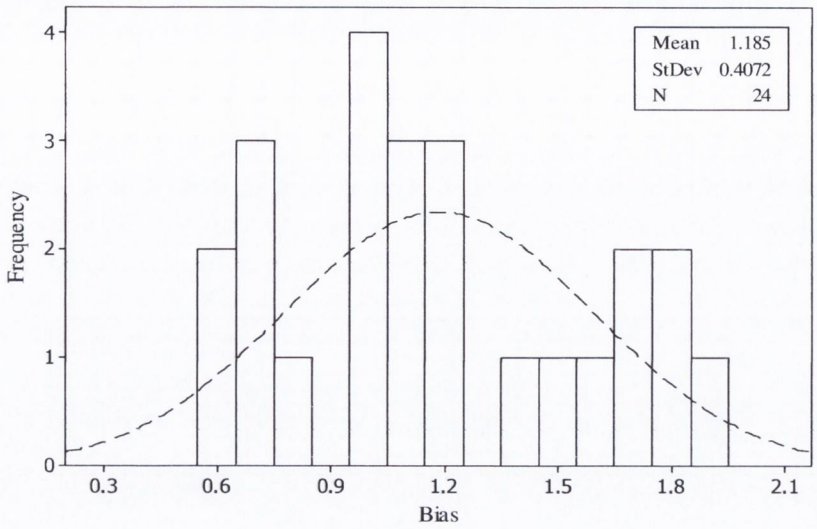


Figure 5.15 – Group 1: Histogram of $R_{c;cal}/R_{c;chin}$

5.5.2 Driven piles in DBC

The same analysis as that presented in Section 5.5.1 was repeated for the 22 driven piles installed in DBC. The parameters for the calculation model were taken as α equal to 0.8, N_c equal to 70 and f_1 equal to 5.5 as outlined in Section 5.4. Chin's method was not applicable to the load-deflection data for one of the piles, thus there are 21 results presented in each of the Figures shown in this Section.

Figure 5.16 shows the ratio $R_{c;cal}/R_{c;chin}$ for these piles and the average value was 1.04 implying that, on average, $R_{c;cal}$ estimates the value of $R_{c;chin}$ rather well. Of the 22 driven piles, 2 were loaded to δ_f and so $R_{c;m}$ was actually known – for the two piles referenced 191 and 192, $R_{c;m}$, $R_{c;cal}$ and $R_{c;chin}$ were 2354, 2162 & 2391 and 2207, 3174 & 2200kN respectively.

In the case of driven piles in DBC $R_{b;cal}/R_{c;cal}$ was 65% on average and ranged from 50-80%, a much greater proportion than that for the CFA piles, which would be expected considering the differences in the method of installation of piles.

The value of $R_{s;cal}$ was computed by the α method and the histogram of the bias, shown in Figure 5.16, displays the spread of the results. The standard deviation was equal to 0.35,

lower than that observed in the case of the CFA piles in the same deposit. This lowered variation may be due to the fact these piles were loaded closer to δ_f with the average ratio δ_{max}/δ_f equal to 35% for this group of piles, compared with just 15% for the previous group of CFA piles. This is thought to be the case as the uncertainty associated with $R_{c;cal}$, expressed as the coefficient of variation in the value, $V(R_{c;cal})$ was equal for both groups at around 34%.

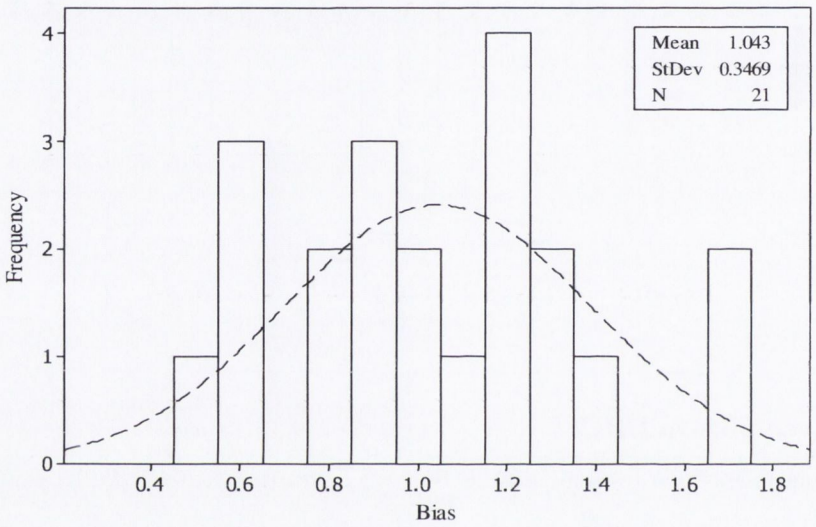


Figure 5.16 – Group 2: Histogram of $R_{c;cal}/R_{c;chin}$

5.5.3 CFA piles in boulder clay other than DBC

The same analysis was applied to the bored piles in boulder clay other than DBC where the values of α and N_c were initially assumed equal to those for the DBC, the results are shown in Table 4.4. The values of the bias, $R_{c;cal}/R_{c;chin}$ are seen in Figure 5.17 to vary around a mean value of 0.97 implying $R_{c;cal}$ and $R_{c;chin}$ are, on average, the same, though there is some variation in the data.

A histogram of the calculated bias, shown in Figure 5.17, reveals the spread of the data, equal to a standard deviation of 0.30 where the mean value is centred close to 1.0.

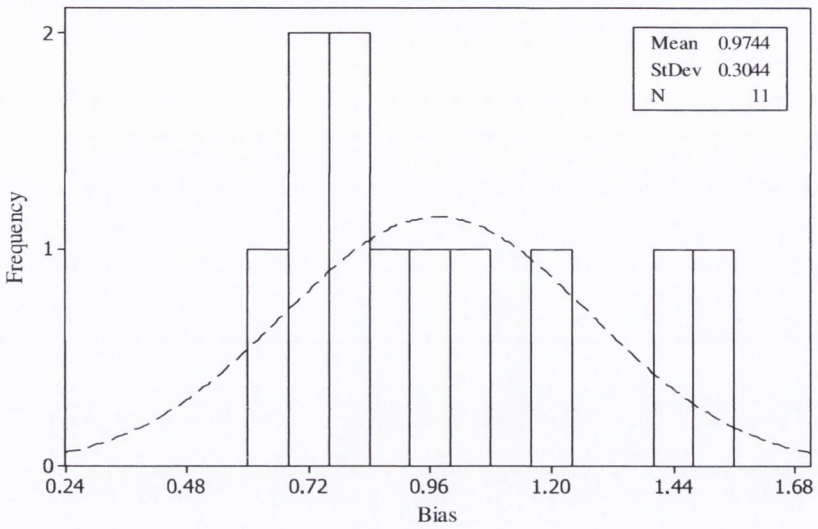


Figure 5.17 – Group 3: Histogram of $R_{c;cal}/R_{c;chin}$

5.5.4 Piles in Sand/Gravel

Though there were no load tests carried out on instrumented piles in coarse grained material (sand/gravel), there were 12 bored piles in coarse grained soil in the PTD that were statically load tested with which to make an appraisal of pile design using Equation 2.3 and Equation 2.9.

The value of N_q was estimated using Figure 2.2 where the value of ϕ' was estimated by correlation of the N_{SPT} as presented by Rahardjo (2001). Prior to estimating N_q, ϕ' was reduced by 3° as suggested by Poulos and Davis (1980) to account for possible loosening of the soil at the pile toe during boring.

The value of R_s was calculated using Equation 2.9 where K was computed using Equation 2.10 and δ was approximated by ϕ' (assuming failure in the soil adjacent to the pile shaft).

A histogram of $R_{c;cal}/R_{c;chin}$ for the 12 piles is shown in Figure 5.18. The mean value of $R_{c;cal}/R_{c;chin}$ is equal to 1.24 indicating that $R_{c;cal}$ is, on average, greater than $R_{c;chin}$. In the case of two of the piles $R_{c;cal}$ was around twice $R_{c;chin}$.

There is considerable uncertainty associated with $R_{c;cal}$ here as N_q is highly sensitive to the estimated value of ϕ' which was based on the highly variable N_{SPT} recorded at the sites.

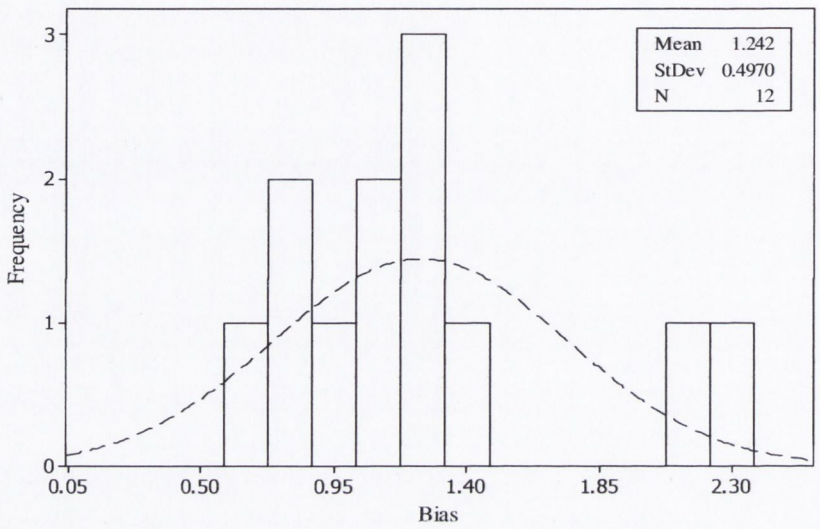


Figure 5.18 – Group 5: Histogram of $R_{c;cal}/R_{c;chin}$

5.6 Conclusions

Using the results of load tests carried out on instrumented piles installed in the DBC, values of α and N_c were evaluated for estimation of $R_{c;cal}$ at δ_f.

The value of α was estimated to be around 0.8 for both CFA and driven piles at δ_f. The base bearing factor N_c was estimated as equal to 6.5 and 65 for the CFA and driven piles respectively at δ_f. These results were computed where the undrained shear strength of the soil s_u was estimated from the N_{SPT} using a multiplication correlation factor f_1 equal to 5.5, which was verified by comparison of the N_{SPT} results for several sites comprising DBC with the results of triaxial tests carried out on the same material.

Appraisal of these calculated factors was then completed using the results of other load tests carried out on bored and driven piles in the DBC deposit and on sites for which SPT results were available. There were 24 No. bored piles over 5 different sites and 21 No. driven piles over 2 different sites, with which to make the assessment.

As the majority of the piles were not loaded to δ_f, the load-deflection data recorded for each of the piles were extrapolated to δ_f using Chin's hyperbolic method, described in Section 4.1, and this parameter was denoted $R_{c;chin}$. The ratio $R_{c;cal}/R_{c;chin}$ was then used to assess the factors calculated from the instrumented tests.

It was found that the average $R_{c;cal}/R_{c;chin}$ was equal to 1.19 and 1.04 for the CFA and driven piles, with standard deviations of 0.41 and 0.35 respectively. This implies that the value of $R_{c;cal}$ using the factors deduced from the instrumented pile load tests, overestimates the value of R_c or alternatively $R_{c;chin}$ underestimates it, in the case of the piles under study.

As these piles were loaded to an average ratio δ_{max}/δ_f equal to 21% it is likely $R_{c;chin}$ is an underestimate of R_c (see Figure 4.12) and it is believed that the combination of $\alpha = 0.8$, $N_c = 6.5$ and $f_1 = 5.5$ leads to an estimate of R_c better than that implied by Figure 5.15.

In the case of the driven piles installed in DBC, the variation in the estimated bias was less than that for the CFA piles, thought to be due to the fact that these piles were loaded to an average ratio δ_{max}/δ_f over twice that for the CFA piles, equal to 35%, and thus leading to a more accurate estimation of $R_{c;chin}$. The fact that the average $R_{c;cal}/R_{c;chin}$ is equal to 1.0, suggests the combination of $\alpha = 0.8$, $N_c = 65$ and $f_1 = 5.5$ leads to a realistic estimate of R_c for driven piles installed in DBC.

The results imply that the base resistance mobilised on static load testing of a driven pile in DBC is significantly greater than that mobilised on loading a CFA pile in the same deposit, thought to be due to the differences in installation effects between the two types of pile and is in agreement with Gavin et al. (2008).

6 Instrumented piles toed in rock

The results of pile load tests carried out on instrumented piles toed in rock were analysed to examine the behaviour of rock rocketed piles in Ireland. The results of load tests in the literature, plus an additional two, instrumented and tested by the Author, are used to produce estimated base and shaft resistance development with pile deflection with respect to the rock socket.

This Chapter details the instrumentation installed in the Author's two piles and the data acquisition equipment used to interrogate and log the data during pile loading. A force-depth profile for each pile is interpreted from the strain-depth measurements taken during pile loading. Additional instrumented load tests, made available to the Author, are then presented to make conclusions on the behaviour of rock socketed piles.

6.1 Instrumented Pile Tests

6.1.1 Site Location

The test site was located at Carranstown, Co. Meath, about 3 km north of Duleek and approximately 130m North-West of the Duleek to Drogheda road. The topography of the field hosting the test site ranges from about 37mOD in the eastern corner to about 31mOD in the north-eastern corner, to about 30 and 32mOD in the western and south-western corners respectively (IGSL 2009).

6.1.2 Pile Installation

Two instrumented CFA piles, 450 and 640mm in diameter and 13.94 and 9.85m in total length, (with 0.6m extending above the ground surface in both cases) were installed at the site using a P135 piling rig and these are hereafter referred to as P450 and P640 respectively. Both piles were reinforced with full length steel cages comprising eight T32 full length longitudinal bars held together by a 10mm helix – the usual 75mm cover was provided to the steel.

P640 was installed by P J Edwards on Wednesday 8th July 2009; and P450 on Thursday 9th July 2009. The pile logs, from the piling rig, for P450 and P640 are shown in Appendix C in Figure C.1 and Figure C.2 respectively.

6.1.3 Ground conditions

A combination of soil resistivity measurements and multichannel analysis of surface wave (MASW) profiling were undertaken at the site to indicate vertical variation and to interpret the stratigraphy. Rotary coring, logs (RC2, RC4, RC6 and RC7) were also carried out to assist with the interpretation of the geophysical data. These indicated between 5.1 and 12.2m of boulder clay overlying strong limestone bedrock.

Cable percussion boreholes (BH1-BH7) were also carried out at the site. Generally the overburden, of minimum thickness 4.5m, could be described as a stiff sandy gravelly clay/silt (boulder clay) with some cobbles. The N_{SPT} values recorded were in the range 12-23 with an average value of 18, as shown in Figure 6.1 and no correction factors were applied to the these values. The cable percussion boreholes refused at depths of between 4.4 and 5.4 m below ground level while the coincident rotary core boreholes recorded rock at between 7.6 and 12.2 m below ground level.

The interpreted stratigraphy in the vicinity of each of the instrumented test piles is shown in Figure 6.2 and Figure 6.3 for P450 and P640 respectively and a legend for use with these Figures is shown in Figure 6.4. The pile head in each case is below the original ground level as shown in Figure 6.3 and Figure 6.2; this is because the site was excavated to the piling platform level after the site investigation was carried out.

The results of uniaxial compressive strength (UCS) tests, carried out on the limestone bedrock, are presented alongside UCS values interpreted from point load tests in Table 6.1. Total core recovery of 100% was achieved close to P450 while a void was identified close to P640 and the rock quality designation and fracture spacing index averaged 80% and 5 respectively.

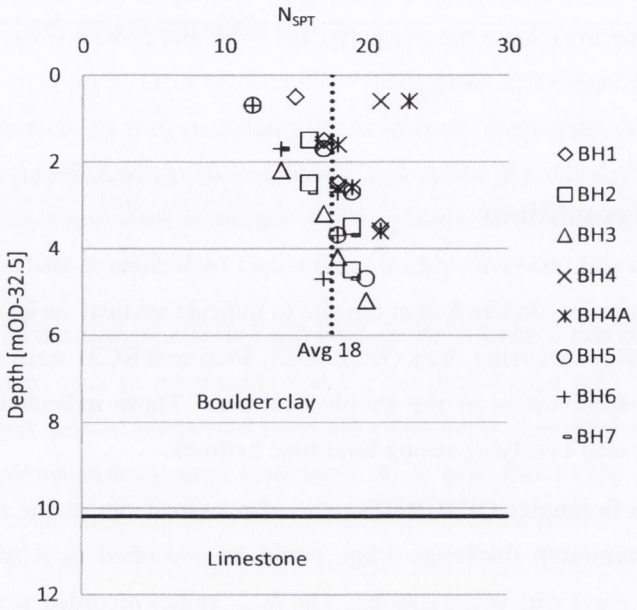


Figure 6.1 – Duleek: N_{SPT} (IGSL 2009)

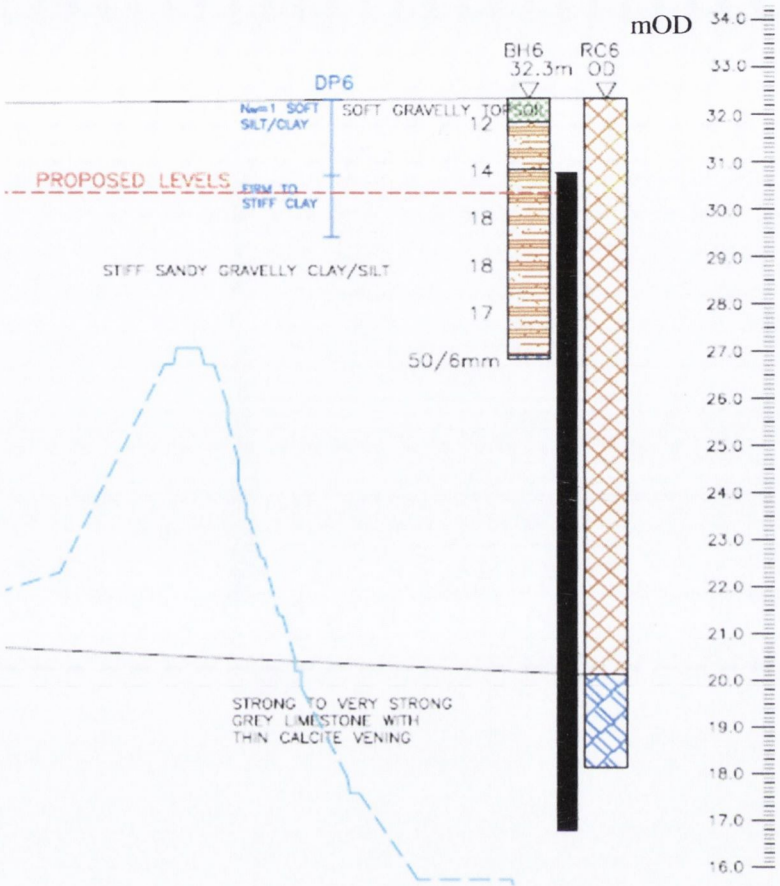


Figure 6.2 – Stratigraphy in vicinity of P450

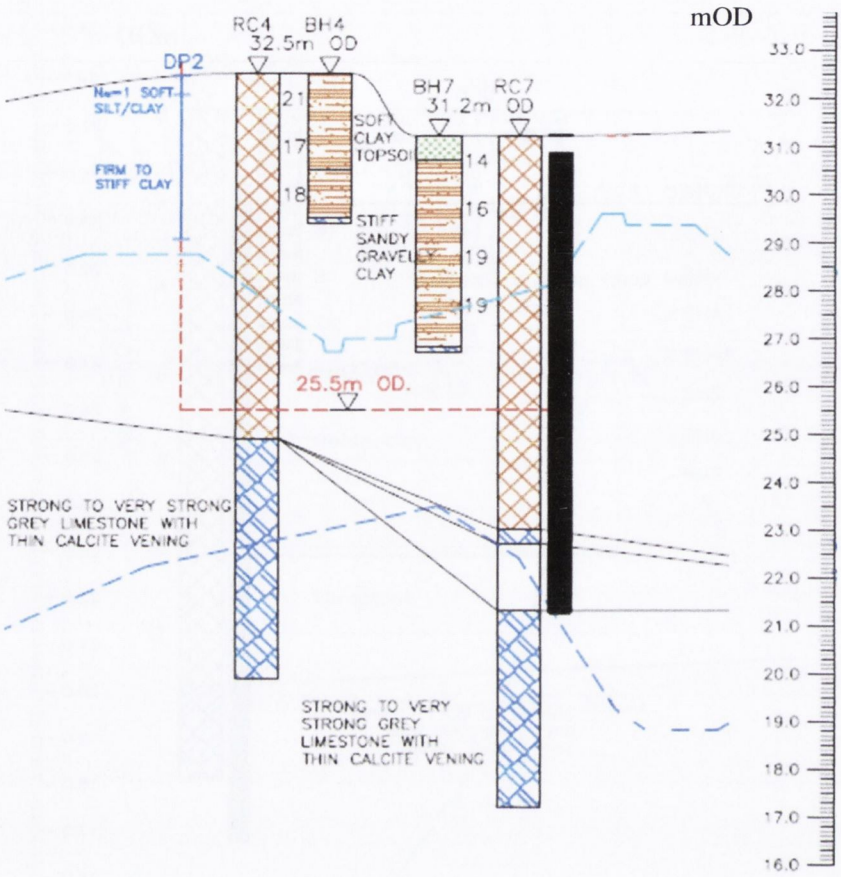


Figure 6.3 – Stratigraphy in vicinity of P640

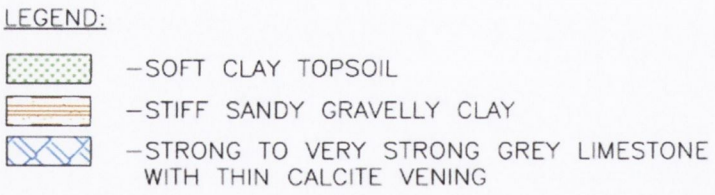


Figure 6.4 – Legend for use with Figure 6.3 and Figure 6.2

	(a)	(b)	(c)
$q_{u;mean}$	45.4	147.3	117.0
z_{mean}	8.6	9.1	9.4
s	15.2	37.9	29.7
n	8.0	8.0	29.0
V	33.4	25.8	25.4
$q_{u;min}$	26.7	93.0	93.0
$q_{u;max}$	72.2	224.0	169.0
L 95% CI	15.7	72.9	58.8
U 95% CI	75.1	221.6	175.1

Table 6.1 – Summary of q_u statistics on rock at Duleek test site (a) from UCS tests and (b) and (c) from point load tests

6.1.4 Load Test Arrangement

The piles were statically load tested simultaneously by the maintained load method using two separate load test frames with separate data acquisition equipment (DAE) allocated to each test. Testing began on Wednesday 15th July 2009, approximately 7 days subsequent to installation.

The test arrangement for P450 is shown in Figure 6.5 and shows the hydraulic jack placed on the pile head, in line with a load cell of maximum capacity 5MN, acting against a reaction frame which comprised a long main beam, two secondary cross beams and four tension anchors – the test arrangement for P640 was similar and both load test frames were capable of resisting a maximum load of 6000kN, applied mid-span, at this spacing.

6.1.5 Instrumentation

The Geotechnical Laboratory of TCD instrumented the steel reinforcement cage for each test pile with an array of strain gauges comprising a combination of foil gauges and vibrating wire gauges at six different levels.

The foil gauges were located in a ring arrangement of four gauges, with one gauge on each alternate bar of the eight longitudinal bars, at each of the levels. Details of the levels of the strain gauges and which type was used and where are shown in Table 6.2 for the two piles.



Figure 6.5 – Test arrangement, P450

Table 6.2 – Strain gauge arrangement

P450 Depth	No. Gauges	Type	P640 Depth	No. Gauges	Type
1.3	1	VW	0.1	4	F
3.3	5	4F & 1VW	0.6	3	VW
5.3	4	F	7.6	4	F
12.5	5	4F & 1VW	8.0	3	VW
12.9	4	F	8.4	4	F
13.2	4	F	9.1	4	F

6.2 Static load test results

The readings taken during the static load tests included pile head load-deflection measurements with time and also strain measurements throughout the depth of the pile at the various load increments, the measured values are presented in this Section.

6.2.1 Pile head load-deflection-time

The measured pile head load-deflection data for each of the test piles is displayed in Figure 6.6. Load cells were used to measure the load applied at the pile head together with the readings from pressure gauges on the hydraulic jacks used to apply the load. The deflection

measurements were taken using a combination of dial gauges on the top of the piles, together with a precise level.

The piles were loaded in accordance with a pre-determined load-time regime as much as possible, while limiting the maximum measured rate of deflection over individual load increments to 0.1mm per hour, in keeping with the Institution of Civil Engineers specification (ICE 2007). The load-time graphs for the two piles are shown in Figure 6.7 (notice F_k was maintained overnight in the case of each pile).

Both the piles were loaded to a maximum test load equal to 2.5 times F_k, which is normal practice for these preliminary test piles. P450 was loaded to a maximum of 2500kN with two unload-reload cycles and the measured deflection at the maximum load was 5.2mm, the residual deflection on unloading was 1.8mm. P640 was loaded to a maximum of 5000kN, over four load cycles and the corresponding deflection was 12.1mm. The residual deflection for P640 was 6.6mm.

The load-deflection plots for P450 and P640 are shown in Figure 6.6 (a) and in Figure 6.6 (b) respectively.

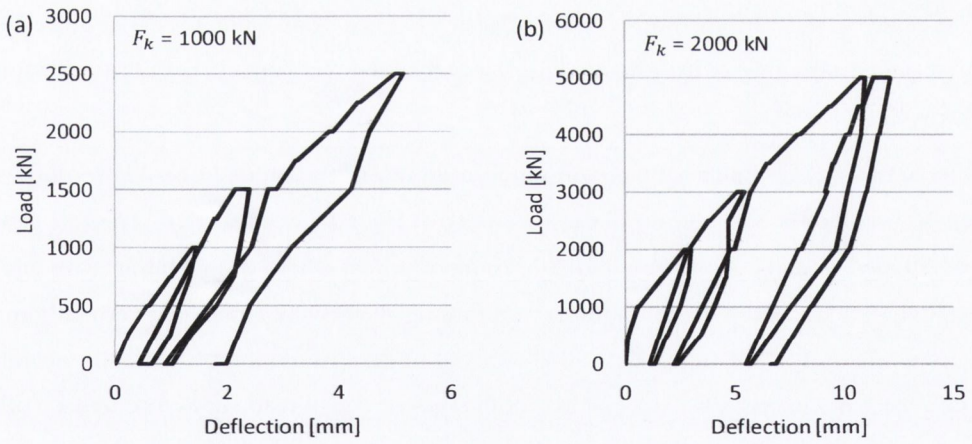


Figure 6.6 - Pile load-deflection data, (a) P450 (b) P640

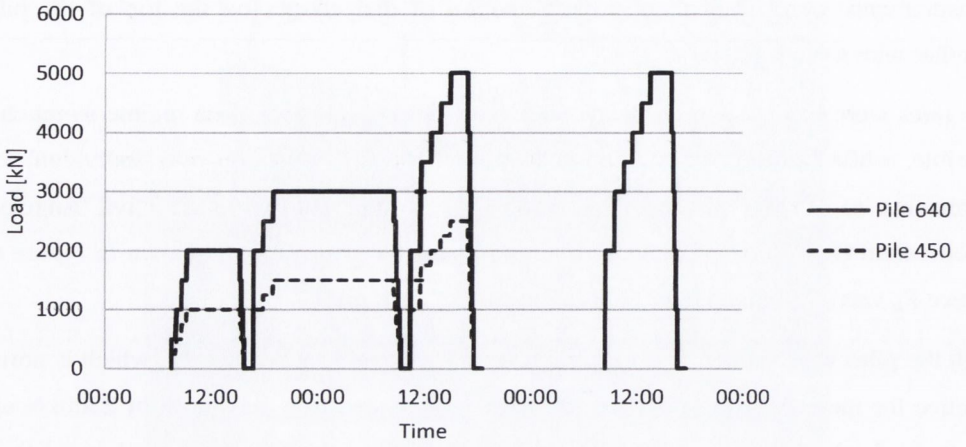


Figure 6.7 – Load-time graphs for instrumented test piles

6.2.2 Strain-depth measurements

The strain values measured at each level in P450 and P640 are displayed in Figure 6.8 and Figure 6.9 respectively and come from a combination of readings from the two types of strain gauge installed. The two types of gauge in P450 agree well yielding almost identical strain values at the various levels at particular head loads. The results for P640 suggest that the vibrating wire gauges may be reading lower than the foil gauges; the reason for this is unknown.

The results validate the common assumption used in estimation of force-depth profiles in piles – that there is equal strain in each element of the pile cross-section. The foil gauges were adhered directly to the longitudinal reinforcing bars where the vibrating wire gauges (although tied loosely to the longitudinal reinforcing steel) were embedded vertically in the concrete adjacent to the steel. A detailed account of the installation of the instrumentation is presented in Appendix C. The fact that both types of gauge read very close to each other, at corresponding levels in the piles, indicates that there is indeed equal strain over each element of the pile cross-section in the case of these piles.

Only the strain readings during load cycle four on P640 are shown in Figure 6.9 due to problems with the DAE used with this pile. The DAE used initially was a new system, on-site for the first time and did not perform as expected. The corrupt/partial data files it produced were sent to the manufacturer who salvaged the data, however, this was not

deemed reliable for interpretation by the Author. During load cycle four the DAE used with P450 was used and there were no problems.

It should be noted that some of the foil strain gauges, of which there were four at each level, were not considered in the analysis due to erroneous readings thought to be due to inadequate moisture proofing. The survival rate of the foil gauges was around 66%.

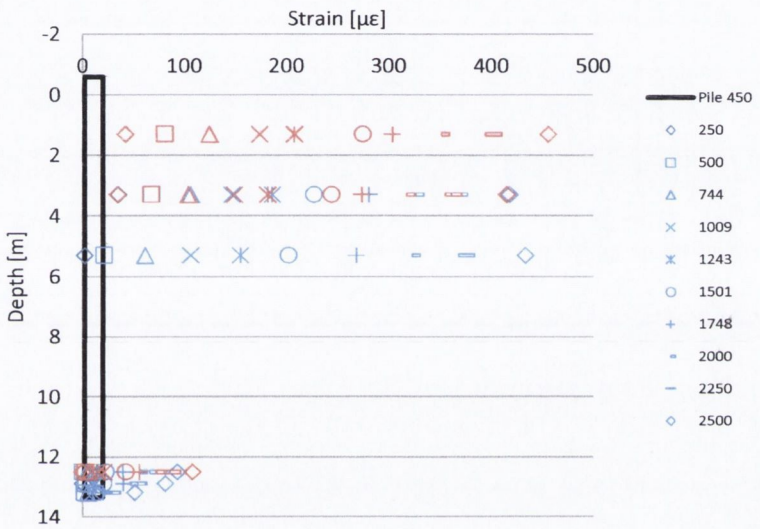


Figure 6.8 – Measured strain-depth P450

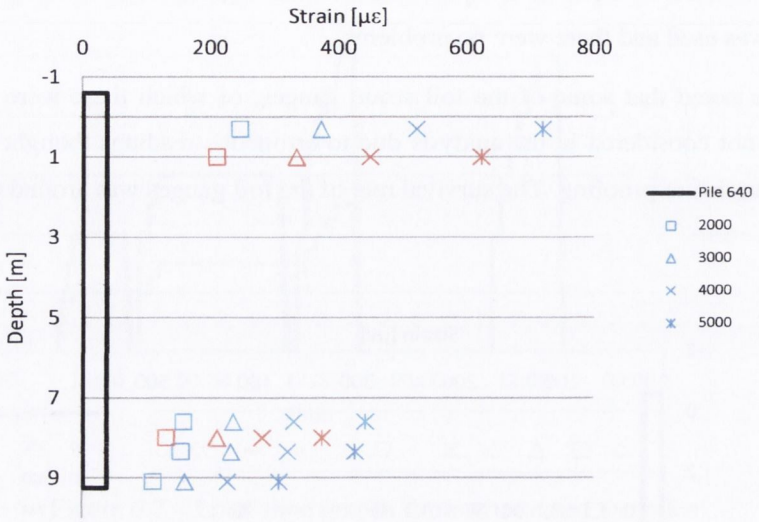


Figure 6.9 – Measured strain-depth P640

6.2.3 Interpreted force-depth profile

The strain readings were logged continuously for intermittent periods throughout the load test sequence and were interpreted to estimate the force-depth profile for each of the two CFA piles tested.

Theoretically the force, F at a given level in the pile is given by Equation 6.1.

$$F = \varepsilon E_G A_G \qquad 6.1$$

where ε is the measured strain, E_G is the gross stiffness of the pile and A_G is the gross cross-sectional area. However, the parameters E_G and A_G may be difficult to ascertain accurately, in particular, where bored piles are installed in-situ or are cast-in-place, as variability of concrete and methods of placement lead to variation in E_G, also A_G may vary along the length of a pile.

The value of E_G depends on the stiffness of the elements making up the cross-section of the pile (often a combination of steel and concrete) at the location of the strain gauge. The stiffness of the steel E_s is fairly accurately known but the stiffness of the concrete E_c is not, and varies with strain level, with time and also with the materials used in the concrete mix. The value of E_c may be estimated from the ACI formula shown in Equation 6.2 (Hayes and Simmonds).

$$E_c = k f_c^{0.5} \qquad 6.2$$

where f_c is the unconfined compressive strength of the concrete (measured from cylinder tests) and k is a constant, usually 4700 (when f_c is in MPa). Concrete cube strength is about 125% of the cylinder strength of the same concrete (CEN 1992).

This method may be used to estimate E_c but, it should be noted that, f_c also depends on the unit weight of the concrete and it has been shown that the usual methods by which concrete cylinders are cured prior to testing may result in significantly reduced values of f_c compared with those achieved in the mass concrete (Khan et al. 1995).

Furthermore, it is not sufficient to estimate the load in the pile at the various depths assuming a constant value of E_G as this may vary considerably with strain level (as stress varies with strain level shown in Figure 6.10) and over a wide strain range an accurate computation of E_G may be required during a pile load test. It should be noted that Figure 6.10 comes from a real measurement.

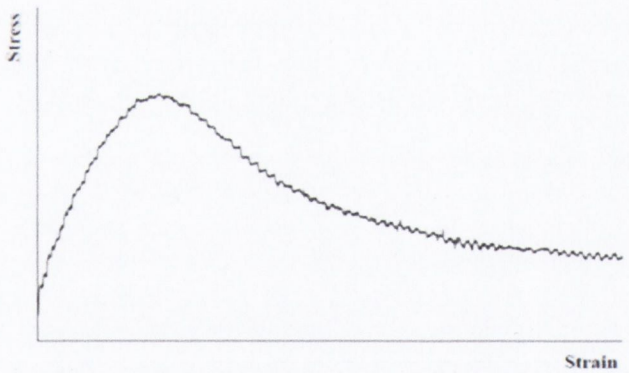


Figure 6.10 - Characteristic stress-strain behaviour of SCC with a thixotropic structure (Billberg 2006)

An alternative method by which E_G may be estimated at varying strain level, is to consider a ring of strain gauges positioned close to the top of the pile (at depth less than or equal to 0.5m) then, in this region, the registered strain readings will be directly due to the applied head load, as close to the top of the pile, there will be minimal reduction in load due to shaft resistance in this short region.

The value of E_G may be estimated close to the pile head within the range of the strain level induced by the applied load (registered by the strain gauges). A polynomial is then used to approximate the relationship between E_G and the strain level in the pile and this may be assumed at each depth where strain gauges are located to estimate the force at that depth using Equation 6.1 (assuming the pile cross section remains constant with depth).

This method is simplified by the Author as outlined in this section. The various loads applied to the piles were plotted against the corresponding strain gauge readings from the strain gauges closest to the top of both of the pile heads to produce a load-strain relationship for each. The load-strain relationships plotted for P450 and P640 are shown in Figure 6.11 and are close to linear up to 400με.

The load-strain relationship for P450, comprising the results of three load cycles, shows that the effects of unload-reload cycles do not much affect the relationship – on reloading the pile subsequent to unloading, the load-strain values appear to reach the original load-strain relationship and continue to follow this relationship on further loading.

The load-deflection data for the piles, shown in Figure 6.6, also imply that the effects of unload-reload does not much affect the interpretation of the results – in the case of both the piles, the load-deflection trend appears to follow the same pattern subsequent to unload-reload cycles and there is no obvious deviation from the load-deflection trend subsequent to an unload-reload cycle.

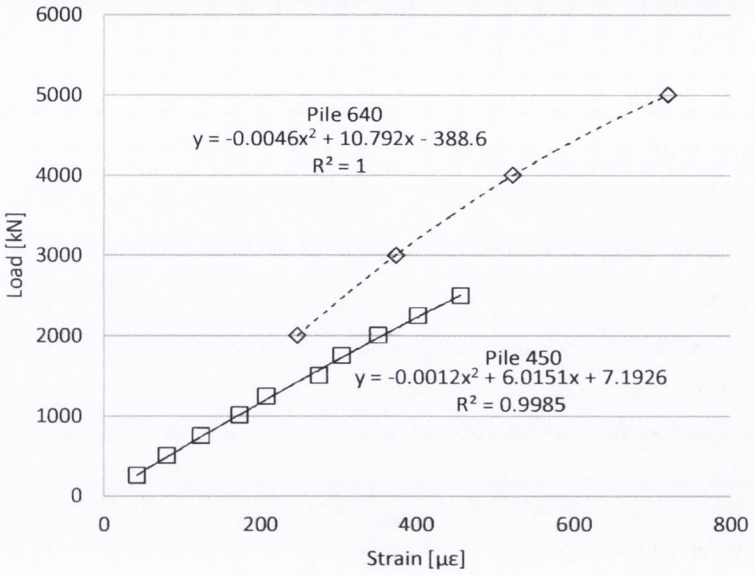


Figure 6.11 - Load-strain relationships, P450 and P640

Interpreting the load from the strain readings in this way overcomes the need for complicated and often unreliable methods of estimation of in situ mass concrete stiffness, E_c which is known to vary with strain level (Fellenius 1980; Fellenius 2001; Billberg 2006); however, these methods are investigated in Section 6.2.5 for completeness.

Concrete stiffness is often estimated using either the results from tests on concrete cylinders or cubes taken from the test pile, which can yield variable results. Also, if a constant value of E_c is assumed over the wide range of strain induced during a pile load test, it is reported this can lead to errors in the range 10-20% in the values of the interpreted force at the various depths, (Fellenius 2001; Fellenius 2002).

The force-strain relationship close to the pile head incorporates the change in E_c with strain level when applied to each instrumented level in the pile. This method of analysis does, however, assume a constant value of E_c with depth which may not be the case.

It has been suggested, that, E_c may vary with depth and that this effect is due to the natural compaction process of the concrete under its own self-weight during placement (Ng et al. 2000). In a static load test on an instrumented barrette in Hong Kong, a continuous concrete core was taken to a depth of 40m, along the central axis of the barrette (Ng et al.

2000). The value of E_c was determined at various depths by laboratory test and the results are shown in Figure 6.12. Although there is a slight increase in the value of E_c with depth (from about 24-28GPa over 40m), this increase is not statistically significant due to the relatively large spread of the data, and therefore, there is not sufficient evidence to indicate that E_c does indeed increase with depth.

The interpreted force-depth profiles are shown for P450 and P640 in Figure 6.13 and in Figure 6.14 respectively. Considering P450, about 20% of the applied load was estimated to have been resisted by shaft resistance in the boulder clay layer overlying the bedrock, with 70-80% being resisted by the pile shaft in the limestone bedrock leaving virtually zero load to be resisted by the toe of the pile. Even at the maximum applied load of 2500kN only about 300kN (12%) was estimated to be resisted in end bearing.

P640 behaved differently, it had a much shorter rock socket – about 1.9m, compared with just over 4m for P450. In this case, again about 20% of the applied load was resisted in the overburden layer with a further 30% resisted by the pile shaft in the bedrock and about 50% of the applied load was estimated to have been resisted in end bearing.

It should be noted that, in the case of P450, there were no strain gauges located between 5.3 and 12.3m depth – the average skin friction developed in the rock and in the overburden layers, interpreted using the other strain gauges, was assumed to be constant within this region of the pile in each of the layers and was extrapolated back to the boundary between the two stratigraphic layers as shown in Figure 6.13 to produce the force-depth profile shown.

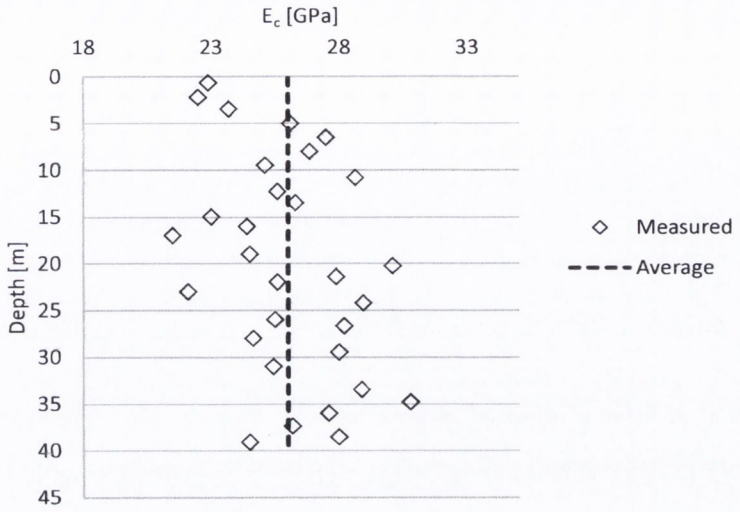


Figure 6.12 – E_c values with depth (mean and best fit interpreted by Author (Ng et al. 2000)

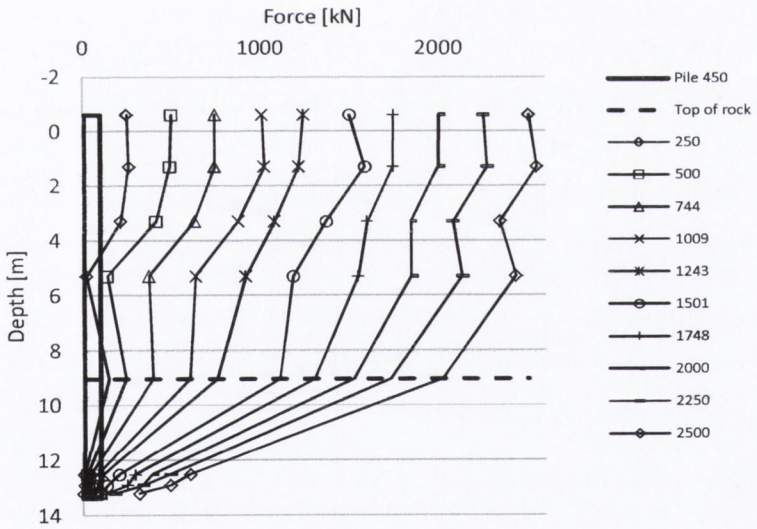


Figure 6.13 – P450: Interpreted force-depth profile

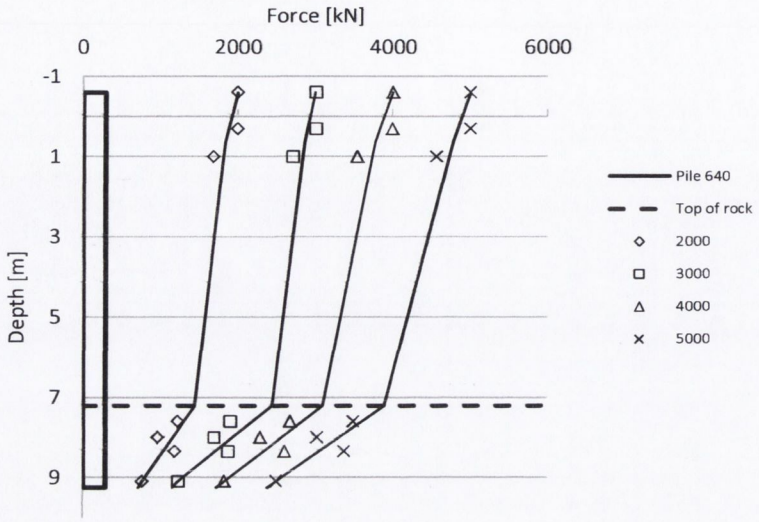


Figure 6.14 – P640: Interpreted force-depth profile

6.2.4 Interpreted shaft resistance

The interpreted shaft resistances developed for P450 and P640 are shown in Figure 6.15 and in Figure 6.16 respectively. The shaft resistance was similar for each pile, with little resistance developed in the boulder clay layer – about 30 and 80kPa for P450 and P640 respectively. The shaft resistance developed in the rock layer, $R_{s;rock}$ was almost 300kPa for P450 and around 370kPa for P640 which was deflected by a greater amount under load.

The calculated values of $R_{s;rock}$ are analysed further in Section 6.3 to consider the design parameters generally used to calculate $R_{s;rock}$ given the properties of the rock in which the pile is installed, measured by laboratory test.

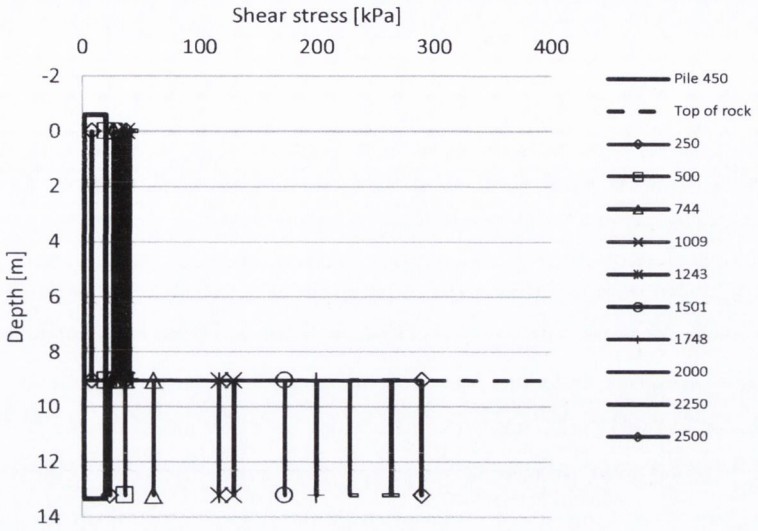


Figure 6.15 – P450: Interpreted shaft resistance

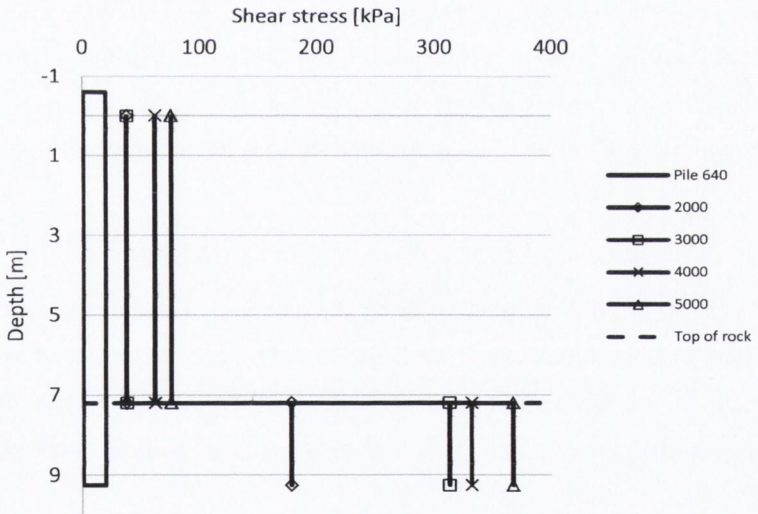


Figure 6.16 – P640: Interpreted shaft resistance

6.2.5 Pile stiffness

This section considers several methods of estimation of the gross pile stiffness's E_G for use with Equation 6.1.

Concrete cylinders were taken from the concrete batches supplied to P450 and these were instrumented with strain gauges and loaded to provide an estimation of E_c for comparison to that back calculated from the load-strain relationship measured at the pile head during the pile load test. The value of E_c from concrete cylinders is affected by differences in curing and due to scale effects between the in situ mass concrete of the pile and the controlled curing in a water bath specified for test cylinders.

In light of the limitations of estimating E_c from concrete cylinders cured in the laboratory, a 2m length instrumented dummy pile was installed immediately after construction of P450 using the same piling rig and only a few metres away at the same elevation. The dummy pile was allowed to cure under the same conditions as P450 itself, for several days, before excavation, transportation and load testing in the geotechnical laboratory at TCD. A detailed account of the installation, instrumentation and testing of the dummy pile is shown in Appendix C.

Figure 6.17 shows both the secant and tangent pile stiffness estimated using the load and strain measurements close to the pile head during load testing, these parameters are denoted $E_{G;secant}$ and $E_{G;tangent}$ respectively. P450 is of higher stiffness than P640, which is to be expected as the cross-section of P450 has a greater proportion of steel then P640. P450 is represented by square symbols and continuous lines in Figure 6.17. As expected, both moduli degrade with increasing strain for both the piles due to a degradation of the stiffness of the concrete in the piles.

A theoretical estimate of $E_{G;secant}$ for P450 and P640 is also shown in Figure 6.17 (horizontal lines) where no degradation in E_c for increase in strain was accounted for. It can be seen that, if this estimate were used with Equation 6.1, it could lead to considerable error in the estimate of the force at a particular level in the pile, especially as the strain in the pile increases under load. The reduction in $E_{G;tangent}$ is more marked than that of $E_{G;secant}$ in the case of both the piles.

Figure 6.18 is a plot of the calculated concrete stiffness, $E_{c;secant}$ and $E_{c;tangent}$ versus strain measured during compression loading of two similar concrete cylinders comprising concrete from the same batch as that used in P450. The cylinders were cured in a water bath at constant temperature at TCD for 14 days prior to compressive testing to estimate concrete stiffness with varying strain. Details of the instrumentation, load testing and of the results of the cylinder tests is presented in Appendix C.

Figure 6.18 clearly indicates degradation of E_c with increasing strain. The value of $E_{c;secant}$ reduces from 35 to 25GPa for one cylinder and from 30 to 20GPa for the other, a reduction of around 35% over the range of strain induced during the load test on P450. The value of $E_{c;tangent}$ is consistently lower than $E_{c;secant}$ over this strain range, with an average value of about 22GPa considering both the cylinders.

The ACI formula (Oluokun et al. 1991), for calculation of the concrete modulus from compressive testing of cylinders, results in a value of $E_{c;secant}$ of 36GPa for both cylinders (both cylinders recorded the same ultimate stress at failure) and this agrees well with the values presented by the Author for cylinder 1 (Figure 6.18) at low strain levels. This formula does not, however, encapsulate concrete stiffness degradation with increasing strain, which is necessary for accurate computation of force from strain measurements taken in instrumented bored piles.

If the stress-strain response observed in carrying out the load tests on the concrete cylinders is interpreted to estimate the gross stiffness of P450, (considering the increased cross-sectional area and also the steel reinforcement in the pile) then the stiffness-strain relationships shown in Figure 6.19 are calculated.

When compared to the stiffness-strain relationship for P450 in Figure 6.17, the results from the stiffer cylinder are almost identical, indicating that it is valid to estimate the gross stiffness of a pile by interpretation of instrumented cylinders of concrete taken from the same concrete used to construct the pile.

The results from the second cylinder, however, contradict this, as it reads about 35% lower in terms of stiffness over the strain range induced during the pile load test, which, if applied in Equation 6.1, would lead to a substantially reduced value of the calculated force at a given strain. The variability associated with laboratory tests on concrete calls for a significant number of tests with which to estimate a mean value of E_c with some confidence for use with Equation 6.1.

Figure 6.20 shows the values of $E_{G;secant}$ and $E_{G;tangent}$ interpreted from load testing of a dummy pile installed at the test site compared with that computed using results recorded during loading of P450. The steel reinforcement was reduced in the dummy pile, but this has been accounted for, and it is seen that the stiffness estimated using the results of loading of the dummy pile are about 20% lower than that interpreted from the stress-strain

response of P450 itself. A detailed account of the interpretation of the measured results during loading of the instrumented dummy pile, are shown in Appendix C.

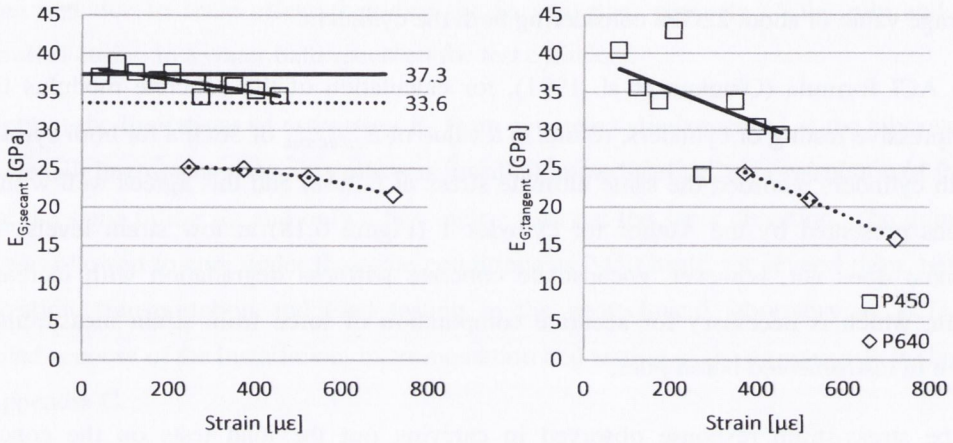


Figure 6.17 – Secant/Tangent stiffness-strain relationship for P450 and P640

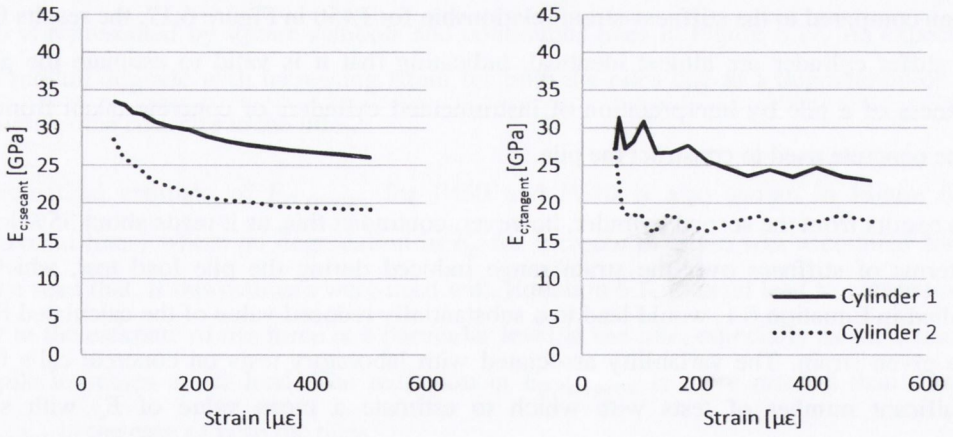


Figure 6.18 – Secant/Tangent stiffness-strain relationship for concrete cylinders

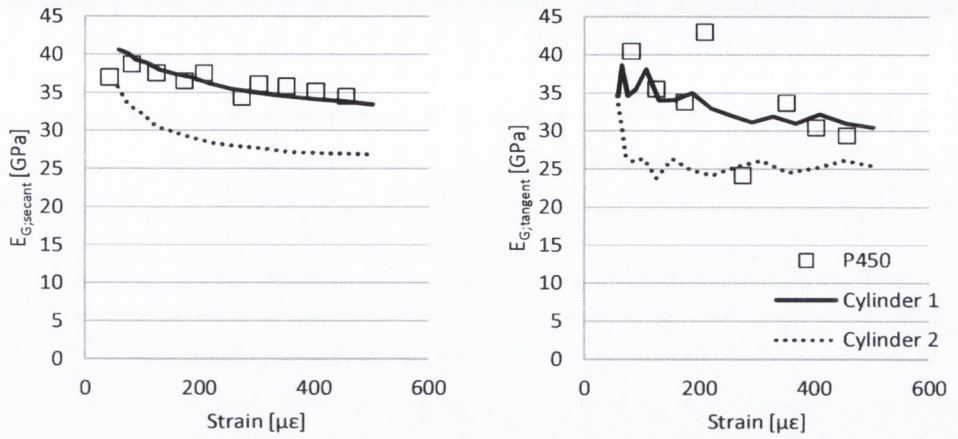


Figure 6.19 – P450: Equivalent Secant/Tangent pile stiffness-strain relationship using concrete stiffness-strain relationship from two concrete cylinders

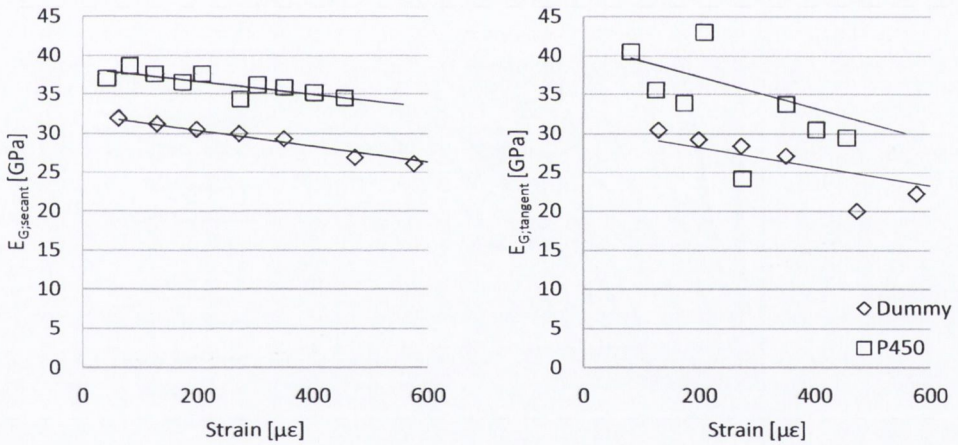


Figure 6.20 – P450 and Dummy pile: Secant/Tangent pile stiffness-strain relationship

6.3 Other instrumented tests on rock

Table 6.3 lists the details of the additional instrumented pile load test results available to the Author, wherein the piles were toed in rock. These instrumented load tests were made available to the Author when compiling the PTD (JK11, PTP1 and PTP2) and during perusal of the literature (TP3). In the case of these pile tests the loads interpreted by others

at the location of each strain gauge were used by the Author for interpretation of the development of shaft and base resistance in the rock socket.

The force-depth profiles for the additional instrumented tests are shown for the other piles toed in rock in Table 6.3. These results are used in combination with the Author's own instrumented tests with a view to demonstrating the behaviour of piles toed in Irish rocks.

Table 6.3 – Pile details: instrumented tests on piles toed in rock

Pile	Location	Length [m]	Diameter [mm]	L_{rock} [m]	D_{rock} [mm]	Comment
Pile 450	Duleek	13.94	450	4.30	450	-
Pile 640	Duleek	9.85	640	2.05	640	-
JK11	Coolkeragh	11.50	450	2.50	450	-
PTP1	Dundrum	18.20	914	4.50	900	Sleeve to 13.7m;
PTP2	Dundrum	20.20	914	6.50	1080	Sleeve to 13.7m; Debris at pile toe;
TP3	Ballsbridge	11.00	762	1.35	762	Loaded in Tension;
DC PTP1	Dublin Central	24.00	1162	2.00	1162	Zero friction assumed to 22m;

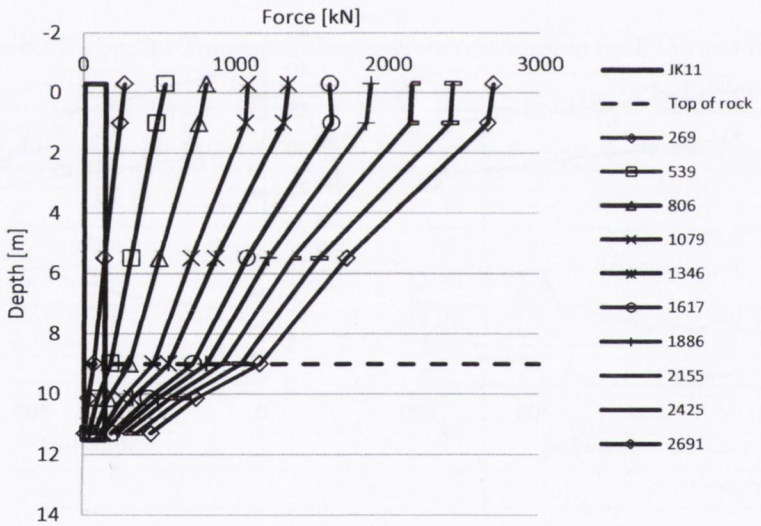


Figure 6.21 – JK11; Force-depth profile

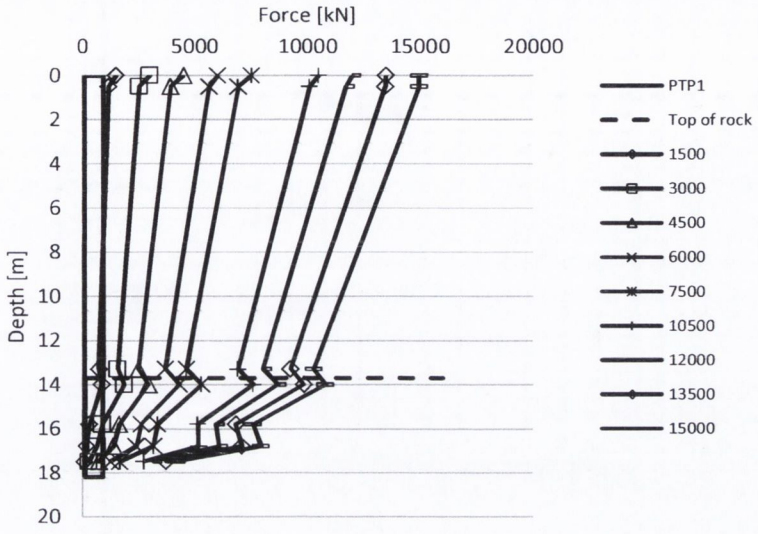


Figure 6.22 – PTP1; Force-depth profile

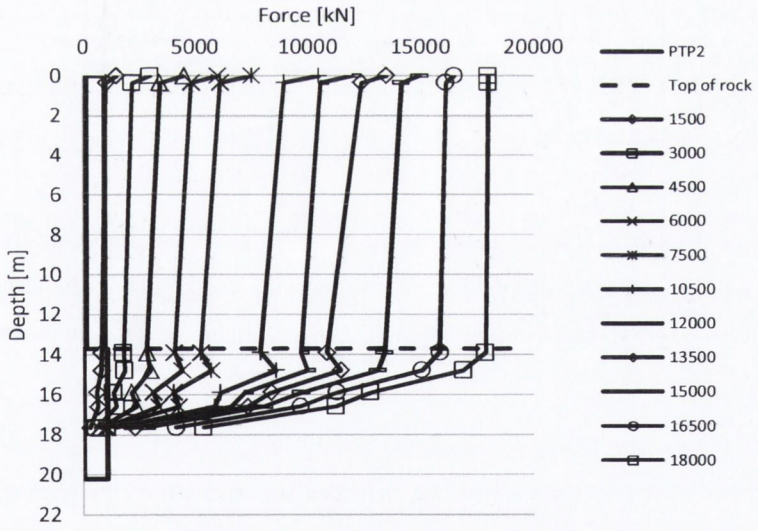


Figure 6.23 – PTP2; Force-depth profile

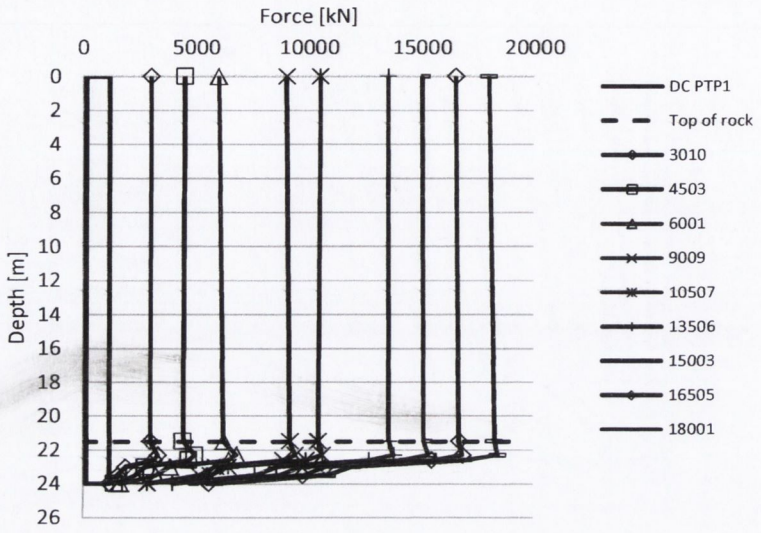


Figure 6.24 – DC PTP1; Force-depth profile

6.3.1 Pile-Rock Interface Shear Stress

The pile-rock interface shear stress $q_{s;rock}$ was calculated from the force-depth profiles for these additional rock socket tests. The results are plotted against the pile head deflection normalised by pile diameter in Figure 6.25 and are plotted separately for each of the test sites for clarity.

The development of $q_{s;rock}$ is very similar for the piles at Duleek and Dundrum where the piles were toed in limestone and in granite respectively. Pile JK11 at the Coolkeragh site, was toed in Sandstone and showed much lower values of $q_{s;rock}$ with normalised deflection.

The calculated $q_{s;rock}$ were extrapolated (assuming a hyperbolic relationship with deflection) and divided by the unconfined compressive strength of the rock q_u for each of the piles to estimate the development of the adhesion factor α_{rock} for the pile-rock system. The results are shown in Figure 6.27. The α_{rock} factor for those piles toed in the limestone bedrock was in the range 0.013 – 0.020 at δ_f.

In the case of pile JK11, toed in the much weaker sandstone, the α_{rock} factor was much higher. It is estimated that a α_{rock} value equal to 0.028 was actually developed on loading the pile and that at δ_f, α_{rock} was estimated as 0.033, twice the average value for the

limestone and granite. Figure 6.27 implies that the weaker the rock the greater the proportion of the strength of that rock is potentially mobilised on loading the pile. This could be due to the load-deflection response at the base of the pile in the different strength rocks.

Figure 6.28 shows the estimated stress developed under the pile toe $q_{b;rock}$ plotted against the normalised base deflection. The piles toed in the limestone and granite developed large base resistance for little deflection, less than 1% of the diameter, and the response is very stiff in comparison to that for pile JK11, which developed only a third of the base resistance in the limestone or granite at three times the normalised base deflection.

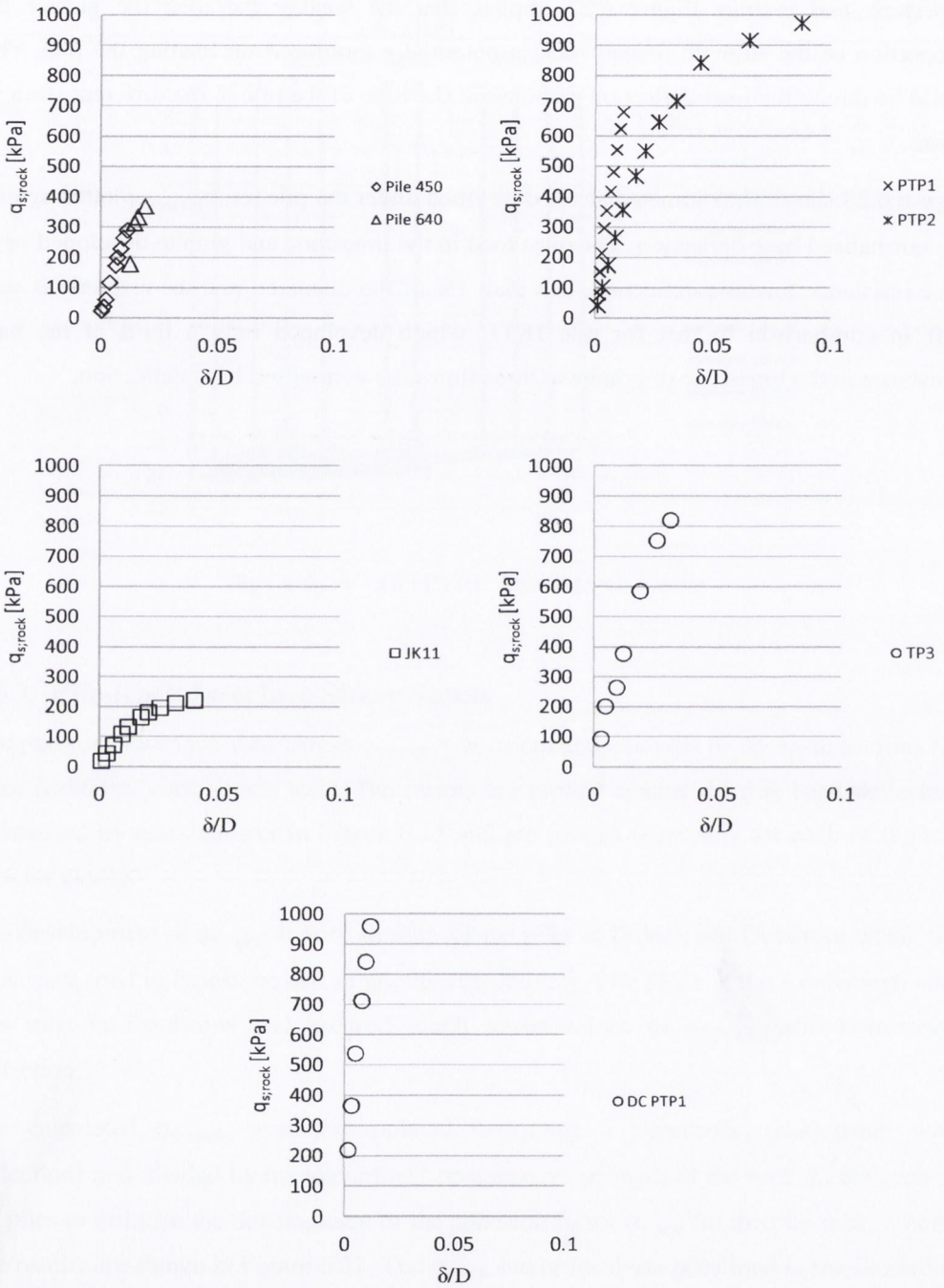


Figure 6.25 – Shear stress development in rock

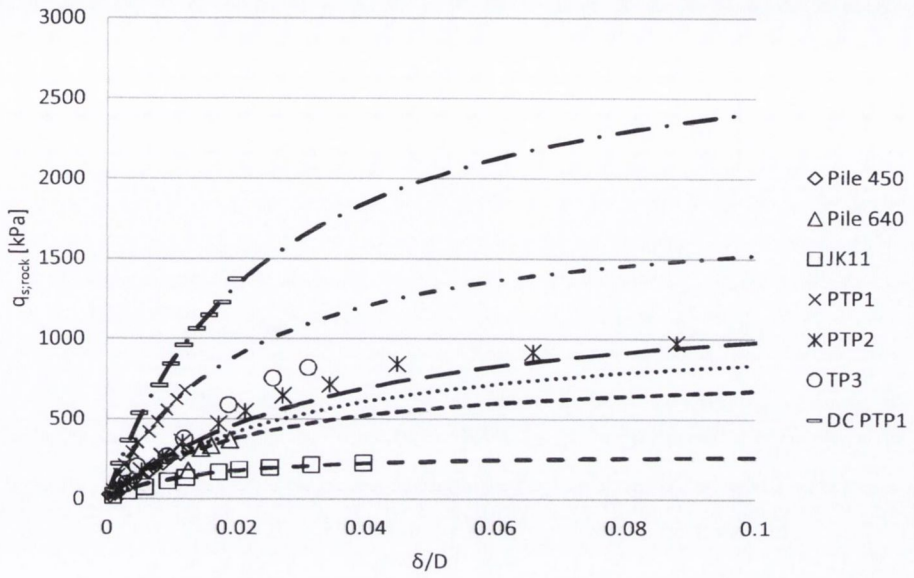


Figure 6.26 – $q_{s;rock}$ vs. normalised deflection

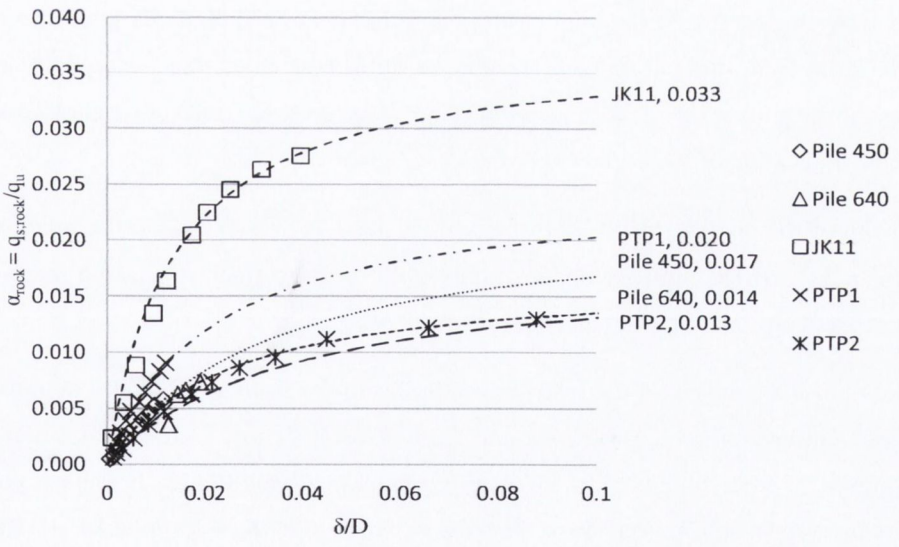


Figure 6.27 – α vs. normalised deflection

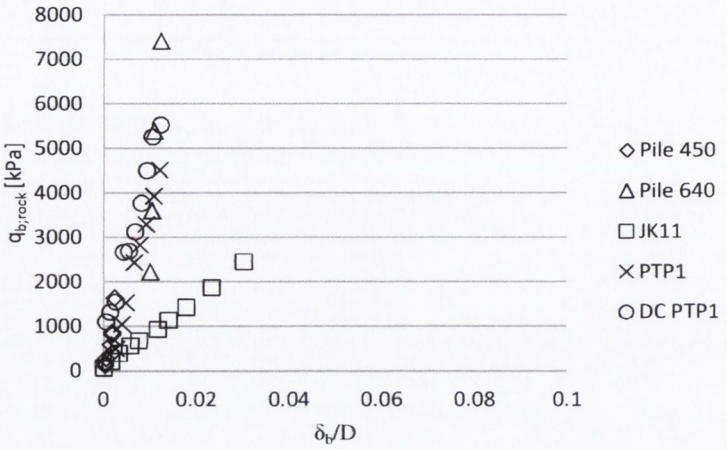


Figure 6.28 – Stress on base vs. normalised base deflection

6.4 Discussion: Rock socketed piles

Long and Collins (1999) compared α_{rock} values calculated for the pile tests in Irish rock with those of Kulhawy and Phoon (1993) and showed that these are not applicable to Irish rock. It was suggested by Long and Collins that this may be due to the generally higher strength of the rock found in Ireland. Long and Collins concluded that rock quality is what governs the development of shaft resistance of rock socketed piles in Ireland and that parameters indicative of rock quality are better indicators of $q_{s;rock}$ than q_u.

The results of the analysis of these instrumented piles were overlaid on the relationships between α_{rock} and rock quality designation (RQD) and the fracture spacing index (FSI) interpreted and presented by Long and Collins (1999).

The results of the analysis of the instrumented piles under study are broadly in agreement with those findings presented by Long and Collins, as shown in Figure 6.29, Figure 6.30 and Figure 6.31, where the piles are labelled individually on the Charts. It was not possible to obtain a value of RQD and FSI for the rock in which pile JK11 and pile DC PTP1 were installed and so these piles do not appear in Figure 6.30 or Figure 6.31.

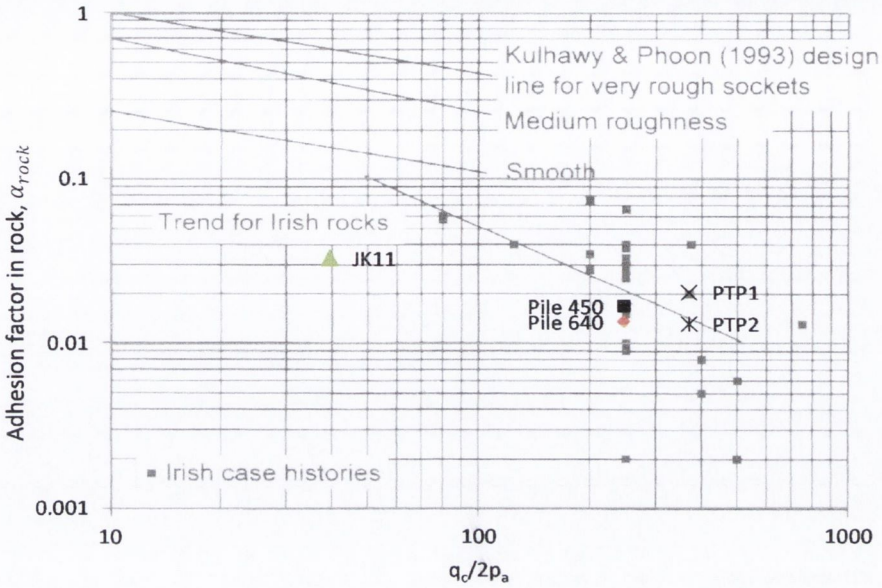


Figure 6.29 – Relationship between α and $q_c / 2p_a$ (Kulhawy and Phoon 1993)

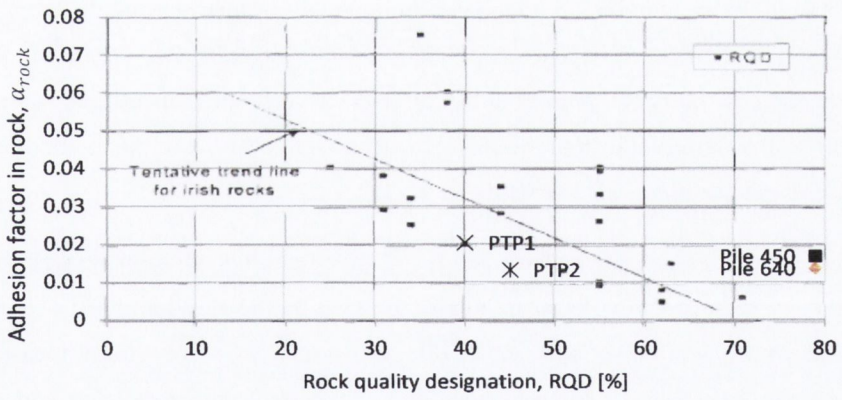


Figure 6.30 – Relationship between α and RQD (Kulhawy and Phoon 1993)

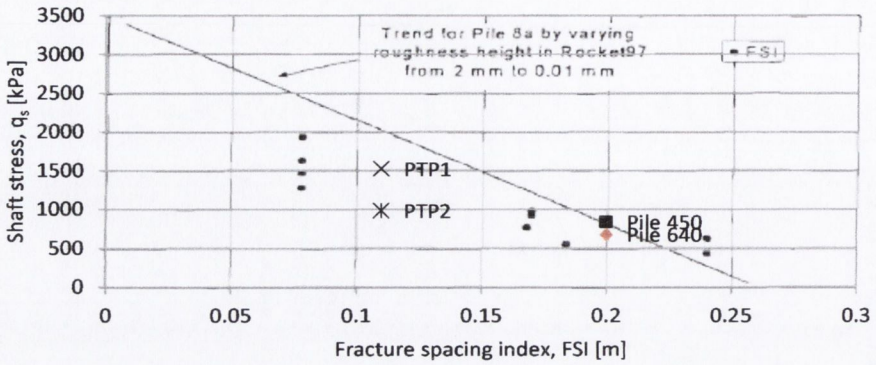


Figure 6.31 – Relationship between q_s and FSI (Kulhawy and Phoon 1993)

6.5 Conclusions

Firstly, the installation and static loading of two instrumented CFA piles, toed in limestone bedrock, were presented, alongside the interpreted stratigraphy at the site using the results of rotary core and shell and auger boreholes in combination with MASW profiling.

Instrumentation, in the form of an array of strain gauges comprising two different types of gauge, namely, electrical resistance (foil) gauges and vibrating wire strain gauges, were installed in each of the two test piles at six different levels. The foil gauges were directly adhered to the longitudinal steel reinforcement in the piles and the embedment type vibrating wire gauges were tied vertically to the same bars.

The two types of strain gauge, at any given level, gave readings of strain very close to each other at the various applied pile head loads, thus validating the common assumption of equal strain under load over the entire pile cross-section – the strain measurements provided by the foil gauges were representative of the steel where those provided by the embedment type vibrating wire gauge were representative of the concrete.

The strain measurements were then converted to force at the various depths over the length of each pile by direct conversion using a load-strain relationship developed using the measured load and the measured strain at the pile head for each of the two piles. This analysis assumes equal strain in each element of the pile cross section and that both the concrete stiffness and the pile cross section remain constant with depth. These assumptions are thought to be justified and reasonable.

The interpreted force-depth profiles are shown for P450 and P640 in Figure 6.13 and in Figure 6.14 respectively. About 20% of the applied load was estimated to have been resisted by the shaft in the boulder clay layer overlying the bedrock in the case of both the instrumented piles. It was estimated that 70-80% and 30% of the applied load was resisted by the shaft in the limestone bedrock for P450 and P640 respectively, the apparently reduced shaft friction in P640 is due to the fact that the rock socket was less than half the length of that for P450.

Very little load was resisted by the toe of the pile in the case of P450 – at the maximum applied load of 2500kN, only about 300kN (12%) was estimated to be resisted in end bearing. Conversely, about 50% of the applied load was estimated to have been resisted in end bearing in P640, probably due to the fact that the rock socket was much shorter than that for P450 and also due to the fact that P640 was loaded to a pile head deflection over twice that of P450.

An investigation was then carried out to assess the gross stiffness of P450 to reveal the uncertainty that can arise when force-depth profiles are interpreted using calculated stiffness values. Concrete cylinders comprising the same concrete as that used in P450 were instrumented with strain gauges on the surface and load tested in uniaxial compression to estimate the concrete stiffness and also to characterise the stiffness-strain relationship for the concrete.

The concrete stiffness, from the results of the cylinder tests, was seen to exhibit stiffness degradation with increasing strain – the stiffness reduced by about a third, from an initial value of between 30 and 35GPa to 20 and 25GPa for the two cylinders over the strain range experienced by P450 during the load test, 0 to 500με.

This stiffness-strain relationship for the concrete was interpreted to estimate the relationship between the gross pile stiffness and increasing strain level. This was seen to be almost identical to the actual relationship measured at the pile head during the load test when the results of Cylinder 1 were used, and was about 35% lower using the results of Cylinder 2. If the results of Cylinder 2 were applied to the measured strain in the pile this would lead directly to an underestimate of the force-depth profile of the same magnitude. The variability associated with laboratory tests on concrete, therefore, calls for a significant number of tests with which to estimate a mean value of concrete stiffness with some

confidence for use with Equation 6.1 to provide an accurate estimate of the force where strain is measured in an instrumented bored pile.

The stiffness-strain relationship was also estimated using the results of a laboratory load test on a short section of an instrumented dummy pile, which was installed at the test site by the same methods as the full-scale pile, and was allowed to cure on the site for several days prior to excavation. The instrumented dummy pile was installed immediately after P450, only a few metres apart, and was installed using the same CFA piling rig and concrete as that for P450.

The results from the dummy pile test also registered similar pile stiffness degradation with increasing strain under load. The interpreted stiffness of the dummy pile was around 20% lower than that of P450 even when the reduced steel reinforcement in the dummy pile was accounted for – the reasons for this are not clear.

In estimating the stiffness of P450, by the various means, both the secant and tangent moduli were computed in each case. The value of the tangent modulus is considered to be a more accurate representation of the varying stiffness of the pile with varying strain level. The tangent modulus is based on the incremental stress-strain relationship computed, where the secant modulus is a calculation of the gradient of the stress-strain curve relative to the origin. If the stress-strain curve were linear, these two values would be equal in magnitude but this is not the case where concrete is present, the tangent modulus tends to be lower than the secant modulus.

The force-depth profiles, interpreted by others, for four additional instrumented piles also toed in rock in Ireland, were then introduced in this Chapter for comparison. Three of the piles were taken from two separate sites in Dublin and the third from a site in Londonderry. The pile-rock interface shear stress, denoted $q_{s;rock}$, was calculated for each of the five piles and was plotted against the pile head deflection normalised by the pile diameter. The development of $q_{s;rock}$ was similar for the piles toed in the limestone and much less for Pile JK11 where the estimate at δ_f was about a third of that of the other piles.

The base resistance $q_{b;rock}$ for each of the piles was also estimated and the development of $q_{b;rock}$ appears to be linear elastic when plotted against the base deflection normalised by

the pile diameter. Again, $q_{b;rock}$ for Pile JK11, toed in the highly weathered rock, is much lower than that calculated for the other piles that are toed in limestone and granite.

When overlaid on relationships presented by Long and Collins (1999), the values of α and q_s computed by the Author are broadly in agreement. The value of q_s decreases with increasing FSI and the value of α decreases with increasing RQD, these results indicate that the more fractured the rock the greater the magnitude of q_s.

The results also indicate that higher strength rock leads to a lower proportion of that strength being potentially mobilised along the shaft of a pile (equivalent to lower α values observed with increasing q_c), however, the actual magnitude of shaft resistance mobilised with higher strength rocks is still much higher than that for rocks of lower strength.

7 Reliability of Piles

The reliability of a pile foundation depends, not only on the magnitude of the applied loads and resistances, whether calculated or measured, but critically on the uncertainty associated with each of these parameters. Uncertainty was estimated in Chapter 4 by application of statistical methods to the test results in the PTD and the results of this analysis are used in this section to evaluate the reliability of single piles and of pile designs specified for a site. The reliability is characterised using the reliability index (β) which may be related to the probability of the occurrence of a limit state.

Many modern geotechnical design codes, such as Eurocode 7, rely on the application of partial factors to measured ground properties used in geotechnical design and it is required that a characteristic value of the ground property is selected using these measured values. Several methods of determination of this characteristic value have been proposed, often derived from or reliant on the use of statistical methods. Characteristic values are determined in this section by applying the various methods of determination of characteristic values to the measured ground test results and are each used to calculate the characteristic resistance of the piles. Appraisal of the different methods may be carried out by comparison to the measured pile resistance using the static load tests in the PTD.

7.1 Background

The margin of safety, M of single pile under load, Q with a resistance, R is given simply by the difference between R and Q, Equation 7.1.

$$M = R - Q \tag{7.1}$$

M is known as a performance function and R and Q are considered as random variables that may be described using some frequency distribution. If R and Q are assumed normally distributed then M is also normally distributed with a mean value, μ_M and variance, σ_M^2 given by Equation 7.2 and Equation 7.3 respectively.

$$\mu_M = \mu_R - \mu_Q \tag{7.2}$$

$$\sigma_M^2 = \sigma_R^2 + \sigma_Q^2 - 2\rho_{RQ}\sigma_R\sigma_Q \tag{7.3}$$

where μ_R & μ_Q and σ_R & σ_Q are the mean and standard deviation of R and Q respectively, and ρ_{RQ} is the correlation coefficient between R and Q.

Where $R > Q$ (equivalent to $M > 0$) then there is some margin of safety for the foundation but there is still a chance that Q may exceed R, this chance is represented by the shaded area in Figure 7.1 and the probability of failure, P_f may be calculated using Equation 7.4.

$$P_f = \Phi(-\beta) \tag{7.4}$$

where $\Phi(\cdot)$ is the standard normal cumulative function and the reliability index, β is defined by Equation 7.5. The relationship between β and P_f is displayed in Figure 2.25 alongside qualitative interpretations of the level of performance of the foundation. If R and Q are uncorrelated then $\rho_{RQ} = 0$ and Equation 7.5 reduces to Equation 7.6.

$$\beta = \frac{\mu_M}{\sigma_M} = \frac{\mu_R - \mu_Q}{\sqrt{\sigma_R^2 + \sigma_Q^2 - 2\rho_{RQ}\sigma_R\sigma_Q}} \tag{7.5}$$

$$\beta = \frac{\mu_R - \mu_Q}{\sqrt{\sigma_R^2 + \sigma_Q^2}} \tag{7.6}$$

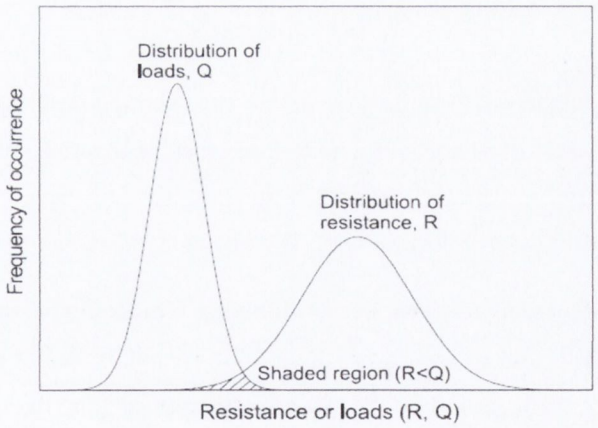


Figure 7.1 - Variation of load and resistance (Zhang et al. 2005)

If R and Q are assumed lognormal (the log of the values R and Q are normally distributed) then β may be calculated using Equation 7.7, (Whitman 1984).

$$\beta = \frac{ln\left(\frac{\mu_R}{\mu_Q}\sqrt{\frac{1+V_Q^2}{1+V_R^2}}\right)}{\sqrt{ln[(1+V_Q^2)(1+V_R^2)]}} \qquad 7.7$$

where V_R & V_Q are the coefficients of variation of R and Q and are equal to σ_R/μ_R and σ_Q/μ_Q respectively. Equation 7.7 reduces to Equation 7.8 where V_Q and V_R are less than or equal to 0.30 (MacGregor 1976).

$$\beta = \frac{ln\left(\frac{\mu_R}{\mu_Q}\right)}{\sqrt{V_Q^2 + V_R^2}} \qquad 7.8$$

7.2 Reliability of a single pile

The reliability of a single pile refers only to those piles that are actually load tested and takes no account of the within-site variation. Various means of determination of R_c and the associated uncertainty have been presented earlier in this thesis and the resulting values are used to assess the reliability of the piles tested.

Most of the piles in the PTD were only deflected by a small amount, much less than δ_f and this implies that the ultimate resistance of the pile is greater than the test load. The reliability of a single pile was calculated based on an extrapolated value of R_c to δ_f using the measured load-deflection data. However, as this extrapolated value is not actually measured, the associated uncertainty was increased to reflect this. A means of quantification of the uncertainty associated with the estimated failure load, by extrapolation of limited load-deflection data, was outlined in Section 4.3.

The β values and relationships shown in the following figures are based on the assumption that the applied load, G and the resistance R_c are lognormal, it should be noted that where these parameters are assumed normal the β values are reduced and the results assuming the normal distribution are shown in Appendix D of this thesis.

The estimated effect of limited load-deflection data on the calculated β value for a single pile is shown in Figure 7.2, Figure 7.3 and Figure 7.4 for CFA and driven piles in DBC and for CFA piles in clay outside Dublin respectively, where β is plotted against δ_{max}/D. Curves of the equivalent OFS (calculated using Equation 7.9 or Equation 7.10) are also

plotted on the same Figures and β values at each OFS were based on Equation 7.7 (by simply choosing values of μ_R and μ_Q such that $OFS = \mu_R/\mu_Q$). The site references are shown in the legend. The target β value at the ULS implied by Eurocode 7 (equal to 3.8) is also shown on the Figures for ease of comparison to the calculated results.

$$OFS = R_{c;m}/F_k \qquad \delta_{max} \geq \delta_f \qquad 7.9$$

$$OFS = R_{c;chin}/F_k \qquad \delta_{max} < \delta_f \qquad 7.10$$

Interpreted, Figure 7.2 implies that, where a pile is loaded to δ_f (equivalent to δ_{max}/D equal to 10%) and the OFS is equal to 2.0 then a β value of 4.8 is achieved. If the same pile were loaded to only δ_{max}/D equal to 1% and extrapolated to δ_f, then the β value would be reduced to 2.1 for the same apparent OFS of 2.0. This analysis shows that, there is substantial benefit in loading a single pile closer to δ_f when load testing. The β value for the pile will be increased for a constant OFS. Thus, the traditional OFS is misleading – a higher OFS does not necessarily equate to a lower probability of failure.

This concept is demonstrated more clearly in Figure 7.5 which shows the OFS against δ/D, for three different sets of load-deflection data that might be observed for a single pile. Figure 7.5 (a) shows that the pile was loaded to δ_f and a value of $R_{c;m}$ was available, there is no need for extrapolation of the data and β may be calculated. Figure 7.5 (b) shows that the load test was only carried out to a deflection equal to 2% of the pile diameter and also shows the extrapolated curve to δ_f (which equates to that measured in Figure 7.5 (a)).

However, the uncertainty associated with the extrapolated value of R_c is much greater than that associated with the measured value - $V(R_{c;chin})$ may be as high as 0.4 while $V(R_{c;m})$ is taken as 0.1, so the β value will be much lower in case (b) than in case (a), while the OFS remains the same (equal to 2.5).

Figure 7.5 (c) demonstrates another set of load-deflection data, here the pile is loaded to the same load as in case (a) (and thus the observed OFS is equal to 2.5) but the pile was not deflected by near as much and extrapolation of the data yields a higher OFS. Obviously this set of load-deflection data would lead to a higher β value than case (a) and case (b) but the OFS at δ_f will be greater also.

It can be seen that all the piles in Figure 7.2 and Figure 7.3 loaded to δ_{max}/D of 5% or more all achieved values of β in excess of 4.0. For low values of δ_{max}/D, in the range 1-4% β values ranged from about 2-7.

Figure 7.4 shows much lower β values and these computed for CFA piles on a single site comprising boulder clay. The relatively low β values indicate a higher probability of failure; the ULS was reached under F_k during the load tests for many of these piles.

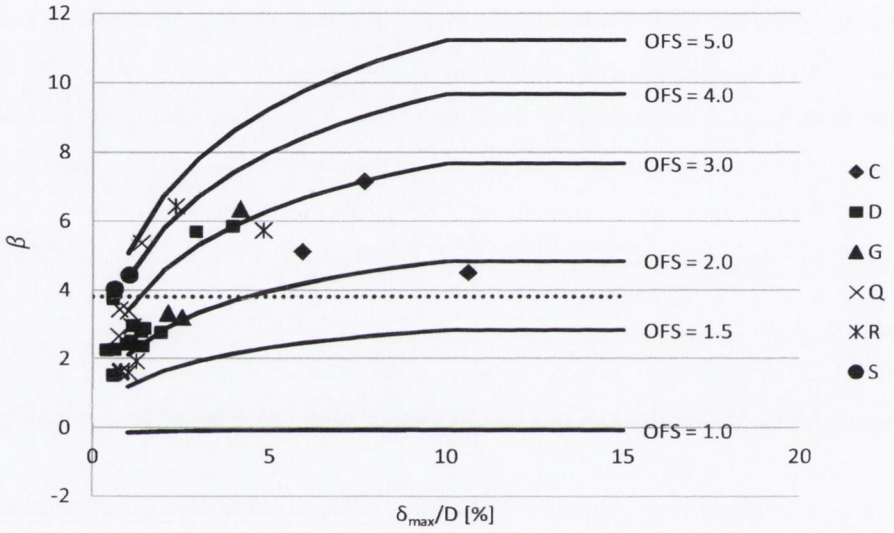


Figure 7.2 – CFA piles in DBC: Calculated β for a single pile

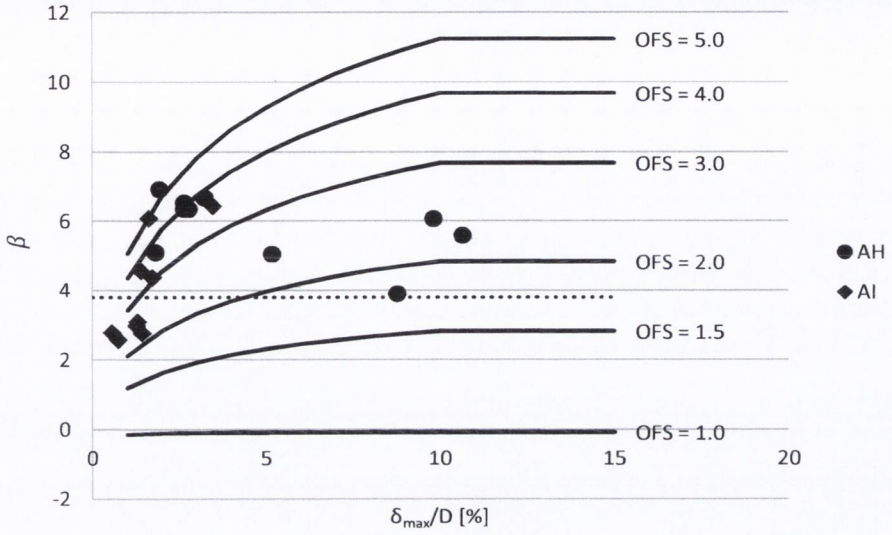


Figure 7.3 – Driven piles in DBC: Calculated β for a single pile

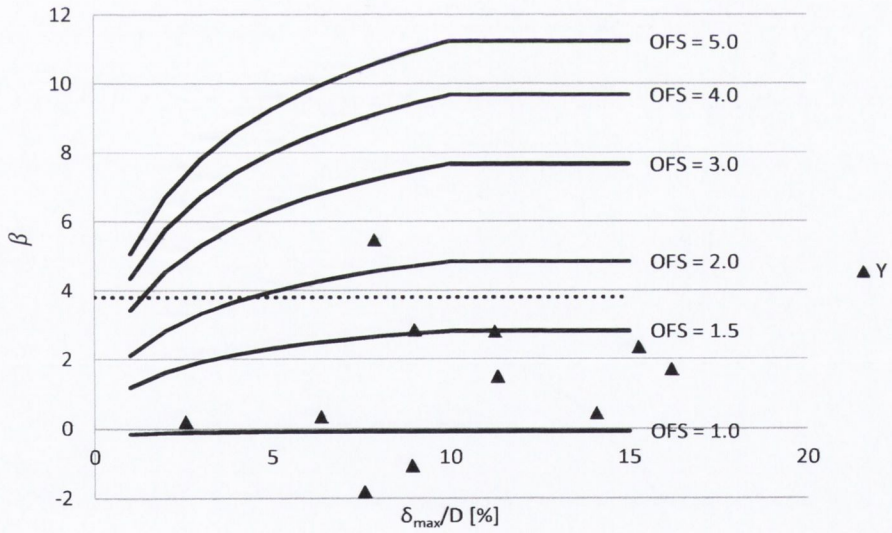


Figure 7.4 – CFA piles in boulder clay: Calculated β for a single pile

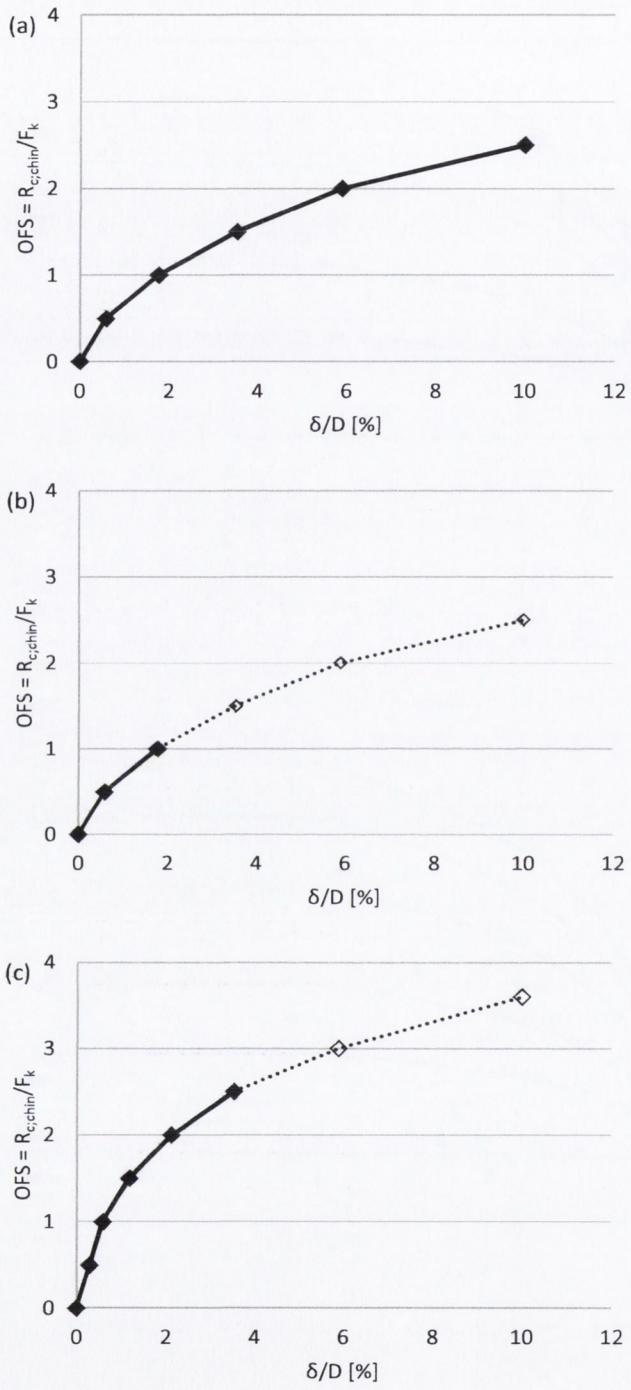


Figure 7.5 – Load-deflection compared

Figure 7.6, Figure 7.7 and Figure 7.8 refer to the other groups of piles outlined in Section 4.3. The calculated β values are seen to be highly variable, even with-in sites, thought to be due mainly to the effect of limited deflection on loading.

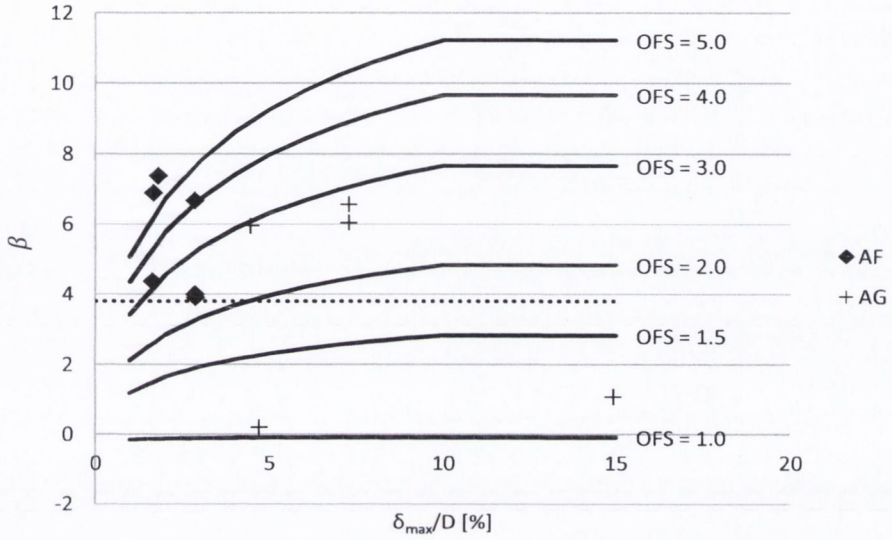


Figure 7.6 – Driven piles in boulder clay: Calculated β for a single pile

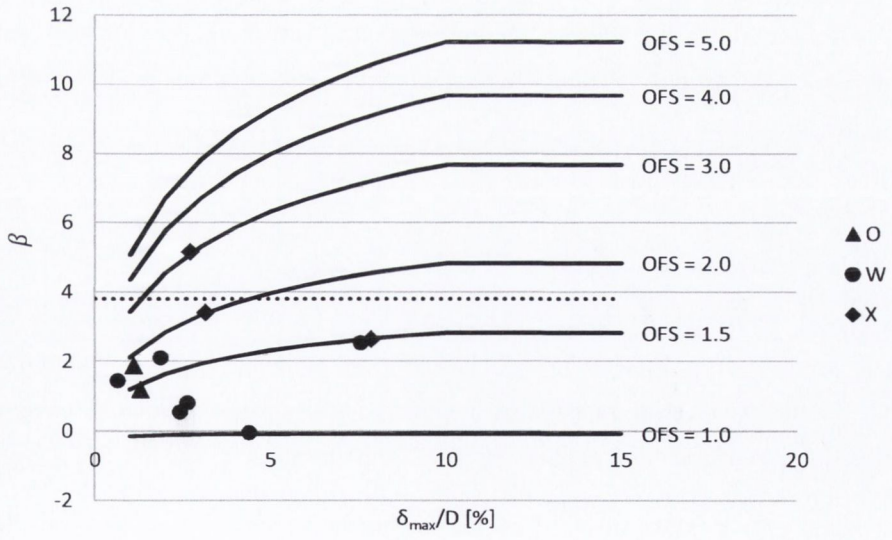


Figure 7.7 – CFA and bored piles in sand/gravel: Calculated β for a single pile

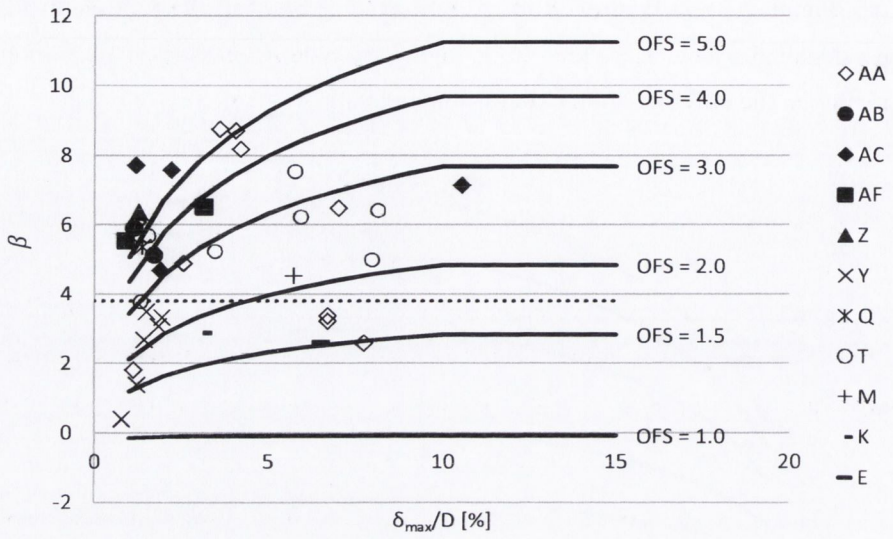


Figure 7.8 – CFA piles in rock: Calculated β for a single pile

7.3 Reliability of a pile design – ULS

Generally in Ireland, a pile design is specified for a given site or for an area within a site where the ground conditions are deemed similar; therefore, it is necessary to consider the reliability of the pile design rather than individual piles. This requires that the within-site variability be combined with the variability associated with a single pile load test. The reliability of a pile design, calculated using ground test results and load test results, is shown in this section.

7.3.1 Using ground test results

The uncertainty associated with the measured ground test results was quantified in Chapter 4 for many sites, from the results of the SPT carried out at those sites. This uncertainty was used to calculate the uncertainty associated with R_b and R_s when calculated using ground test results and these were combined to estimate the uncertainty in R_c.

The calculated uncertainties are used in this section to assess the reliability of piles and also to assess the effects of spatial variation for variance reduction on the calculated reliabilities.

Using the CFA and driven piles in DBC, for which the results of the SPT were available at the sites of the pile load tests, the effect of spatial averaging and pile length on the reliability of the pile design for installation over the sites, was assessed.

The value of $V(R_b)$ and $V(R_s)$ were, on average, both equal to 0.40 using the N_{SPT} results measured at the various sites in the PTD. The same value was assumed for calibration of partial factors in the National Building Code of Canada (Becker 1996). These values apply to both CFA and driven piles as the variability in the ground measured using the SPT is not affected by the pile type that is subsequently installed. However, spatial averaging of the N_{SPT} will affect the value of $V(R_c)$ for the CFA and driven piles differently for two main reasons.

Spatial averaging only has an effect where the length of the failure surface, L_f is larger than the vertical scale of fluctuation, Θ_z (see Equation 2.32 and Equation 2.33). This may be true for the failure surface governing shaft resistance, which may be assumed to be equal to the length of the pile, however, L_f in bearing at the pile toe is relatively short and thus it is unlikely that spatial averaging will have an appreciable effect on $V(R_b)$, if any effect at all.

The way in which CFA and driven piles resist load may be different, as indicated in Chapter 5 for the piles installed in DBC, (the ratio $R_{s;cal}/R_{b;cal}$ was equal to 4.00 and 0.54 for the CFA and driven piles respectively). This means that, in the case of CFA piles, where a much greater proportion of the load is resisted by the pile shaft than in driven piles installed in similar ground conditions, the application of spatial averaging to the measured N_{SPT} values will result in a greater overall reduction in the value of $V(R_c)$ in the case of the CFA piles.

Secondly, the dimensions of CFA piles tend to be greater than those of driven piles. In the PTD, the CFA piles in DBC were of average length 12m and ranged from 9-15m, while the driven piles were, on average, 7m in length and in the range 5-11m. As the piles are installed in the same deposit, then the value of Θ_z should be similar for each but the variance reduction factor Γ^2 is calculated as Θ_z/L_f as shown in Equation 2.33, therefore, longer piles result in a reduced value of Γ^2 thus reducing $V(R_s)$ by more than that for a shorter pile, which, in turn results in a lower value of $V(R_c)$.

These points are illustrated in Figure 7.9 where β values, computed based on the measured N_{SPT} and its associated uncertainty, are plotted against the equivalent OFS for CFA and driven piles in DBC. Figure 7.9 (a-d) each show the calculated β values for three scenarios: where no spatial averaging is applied, equivalent to Θ_z greater than or equal to L_f (represented by diamonds), and where Θ_z is equal to 6m and 2m (represented by square and triangle symbols respectively).

In Figure 7.9 (a) and Figure 7.9 (b) the pile length was assumed equal to 12m (the average for CFA piles installed in DBC in the database) and Figure 7.9 (a) and Figure 7.9 (b) refer to CFA and driven piles respectively. It is seen that, where no spatial averaging is applied, the β-OFS relationship is the same for both types of pile, but where spatial averaging is applied, CFA piles enjoy a much greater enhancement in β, for a given OFS. This is because the ratio $R_{s;cal}/R_{b;cal}$ is about eight times larger for bored piles than it is for driven piles.

Interpreting Figure 7.9 (a), the β value for the average CFA pile installed in DBC is 1.6 & 2.6 where the equivalent OFS is 2 and 3 respectively and where no spatial averaging is considered. Applying spatial averaging, where Θ_z is assumed equal to 6m and 2m, the β values are increased to 2.3 & 3.7 and 3.9 & 6.3, where the equivalent OFS is equal to 2 and 3 respectively.

Comparing this with Figure 7.9 (b), which applies the same methodology to an equivalent sized driven pile in the same deposit, the β values at equivalent OFS of 2 and 3 and where Θ_z is assumed equal to 6m and 2m were 1.8 & 3.0 and 2.2 & 3.6 respectively, much lower than those for the equivalent sized CFA pile in the same deposit.

Figure 7.9 (c) and Figure 7.9 (d) display the same results but where a pile length more akin to those driven piles in the PTD was assumed, equal to 6m. Where Θ_z was assumed equal to 6m there is no reduction in uncertainty and no enhancement of β as Θ_z is equal to L_f. Figure 7.9 (d) shows that the average driven pile in DBC would not benefit from spatial averaging if Θ_z is around 6 while a value of Θ_z equal to 2m would result in an increase in β from 1.6 & 2.6 to 1.9 & 3.1 again at equivalent OFS of 2 and 3 respectively.

This analysis shows that, based on the uncertainty in the measured N_{SPT} in DBC, without spatial averaging, a β value of 3.8 is achieved only where the equivalent OFS is equal to

5.0. To apply such a high factor of safety, given that piles proved to 2.5-3.0 times their F_k under test were generally deflected by a small amount, is clearly much too conservative.

Spatial averaging provides a means to reduce $V(R_s)$ and increase β, however, the Θ_z value has a large effect on the β value and should be chosen carefully. More research is required to estimate the value of Θ_z so that β may be determined more accurately for piles, where R_c is calculated based on ground test results.

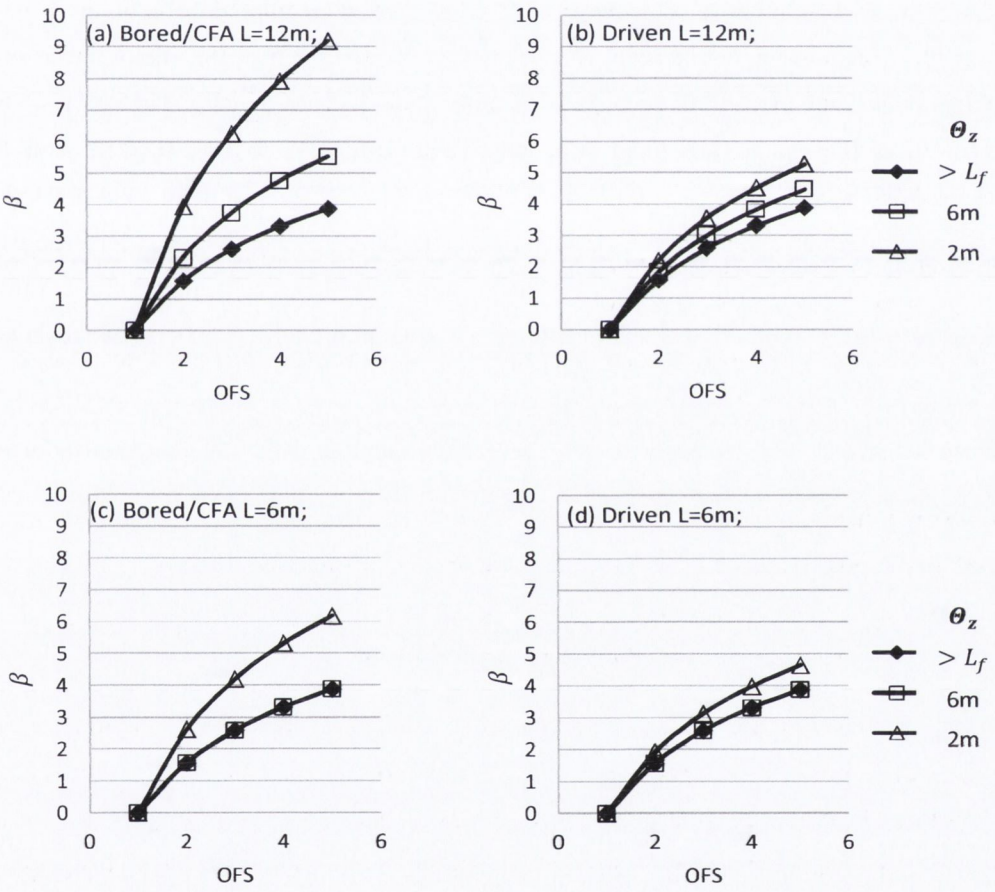


Figure 7.9 – Effect of spatial averaging and pile length on calculated β

7.3.2 Using load test results

In Section 4.6 the value of the within-site variation was estimated using groups of load test results on similar piles in various sites and was seen to tend to a level of variation in R_c of about 20%, in agreement with that suggested by other Author's. This level of within-site variation is assumed to be representative of the sites within the PTD and is used to estimate the reliability of the pile designs, given F_k.

The uncertainty associated with a single pile load test was quantified in Section 4.3 and the resulting β values were calculated in Section 7.1. Figure 7.2 to Figure 7.4 were used to show the relationship between β and δ_{max}/D at equivalent traditional OFS. Figure 7.10 to Figure 7.12 are similar, but include the within-site variation, so that, the pile design is now being assessed for the installation of many similar piles across the site. The result is that the calculated β values are much reduced overall, which is to be expected with the increased uncertainty due to within-site variability. The effect of limited load-deflection data is also reduced such that, above δ_{max}/D of about 5%, β values do not increase by a lot, for an equivalent traditional OFS. Where the OFS is equal to 2 and 3, the β values range from 2.6-2.8 and 4.1-4.4 where piles are loaded such that δ_{max}/D is equal to 5 and 10% respectively.

As already stated, this analysis assumes a level of within-site variation, characterised using $V(R_c)$ equal to 20%.

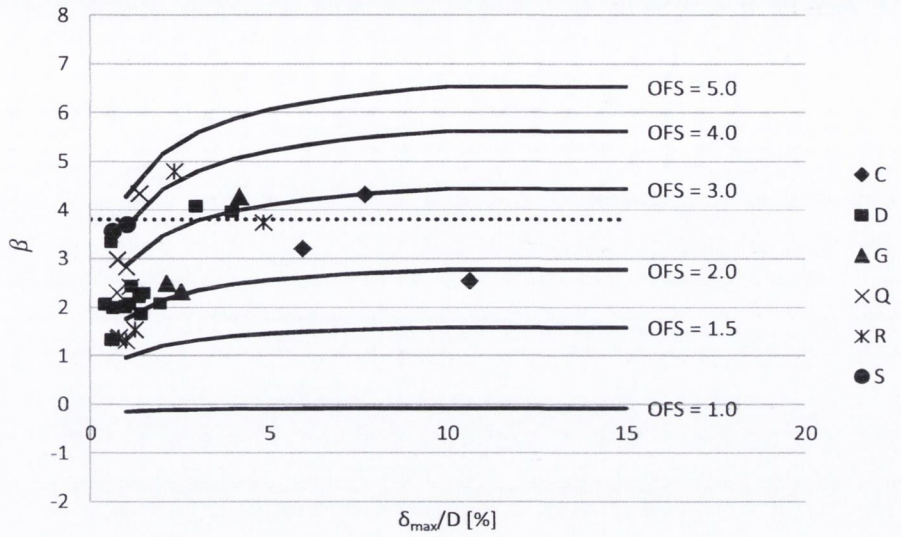


Figure 7.10 – CFA piles in DBC: Calculated β for a pile including within-site variation

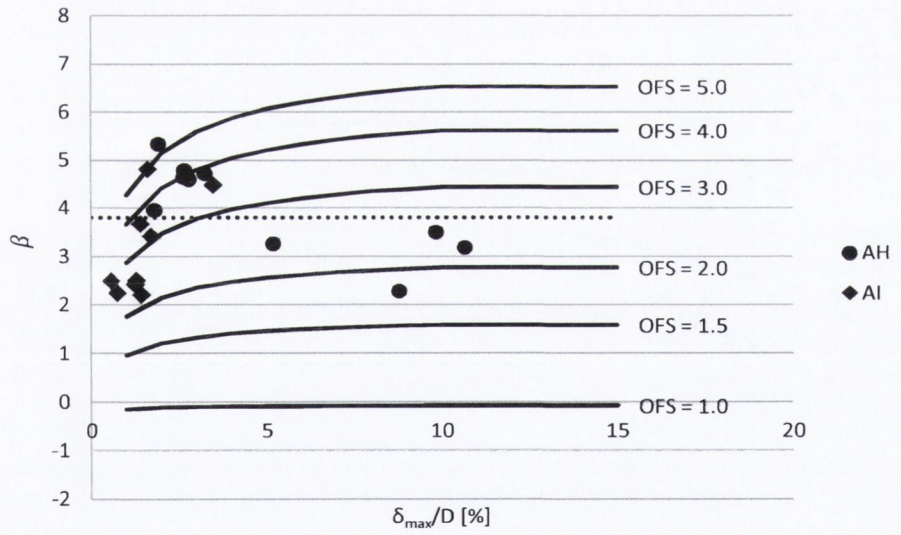


Figure 7.11 – Driven piles in DBC: Calculated β for a pile including within-site variation

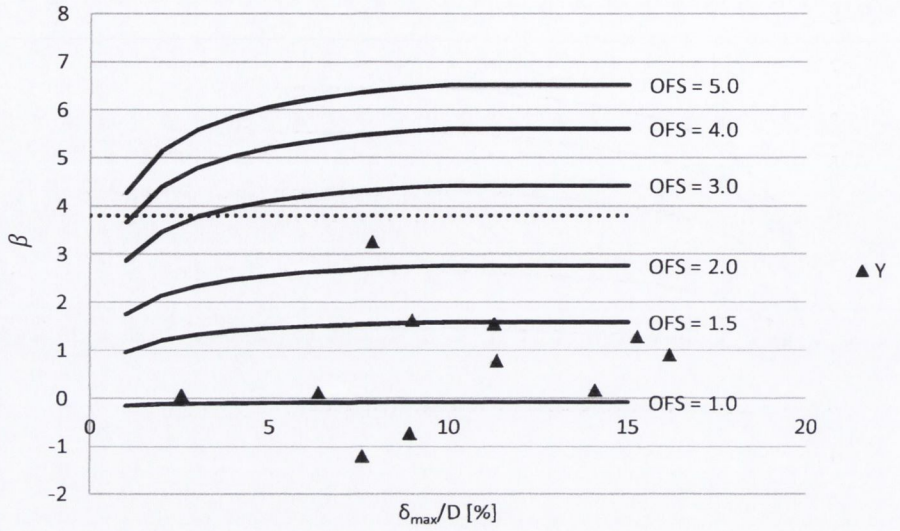


Figure 7.12 – CFA piles in boulder clay: Calculated β for a pile including within-site variation

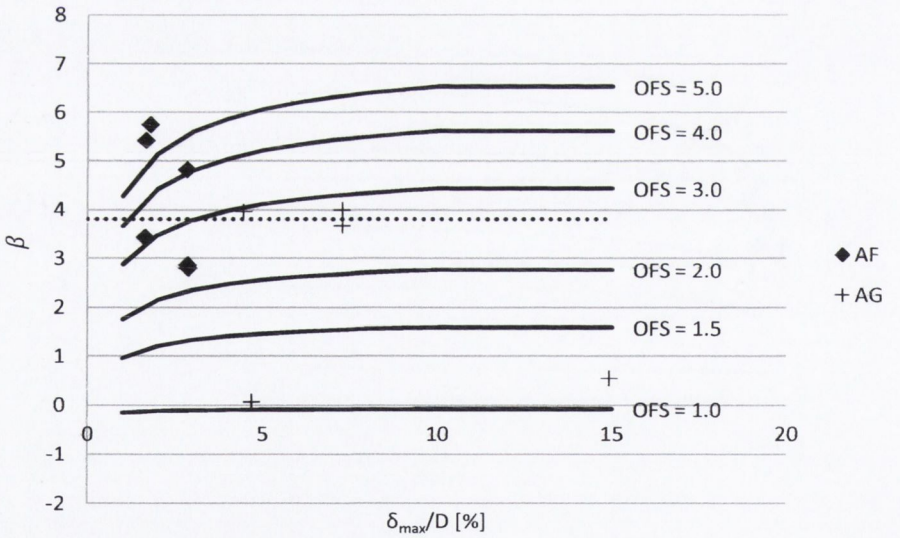


Figure 7.13 – Driven piles in boulder clay: Calculated β for a pile including within-site variation

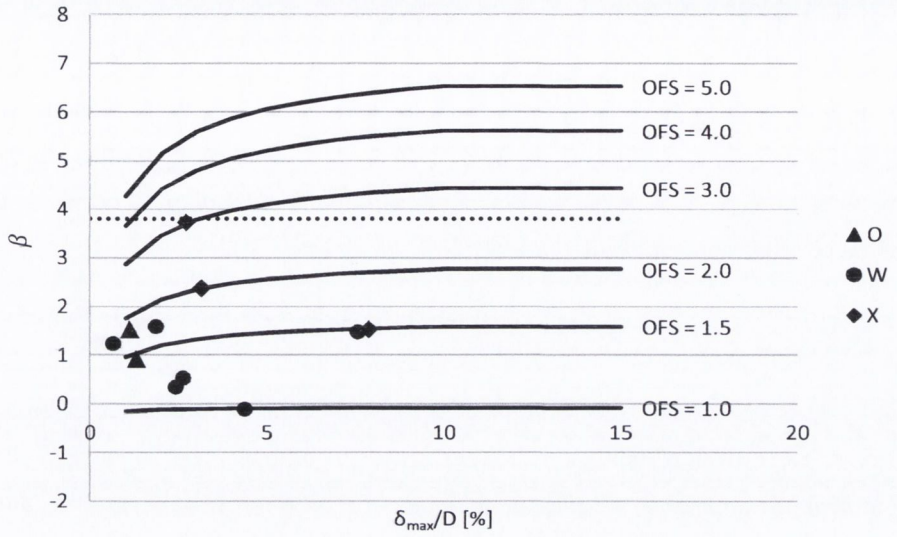


Figure 7.14 – CFA and bored piles in sand/gravel: Calculated β for a pile including within-site variation

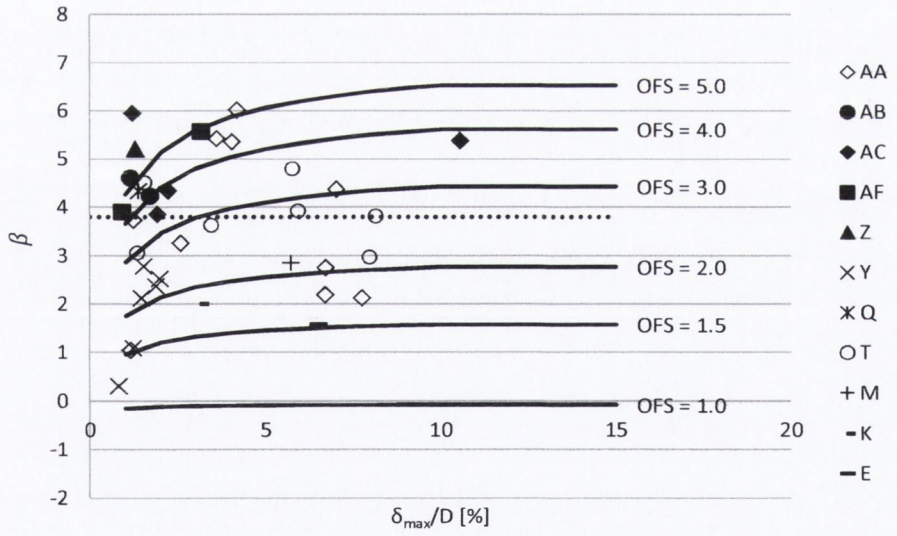


Figure 7.15 – CFA piles in rock: Calculated β for a pile including within-site variation

7.4 Correlation factors

The uncertainty in R_c from load test results on similar piles on the same site, characterised using $V(R_c)$ was seen to tend to 20% where many load test results were available, (Figure 4.20). Therefore, 20% is the best estimate of $V(R_c)$ by calculation using the sample data and may be assumed representative of the variability in a population of pile load tests on a single site due to ground variation.

This estimate of the variability of the population may be used to calculate the minimum resistance of the piles tested such that a particular level of confidence in the mean measured value of R_c is achieved and conventionally the level of confidence taken is 95%. Since the number of load tests carried out within a single site is generally limited, statistical methods applied to the measured values of R_c should account for this. One such probabilistic distribution that does take account of the number of data points in a sample is the Student-t distribution.

This section assesses the partial factors that should be applied to the loads and resistances considering the levels of uncertainty calculated using the PTD. The within-site variability was combined with the uncertainty in the measured value of R_c for a single pile using Equation 4.4, yielding a value of the overall uncertainty for a pile installed across a site of 22.4%. The uncertainty associated with the applied load was assumed equal to a coefficient of variation in the parameter $V(F_k)$ of 10% for purposes of the analysis.

The mean value of $R_{c;m}$ was assumed equal to unity for purposes of the analysis. The value of R_c such that the mean value of $R_{c;m}$ should lie above this value 95% of the time, denoted $R_{c;P5}$, was calculated using Equation 7.11.

$$R_{c;P5} = \mu(R_{c;m}) - t_c \sqrt{\left(\frac{1}{n}\right)}\,\sigma(R_{c;m}) \qquad 7.11$$

where $\mu(R_{c;m})$ is the mean value of the measured R_c from the load tests, t_c is the critical t value for the lower tail 95% confidence level of the Student t-distribution with $n-1$ degrees of freedom, n is the number of load tests results available and $\sigma(R_{c;m})$ is the standard deviation of $R_{c;m}$ (assumed known from experience and taken as 0.22).

The reciprocal of the result of Equation 7.11 at each n is the factor that should be applied to $\mu(R_{c;m})$ such that 95% confidence in the mean value is achieved. However, using

Equation 7.11 alone does not account for any variation in the applied load. Taking the applied load as unity also, the value of F_k may be calculated, such that the mean value of the applied load is below this value 95% of the time, using Equation 7.12 (assuming F is normally distributed).

$$F_k = \mu(F) + 1.645\sigma(F) \qquad 7.12$$

Dividing the reciprocal of Equation 7.11 by Equation 7.12 yields the partial factor that should be applied to the value of $\mu(R_{c;m})$ at each n such that a level of variation in the loads and resistances, characterised by $V(R_c)$ and $V(F_k)$, equal to 22.4 and 10% respectively, is covered by the partial factors.

The computed values at each n are denoted ξ_1 (as are the equivalent factors written in Eurocode 7) and are shown in Figure 7.16 alongside those in Eurocode 7 for comparison. It should be noted, that, the values shown at n equal to 1 and n equal to 2 were interpreted using backward extrapolation of the values calculated where n was greater than 2.

Eurocode 7 also specifies that a correlation factor to be applied to the minimum value of the measured R_c from pile load test results, this factor is denoted ξ_2. The smaller of $\mu(R_{c;m})/\xi_1$ and $min(R_{c;m})/\xi_2$ should then be taken as the value of $R_{c;k}$, according to Eurocode 7. The value of $min(R_{c;m})/\xi_2$ should only be smaller than $\mu(R_{c;m})/\xi_1$ when the variation in $R_{c;m}$ is large, equivalent to the case where $min(R_{c;m}) < R_{c;P5}$.

Thus, there is a critical value of $V(R_{c;m})$, below which $\mu(R_{c;m})/\xi_1$ and above which $min(R_{c;m})/\xi_2$ will govern $R_{c;k}$. This value is equal to 22.4%, as observed from the pile load test results. The ξ_2 factors may then be calculated such that a higher level of $V(R_{c;m})$ is covered by application of a factor to the $min(R_{c;m})$. If a maximum value of $V(R_{c;m})$ equal to 35% is allowed for (which represents a maximum value of $V(R_{c;m})$ observed in the actual load test results in the PTD shown in Table 4.14), then values of ξ_2 shown in Figure 7.17, are applicable. The values of ξ_2 were calculated such that $R_{c;P5}$ calculated using the higher value of $V(R_{c;m})$, achieved the value of $R_{c;P5}$ calculated using the lower value of $V(R_{c;m})$.

Similar analysis was applied to the mean value of R_c estimated by calculation from profiles of ground test results, in this case, the variation was characterised by $V(R_{c;cal})$ which was equal to 40% as calculated in Section 4.5. A ground test profile is defined as a number of

tests carried out at various depths in a single line and over a depth that is representative of the ground in which the foundation element is to be installed. The results are shown in Figure 7.18, here the partial factor for application to $\mu(R_{c;cal})$ is denoted ξ_3 (in keeping with Eurocode 7) and again the equivalent values written in Eurocode 7 are shown for comparison.

Similar to the ξ_2 factor outlined previously, there exists a ξ_4 factor in Eurocode, to be applied to the minimum value of the calculated resistance of a pile, $min(R_{c;cal})$. Again this procedure allows for greater variation in $R_{c;cal}$ to be accounted for, where $V(R_{c;cal})$ is larger than 40%, then $min(R_{c;cal})/\xi_4$ will govern the value of $R_{c;k}$. The ξ_4 factors shown in Figure 7.19 cover the situation where $V(R_{c;cal})$ is as high as 50%.

The ξ values are shown together in Figure 7.20 and Figure 7.19 and it is seen that ξ_3 is larger than ξ_1 and that ξ_4 is larger than ξ_2, which is intuitively correct as direct determination of R_c from pile load tests should lead to greater confidence in the value than that by calculation using ground test results, as the uncertainty in R_c is reduced when load tests are carried out.

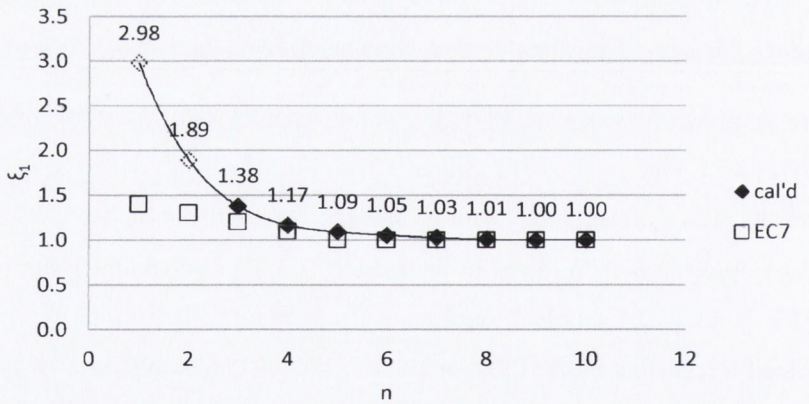


Figure 7.16 – ξ_1 factors: for application to mean $R_{c;m}$ from a group of load tests

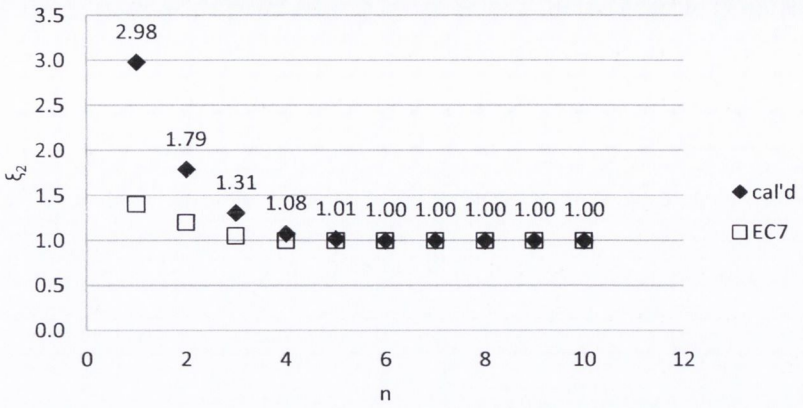


Figure 7.17 – ξ_2 factors: for application to minimum $R_{c;m}$ from a group of load tests

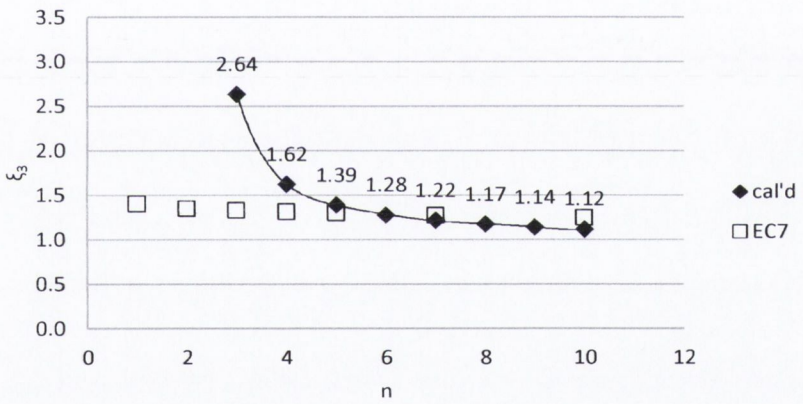


Figure 7.18 – ξ_3 factors: for application to mean $R_{c;cal}$ from ground test profiles

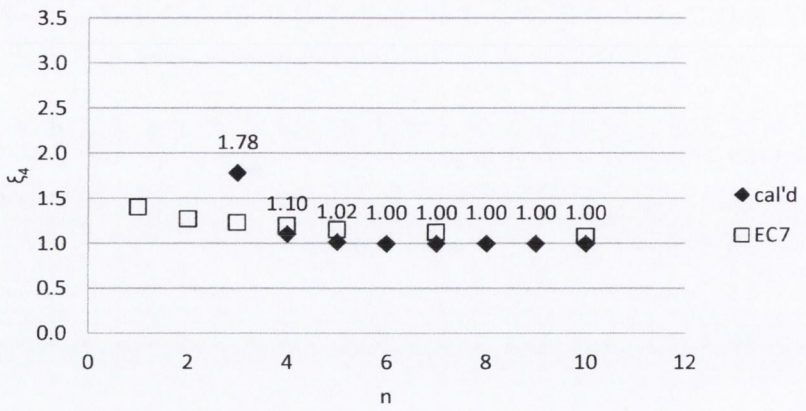


Figure 7.19 – ξ_4 factors: for application to minimum $R_{c;cal}$ from ground test profiles

The ξ factors calculated indicate the following:

where $V(R_{c;m}) \leq 22.4\%$

1) There is substantial benefit in carrying out two load tests as opposed to just one, the ξ_1 factor reduces from 3.0 to 1.9 where one and two load tests are carried out respectively.
2) Where a third load test result is available ξ_1 reduces further, to 1.4.
3) If five or six load test are carried out ξ_1 gets close to one and where there are eight load tests result ξ_1 is equal to 1.0, indicating that $R_{c;k}$ be taken as $\mu(R_{c;m})$.

where $22.4\% < V(R_{c;m}) \leq 35.0\%$

1) The variation in the measured load test results is large and $R_{c;k}$ is governed by the minimum $R_{c;m}$.
2) Where there is one load test result, ξ_2 is equal to ξ_1 as the mean and minimum value of $R_{c;m}$ are the same value.
3) If there are at least five load test results, the value of $R_{c;k}$ equals the minimum $R_{c;m}$, equivalent to ξ_2 equal to one.

where $V(R_{c;cal}) \leq 40\%$

1) The level of variation is very high, such that, the ξ_3 factors are extremely large where there are only one or two ground test profiles, these are not shown in Figure

7.18 as it is implied that design based on such a limited number of tests carries high risk.

2) Three ground test profiles lead to a ξ_3 value of 2.6 and four to a value of 1.6, thus, it is probably more economical to carry out four ground test profiles across the site as opposed to just three so that, the much reduced ξ_3 factor is taken advantage of when designing the piles.
3) Where many ground test profiles are carried out (n>10), the ξ_3 factor reduces to about 1.1.

where $40\% < V(R_{c;cal}) \leq 50\%$

1) Again, it is implied at least three ground test profiles are required.
2) The value of ξ_4 is equal to 1.8 where there are three ground test profiles and reduces to 1.1 where there are four again indicating it is beneficial to carry out at least four ground test profiles.
3) When there are at least five ground test profiles, the value of ξ_4 approaches unity indicating that $R_{c;k}$ be taken as the minimum $R_{c;cal}$ at these high levels of variation.

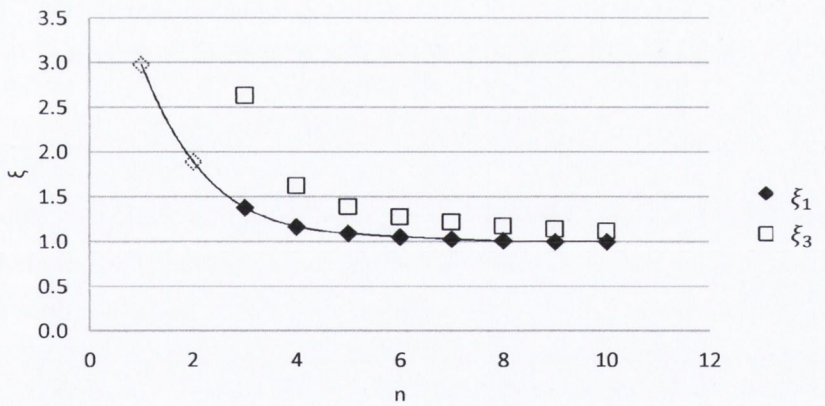


Figure 7.20 – Comparison of calculated ξ_1 and ξ_3 factors

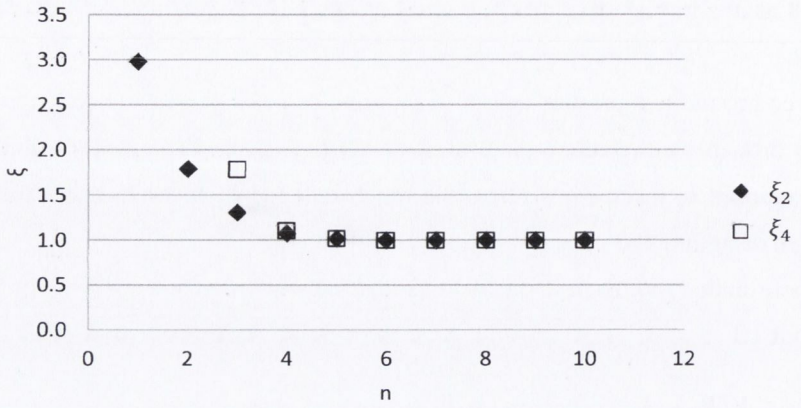


Figure 7.21 – Comparison of calculated ξ_2 and ξ_4 factors

7.5 Reliability of a pile design – SLS

Though it is important to quantify properly the ultimate capacity of a single pile under load, it is often the case with deep foundations that the governing limit state will be serviceability of the foundation. It is common practice to specify an allowable pile head deflection for a given load, usually the F_k for the pile under test, and to prove the design adequate by proof testing to 1.5 times the F_k, while monitoring deflection. In Ireland, where deep foundations are concerned, the allowable deflection under the F_k is usually limited to 10mm.

This section presents analysis of the PTD to assess the serviceability of each of the piles. The SLS is defined whereby the allowable pile head deflection is equal to 10mm and the pile resistance developed at this deflection is denoted $R_{c;10}$ (where piles were not loaded to cause 10mm deflection at the pile head the measured load-deflection data were extrapolated to 10mm).

As $R_{c;10}$ values are measured values (in most cases) the uncertainty $V(R_{c;10})$ was taken as 10%. The performance of the piles at the SLS, as for the ULS, was assessed at F_k for which the associated uncertainty, $V(F_k)$ was again taken as equal to 10%. Within-site variation was also included and taken as contributing $V(R_c)$ equal to 20% as described previously.

Table 7.1 summarises the calculated β values at the SLS. The values are lower than those calculated for the same piles at the ULS as the piles are more likely to reach 10mm deflection under F_k than they would be to reach δ_f under the same load (excepting, of course, the case where 10mm > δ_f equivalent to D < 100mm).The average β value for bored piles in DBC (Group 1) was around 2.0 compared with 2.9 for driven piles in the same deposit. Driven piles are, on average, less likely to reach the SLS under the F_k. This difference is likely due to the method of installation of the piles.

The average β value for CFA piles in boulder clay (Group 3) was -1.3 indicating the piles are extremely likely to be deflected by 10mm under F_k.

Table 7.1 – Summary of calculated pile design reliabilities: SLS

Pile Group	Ground Type	Pile Type	n	β - pile design	
				μ	Range
1	DBC	CFA	32	1.81	-1.72 to 5.09
2	DBC	Driven	22	2.89	0.29 to 5.14
3	Boulder Clay	CFA	13	-1.31	-3.14 to 1.45
4	Boulder Clay	Driven	12	0.91	-1.12 to 3.63
5	Sand/Gravel	Bored/CFA	12	-0.52	-2.76 to 1.71
6	Rock	Bored (2 Driven)	38	1.84	-1.54 to 4.82
7	Mixed	Bored/CFA	16	-0.02	-2.79 to 2.42
8	Rock (Tension)	Bored/CFA	11	-	- to -
9	Unknown	Bored (4 Driven)	18	1.14	-3.04 to 4.07

7.6 Characteristic values

When estimating $R_{c;cal}$ from ground test results, a characteristic value of the measured soil parameter may be used instead of the mean value to estimate the characteristic resistance of the pile, $R_{c;k}$. The choice of this characteristic value may be determined by statistical methods based on the observed sample mean and standard deviation of the measured parameters at a particular site.

Given a set of N_{SPT} profiles carried out across a site, the mean and standard deviation of the sample data may be calculated and in order to take into account the variation in the

material properties it is suggested by some, that statistical methods be applied directly to these.

In structures, the characteristic material property is defined as the lower 5% fractile of the parameter, that value above which the mean value of the material property should lie 95% of the time and this may be calculated, for a parameter X, assuming X is normally distributed, as shown in Equation 7.13.

$$X_k = \mu(X) - 1.645\,\sigma(X) \qquad 7.13$$

where X_k is the characteristic value of the parameter with mean value $\mu(X)$ and standard deviation $\sigma(X)$.

The effects of spatial variation in soils and the fact that soil properties measured close to each other are not probabilistically independent, but may show some correlation, suggest that Equation 7.13 be adapted to reflect this.

In Geotechnical design, it is the mean value of the soil parameter over the failure domain that will govern the occurrence of a limit state (Orr 2002). Lo and Li (2007) summarised the methods by which the characteristic value may be obtained in the case of soils. Where the failure domain is large, where $L_f > \Theta_z$ then X_k may be calculated by Equation 7.14. Equation 7.14 is applicable for determination of X_k for calculation of the shaft resistance, as L_f is generally large when compared to Θ_z and where L_f is taken as equal to the length of the pile L minus 2m.

In determining the base resistance, L_f is considered comparable to Θ_z and thus the effect of spatial averaging will be negligible and Equation 7.14 reduces to Equation 7.15.

$$X_k = \mu(X) - K\sqrt{\left(\frac{1}{n} + \Gamma^2\right)}\,s(X) \qquad 7.14$$

$$X_k = \mu(X) - K\sqrt{\left(\frac{1}{n}\right)}\,s(X) \qquad 7.15$$

The value of K for use in Equation 7.14 and Equation 7.15 may be calculated using the Student-t distribution and the value depends on n and on the significance level. As $n \to \infty$ then the difference between the population and sample standard deviations $\sigma(X) - s(X) \to$

0 in fact for $n \geq 30$ this difference is negligibly small, thus, for $n \geq 30$ the value of K may be approximated by 1.645.

Schneider (1997), suggested X_k be defined as the mean value minus one half the standard deviation, which is simply Equation 7.15 where $K/\sqrt{n}$ is always taken as equal to 0.5, however, in reality, K depends on n and this should be reflected in Equation 7.14 and in Equation 7.15.

These equations were applied to the N_{SPT} profiles in the PTD. An example of the characteristic values of the N_{SPT}, denoted $N_{SPT;k;s}$ and $N_{SPT;k;b}$, referring to the characteristic value over the length of the shaft and at the pile toe respectively, is shown in Figure 7.22, calculated by the various equations applied to the data measured at Site D and assuming a pile length equal to 10m.

Each of the following list may be suggested as a characteristic value and these are shown in Figure 7.22 for Site D.

(a) The mean value of the N_{SPT}, $\mu(N_{SPT;s})$ over the length of the failure domain $L_{f;s}$ (the length of the shaft of the pile minus the top 2m)
(b) The lower tail 5% fractile of $\mu(N_{SPT;s})$ over $L_{f;s}$
(c) 95% confidence in $\mu(N_{SPT;s})$ assuming a value of Θ_z equal to 1m over $L_{f;s}$
(d) 95% confidence in $\mu(N_{SPT;s})$ assuming a value of Θ_z equal to 4m over $L_{f;s}$
(e) Schneider's method applied to the pile shaft
(f) The mean value of the N_{SPT}, $\mu(N_{SPT;b})$ at the toe of the pile
(g) The lower tail 5% fractile of $\mu(N_{SPT;b})$ at the pile toe
(h) Schneider's method applied to the pile toe

Though the characteristic values are presented as increasing with depth in Figure 7.22, their average over the length of the pile is referred to here for convenience. Considering the pile shaft, $\mu(N_{SPT;s})$ was equal to 53 for this pile assumed 10m in length. The lower tail 5% fractile was equal to 29 and is the most conservative estimate of the characteristic value calculated here. Assuming Θ_z equal to 1 and 4m for purposes of spatial averaging over the failure domain governing shaft resistance, the characteristic value of the N_{SPT} was 45 and 39 respectively. Schneider's method was least conservative and led to a characteristic value of 46, very similar to that value representing 95% confidence in $\mu(N_{SPT;s})$ where Θ_z was equal to 1m.

At the pile toe $\mu(N_{SPT;b})$ was calculated at 10m depth using the least squares regression line and was computed as 75. The lower tail 5% fractile and Schneider's method were used to interpret other values of the characteristic value at the pile toe, these values were calculated as 51 and 68 respectively. Spatial averaging was not applied to estimate the characteristic value at the pile toe as the value of $L_{f;b}$ is short.

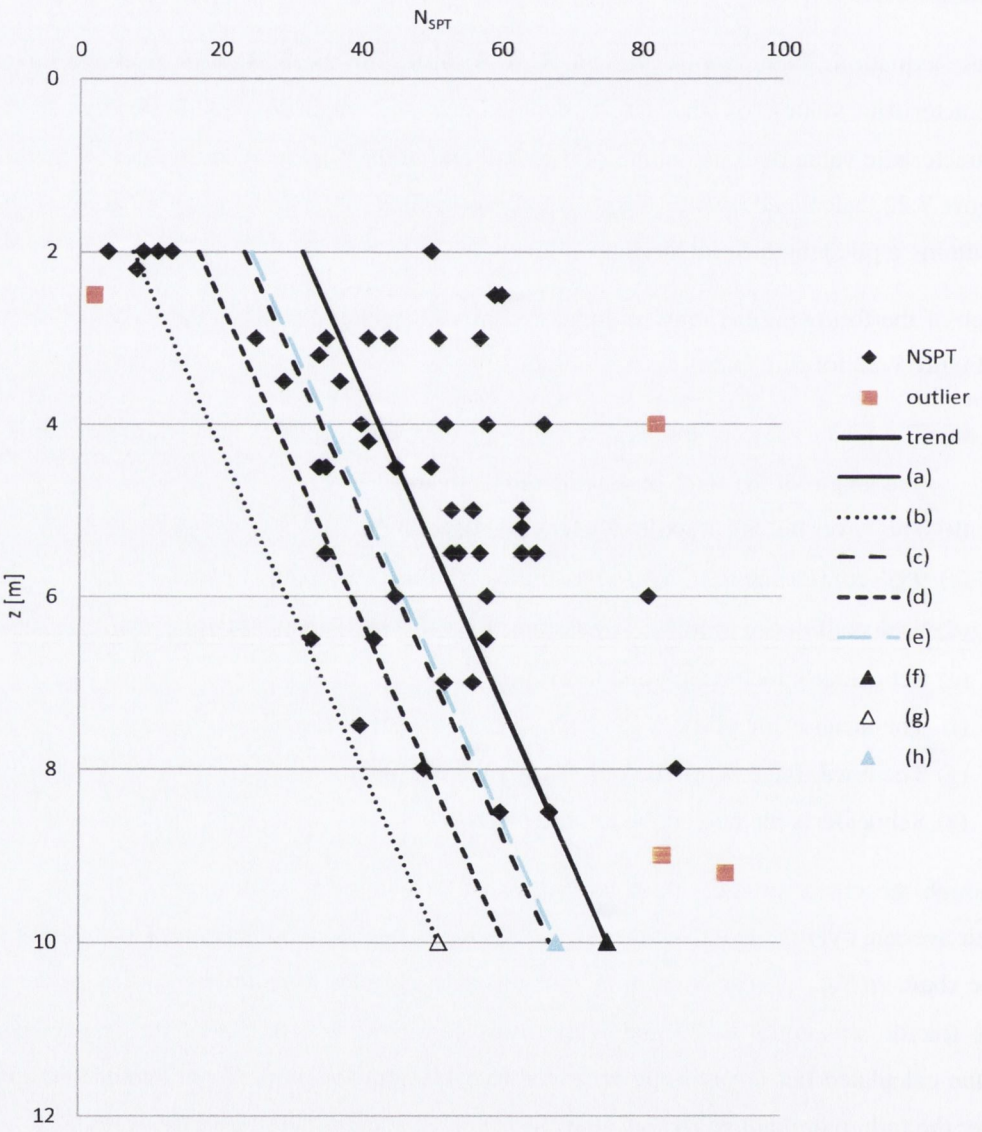


Figure 7.22 – Calculated characteristic values by various methods applied to Site D data

The values of $N_{SPT;k;s}$ and $N_{SPT;k;b}$ were used to compute the characteristic value of R_c, denoted $R_{c;k}$ for a pile of length 10m and 900mm diameter installed at Site D and these values were compared to the value of $R_{c;k}$ interpreted using the results of 8 load tests carried out on similar piles actually installed at the site (Group 2 in Table 7.2). The results are shown in Table 7.2.

The value of $R_{c;k}$ was assessed in accordance with Eurocode 7 by applying the ξ factors outlined in Eurocode 7 to the static load test results. The value of $R_{c;k}$ assessed in this way was 5821kN. This is lower than $R_{c;k}$ computed based on the mean value of the N_{SPT} and when Schneider's method was used where the value of $R_{c;k}$ was equal to 6751 and 5887kN respectively. Where no spatial averaging was applied over the shaft, equivalent to $\Theta_z > L_{f;s}$, the most conservative estimate of $R_{c;k}$ was calculated – 3909kN. Assuming Θ_z equal to 4 and 1m, $R_{c;k}$ was calculated as 4530 and 5217kN respectively.

Considering Group 2 of Table 7.2, if the eight load test results are considered alone, and assumed to follow the Student-t distribution with 7 (equal to n-1) degrees of freedom, then a lower tail 5% fractile value for $R_{c;m}$ denoted $R_{c;P5}$ is equal to 6032kN which corresponds closely with the value of $R_{c;k}$ approximated using Schneider's method.

Table 7.2 – Interpreted values of $R_{c;k}$ by different methods

					$R_{c;k}$ [kN]					
Group [_]	n [_]	$V(R_{c;chin})$ [%]	$V(N_{SPT})$ [%]	$R_{c;P5}$ [kN]	from $R_{c;m}$	(a & f) μ	(b & g) $\Theta_z > L_f$	(c & g) $\Theta_z = 4$	(d & g) $\Theta_z = 1$	(e & h) Schneider
1	4	37	-	1416	1631	-	-	-	-	-
2	8	22	32	6032	5821	6751	3909	4530	5217	5887
3	3	26	29	2784	3874	-	-	-	-	-
4	5	15	20	9011	8643	-	-	-	-	-
5	3	26	-	2348	2841	-	-	-	-	-
6	3	26	-	2322	3264	-	-	-	-	-
7	5	29	25	956	950	910	244	643	681	627
8	4	31	25	926	1060	1289	363	888	946	899
9	3	37	39	977	1783	-	-	-	-	-
10	3	30	39	693	882	-	-	-	-	-
11	2	2	39	2623	2197	-	-	-	-	-
12	3	54	23	304	2373	4366	2961	3135	3624	3939
13	3	27	23	2040	2912	5153	3446	3616	4189	4634
14	6	29	36	2511	1782	2191	975	939	1146	567
15	7	24	48	1828	1534	2361	943	1037	1208	601

Figure 7.23 shows a plot of the difference between $R_{c;P5}$ and $R_{c;k}$ (interpreted from load test results) normalised by $R_{c;k}$ against the variation in $R_{c;m}$, $V(R_{c;m})$. A least squares regression line indicates that the partial factors proposed in Eurocode 7 cover the situation of a maximum value of $V(R_{c;m})$ of around 20%, i.e. where y is equal to zero in Figure 7.23. This is in close agreement with the value the within-site variability of a pile characterised using $V(R_{c;chin})$ (and assumed representative of $V(R_{c;m})$) in Figure 4.20 where many load test results are available.

The values on the y axis in Figure 7.23 are negative above a value of $V(R_{c;m})$ of about 20% indicating that $R_{c;P5}$ is less than $R_{c;k}$ and this is thought to be due to a limited number of load test results which tends to lead to a larger value of $V(R_{c;m})$, as shown earlier in Figure 4.20.

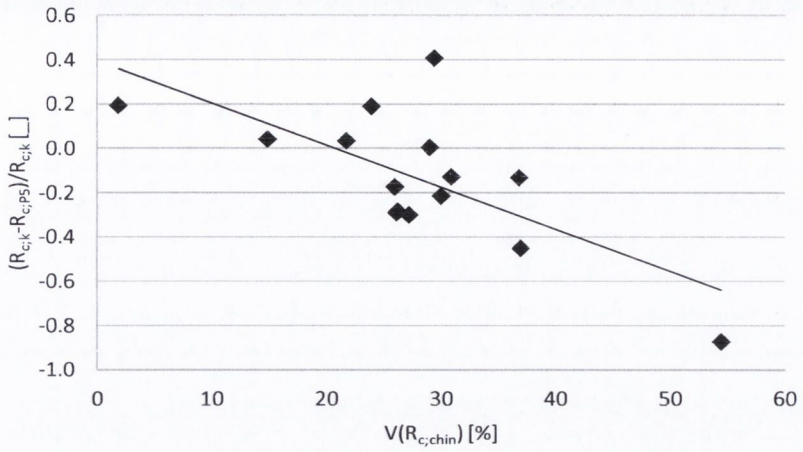


Figure 7.23 – Plot showing variation in $R_{c;k}$ and $R_{c;P5}$ with $V(R_{c;chin})$

Examination of Table 7.2 highlights the difficulties involved in choosing the characteristic value for design from ground test results. Design based on the mean value of the N_{SPT} tends to over predict the value of $R_{c;k}$ when compared with that value computed using the load test results with the factors in Eurocode 7 or when computed using $R_{c;P5}$ where a Student-t distribution was assumed. The other methods neither consistently over predict nor under predict the value of $R_{c;k}$ when compared with that computed based on load test results.

The differences in the calculated $R_{c;k}$ values depend on the variation observed in the load test results and the variation in the ground test results. Where $V(N_{SPT})$ is relatively high, then the $R_{c;k}$ values, computed based on the ground test results, will be substantially lower where the 5% fractile or 95% confidence in the mean value is used, compared to the situation where the mean value itself is used. This is the case for Group 14 and 15 in Table 7.2.

Group 12 demonstrates that $R_{c;P5}$ can be substantially lowered where the value of $V(R_{c;m})$ is high. The value of $R_{c;P5}$ equal to 300kN is clearly non-sensical, based on the results of 3 pile tests loaded in the range 2100-3150kN with corresponding deflections in the range 4-10mm at the pile head. The value of $R_{c;k}$ using the correlation factors in Eurocode 7 ignores the large variability that was observed from the load tests and results in a much increased and more realistic value of $R_{c;k}$ equal to 2400kN. Group 12 highlights the fact

that the variation in the sample of load tests is sometimes not representative of the variation in the population.

In the case of Group 2 there were 8 load tests in number and based on these, the within-site variation was 22% and the mean value of $V(N_{SPT})$ was equal to 34% (Table 4.12). Based on these levels of variation the values of $R_{c;P5}$ and $R_{c;k}$ from the load test results using the correlation factors in Eurocode 7 are considered to give realistic values of $R_{c;k}$. Also, $R_{c;k}$ from ground test results using Schneider's method and using 95% confidence in the mean, where an appropriate value of Θ_z is chosen for application of spatial averaging to the shaft resistance, are also considered to give representative values of $R_{c;k}$.

In the absence of many load test results, in excess of about 4, then the value of $V(R_{c;m})$ is difficult to quantify with any degree of certainty and can lead to over conservative values of $R_{c;k}$, Eurocode 7 overcomes this problem by application of correlation factors which are thought to cover values of $V(R_{c;m})$ equal to 20%. Where the value of $V(N_{SPT})$ is large, in excess of 30%, then the methods of estimation of $R_{c;k}$ from ground test results become too conservative.

The levels of variation shown in Table 7.2 are typical of sites in Ireland, as these can often be large, it is, therefore, suggested that sites be zoned such that the variation within each zone is limited and piles are designed specific to each zone. This would mean that piles within each zone would achieve the target levels of reliability when statistical methods are applied to ground test results and load test results and methods of estimation of $R_{c;k}$ would yield reliable results.

7.6.1 Summary

The calculated reliabilities using the static load test results and using the ground test results are summarised in this section in Table 7.3 and Table 7.4 respectively.

Table 7.3 – ULS: Summary of β calculated from static load test results

Pile Group	Ground Type	Pile Type	n	β - single pile			β - pile design		
				μ	Range		μ	Range	
1	DBC	CFA	32	3.53	1.53	7.16	2.69	1.31	4.79
2	DBC	Driven	22	4.85	2.58	6.91	3.49	2.20	5.32
3	Boulder Clay	CFA	13	1.34	-1.83	5.46	0.72	-1.20	3.26
4	Boulder Clay	Driven	12	4.83	0.22	7.38	3.39	0.07	5.75
5	Sand/Gravel	Bored/CFA	12	2.01	-0.07	5.14	1.39	-0.12	3.73
6	Rock	Bored (2 Driven)	38	5.00	0.40	8.74	3.55	0.30	6.01
7	Mixed	Bored/CFA	16	3.10	0.56	6.27	2.10	0.27	3.57
8	Rock (Tension)	Bored/CFA	11	1.11	-8.72	8.24	0.90	-5.16	5.15
9	Unknown	Bored (4 Driven)	18	4.61	2.08	7.77	3.29	1.30	5.69

Table 7.4 – ULS: Summary of β calculated from ground test results

Pile Group	Ground Type	Pile Type	β ($\Theta_z > L_t$)			β ($\Theta_z = 1$)			β ($\Theta_z = 4$)		
			μ	Range		μ	Range		μ	Range	
1	DBC	CFA	0.98	0.02	1.85	1.07	0.05	1.95	1.04	0.04	1.92
2	DBC	Driven	2.29	1.50	4.12	2.60	1.67	4.77	2.41	1.50	4.54
3	Boulder Clay	CFA	-0.24	-0.63	0.64	-0.20	-0.61	0.74	-0.21	-0.62	0.72
5	Sand/Gravel	Bored/CFA	1.38	0.38	3.27	-	-	-	-	-	-

Figure 7.24 compares the average β values calculated using the ground test results and those calculated using the load test results; a line representing a one-to-one relationship is also shown. The β values for Groups 1, 2 & 3 are seen to lie to the left of the one-to-one line, consistent with the fact that $R_{c;cal}$ based on ground tests results carries more uncertainty than $R_{c;m}$ from actual load tests.

Furthermore, the β values shown in Figure 7.24 from the ground test results are those calculated where no spatial averaging was applied to the N_{SPT}. Table 7.4 indicates that the effect of spatial averaging is limited even where Θ_z is assumed small (equal to 1m). The Reader is reminded that where spatial averaging was applied it was only applied for

variance reduction of the shaft resistance and thus the observed variation was carried through for estimation of $V(R_b)$.

It should be noted that Figure 7.24 and Figure 7.25 are based on the average β values for each of the groups of piles, the range of values based on individual piles was quite large as shown in Table 7.3.

Figure 7.25 is a plot of the average β values for each group, calculated from load test results, at the ULS and SLS. There is seen to be a relationship between β_{ULS} and β_{SLS} where β_{SLS} is about 2.1 less than β_{ULS}. The value of β_{SLS} is based on the recorded load corresponding to a measured deflection equal to 10mm, $R_{c;10}$. Figure 7.25 implies that the more likely a pile is to reach the ULS, then the more likely it is to reach the SLS, which is intuitively what would be expected.

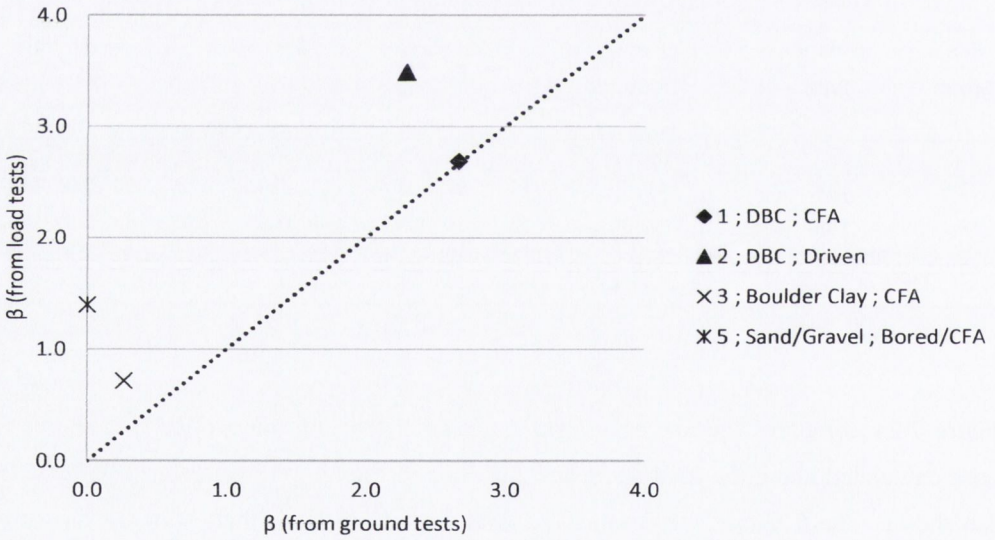


Figure 7.24 – Comparing average β from load tests and that from ground tests at ULS

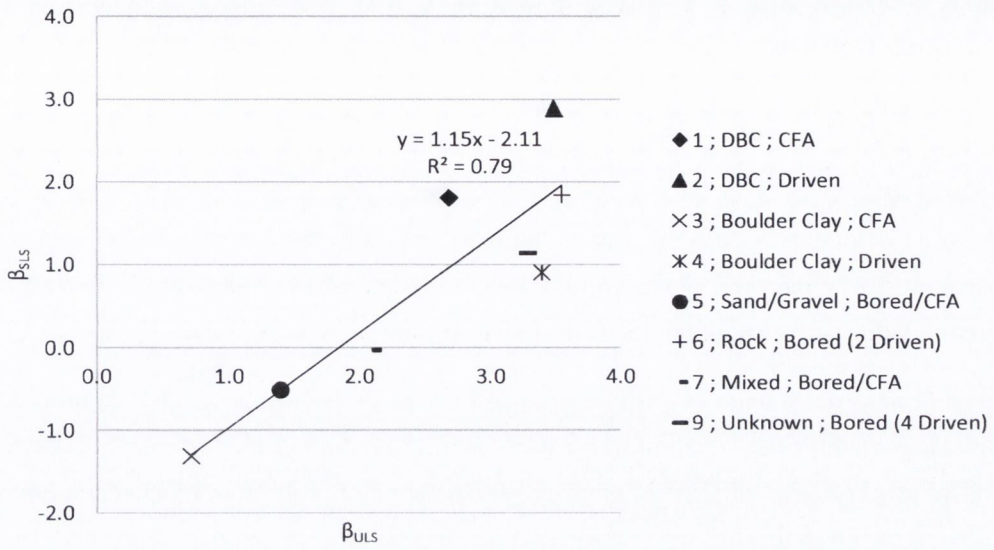


Figure 7.25 – Comparing β_{ULS} with β_{SLS}

8 Conclusions

A single pile under load offers resistance on deflection through a complex pile-soil interaction that depends on the pile geometry, the strength properties of the ground and on the method of installation of the pile. It is recognised that precise estimation of the pile resistance at failure is difficult, due to the relatively high level of uncertainty including spatial variation inherent to the ground, measurement errors arising during testing and variability due to pile installation effects.

Traditionally, this ambiguity was accounted for by the global factor of safety approach, in combination with engineering judgement, usually informed by past experience. However, modern day accountability of the engineer demands a more robust and logical analysis of data collected during site investigation and preliminary testing and has necessarily led to the application of statistical methods to geotechnical design problems.

Reliable pile design requires an appreciation of the overall uncertainty and mitigation of this uncertainty requires quantification of the individual contributory sources of uncertainty based on site investigation and testing that is relevant to, and representative of, the complete area over which a pile design is specified.

During the course of this study, a database of static load tests carried out on piles installed in varying ground conditions in Ireland, including fine and coarse grained material and rock, was compiled. Site investigation data, including borehole logs and in-situ and laboratory test results pertaining to the ground at the various test sites, formed an essential part of the database.

This pile test database (PTD) was used to assess the methods by which the load resisting capacity of the ground against a pile (R_c) is estimated. Pile load tests carried out on instrumented piles, were particularly useful, and enabled the separation of the development of shaft and base resistances with pile deflection. The development of shaft stress along the length of the piles and also the stress in the soil at the pile toe, could also be estimated using these instrumented test results, thus revealing the mechanism by which the applied load is shed from the pile into the adjacent soil.

The Author also installed and instrumented several piles throughout the course of the study, including two CFA piles toed in rock, which were used to assess the methods by which instrumented load tests are interpreted. Other full-scale load testing included the

installation of four micro piles on a separate site to highlight the effects of spatial variation in the soil on pile behaviour and on the value of R_c.

The PTD compiled was also used to assess the variability associated with the expected values of R_c when estimated using ground test results and using the load test results. Where a pile design is specified for a particular site, such that where it is proposed many *similar* piles be installed across the site, then it is required that the within-site variability be assessed in addition to the uncertainty associated with R_c for a single pile.

Methods of estimation of R_c were assessed based on the results of pile load tests for which the piles were taken to failure, and it was concluded that, extrapolation of load-deflection data to a pile head deflection equal to 10% of the pile diameter, denoted δ_f, assuming a hyperbolic relationship as proposed by Chin (1970), yielded a good practical estimate of R_c and this estimate was denoted $R_{c;chin}$. It was found, that, where piles are loaded such that they are deflected by at least 5% of the pile diameter, then the value of $R_{c;chin}$ was in the range 85-100% of $R_{c;m}$ where $R_{c;m}$ is the measured value of R_c at δ_f.

A relationship was developed, such that, the variation associated with the value of $R_{c;chin}$, characterised by the coefficient of variation of the parameter $V(R_{c;chin})$ for a single pile, could be estimated based on the ratio of the maximum deflection recorded during the load test to the pile diameter, δ_{max}/D . The value of $V(R_{c;chin})$ was found to reduce from 0.40-0.10 where δ_{max}/D increased from 1-10% and this included an allowance for measurement error equivalent to a value of $V(R_{c;m})$ equal to 0.10.

Using the load-deflection data for the piles loaded to δ_f, $R_{c;chin}$ was estimated for each of the piles in the PTD. Groups of *similar* piles were identified, where *similar* was defined as piles of equal diameter and within 1m length of each other installed on the same site and in similar ground. These groups contained between 2 and 8 pile load test results and were used to assess the within-site variation, characterised by $V(R_{c;chin})$ assumed equivalent to $V(R_{c;m})$. A simulation exercise was completed whereby all combinations of n load tests in each of the 15 groups were generated and the results were used to estimate the maximum expected value of $V(R_{c;m})$ where a limited number of load tests are carried out, which is generally the case in practice. It was found, that, where two load tests are carried out, the expected value of $V(R_{c;m})$ was around 0.38, and this reduced to 0.20 where 8 load tests are carried out.

Having characterised the uncertainty associated with R_c for a single pile, and also the within-site variability representative of the test sites, the performance of the piles were assessed at the ultimate and serviceability limit states with respect to single piles and for many piles installed across a site. The performance was characterised using the reliability index β which is related to the probability of a limit state occurring.

On average, the β value for CFA and driven piles in DBC at the ULS was 2.7 and 3.5 respectively when calculated using pile load test results. A possible explanation for the higher value estimated for the driven piles, is the fact that these were loaded to a higher value of the ratio of δ_{max}/D, where the mean value of δ_{max}/D was equal to 2.1 and 3.5% for the CFA and driven piles respectively – $V(R_{c;chin})$ is increased where load-deflection data is limited, thus reducing β. The β values for the other types of piles including those in sand/gravel and in rock were seen to be highly variable over the different sites in the PTD.

Pile designs were found to realise their maximum potential β value when loaded to a deflection at the pile head, of at least 5% of the diameter, thus, the calculated β values could potentially have been increased had the pile load tests been conducted such that greater deflections had taken place.

The variability in the shaft and base resistances, denoted $V(R_s)$ and $V(R_b)$ were both found to be about 0.40, when computed based on the results of the N_{SPT} and thus combined to yield a value of $V(R_{c;cal})$ also equal to 0.40, about double $V(R_{c;m})$.

Correlation factors (ξ) may be applied to the mean and minimum values of $R_{c;m}$ or $R_{c;cal}$, so that, the occurrence of a limit state remains sufficiently unlikely – a philosophy in line with the recently introduced Eurocode 7. The ξ factors depend on the level of variation in the measured or calculated results, the number of pile load tests or ground test profiles carried out at the site and on the level of risk deemed appropriate for the foundation under design.

The ξ factors were evaluated by the Author for the case where the likelihood of the occurrence of the ULS was not greater than 5% and based on the levels of variation observed in the PTD ($V(R_{c;m})$ equal to 0.22 and $V(R_{c;cal})$ equal to 0.40). It was found, that, higher ξ values should be applied to $R_{c;cal}$ than to $R_{c;m}$, to achieve a consistent level of safety in the foundation, as the uncertainty associated with $R_{c;cal}$ is greater.

Where one pile load test result is available, resulting in one value of $R_{c;m}$, this should be divided by about 3.0 to estimate the characteristic resistance $R_{c;k}$ and this factor is ξ, and reduced to 1.9 to be applied to the mean of the load test results where two load test results were available, indicating the potential benefits in carrying out a second test. The ξ_1 factor approached unity where six load tests were carried out, indicating that the mean value of $R_{c;m}$ be taken as equal to $R_{c;k}$ where at least this number of load test results is available.

In the case of $R_{c;cal}$ (based on ground test profiles) it was concluded that at least three profiles are required for pile design and that there is substantial benefit in carrying out a fourth. The level of uncertainty in $R_{c;cal}$ is such that the ξ_3 factor, applied to the mean of the $R_{c;cal}$ values, does not reach unity and only approached 1.1 where ten ground test profiles were available.

Higher levels of uncertainty may also be allowed for by application of ξ_2 and ξ_4 factors to the minimum $R_{c;m}$ and $R_{c;cal}$ respectively. These factors were also calculated for the case where the maximum uncertainty $V(R_{c;m})$ equalled 0.35 and $V(R_{c;cal})$ equalled 0.5.

The PTD is evidence that, very rarely do piles reach the ULS, or even the SLS, even under loads in the range 2-3 times F_k and this would indicate that high β values are achieved in reality. Additional favourable effects, such as, the transfer of load from weaker to stronger piles in the case of stiff structures and also pile group effects, are thought to lead to the low failure rate of piled foundations observed. Such favourable effects may be allowed for by varying the value of the target reliability, β_T in particular cases.

Using the results of load tests on instrumented piles installed in DBC, together with ground test results carried out at the same sites, the factors used for calculation of R_c from ground test results were interpreted. Considering CFA piles, it was found that the adhesion factor α reached values as high as 0.7 during the load tests, with a value of 0.8 predicted at δ_f. The base bearing factor N_c reached about 5 during the load tests and was predicted as 6.5 at δ_f, with a predicted limiting value of around 9, had the pile been deflected further.

This analysis was based on a f_1 multiplication factor of 5.5 for application to the N_{SPT} to estimate s_u and this value of f_1 was verified using the results of triaxial tests on samples of DBC taken from various sites, in combination with the N_{SPT} recorded at several sites also comprising DBC. These results were also used to estimate the uncertainty associated with

the f_1 factor, $V(f_1)$ assuming a constant value of α. The value of $V(f_1)$ was found to be about 0.30.

The values of these factors were then applied to the ground test results to estimate $R_{c;cal}$ for 24 CFA piles that were statically load tested in DBC. Appraisal of the calculation factors, interpreted from the instrumented tests, was carried out by evaluation of the ratio $R_{c;cal}/R_{c;chin}$ for each pile. The average value of $R_{c;cal}/R_{c;chin}$ was equal to 1.2 for the 24 CFA piles, suggesting that, on average, $R_{c;cal}$ overestimates the value of R_c or that $R_{c;chin}$ underestimates it.

Also, the standard deviation associated with the ratio was very large, equal to 40%, thought to be due to the relatively high level of variation associated with the N_{SPT} results on which $R_{c;cal}$ is based. Uncertainty in the value of $R_{c;chin}$, based on interpreted limited load-deflection data from the pile load tests may also have contributed to the overall uncertainty.

A similar analysis was applied to driven piles in DBC and it was found that α was similar to that of CFA piles, around 0.8 with a suggestion that it could reach unity at higher deflections. However, the applicability of the α factor to driven piles is questionable given the shear stress profile observed in the case of driven piles. The interpreted N_c value was around 10 times that for the CFA piles, around 65 at δ_f, with a limiting value approaching 90 on further deflection. The marked increase in the N_c factor, in the case of the driven piles, is thought to be due to differences in the method of installation of CFA and driven piles.

Appraisal of the calculated factors (α, f_1 and N_c) was carried out by application to ground test results at two sites comprising DBC and in which 21 driven piles had been installed and load tested. The average value of $R_{c;cal}/R_{c;chin}$ was equal to 1.1, indicating that on average, the factors interpreted predict the value of R_c rather well. However, the standard deviation of the ratio was again large, equal to 34%. These results indicate that, on average, R_c can be predicted from the ground test results using the factors interpreted by the Author, but it is critical that the variability be appreciated also.

Further Research

It is intended that the pile test database, comprising the details of piles installed and statically load tested in Ireland and also including the ground conditions pertaining to the same sites, be made available for use by others and also be extended when more pile load test results become available in the future. This database will become an increasingly valuable resource if expanded upon in an age where statistical methods, whose power depends on the number of test results, are increasingly used.

Verification of the design parameters required to estimate the shaft and base resistances of driven piles from ground test results in DBC is required. Values of α and N_c were estimated from the results of three load cycles applied to just one pile and were verified by application to ground test results for two sites in which around twenty driven piles were statically load tested. More pile load tests on instrumented driven piles is suggested to verify the conclusions made here.

More accurate quantification of the within-site variability of the ground, measured using both in-situ and laboratory tests, is required, if reliability analyses are to be applied to geotechnical problems properly to assess the true probability of failure of foundations when designed using ground test results.

Within-site variability requires characterisation of the spatial variation of the ground in both the horizontal and vertical planes and for various types of soils. These parameters may be quantified by carrying out a comprehensive desk study of measured ground properties, knowing the relative location of boreholes in which tests are carried out in-situ, or in the case of laboratory testing, knowing the horizontal and vertical distance between which test samples were retrieved.

Probabilistic distributions affect the calculated reliability. The choice of probabilistic distribution needs to be investigated further to ensure the reliability estimated is realistic.

Eurocode 7 outlines correlation factors used to calculate $R_{c;k}$ from ground test results or pile load test results. The correlation factors depend on the number of tests carried out in each case, but do not allow for combination of the information gained in carrying out both ground test and load tests, which is often the case in practice. Bayesian methods, which have the potential to do this, should be investigated to enable combination of the various sources of information for use in pile design.

References

Abdelhamid, M. S. and R. J. Krizek (1976). "At rest lateral earth pressure of consolidating clay." ASCE 102(GT7): 721-738.

Abdelrahman, G. E., E. M. Swaarawi and K. S. Abouzaid (2003). Interpretation of axial pile load test results for continuous flight auger piles. The 9th Arab Structural Engineering Conference, Abu Dhabi, UAE.

API, A. P. I. (2000). Recommended practice for planning, designing, and constructing fixed offshore platforms: Working stress design 21st Ed. Washington, D.C.

Armishaw, J. W. (1987). Report on driven precast concrete piles in lodgement till at Tallaght town centre development. Dublin.

Baecher, G. B. and J. T. Christian (2003). Reliability and statistics in geotechnical engineering. Chichester, Wiley.

Baecher, G. B. and R. Rackwitz (1982). "Factors of safety and pile load tests." International Journal for Numerical and Analytical methods in Geomechanics 6: 409-424.

Baguelin, F. (1990). A study of the influence of the number of pile load.ing tests on the safety factor.

Becker, D. E. (1996). "Eighteenth Canadian Geotechnical Colloquium: Limit states design for foundations. Part II. Development for the National Building Code of Canada." Canadian Geotechnical Journal 33: 984-1007.

Berezantzev, V. C., V. Khristoforov and V. Golubokov (1961). Load bearing capacity and deformation of piled foundation. 5th International Conference Soil Mechanics and Foundation Engineering, Paris.

Billberg, P. (2006). Form Pressure Generated by Self-Compacting Concrete — Influence of Thixotropy and Structural Behaviour at Rest. School of Architecture and the Built Environment Division of Concrete Structures. Stockholm, Royal Institute of Technology. PhD: 91.

Bolton, M. D. (1991). Geotechnical stress analysis for bridge and abutment design, Crowthorne: Transport and road research laboratory.

Bond, A. J. and R. J. Jardine (1991). "Effects of installing displacement piles in high OCR clay." Géotechnique 41(3): 341-363.

Borel, S., M. Bustamante and L. Gianeselli (2004). An appraisal of the Chin method based on 50 instrumented pile tests. New Civil Engineer.

Brooker, E. W. and H. O. Ireland (1965). "Earth pressures at rest related to stress history." Canadian Geotechnical Journal 2(1): 1-15.

Bustamante, M. and L. Gianeselli (1982). Pile bearing capacity prediction by means of static penetrometer CPT. Proceedings of the 2nd European Symposium on Penetration Testing, Amsterdam.

CEN (1992). Draft for Development. DD ENV 206:1992: Concrete. Performance, production, placing and compliance criteria. London, British Standards Institution.

CEN (2001). Eurocode 7 Part 1: Geotechnical design: General rules. E. C. f. Standardisation. Brussels.

Cheng, Y. M. (2004). "Technical Note: Nq factor for pile foundations by Berezantzev." Géotechnique 54(2): 149-150.

Cherubini, C. and G. Vessia (2007). "Reliability approach for the side resistance of piles by means of total stress analysis (alpha method)." Canadian Geotechnical Journal 44: 1378-1390.

Chin, F. K. (1970). Estimation of the ultimate load of piles from tests not carried to failure. Proc. 2nd S.E. Asian Conference, Singapore.

Ching, J., H.-D. Lin and M.-T. Ten (2009). Reliability-based code calibration of piles based on incomplete proof load tests. The 2nd international symposium on geotechnical safety and risk, Gifu, Japan.

Clausen, C. J. F., P. M. Aas and K. Karlsrud (2005). Bearing capacity of driven piles in sand, the NGI approach. Proc., Int. Symp. on Frontiers in Offshore Geomechanics, ISFOG, Taylor & Francis, London.

Collins, F. and J. M. Mitchell (1990). Piling in Gravels. Geotechnical Society of Ireland. Institution of Engineers of Ireland.

Davisson, M. (1972). High Capacity Piles. Soil Mechanics Lecture Series on Innovations in Foundation Construction, Illinois Section, Chicago, ACSE.

Decourt, L. (1999). Behaviour of foundations under working load conditions. The 11th Pan-American conference on soil mechanics and geotechnical engineering, Brasil.

DeNicola, A. and M. F. Randolph (1993). "Tensile and compressive shaft capacity of piles in sand." Journal of Geotechnical Engineering 119(12): 1952-1973.

Farrell, E. R. and M. L. Lawler (2008). "CFA pile behaviour in very stiff lodgement till." Institution of Civil Engineers-Geotechnical Engineering 161(1): 49-57.

Farrell, E. R., B. Lehane and M. Looby (1998). "An instrumented driven pile in Dublin boulder clay." Proceedings of the Institution of Civil Engineers - Geotechnical Engineering 131(4): 233-241.

Farrell, E. R. and D. Wall (1990). "Soils of Dublin." Institutior

Fellenius, B. H. (1980). "The analysis of results from routi Engineering 13(6): 19-31.

Fellenius, B. H. (2001). From strain measurements to lo: Geotechnical News Magazine. 19: 35-38.

Fellenius, B. H. (2001). "What capacity value to choose fro test." Deep foundation institute, Fulcrum: 19-22.

Fellenius, B. H. (2002). "Determining the True Distributio Piles." American Society of Civil Engineers, Foundation Congress 116.

Fenton, G. A. and D. V. Griffiths (2003). "Bearing capacity p c-f soils." Canadian Geotechnical Journal 40(1): 5

Fenton, G. A. and D. V. Griffiths (2007). "Reliability-bas Probabilistic Applications in Geotechnical Engi Specialty Publication No. 170.

Fleming, W. G. K. and S. Thorburn (1983). Recent pilin Report. Proceedings of Conference on Adva Treatment for Foundations, London.

Fleming, W. G. K., A. J. Weltman, M. Randolph and K. Els London, Taylor & Francis.

Foye, K. C., R. Salgado and B. Scott (2006). "Assessment of Variable Uncertainties for Reliability-Based Design of Foundations." American Society of Civil Engineers, ASCE 132(9): 1197-1207.

Gavin, G. K. and B. C. O'Kelly (2007). "Effect of Friction Fatigue on Pile Capacity in Dense Sand." Journal of geotechnical and geoenvironmental engineering 133(1): 63-71.

Gavin, K. G. (2010). Full-scale instrumented load tests on CFA piles in Irish glacial soils - lessons learnt. Presentation given to Engineers Ireland - Geotechnical sector, Dublin.

Gavin, K. G., D. Cadogan and P. Casey (2009). "Shaft Capacity of Continuous Flight Auger Piles in Sand." Journal of geotechnical and geoenvironmental engineering 135(6): 790-798.

Gavin, K. G., D. Cadogan and L. Twomey (2008). "Axial resistance of CFA piles in Dublin Boulder Clay." Proceedings of the Institution of Civil Engineers - Geotechnical Engineering 161(GE4): 171-180.

Gavin, K. G. and B. M. Lehane (1998). Estimating end bearing capacities of driven piles in sand from in-situ tests. Proc. VII Int. Conf. on Piling and Deep foundations, Vienna.

Goh, A. T. C., F. Kulhawy and C. G. Chua (2005). "Bayesian Neural Network Analysis of Undrained Side Resistance of Drilled Shafts." ASCE 131(1): 84-93.

Haldar, S. and G. L. S. Babu (2008). "Load Resistance Factor Design of Axially Loaded Pile Based on Load Test Results." JOURNAL OF GEOTECHNICAL AND GEOENVIRONMENTAL ENGINEERING © ASCE.

Haldar, S. and G. L. S. Babu (2009). "Design of laterally loaded piles in clays based on cone penetration data: a reliability-based approach." Géotechnique 59(7): 593-607.

Hansen, J. B. (1963). "Discussion on hyperbolic stress-strain response. Cohesive soils." American Society of Civil Engineers, ASCE, Journal for Soil Mechanics and Foundation Engineering 89(SM4): 241-242.

Hansen, J. B. (1965). Philosophy of foundation design: Design criteria, safety factors and settlement limits. Symposium on Bearing Capacity and Settlement of Foundations, Duke University, Durham.

Hayes, J. and T. Simmonds "Interpreting strain measurements from load tests in bored piles."

Hight, D. W., R. A. Ellison and D. P. Page (2004). Engineering in the Lambeth Group. London, CIRIA.

ICE, T. F. o. P. S. i. a. w. B. (2007). ICE Specification for piling and embedded retaining walls. London, Thomas Telford Ltd.

IGSL (2009). Meath waste management facility, Carranstown, Duleek, Co. Meath - Factual geotechnical investigation report.

Jaky, J. (1948). Pressure in soils. The 2nd international conference on soil mechanics and foundation engineering, Rotterdam.

Jardine, R. J. and F. C. Chow (1996). New design methods for offshore piles. Marine Technology Directorate, London.

Jardine, R. J., F. C. Chow, R. Overy and J. Standing (2005). ICP design methods for driven piles in sands and clays. London, Thomas Telford.

Kay, J. N. (1976). "Safety factor evaluation for single piles in sand." ASCE 102: 1093-1108.

Kay, J. N. (1977). Factor of safety for piles in cohesive soils. 9th International Conference on Soil Mechanics and Foundation Engineering, Tokyo.

Khan, A. A., W. D. Cook and D. Mitchell (1995). "Early Age Compressive Stress-Strain Properties of Low-, Medium, and High-Strength Concretes." ACI Materials Journal 92(6): 617-624.

Kishida, H. and M. Uesugi (1987). "Tests of interface between sand and steel in the simple shear apparatus." Géotechnique 37(1): 46-52.

Kolk, H. J., A. E. Baaijens and M. Senders (2005). Design criteria for pipe piles in silica sands. Proceedings of International Symposium on Frontiers in Offshore Geomechanics, ISFOG, Taylor & Francis, London.

Kraft, L. M. (1990). "Computing axial pile capacity in sands for offshore conditions." Marine Geotechnology 9: 61-92.

Kulhawy, F. and P. W. Mayne (1990). Manual on estimating soil properties for foundation design. California, Electric Power Reasearch Institute.

Kulhawy, F. H. and C. Jackson (1989). "Some observations on undrained side resistance of drilled shafts." ASCE: 1011-1025.

Kulhawy, F. H. and K. K. Phoon (1993). Drilled shaft side resistance in clay soil to rock. Design and performance of deep foundations: Piles and piers in soil and soft rock.

Ladanyi, B. (1963). "Expansion of a cavity in a saturated clay medium." American Society of Civil Engineers, ASCE 89(SM4): 127-161.

Lee, J. H. and R. Salgado (1999). "Determination of pile base resistance in sands." ASCE Journal of Geotechnical and Geoenvironmental Engineering 125(8): 673–683.

Lehane, B. (1997). Design of axially loaded piles - Irish Practice. Proceedings of Seminar on design of axially loaded piles in Europe, Int. Soc, Soil Mech. & Geotech. Engrg, Brussels.

Lehane, B. M. and R. J. Jardine (1994). "Displacement pile behaviour in glacial clay." Canadian Geotechnical Journal 31: 79-90.

Lehane, B. M. and M. F. Randolph (2002). "Evaluation of a Minimum Base Resistance for Driven Pipe Piles in Siliceous Sand." Journal of geotechnical and geoenvironmental engineering 128(3): 198-205.

Lehane, B. M., J. A. Schneider and X. Xu (2005). A review of design methods for offshore driven piles in siliceous sand. Perth, Australia, The University of Western Australia.

Lehane, B. M. and B. Simpson (2000). "Modelling glacial till under triaxial conditions using a BRICK soil model." Canadian Geotechnical Journal 37: 1078-1088.

Li, K. S. and S. R. Lo (2006). Variance of soil parameters: some common misconceptions. International Symposium on New Generation Design Codes for Geotechnical Engineering Practice. Taipei.

Lo, S. R. and K. S. V. Li (2007). "Characteristic and design soil parameters: Use of statistics." Institution of Civil Engineers Geotechnical Engineering 160(GE3): 141-146.

Long, M. and F. Collins (1998). Rock socketed piling in Ireland. Proceedings of Deep Foundation Institute Conference, Vienna, Austria.

Long, M. and F. Collins (1999). Piling in Rock. The Institution of Engineers Ireland, Cork.

Long, M. and C. O. Menkiti (2007). "Geotechnical properties of Dublin Boulder Clay." Géotechnique 57(7): 595-611.

MacGregor, J. G. (1976). "Saferty and limit states design for reinforced concrete." Canadian Geotechnical Journal 3(484-513).

Mandolini, A., G. Russo and C. Viggiani (2005). "Pile foundations: experimental investigations, analysis and design." Proceedings of the International conference on soil mechanics and geotechnical engineering 1: 177-216.

Mayne, P. W. and F. H. Kulhawy (1982). "K0-OCR relationships in soil." Journal of the geotechnical engineering division 108(GT6): 851-872.

Meyerhof, G. G. (1951). "The ultimate bearing capacity of foundations." Géotechnique(2): 301-332.

Meyerhof, G. G. and L. J. Murdock (1953). "An investigation of teh bearing capacity of some bored and driven piles in London clay." Géotechnique(3): 267-282.

Nadim, F. (2007). Tools and strategies for dealing with uncertaintiy in geotechnics. Probabilistic methods in geotechnical engineering. D. V. Griffiths and G. A. Fenton. New York, Springer Wien: 71-95.

NeSmith, W. M. and T. C. Siegel (2009). Shortcomings of the Davisson Offset Limit Applied to Axial Compressive Load Tests on Cast-In-Place Piles, ASCE.

Ng, C. W. W., D. B. Rigby, S. W. L. Ng and G. H. Lei (2000). "Field studies of well-instrumented barrette in Hong Hong." Journal of geotechnical and geoenvironmental engineering 126(1).

Nordlund, R. L. (1963). "Bearing capacity of piles in cohesionless soils." ASCE Journal of Soil Mechanics and Foundation Engineering Division 89(SM3): 1-35.

O'Neill, M. W. and L. C. Reese (1999). Drilled shaft: Construction procedures and design methods. U. S. D. o. Transportation. Washington, D.C, Federal Highways Administration. Publication No. FHwA-IF-99-025.

Oka, T. and H. Tanaka (2009). Soil variability calculated from CPT data. The 2nd international symposium on geotechnical safety and risk, Gifu, Japan, Taylor & Francis.

Oka, T. and H. Tanaka (2009). Soil variability calculated from CPT data. The 2nd International symposium on geotechnical safety & risk, Gifu, Japan, Taylor & Francis Group.

Oluokun, F. A., E. G. Burdette and J. H. Deatherage (1991). "Elastic Modulus, Poisson's Ratio, and Compressive Strength Relationships at Early Ages." American Concrete Institute 88(1): 3-10.

Orr, T. L. L. (2002). Eurocode 7: a code for harmonized geotechnical design. International Workshop on Foundation Design Codes and Soil Investigation in View of International Harmonization and Performance Based Design, Balkema, Tokyo.

Paikowsky, S. G. (2004). Load and Resistance Factor Design (LRFD) for Deep Foundations. Washington, National Cooperative Highway Research Program.

Peck, R. B. (1969). "Ninth Rankine Lecture: Advantages and limitations of the observational method in applied soil mechanics." Géotechnique 19(2): 171-187.

Phoon, K.-K. and F. H. Kulhawy (2002). "Characterization of geotechnical variability." Canadian Geotechnical Journal 36: 612-624.

Phoon, K. K. (2004). Towards reliability-based design for geotechnical engineering. Special lecture for Korean Geotechnical Society. Seoul.

Phoon, K. K. and F. H. Kulhawy (1999). "Characterization of geotechnical variability." Canadian Geotechnical Journal 36: 612-624.

Poulos, H. G. and E. H. Davis (1980). Pile foundation analysis and design, Rainbow-Bridge Book Company.

Pula, W. (2007). Reliability of laterally loaded rigid piles. Probabilistic methods in geotechnical engineering. D. V. Griffiths and G. A. Fenton. New York, Springer Wien: 169-183.

Radionics. "Foil strain gauges and accessories." from http://docs-europe.origin.electrocomponents.com/webdocs/0077/0900766b80077de6.pdf.

Radionics. (1997). "Strain gauges and load cells - Datasheet." 1997, from http://radionics.rs-online.com/.

Rahardjo, P. P. (2001). In situ testings and Soil Properties Correlations. International conference on In Situ Measurement of Soil Properties and Case Histories, Bali, Indonesia.

Randolph, M. F. and B. S. Murphy (1985). Shaft capacity of driven piles in clay. The 17th offshore technology conference, Houston.

Saldivar, E. E. and R. J. Jardine (2005). "Application of an effective stress design method to concrete piles driven in Mexico City clay." Canadian Geotechnical Journal 42: 1495-1508.

Schneider, H. A. (1997). Panel discussion: definition and determination of characteristic soil properties. The 14th International Conference on Soil Mechanics and Foundation Engineering, Hamburg, Balkema, Rotterdam.

Schneider, J. A. (2007). Analysis of piezocone data for displacement pile design. School of Civil and Resource Engineering, The University of Western Australia. Doctor of Philosophy: 340.

Schneider, J. A., X. Xu and B. M. Lehane (2008). "Database Assessment of CPT-Based Design Methods for Axial Capacity of Driven Piles in Siliceous Sands." Journal of geotechnical and geoenvironmental engineering 134(9): 1227-1244.

Simpson, B. (1992). "Retaining structures: displacement and design." Géotechnique 42(4): 541-576.

Sivakumar, V., T. Navaneethan, D. Hughes and G. Gallagher (2009). "An assessment of the earth pressure coefficient in overconsolidated clays." Géotechnique 59(10): 825-838.

Skempton, A. W. (1951). The bearing capacity of clays. Building Research Congress.

Skempton, A. W. (1959). "Cast in-situ bored piles in London Clay." Géotechnique 9: 153-173.

Skipper, J., B. Follett, C. O. Menkiti, M. Long and J. Clark-Hughes (2005). "The engineering geology and characterization of Dublin Boulder Clay." Quarterly Journal of Engineering Geology and Hydrogeology 38: 171-187.

Spry, M. J., F. H. Kulhawy and M. D. Grigoriu (1988). Reliability-based foundation design for transmission line structures: geotechnical site characterisation strategy. Palo Alto, California, Electric power research institute.

StJohn, H. D. (1980). A Review of Current Practice in the Design and Installation of Piles for Off shore Structures, Technology Paper 5. London, Building Research Station, Department of Engineering: 150.

Stroud, M. A. (1974). The standard penetration test in insensitive clays and soft rocks. Proceedings of European Symposium on Penetration Testing. Stockholm. 2.2: 367-375.

Stroud, M. A. (1989). The SPT test: its application and interpretation. Proceedings of the Institution of Civil Engineers Conference on Penetration Testing, Birmingham.

Terazaghi, K. (1943). Theoretical soil mechanics, J. Wiley New York.

Terazaghi, K. and R. Peck (1967). Soil mechanics in engineering practice, John Wiley, New York.

Tomlinson, M. J. (2001). Foundation Design and Construction, Pearson Education Limited.

Trenter, N. A. (1999). Engineering in glacial tills. Oxford, Alden Press.

Vanmarke, E. H. (1983). Random fields: Analysis and synthesis. Cambridge, MA, MIT Press.

Weltman, A. J. and J. M. Healy (1978). Piling in boulder clay and other glacial tills. London, DoE/CIRIA. PG5.

Whitman, R. V. (1984). "Evaluating calculated risk in geotechnical engineering." Journal of Geotechnical Engineering 110(2): 145-188.

Williams, A. F. and P. J. N. Pells (1981). "Side resistance rock sockets in sandstone, mudstone and shale." Canadian Geotechnical Journal 18: 502-513.

Wu, T. H. (2009). Reliability of geotechnical predictions. The 2nd international symposium on geotechnical safety and risk, Gifu, Japan, Taylor & Francis.

Zhang, L. (2004). "Reliability Verification Using Proof Pile Load Tests." ASCE 130(11): 1203-1213.

Zhang, L. M. (2008). Reliability verification using pile load tests. Reliability-based design in geotechnical engineering: Computations and Applications. K.-K. Phoon, Taylor & Francis.

Zhang, L. M., D. Q. Li and W. H. Tang (2005). "Reliability of bored pile foundations considering bias in failure criteria." Canadian Geotechnical Journal 42: 1086-1093.

Zhang, L. M. and W. H. Tang (2001). Bias in axial capacity of single bored piles arising from failure criteria. The 8th International Conference on Structural Safety and Reliability, Newport Beach, California, A.A. Balkema, Rotterdam.

A. Ground Test Results

A.1 Introduction

This Appendix contains ground test results pertaining to the various sites in which pile load tests were carried out referred to in the main text of the thesis. A simplified stratigraphic profile for each of the sites is presented alongside an N_{SPT}-depth profile (where SPT results were available) for many of the sites referred to. The simplified stratigraphy presented for each of the sites was based on the results of site investigation carried out at each of the sites.

The results of laboratory tests carried out on material retrieved during site investigation, is also presented where this was available.

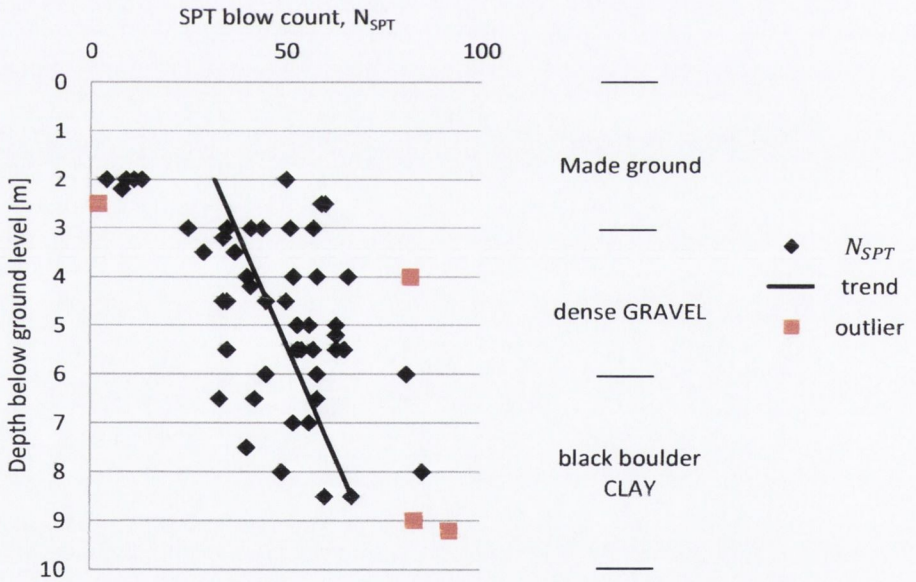


Figure A.1 - Site D N_{SPT}

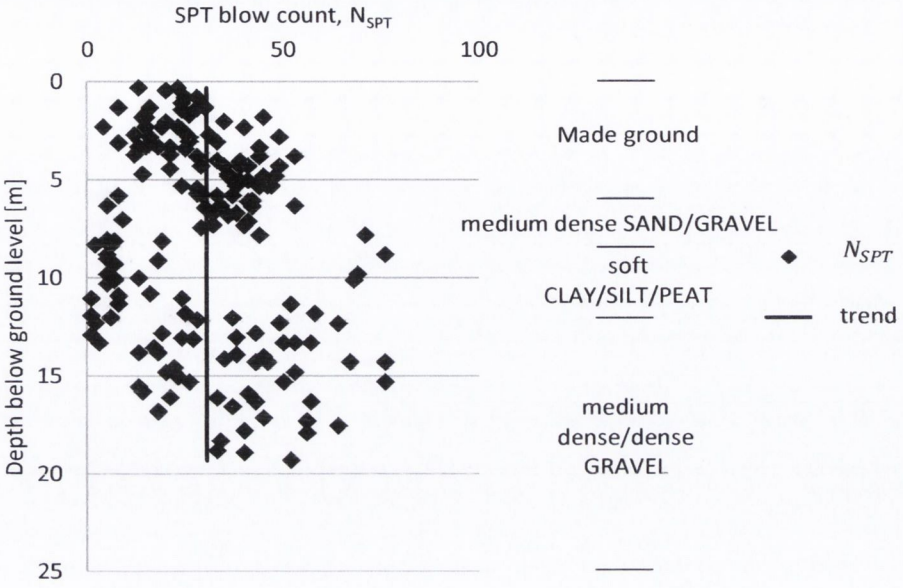


Figure A.2 - Site F N_{SPT}

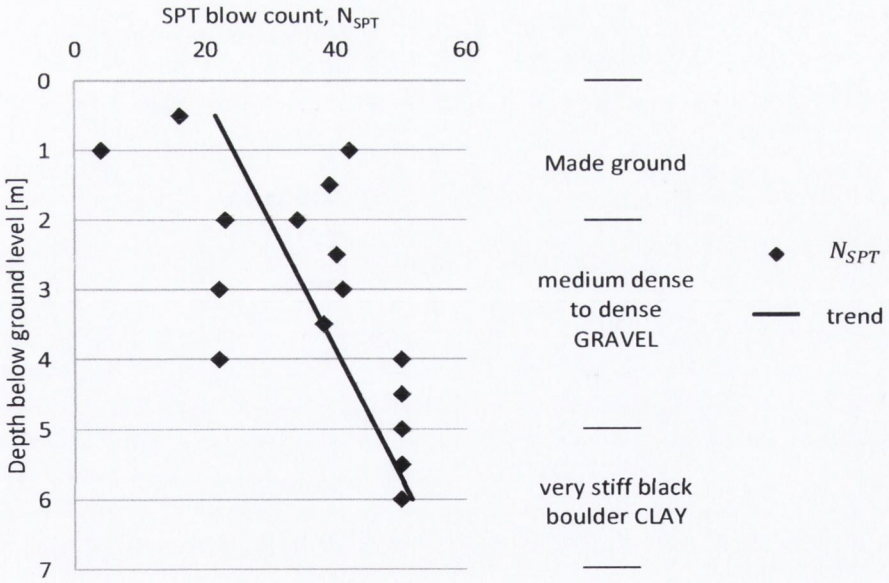


Figure A.3 - Site G N_{SPT}

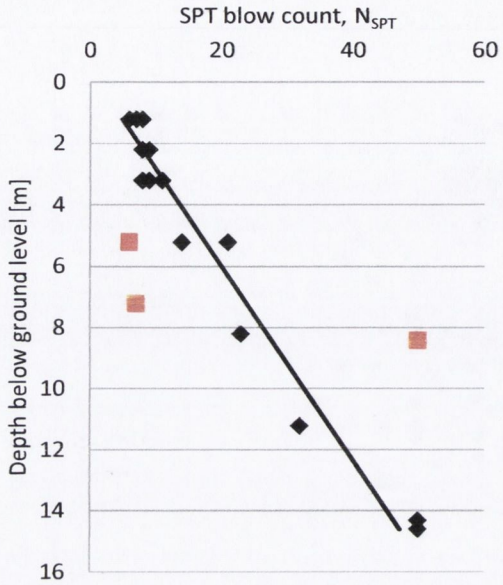


Figure A.4 - Site J N_{SPT} (ground conditions mixed and with old foundations/rubble)

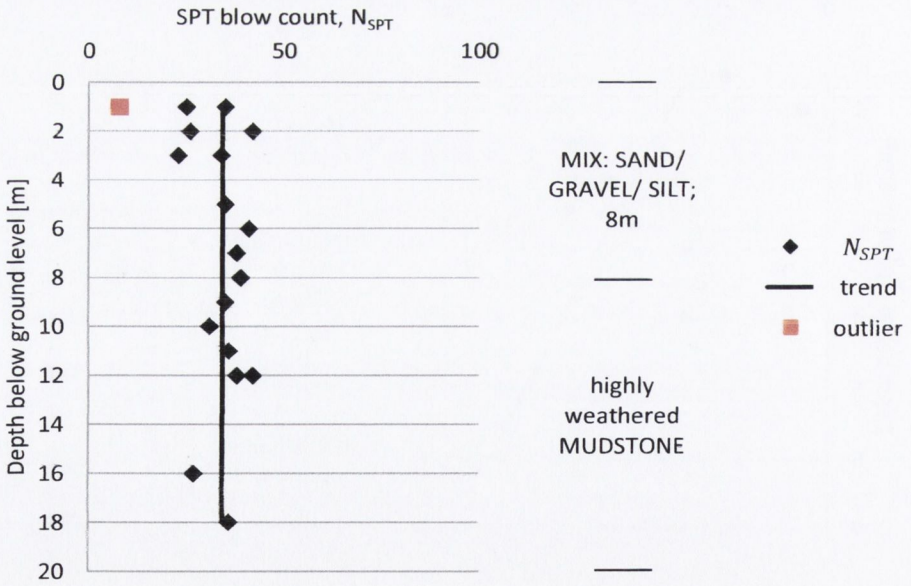


Figure A.5 – Site M N_{SPT}

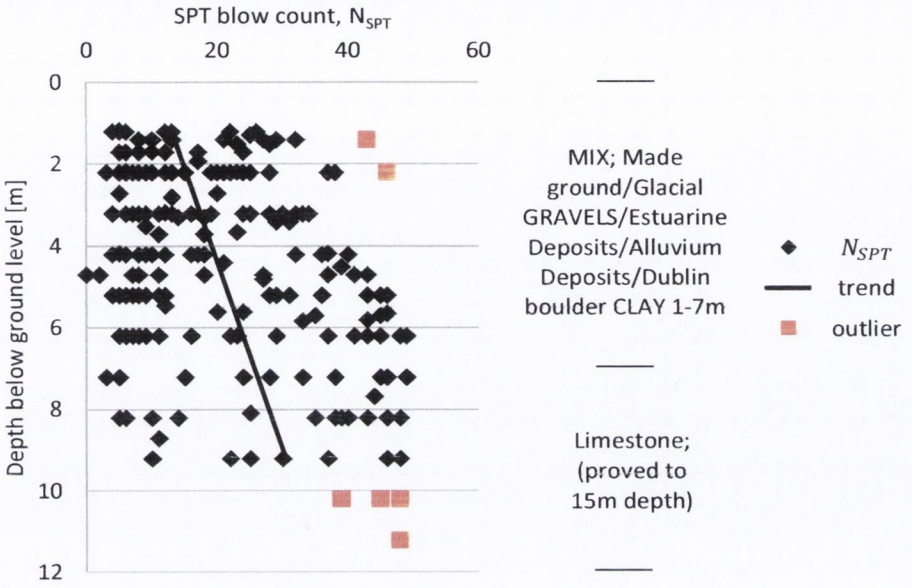


Figure A.6 – Site N N_{SPT}

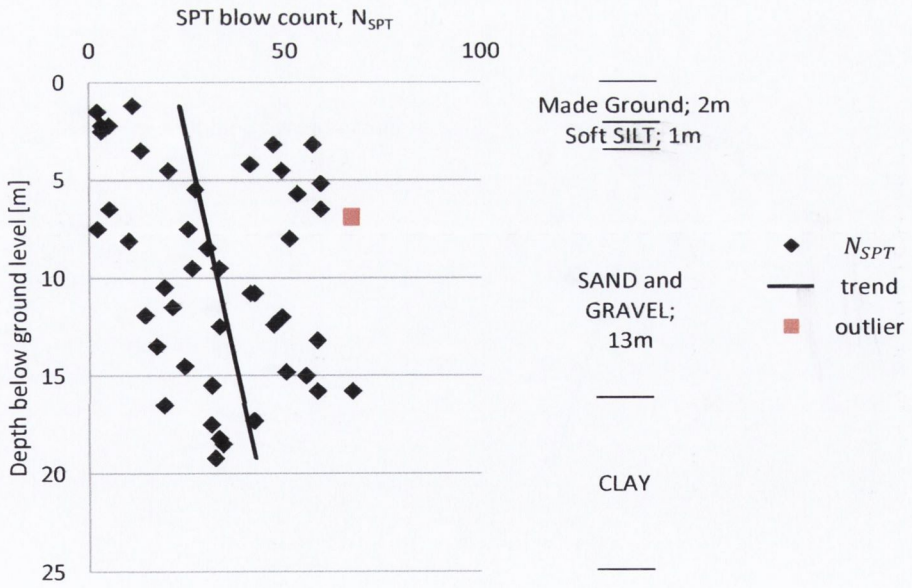


Figure A.7 – Site O N_{SPT}

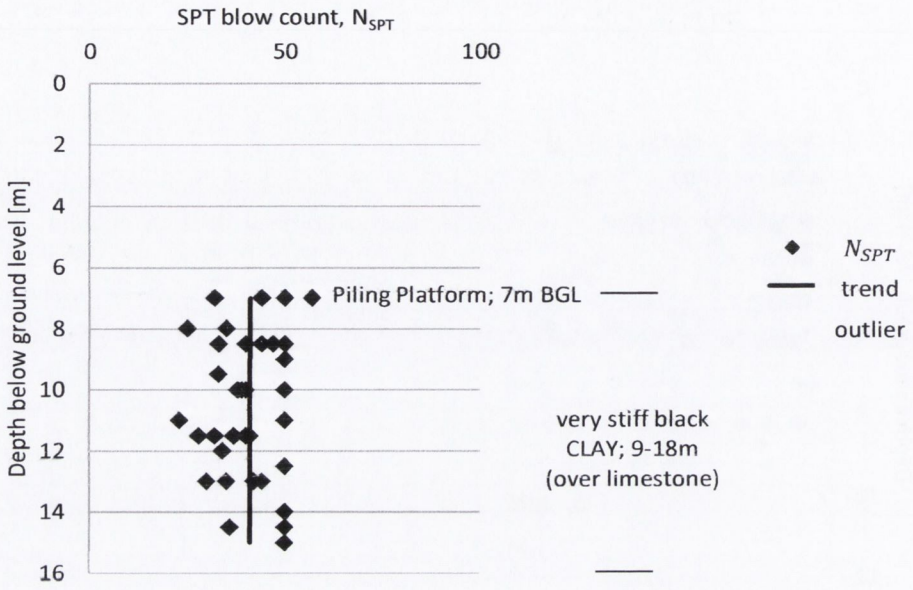


Figure A.8 – Site Q N_{SPT}

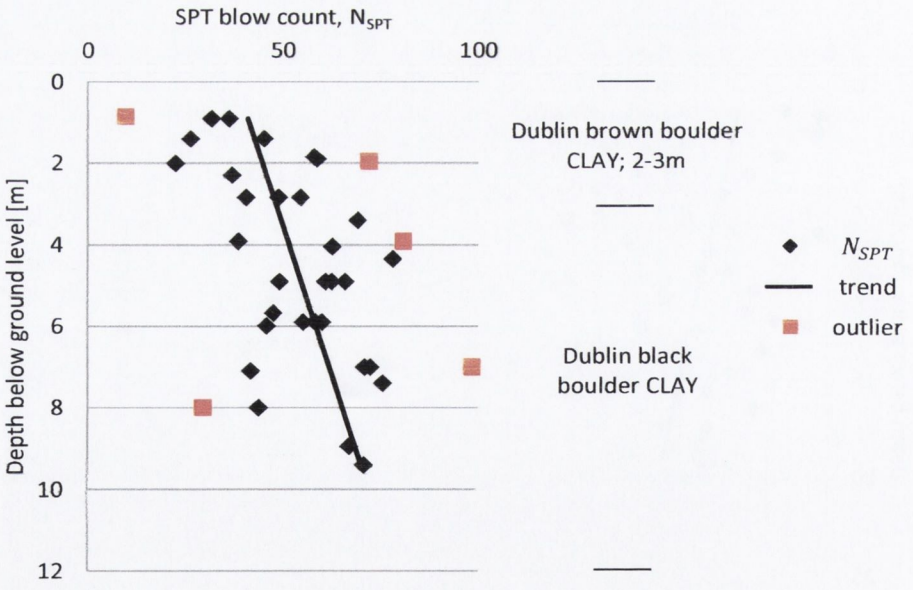


Figure A.9 – Site R N_{SPT}

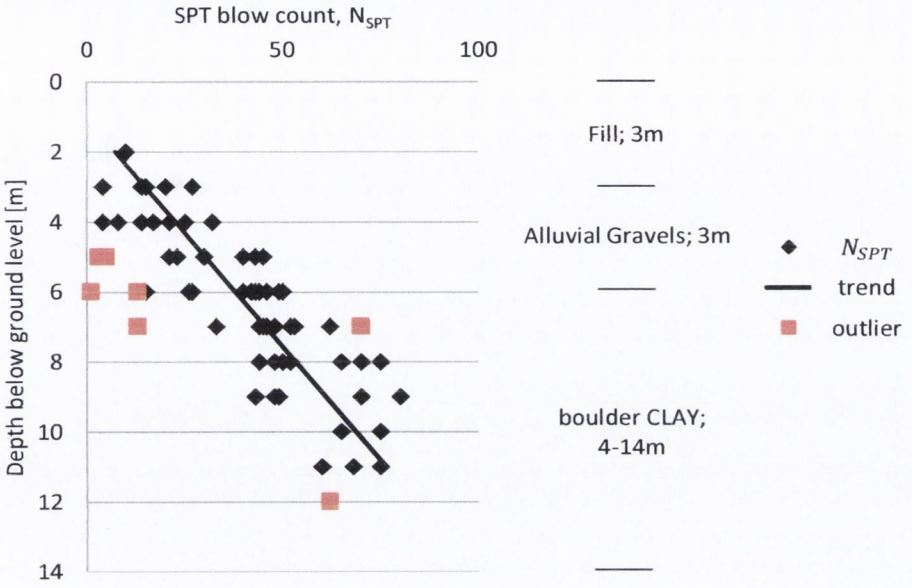


Figure A.10 – Site S N_{SPT}

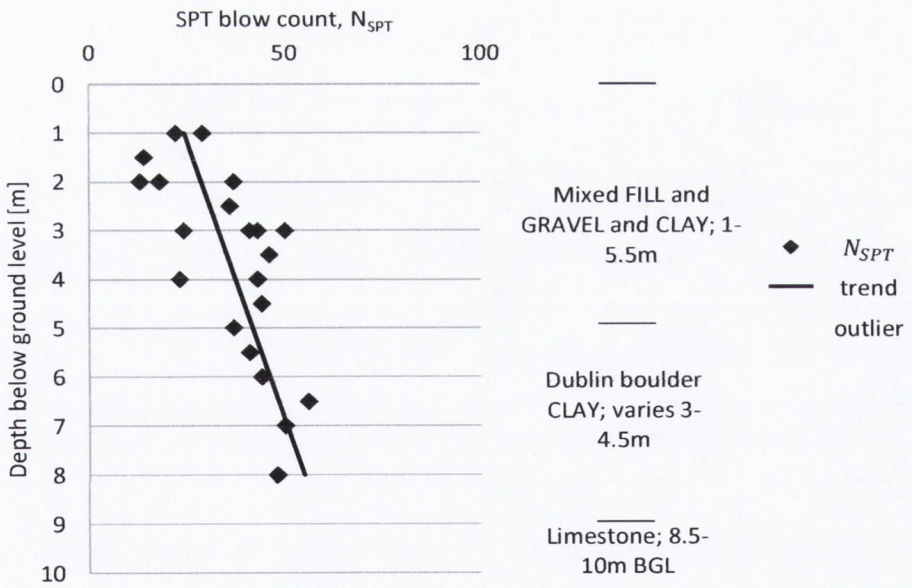


Figure A.11 – Site T N_{SPT}

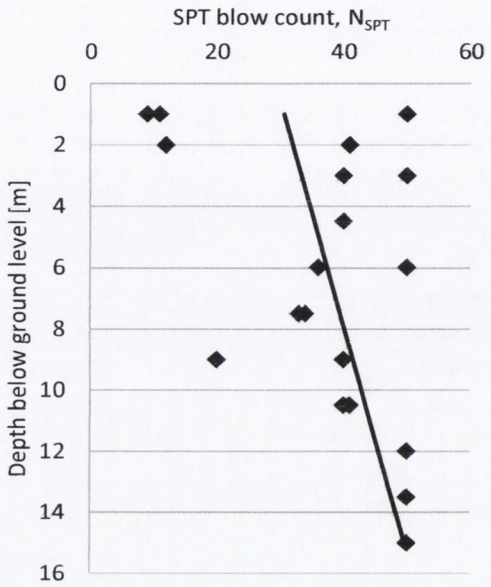


Figure A.12 – Site U N_{SPT} (ground conditions not known)

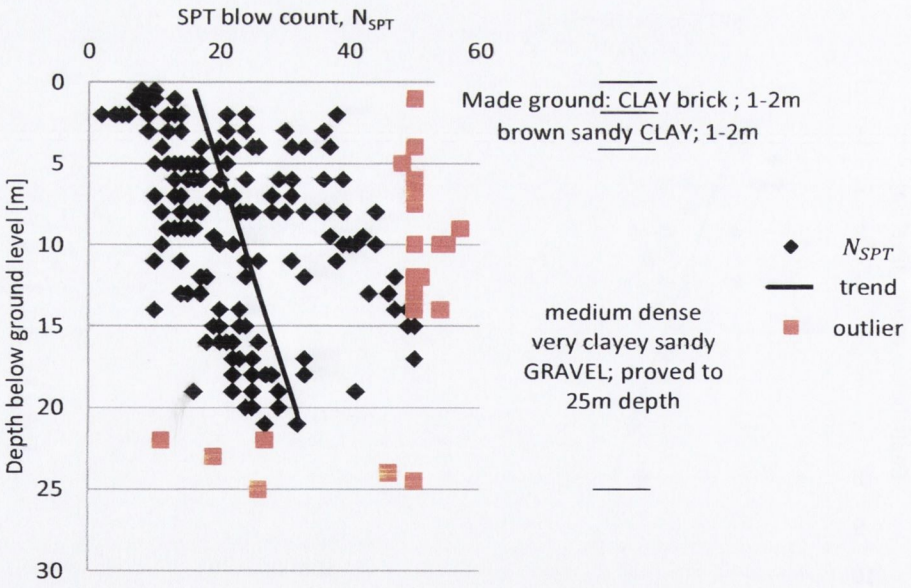


Figure A.13 – Site W N_{SPT}

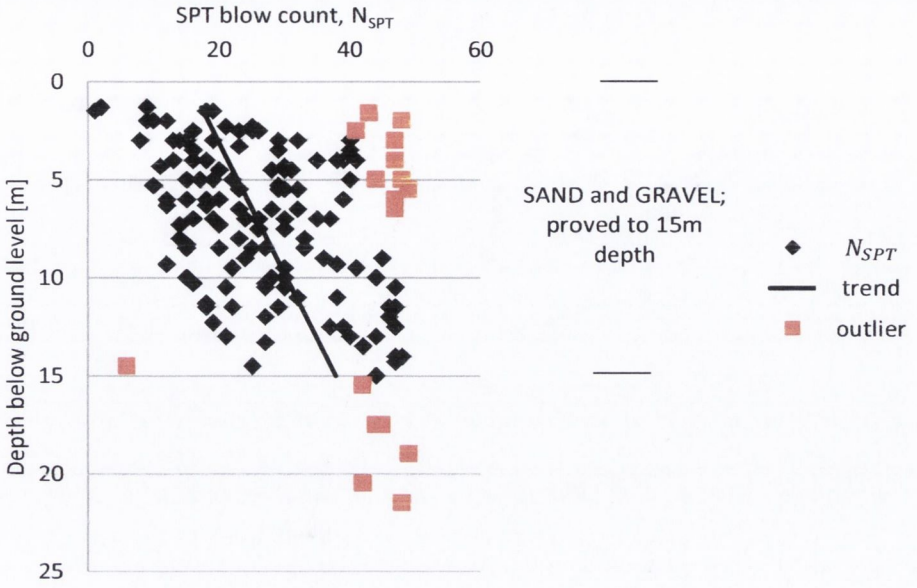


Figure A.14 – Site X N_{SPT}

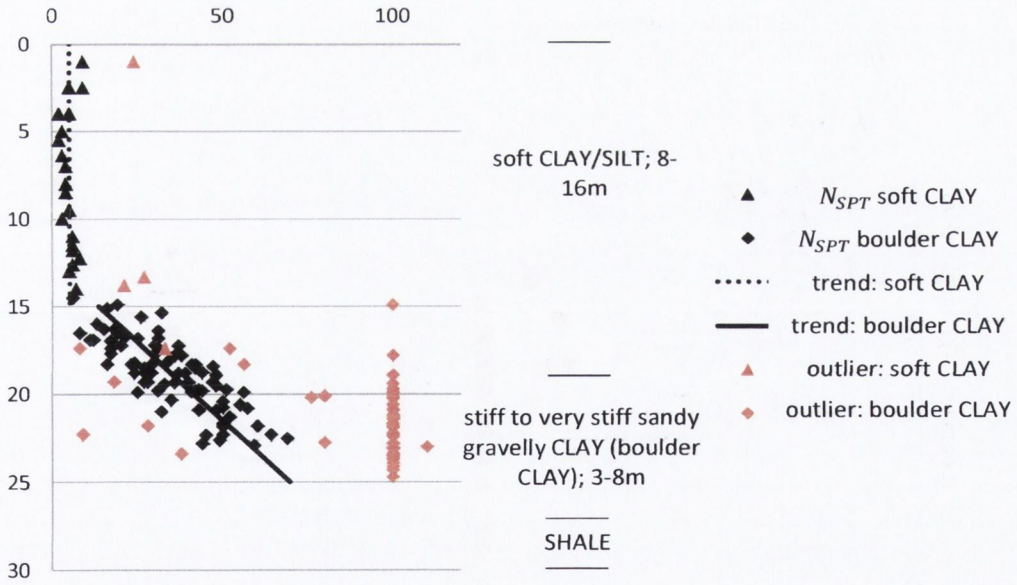


Figure A.15 – Site Y N_{SPT}

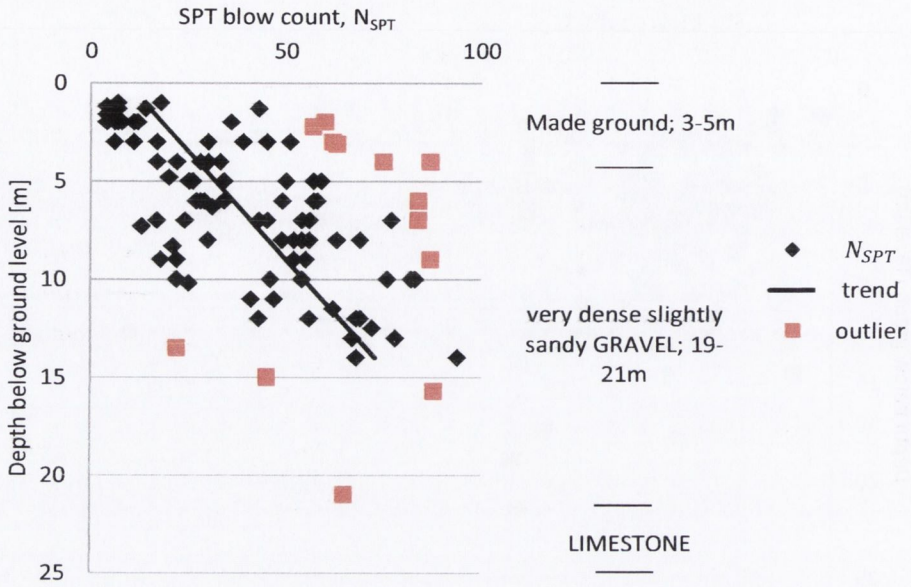


Figure A.16 – Site Z N_{SPT}

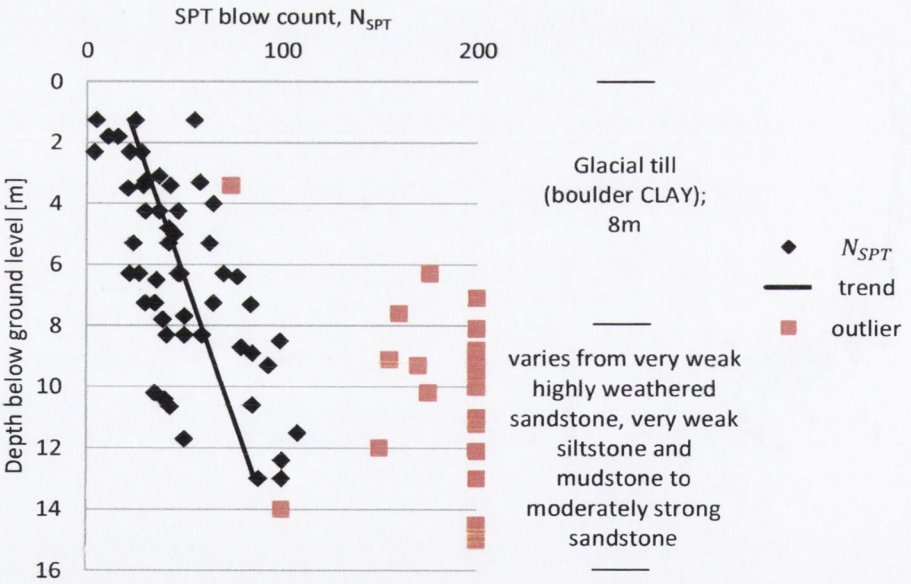


Figure A.17 – Site AA N_{SPT}

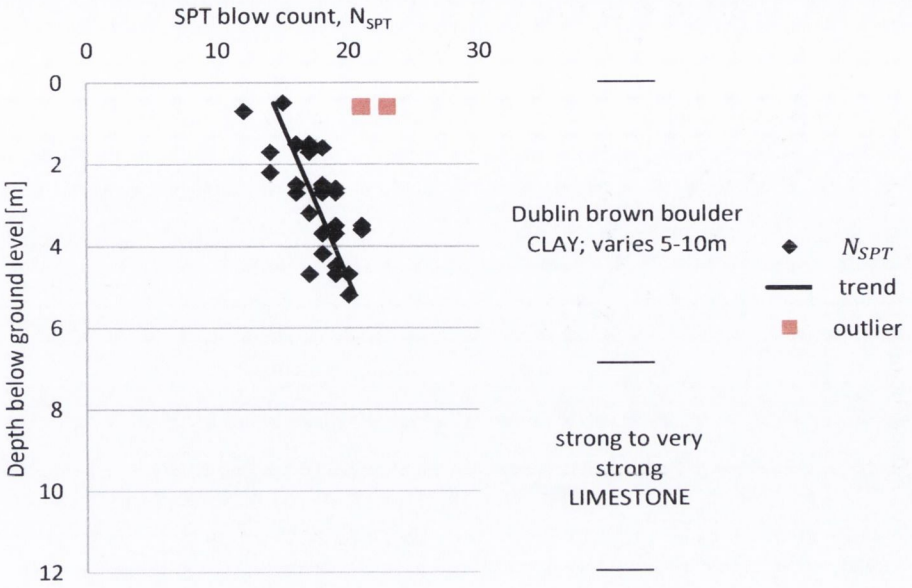


Figure A.18 – Site AB N_{SPT}



Figure A.19 – Site AH N_{SPT}

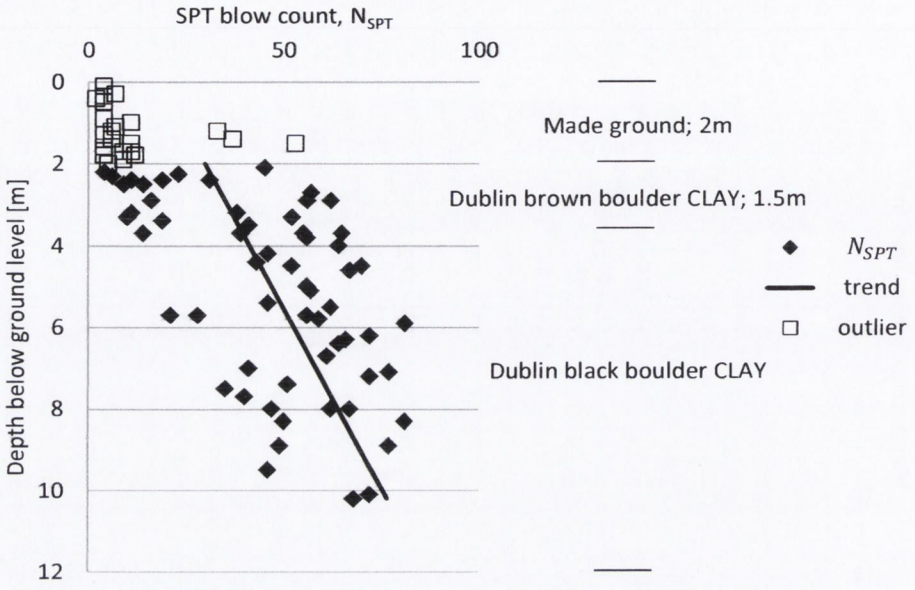


Figure A.20 – Site AG N_{SPT}

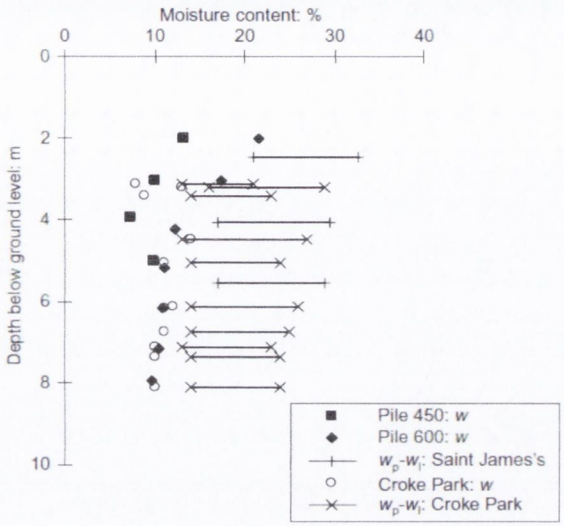


Figure A.21 – Site R: Water content, liquid and plastic limits (Farrell and Lawler 2008)

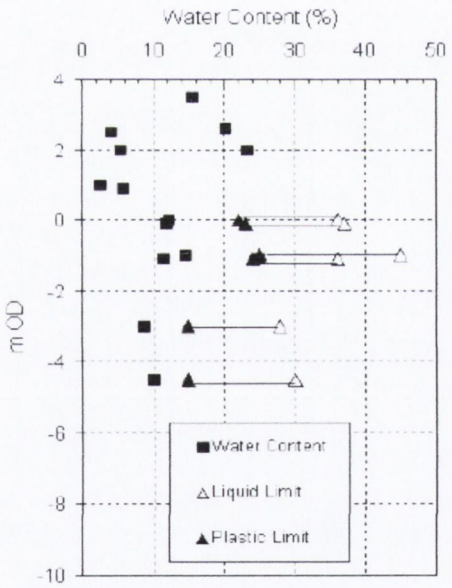


Figure A.22 – Site S: Water content, LL and PL: (Gavin et al. 2008)

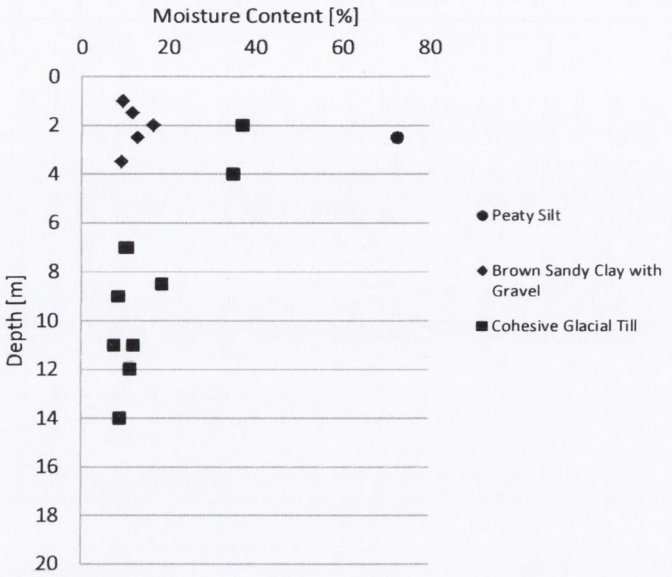


Figure A.23 – Site W: Moisture Content

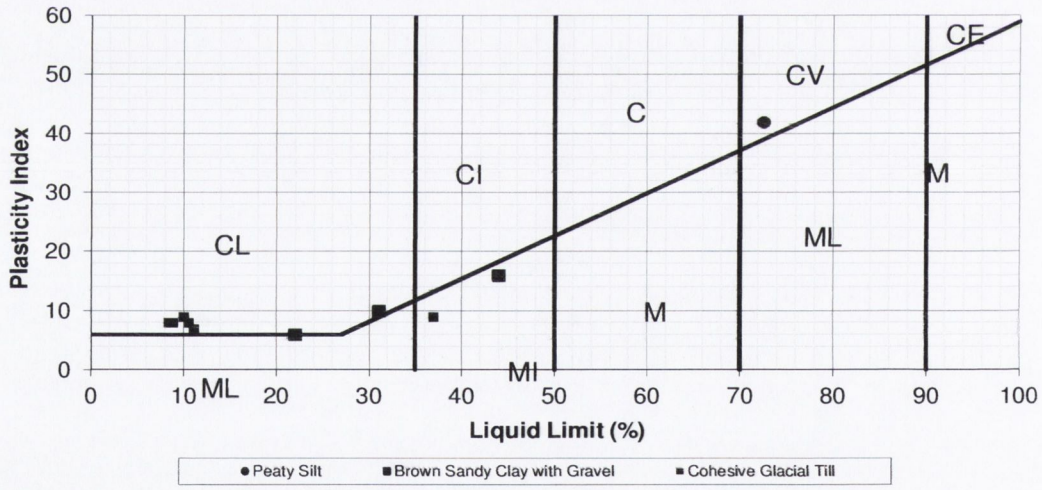


Figure A.24 – Site W: Plasticity Chart

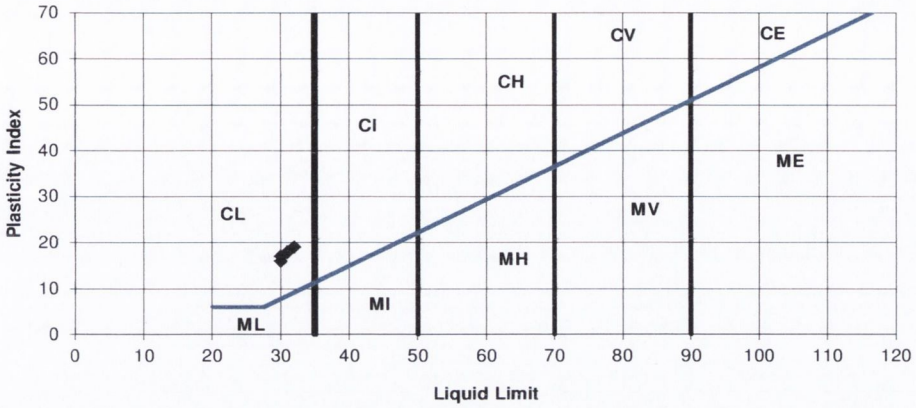


Figure A.25 – Site Y: Plasticity Chart

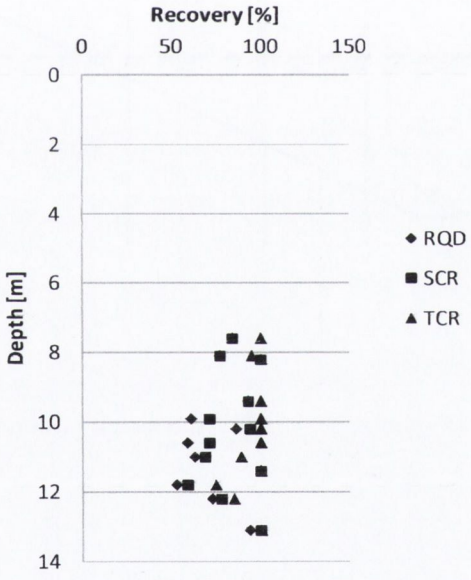


Figure A.26 – Site AB: Rock cores

Table A.1 – Site AB: Rock core test results

BH [_]	Depth [m]	q_u [MPa]	Bulk Density [Mg/m3]
RP5	10.2	59.62	2.68
RP2	7.7	54.51	2.68
RP1	8.1	36.84	2.68
RCGC6	9.2	39.37	2.66
RCGC5	7.9	38.04	2.68
RCGC4	10.3	35.93	2.69
RCGC2	6.5	72.18	2.68
RCGC1	8.8	26.67	2.66

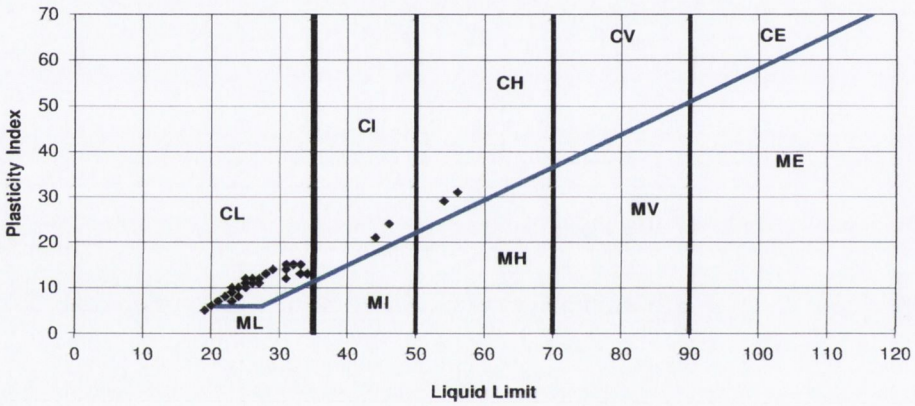


Figure A.27 – Site AH: Plasticity Chart

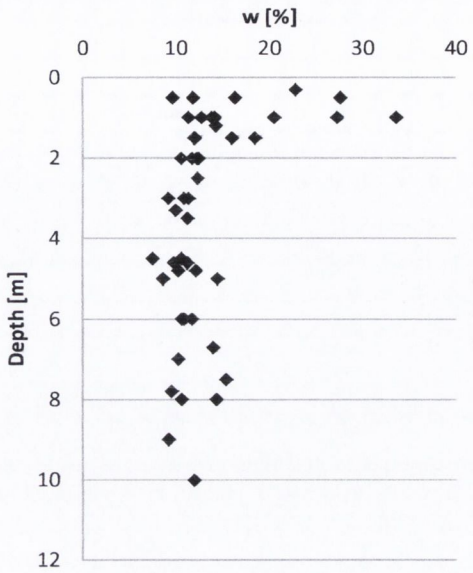


Figure A.28 – Site AH: Moisture Content

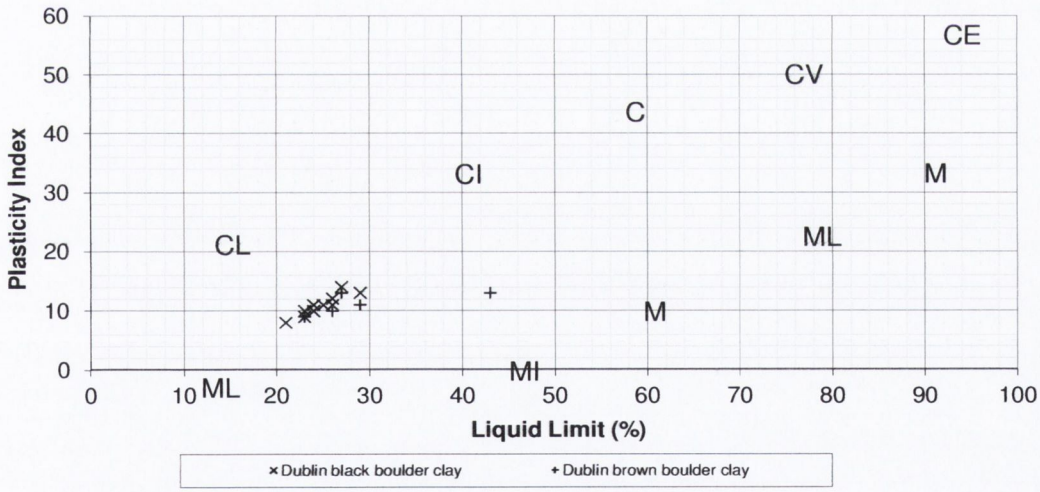


Figure A.29 – Site AG: Plasticity Chart

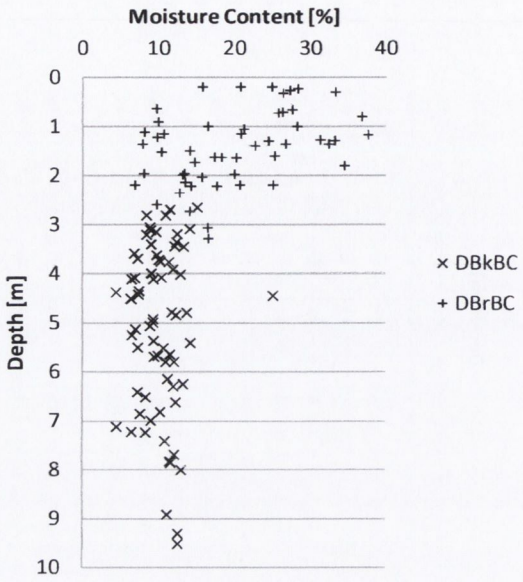


Figure A.30 – Site AG: Moisture Content

B. Pile Load Tests

B.1 Introduction

This Appendix contains the results of each of the 181 No. static pile load tests referred to in the pile test database presented in Chapter 3 of this thesis. The measured load-deflection data recorded at the pile head is plotted for each pile load test and this also includes any load-reload cycles where these were carried out.

Each of the pile load tests were carried out slowly enough such that the effects of creep were allowed to manifest themselves and this is apparent in many of the pile load test results where there is a substantial increase in the deflection at the pile head with time for no increase in the load applied to the pile head. One such example where the effects of creep are rather pronounced is apparent in the load-deflection results for Pile No. 137, shown in Figure B.123, where the pile head deflection increased from 9-19mm over time under a constant applied head load of around 1600kN.

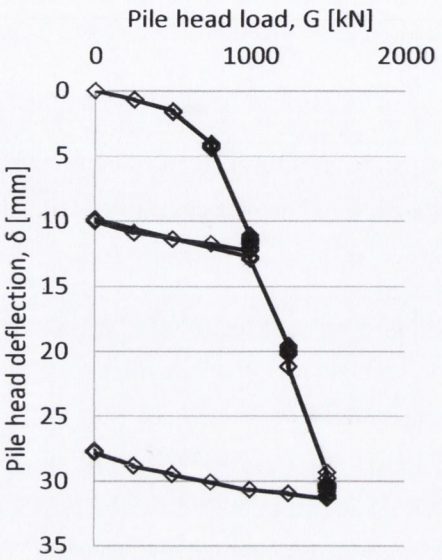


Figure B.1 – Pile 1

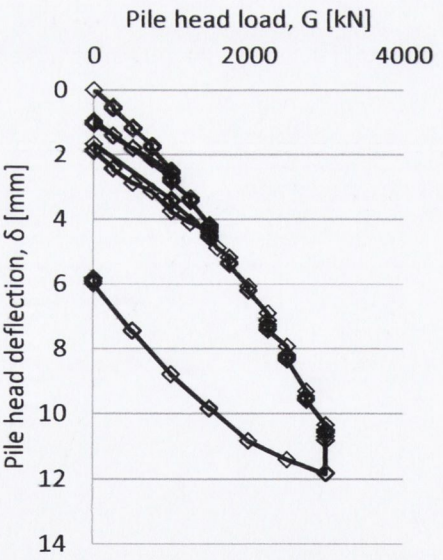


Figure B.2 – Pile 2

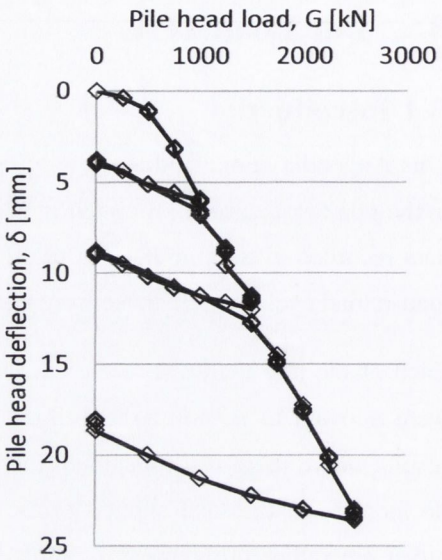


Figure B.3 – Pile 4

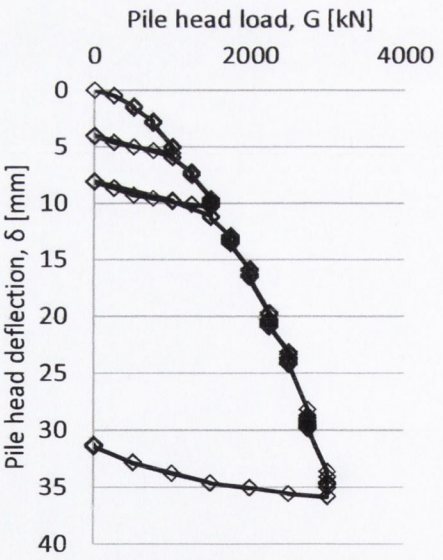


Figure B.4 – Pile 6

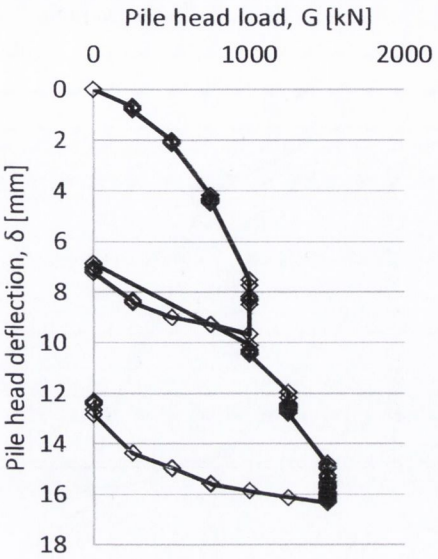


Figure B.5 – Pile 8

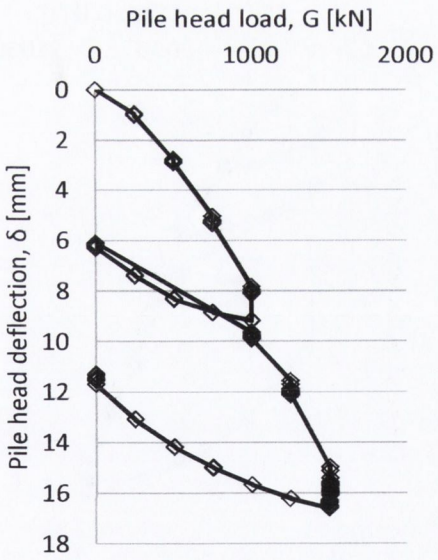


Figure B.6 – Pile 9

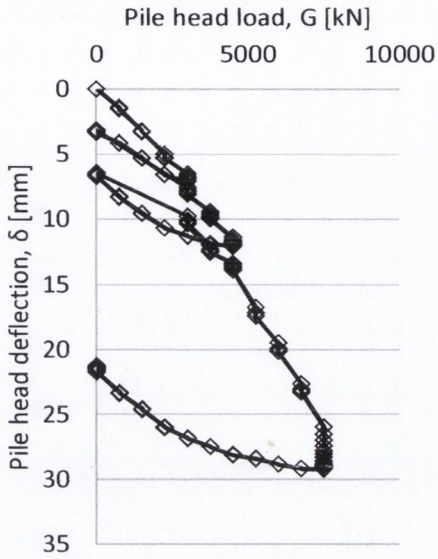


Figure B.7 – Pile 10

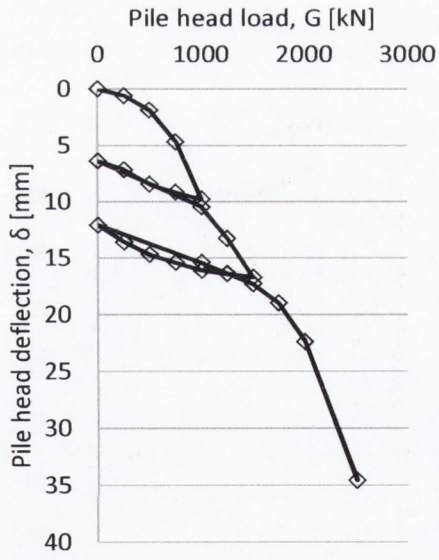


Figure B.8 – Pile11

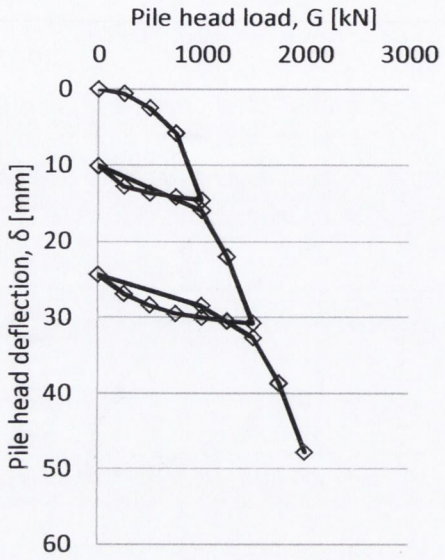


Figure B.9 – Pile 12

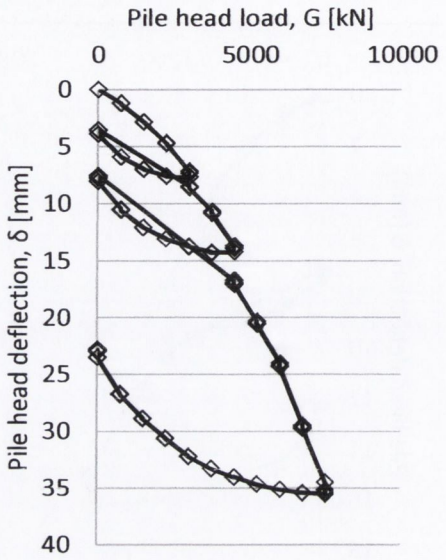


Figure B.11 – Pile 15

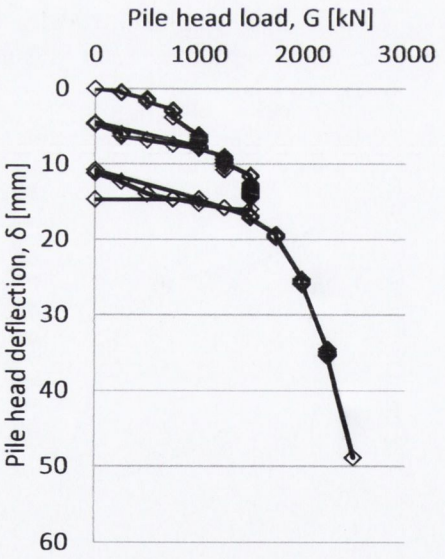


Figure B.10 – Pile 13

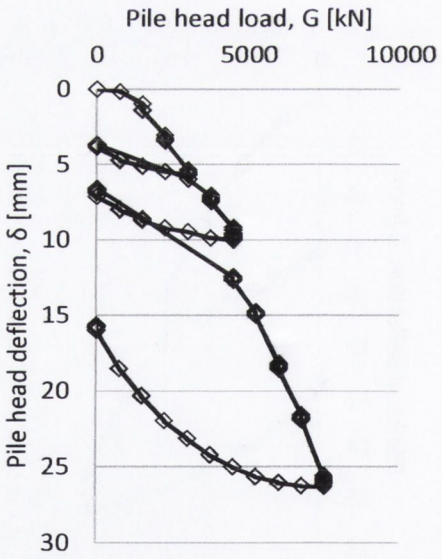


Figure B.12 – Pile 16

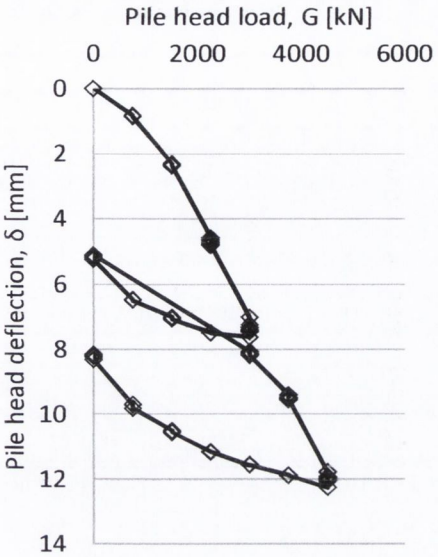


Figure B.13 – Pile 18

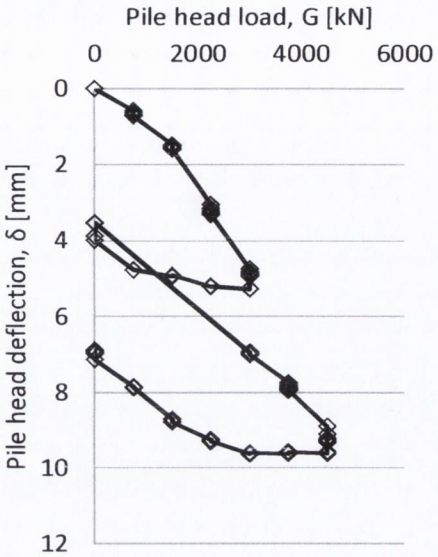


Figure B.15 – Pile 20

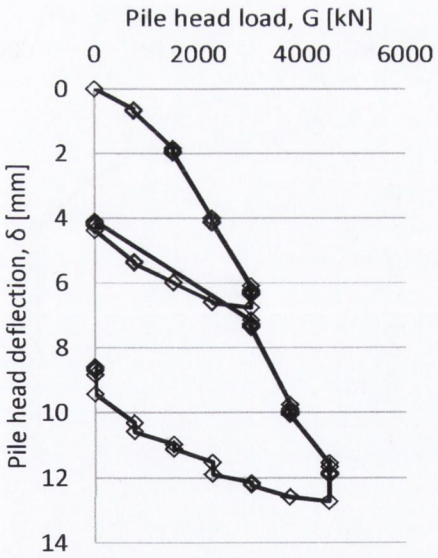


Figure B.14 – Pile 19

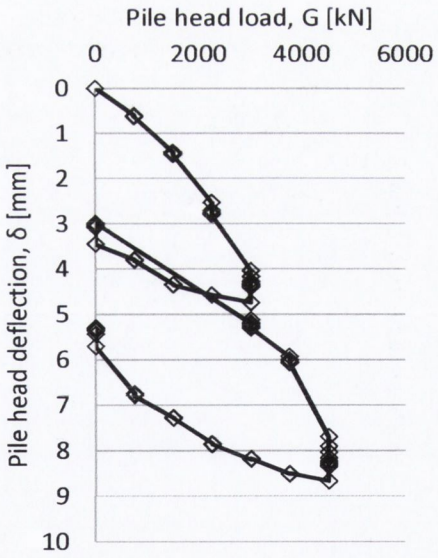


Figure B.16 – Pile 21

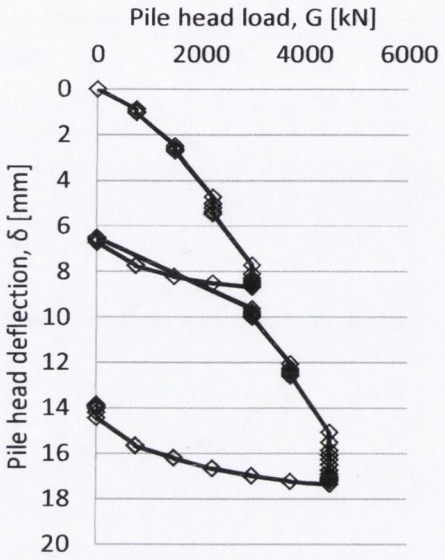


Figure B.17 – Pile 22

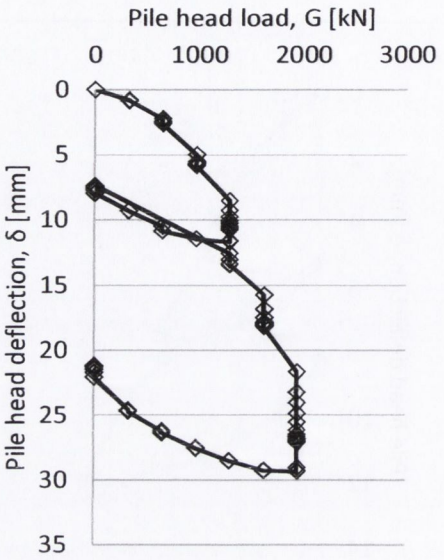


Figure B.19 – Pile 24

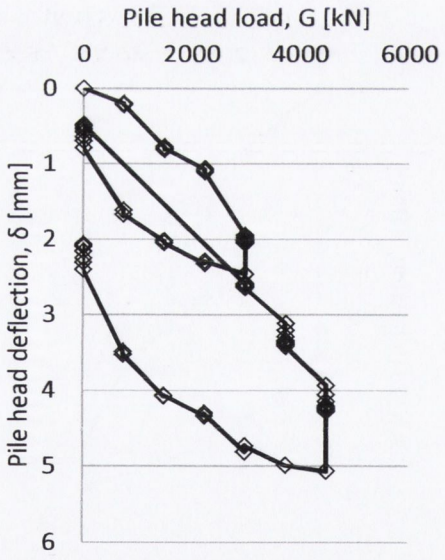


Figure B.18 – Pile 23

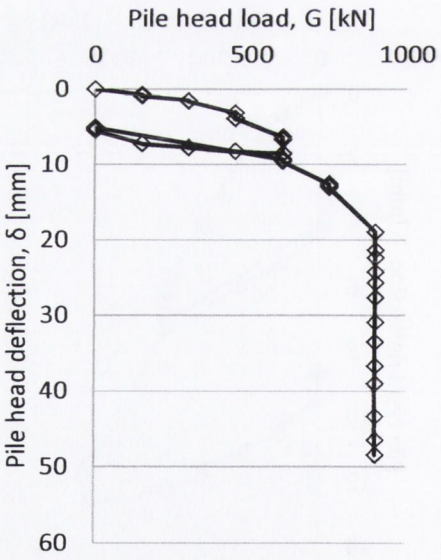


Figure B.20 – Pile 25

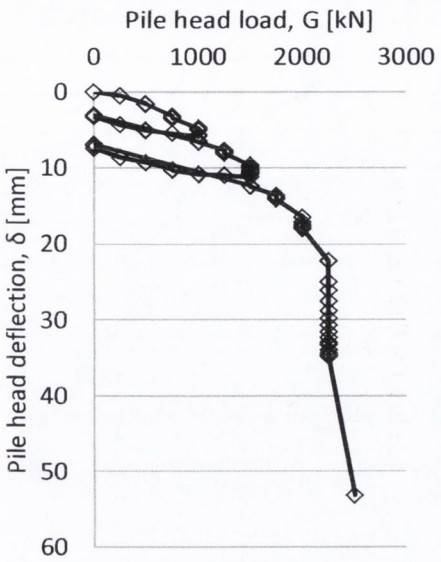


Figure B.21 – Pile 26

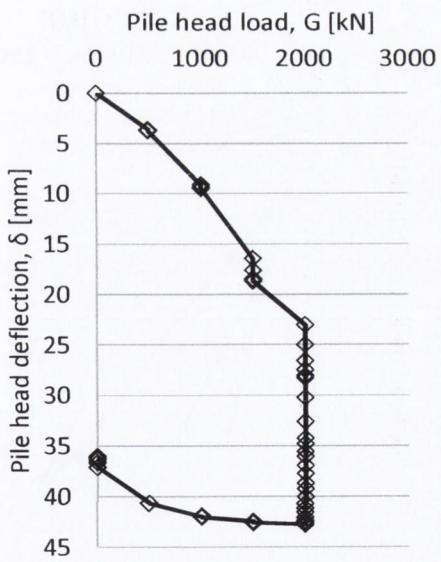


Figure B.22 – Pile 27

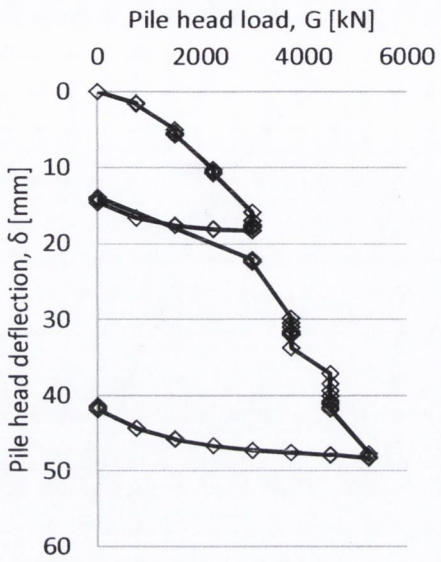


Figure B.23 – Pile 28

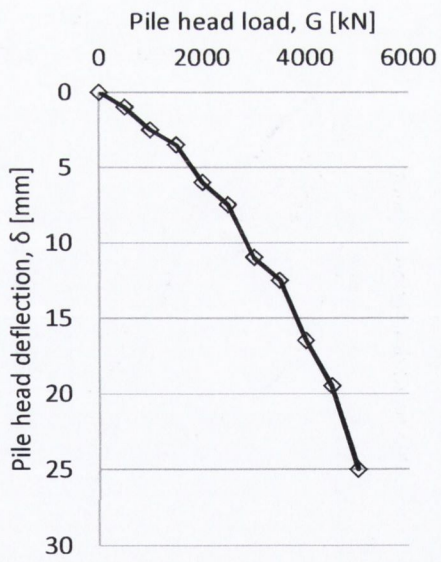


Figure B.24 – Pile 30

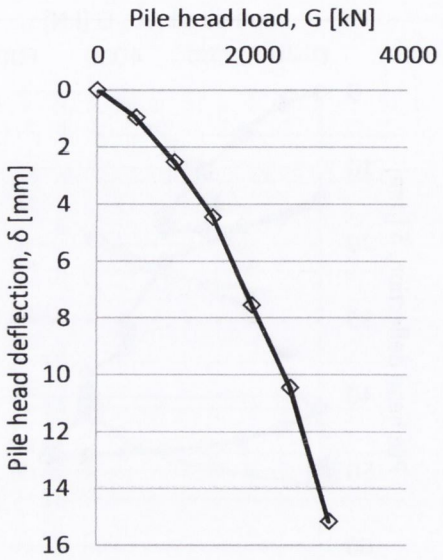


Figure B.25 – Pile 31

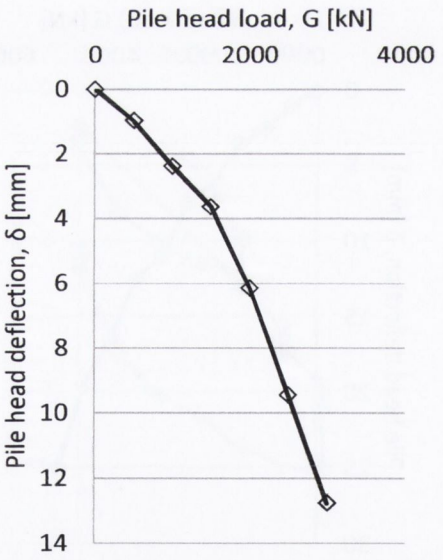


Figure B.26 – Pile 32

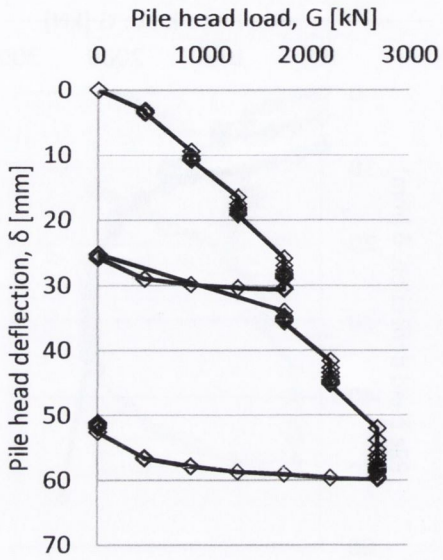


Figure B.27 – Pile 34

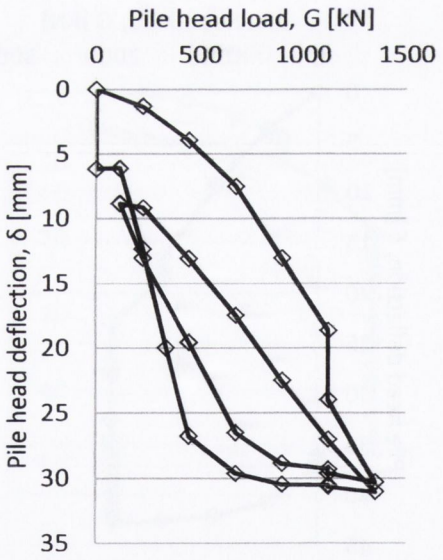


Figure B.28 – Pile 35 (Tension)

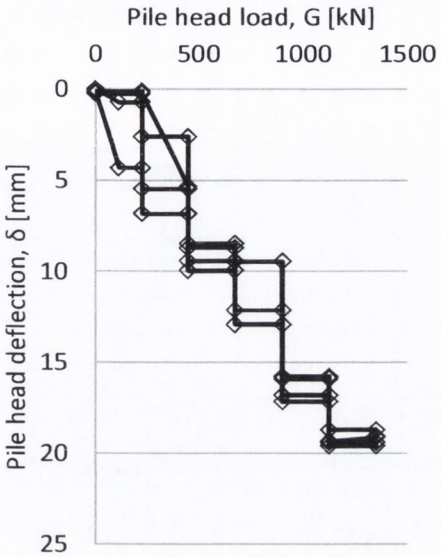


Figure B.29 – Pile 36 (Tension)

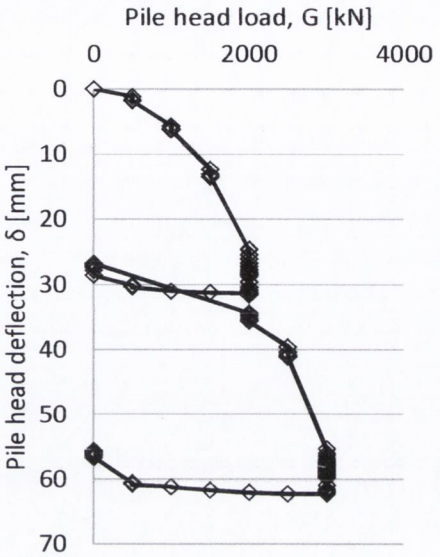


Figure B.31 – Pile 38

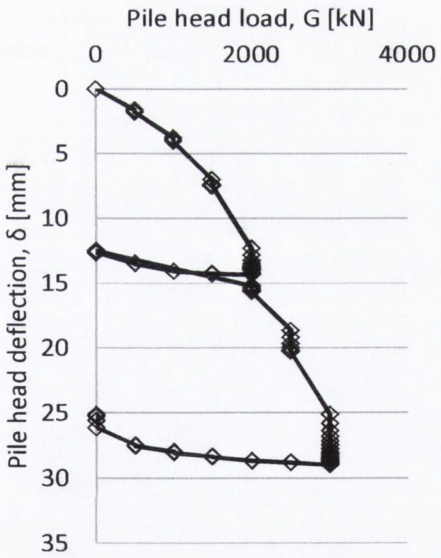


Figure B.30 – Pile 37

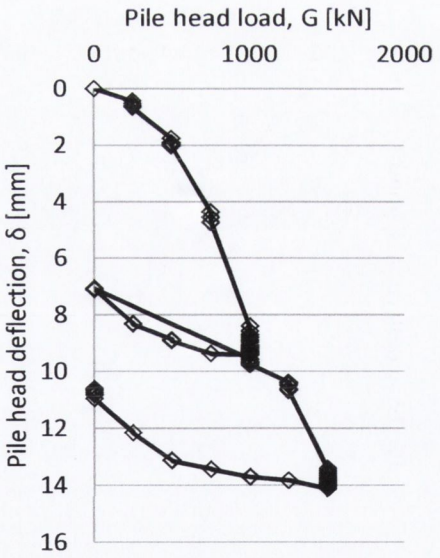


Figure B.32 – Pile 39

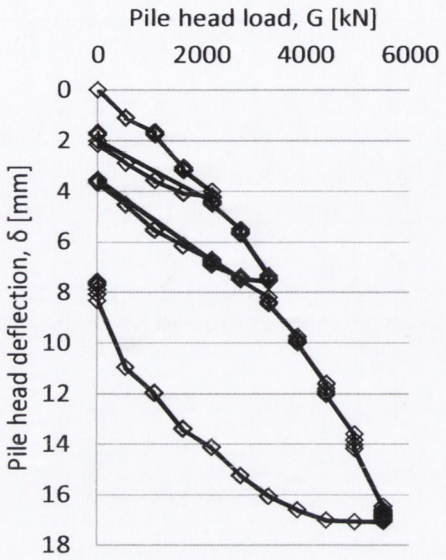


Figure B.33 – Pile 40

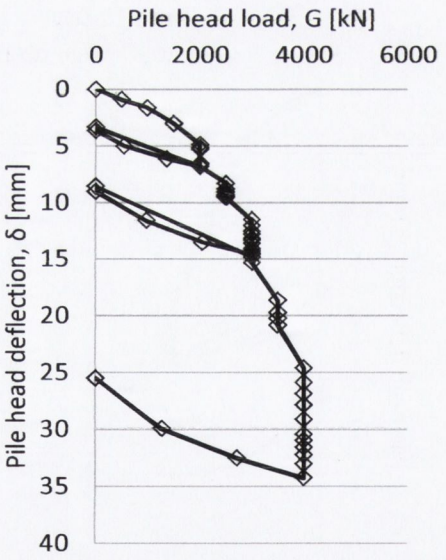


Figure B.34 – Pile 41

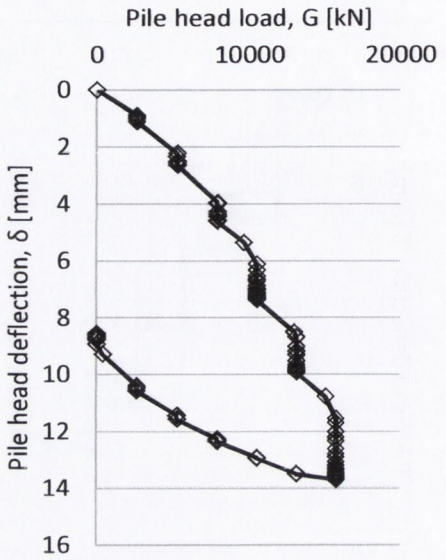


Figure B.35 – Pile 42

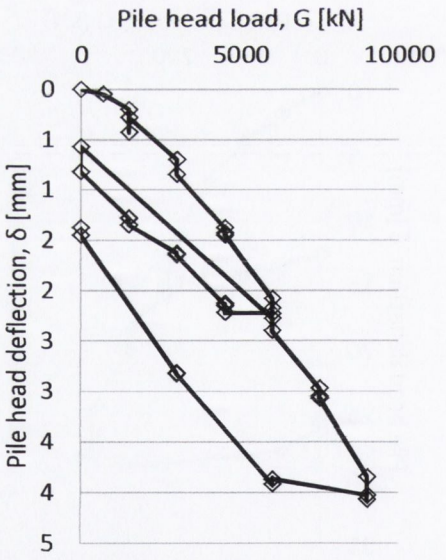


Figure B.36 – Pile 43

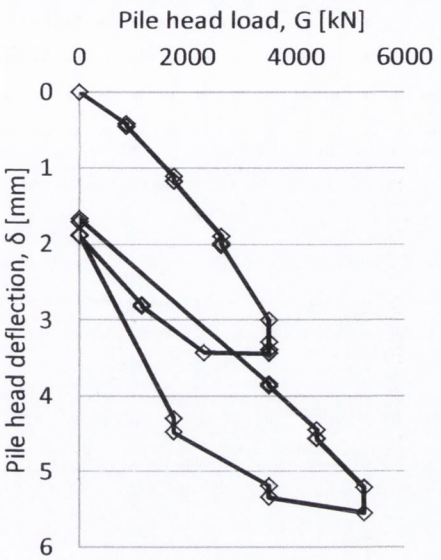


Figure B.37 – Pile 44

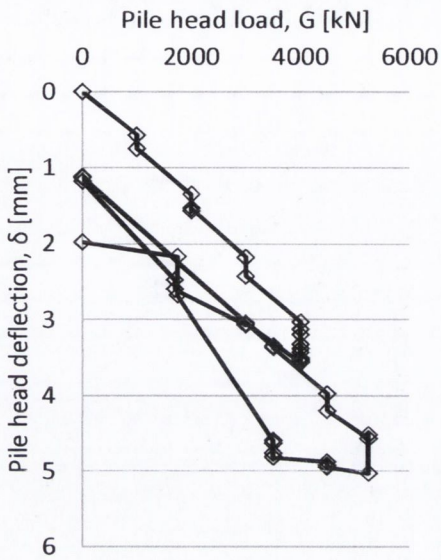


Figure B.39 – Pile 47

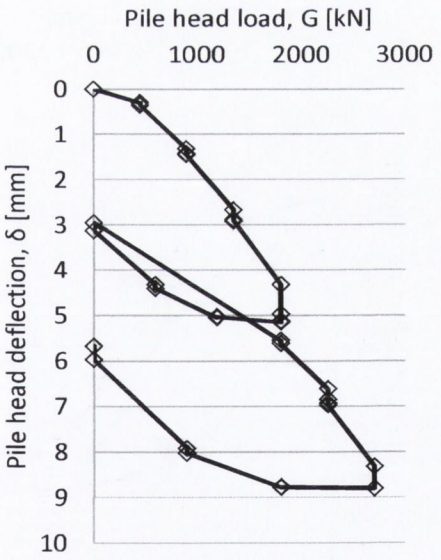


Figure B.38 – Pile 46

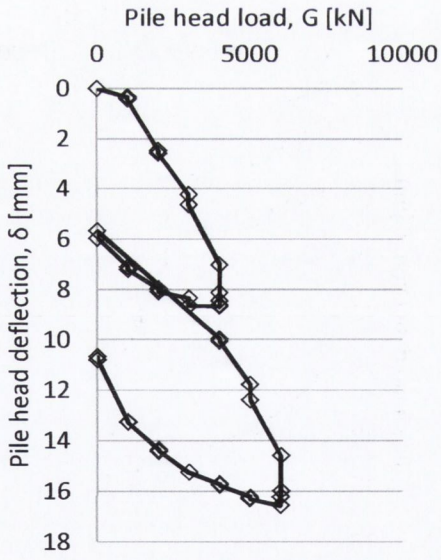


Figure B.40 – Pile 48

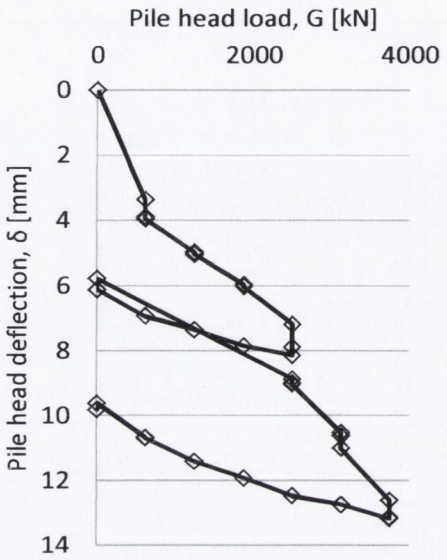


Figure B.41 – Pile 49

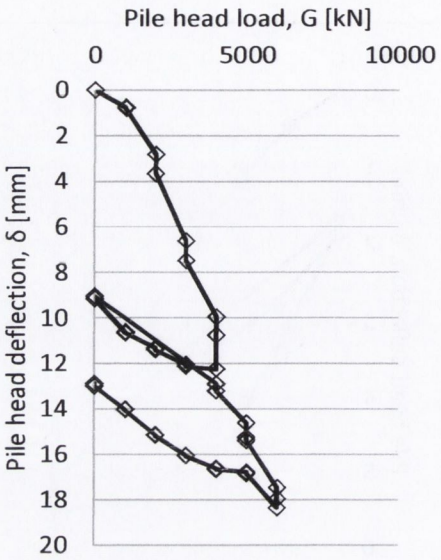


Figure B.43 – Pile 51

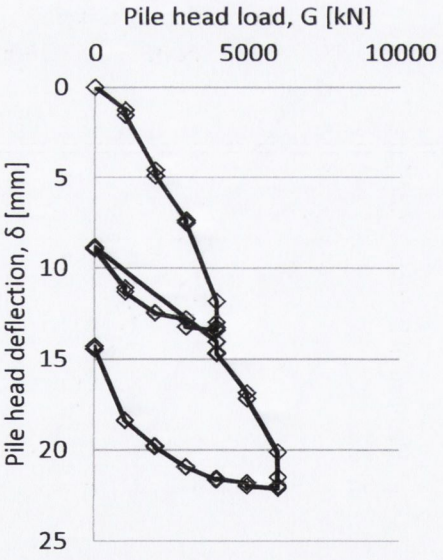


Figure B.42 – Pile 50

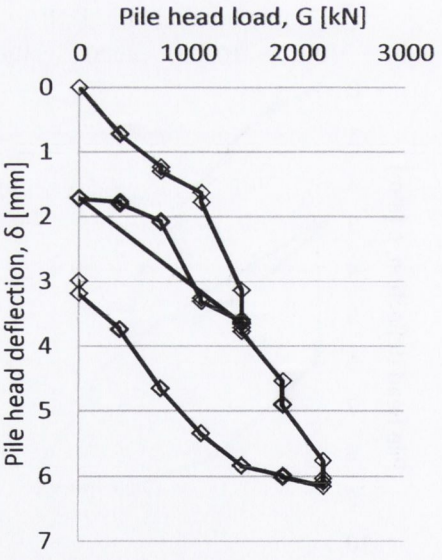


Figure B.44 – Pile 52

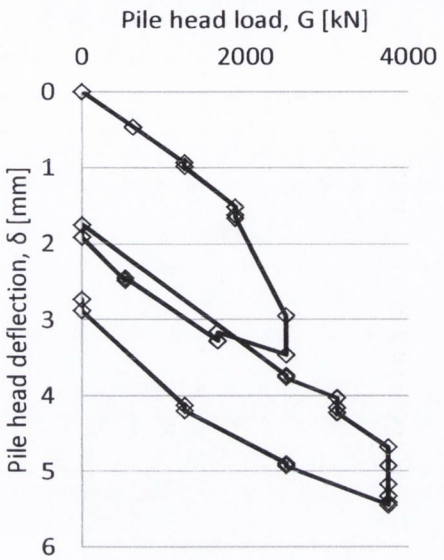


Figure B.45 – Pile 53

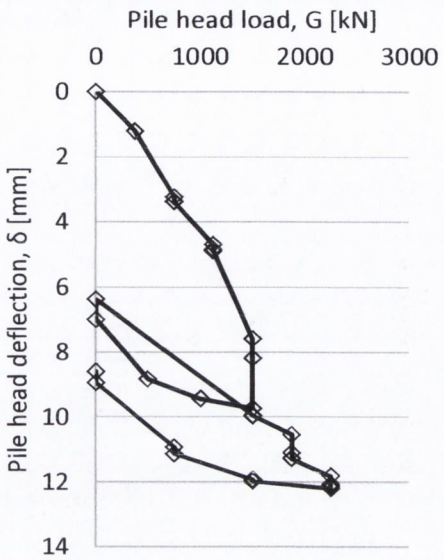


Figure B.47 – Pile 55

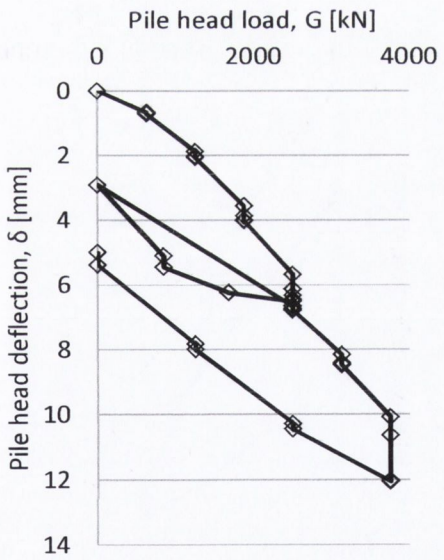


Figure B.46 - Pile 54

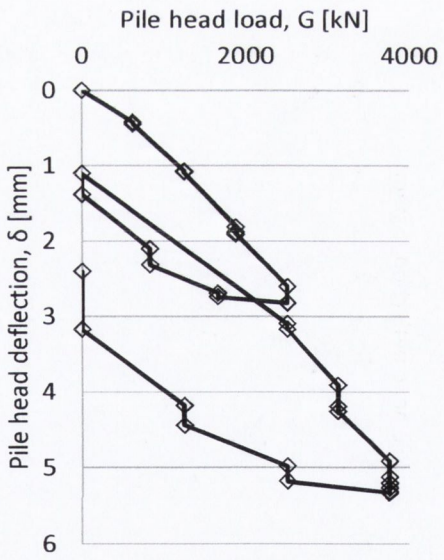


Figure B.48 – Pile 56

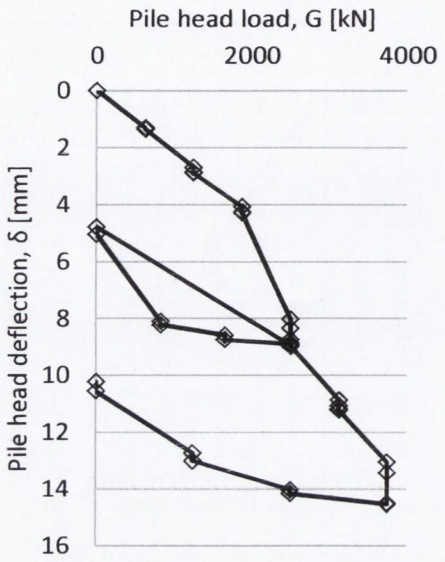


Figure B.49 – Pile 57

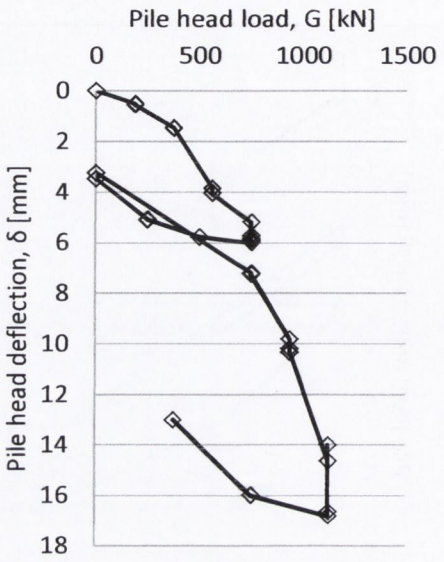


Figure B.51 - Pile 59

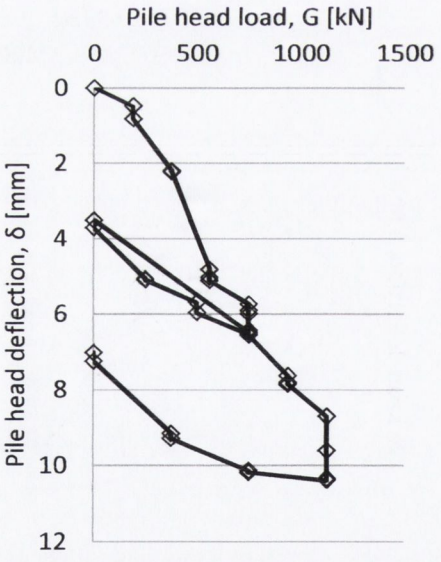


Figure B.50 – Pile 58

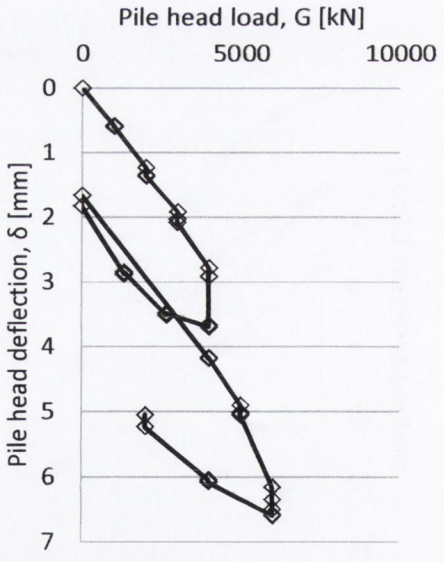


Figure B.52 – Pile 60

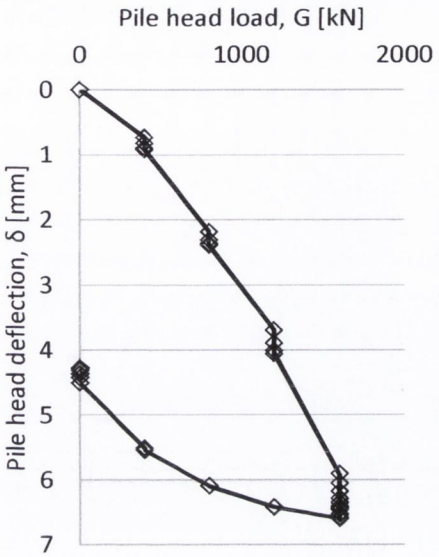


Figure B.53 – Pile 61

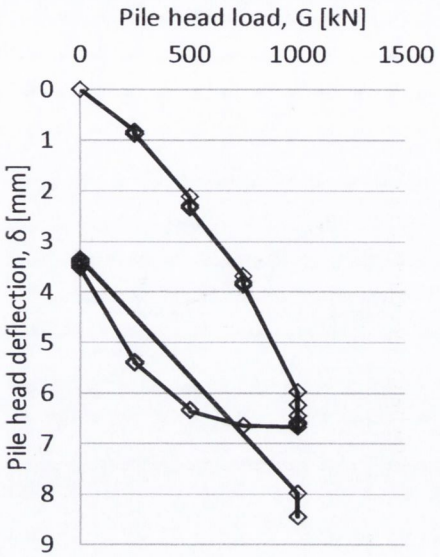


Figure B.55 – Pile 63

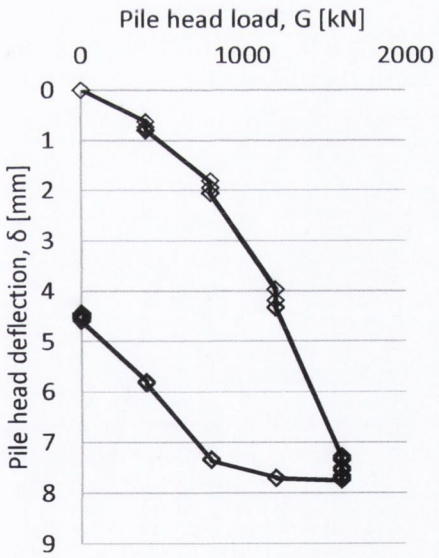


Figure B.54 – Pile 62

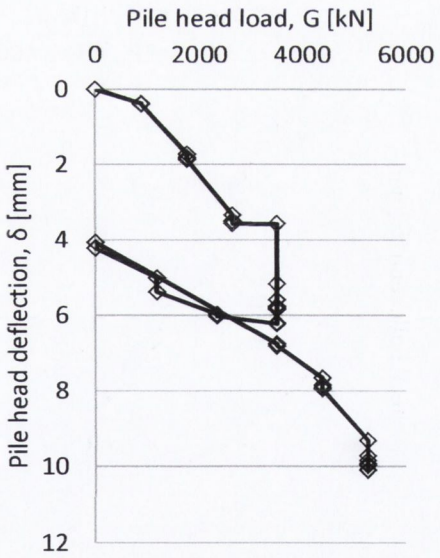


Figure B.56 – Pile 64

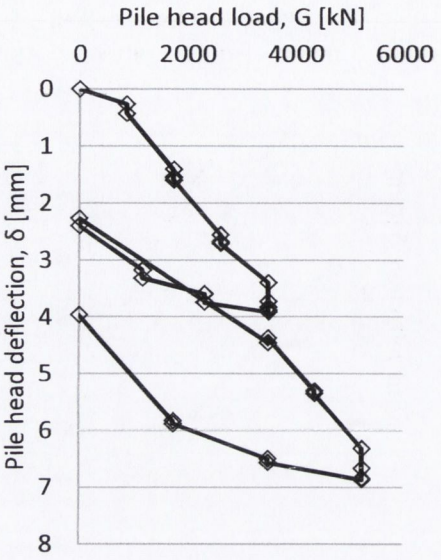


Figure B.57 – Pile 65

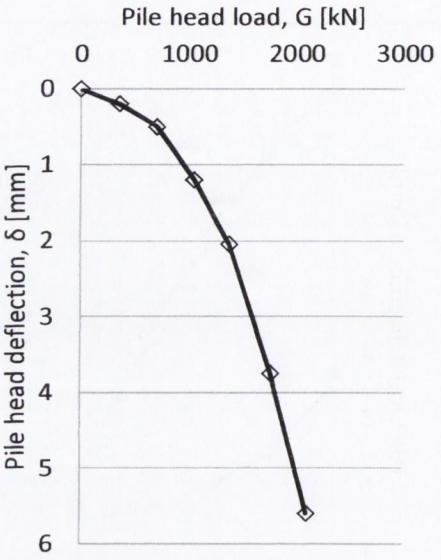


Figure B.59 – Pile 67

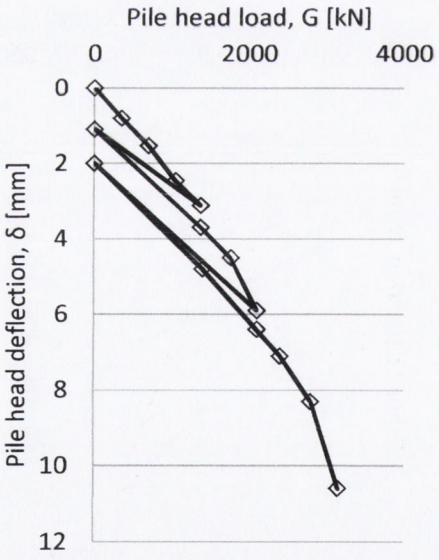


Figure B.58 – Pile 66

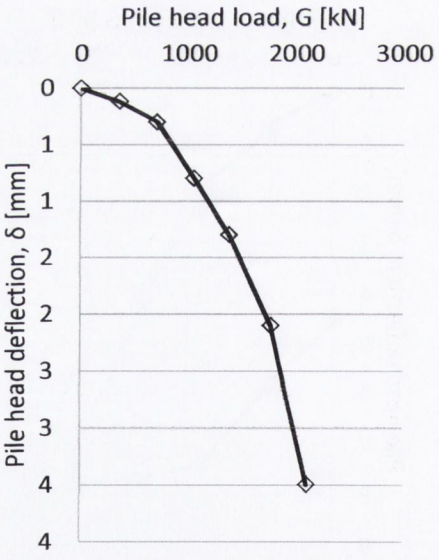


Figure B.60 – Pile 68

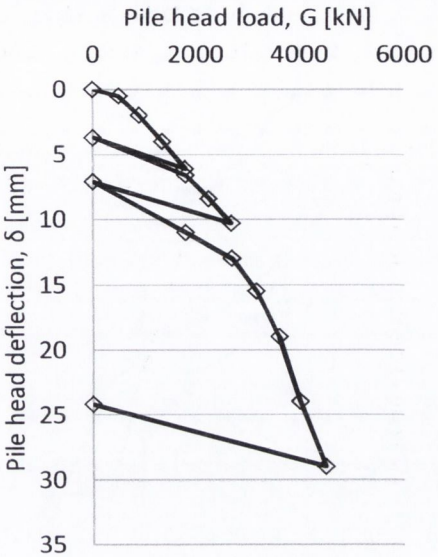


Figure B.61 – Pile 69

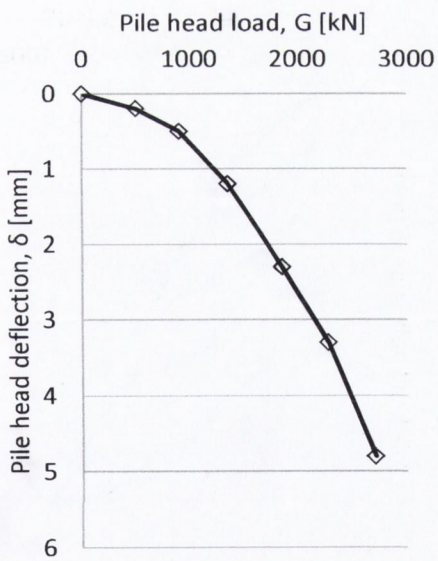


Figure B.62 – Pile 70

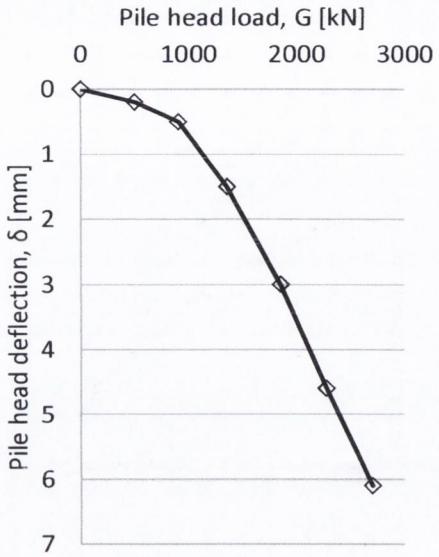


Figure B.63 – Pile 71

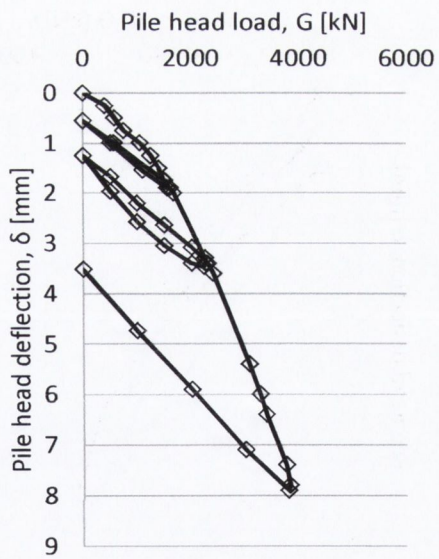


Figure B.64 – Pile 72

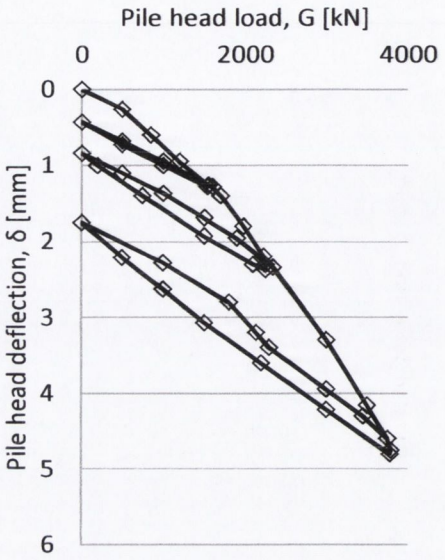


Figure B.65 – Pile 73

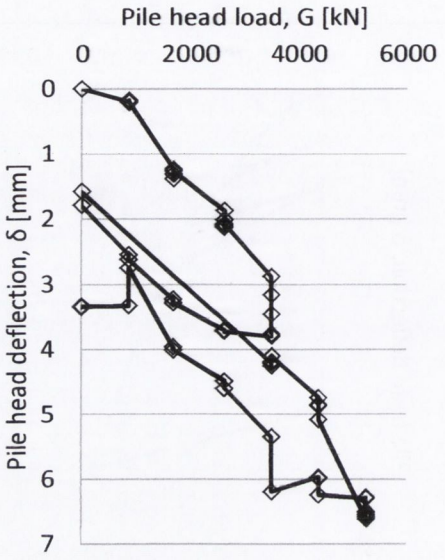


Figure B.67 – Pile 75

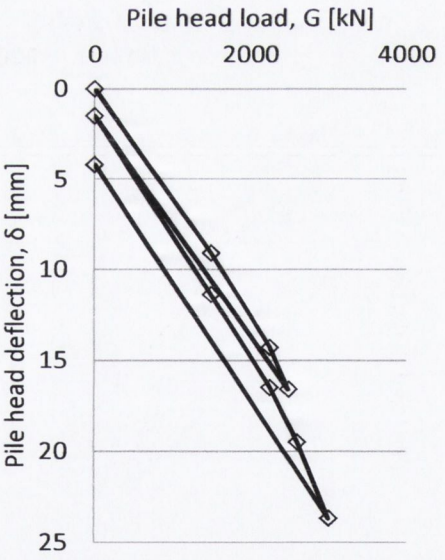


Figure B.66 – Pile 74 (Tension)

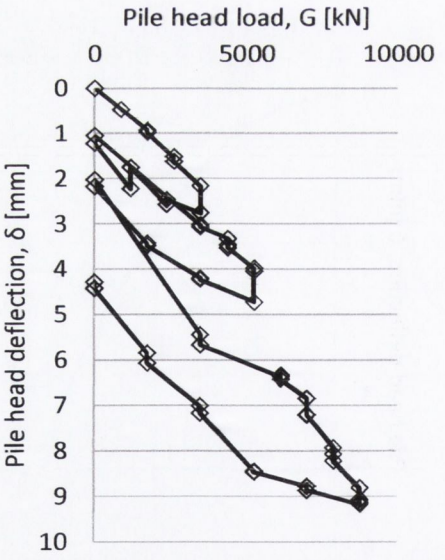


Figure B.68 – Pile 76

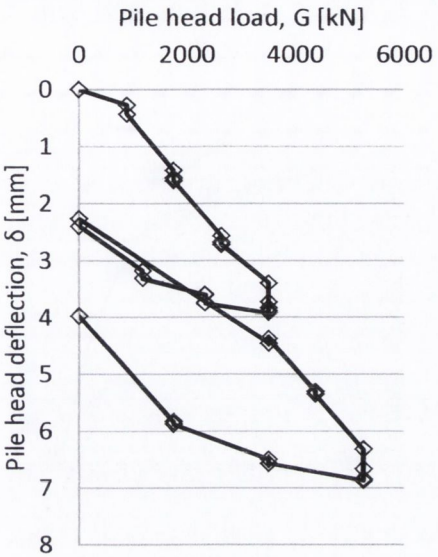


Figure B.69 – Pile 77

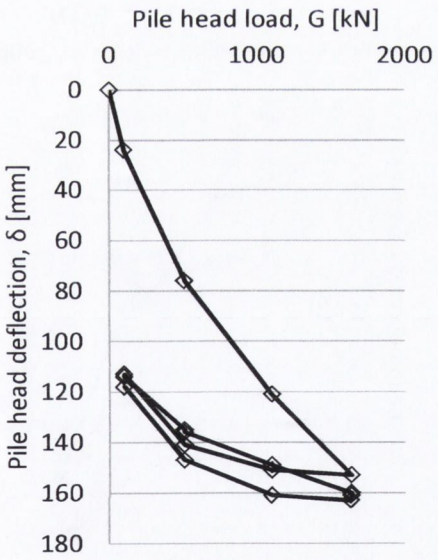


Figure B.70 – Pile 78 (Tension)

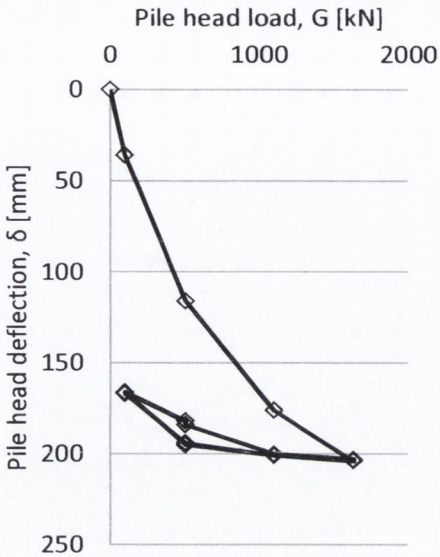


Figure B.71 – Pile 79 (Tension)

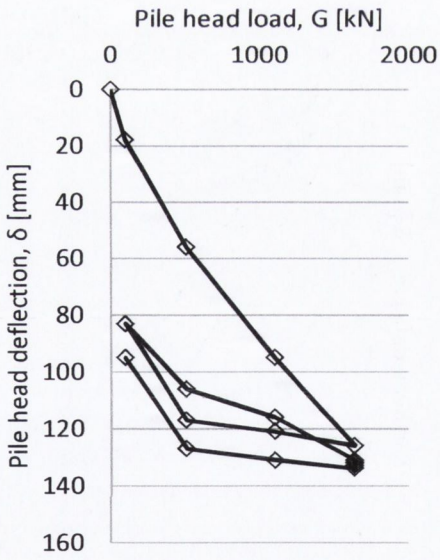


Figure B.72 – Pile 80 (Tension)

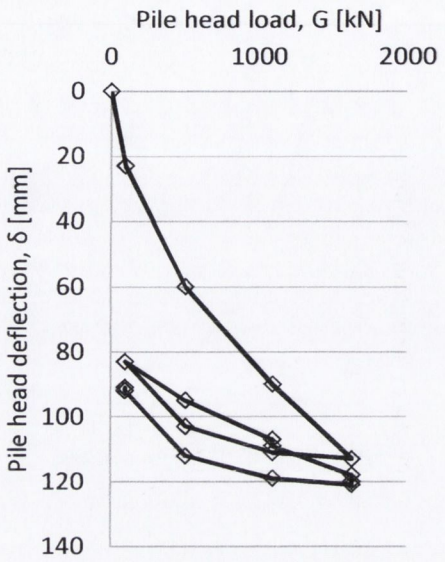


Figure B.73 – Pile 81 (Tension)

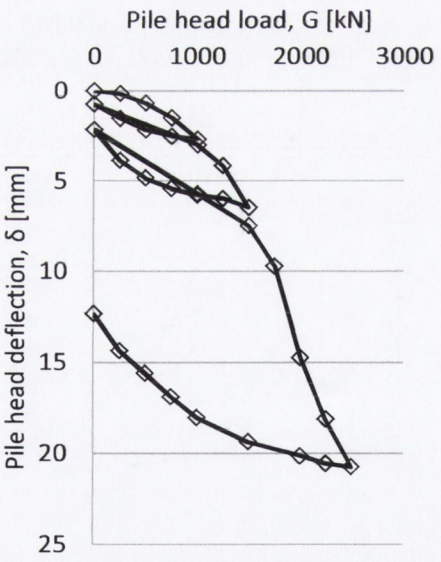


Figure B.74 – Pile 82

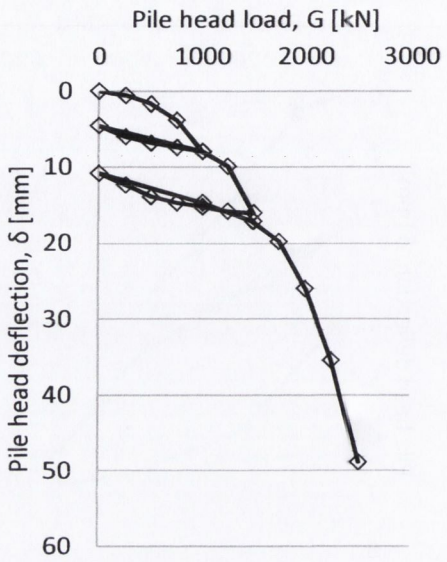


Figure B.75 – Pile 83

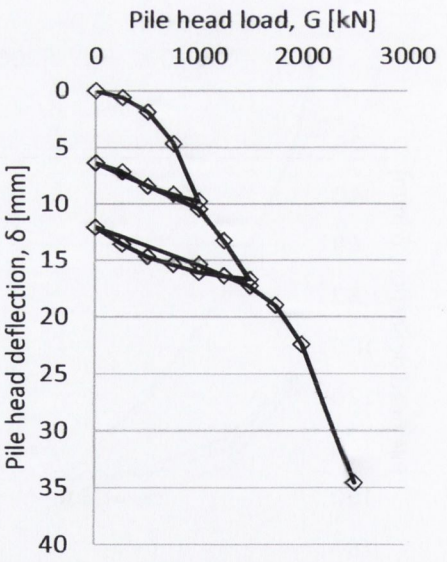


Figure B.76 – Pile 84

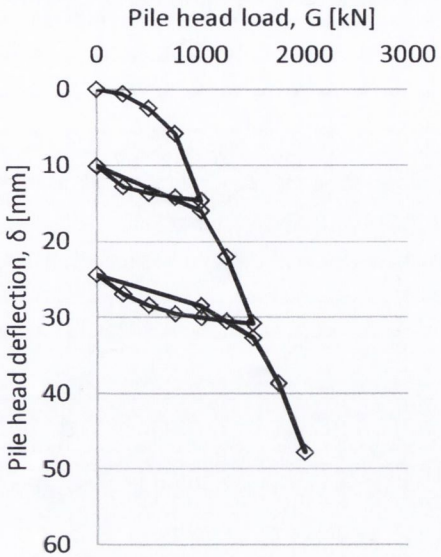


Figure B.77 – Pile 85

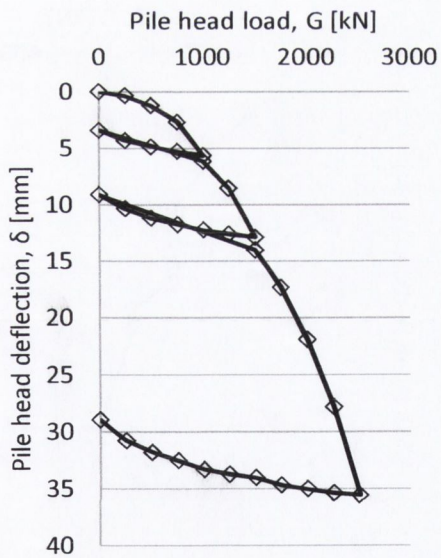


Figure B.78 – Pile 87

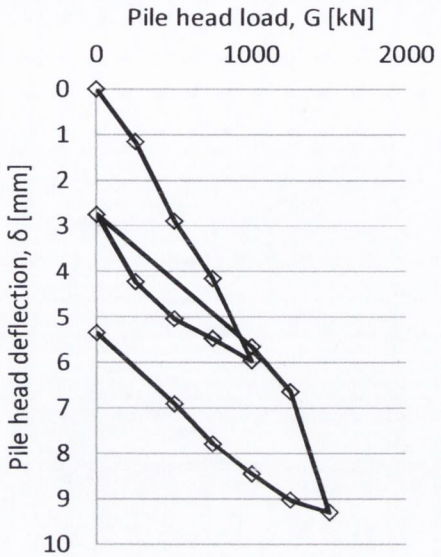


Figure B.79 – Pile 88

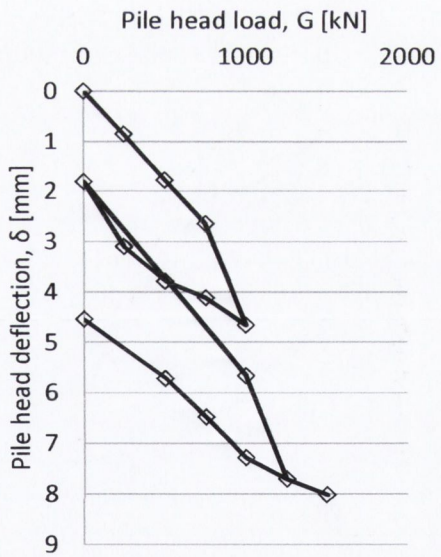


Figure B.80 – Pile 89

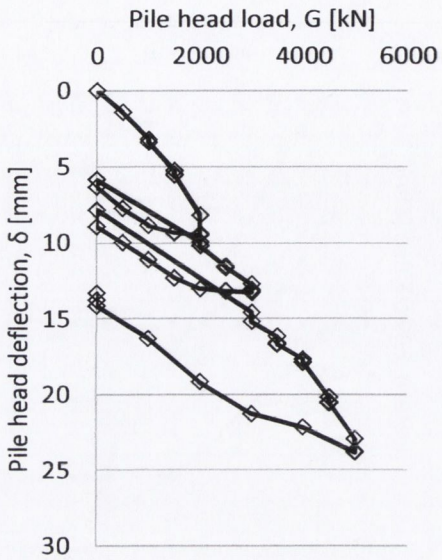


Figure B.81 – Pile 90

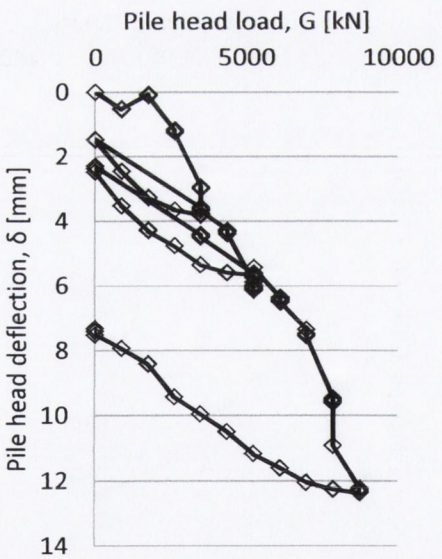


Figure B.82 – Pile 91

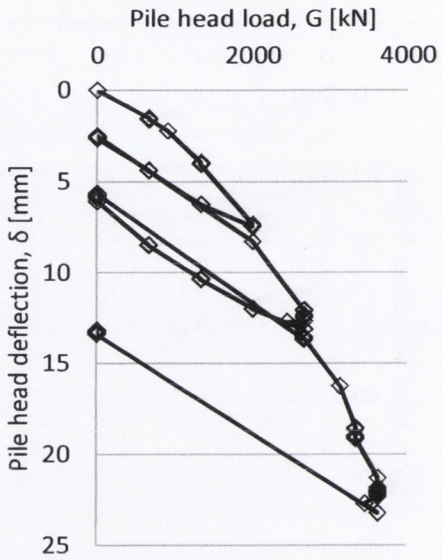


Figure B.83 – Pile 93

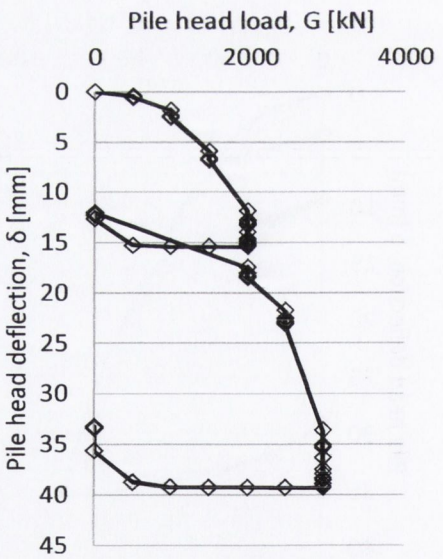


Figure B.84 – Pile 94

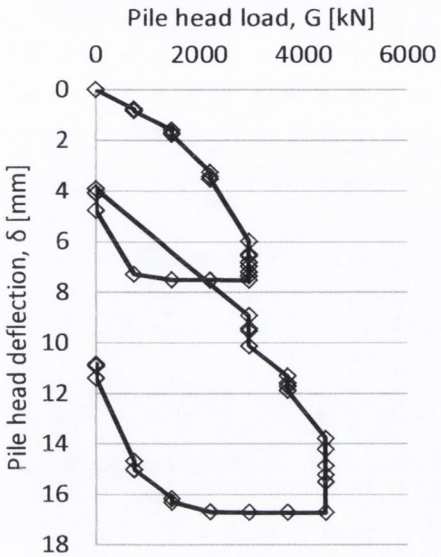


Figure B.85 – Pile 95

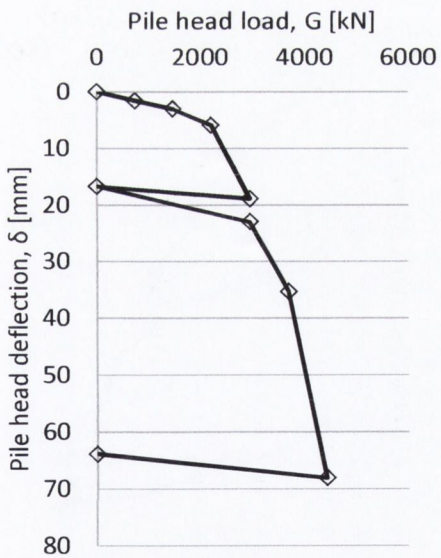


Figure B.86 – Pile 96

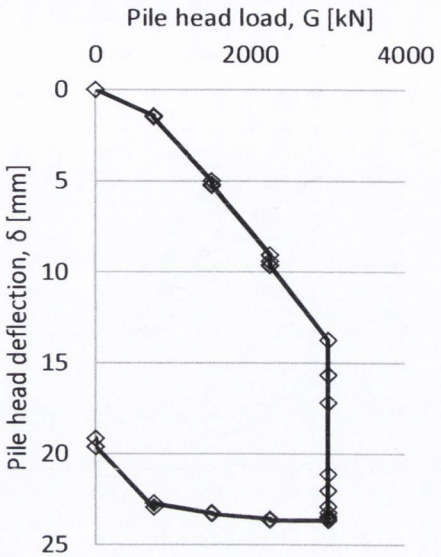


Figure B.87 – Pile 97

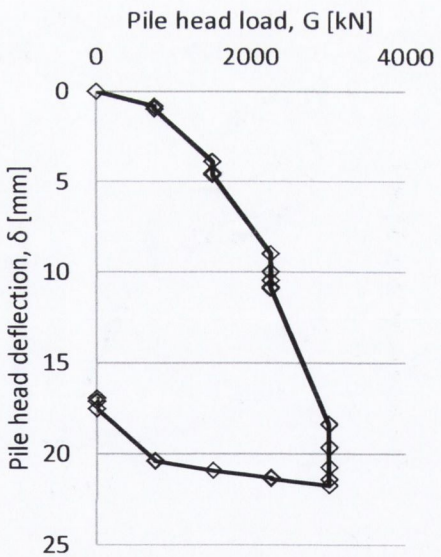


Figure B.88 – Pile 98

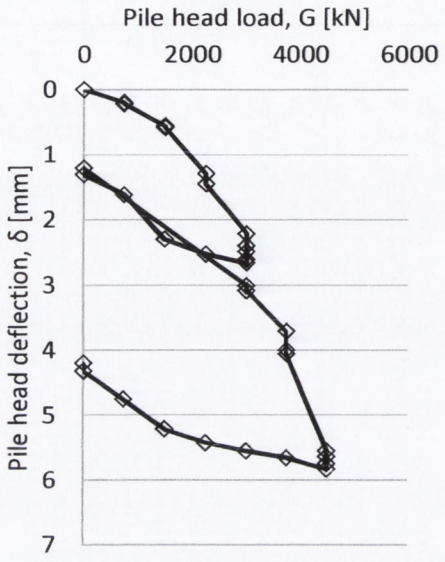


Figure B.89 – Pile 99

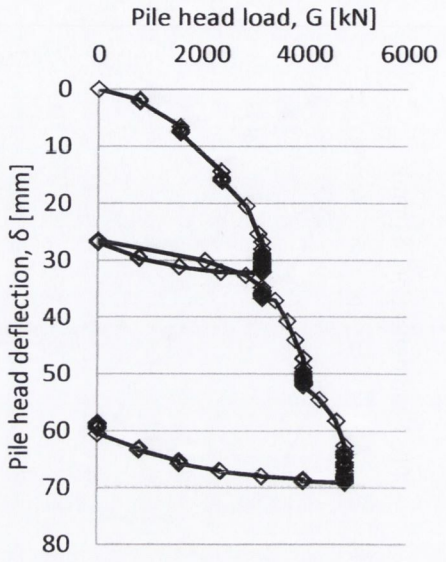


Figure B.91 – Pile 102

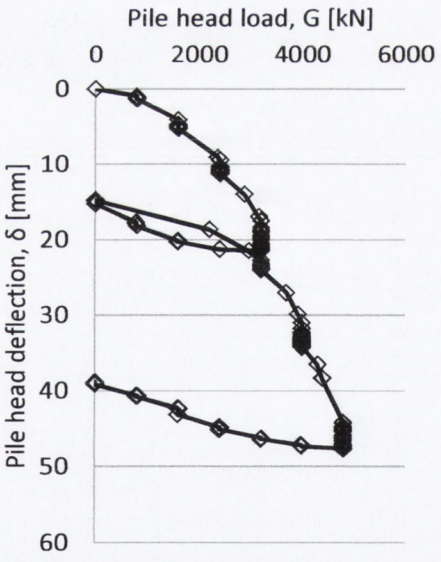


Figure B.90 – Pile 100

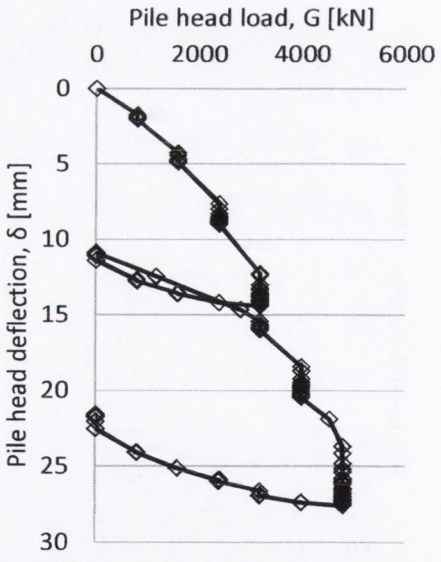


Figure B.92 – Pile 103

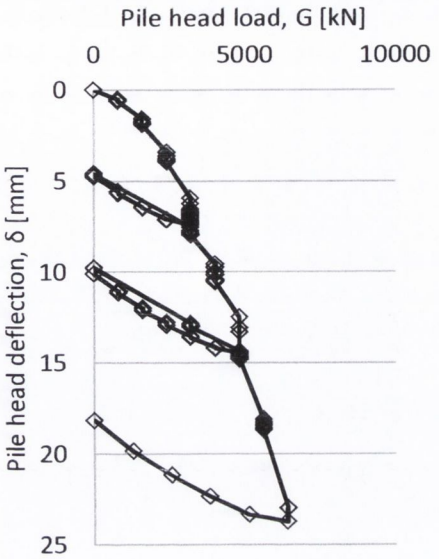


Figure B.93 – Pile 104

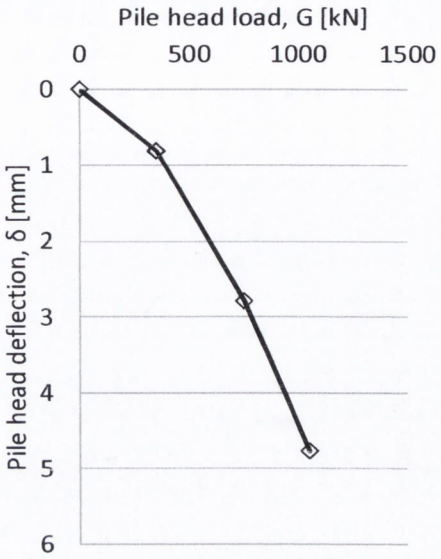


Figure B.95 – Pile 108

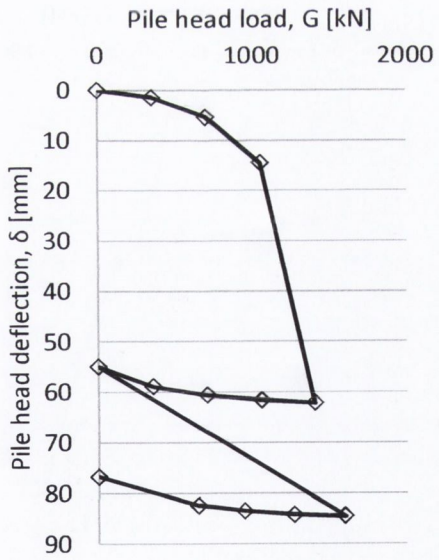


Figure B.94 – Pile 107

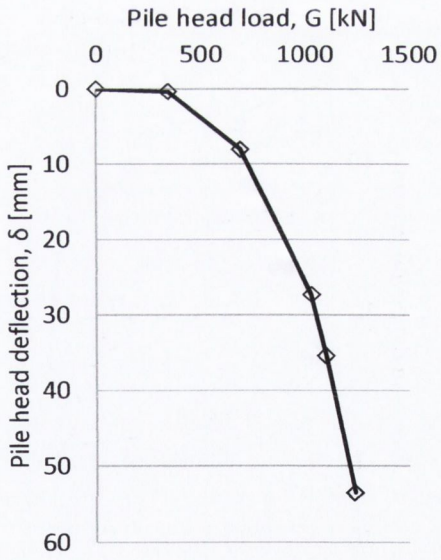


Figure B.96 – Pile 109

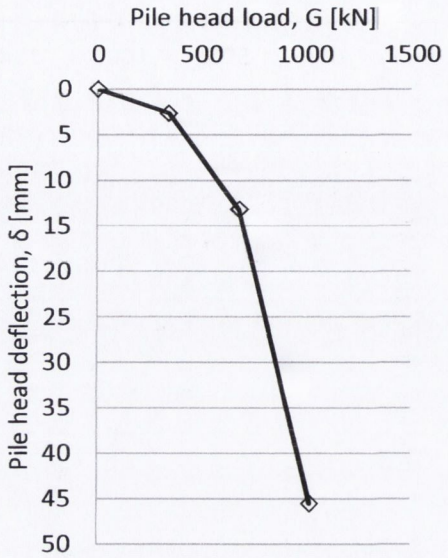


Figure B.97 – Pile 110

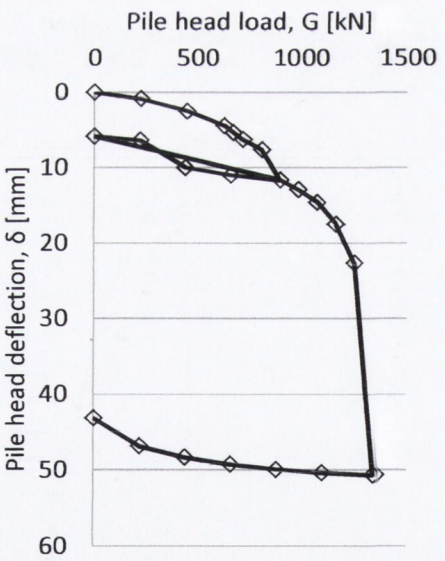


Figure B.98 – Pile 111

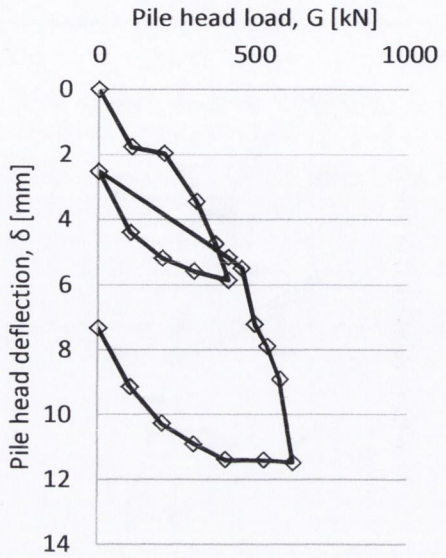


Figure B.99 – Pile 112

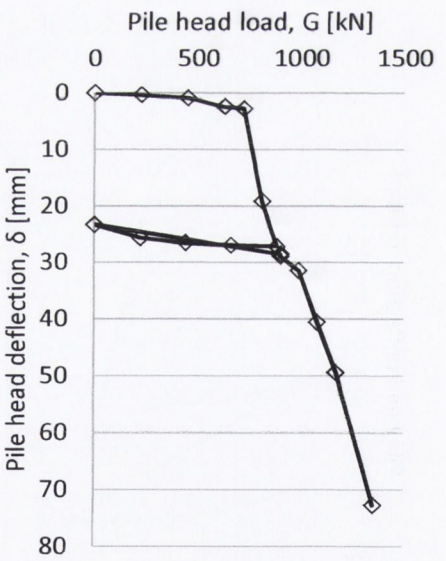


Figure B.100 – Pile 113

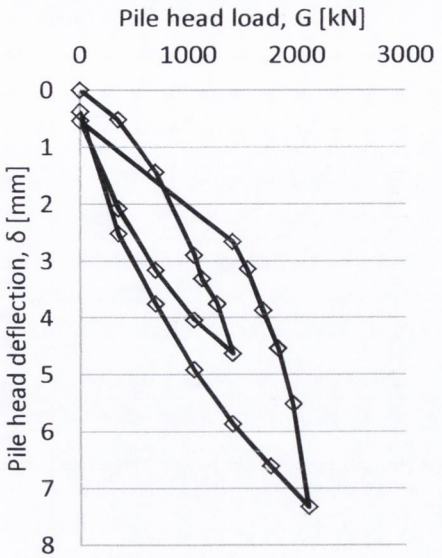


Figure B.101 – Pile 114

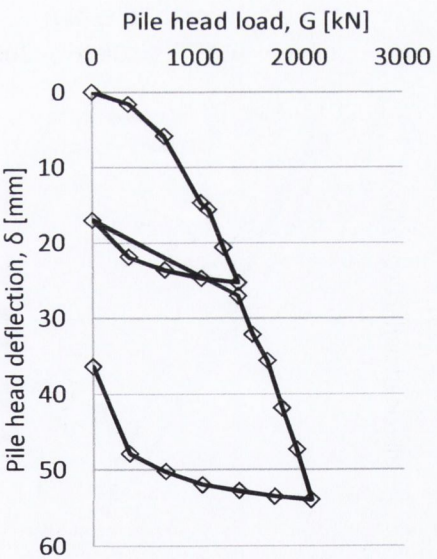


Figure B.102 – Pile 115

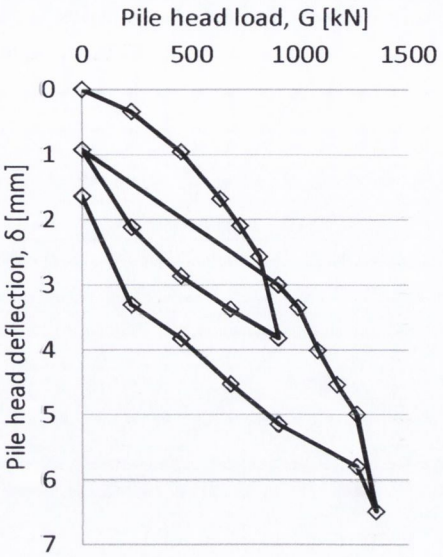


Figure B.103 – Pile 116

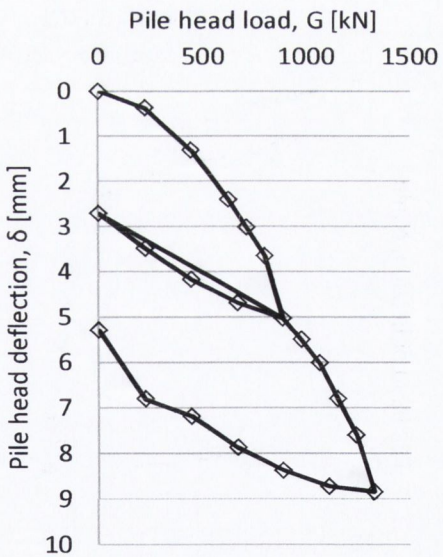


Figure B.104 – Pile 117

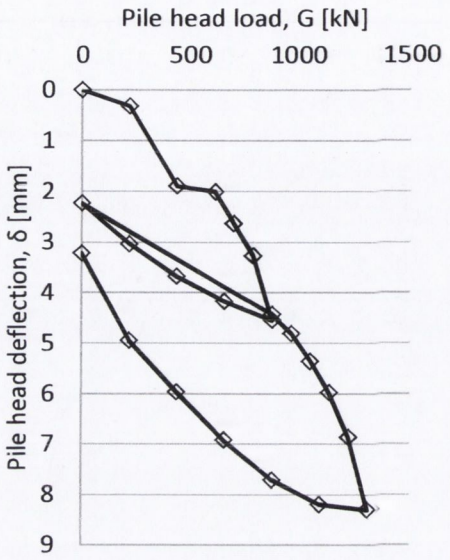


Figure B.105 – Pile 118

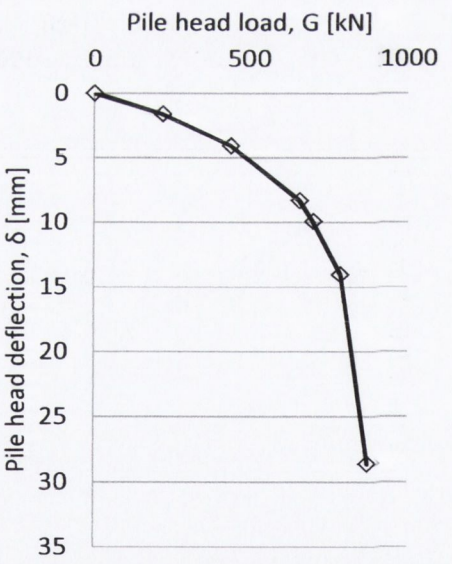


Figure B.106 – Pile 119

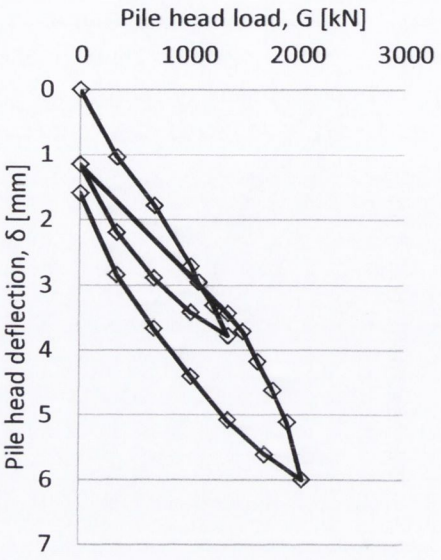


Figure B.107 – Pile 120

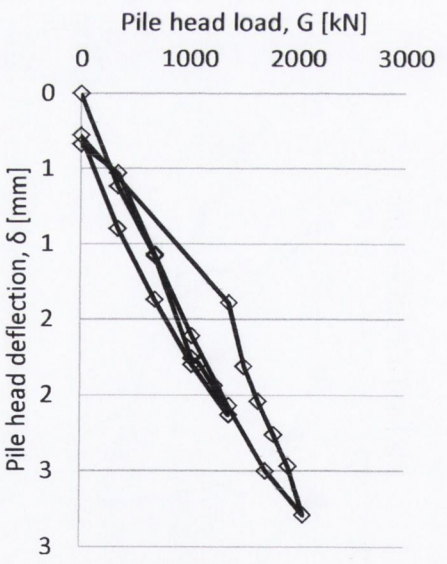


Figure B.108 – Pile 121

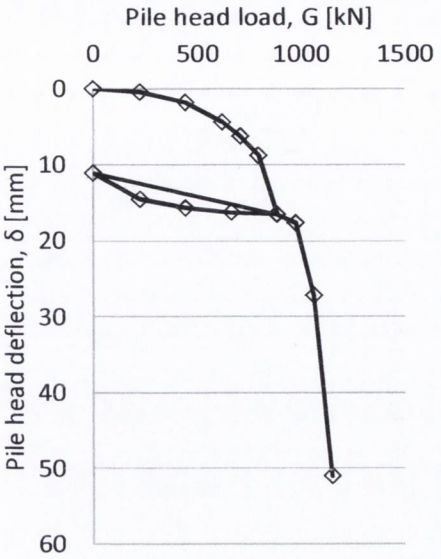


Figure B.109 – Pile 122

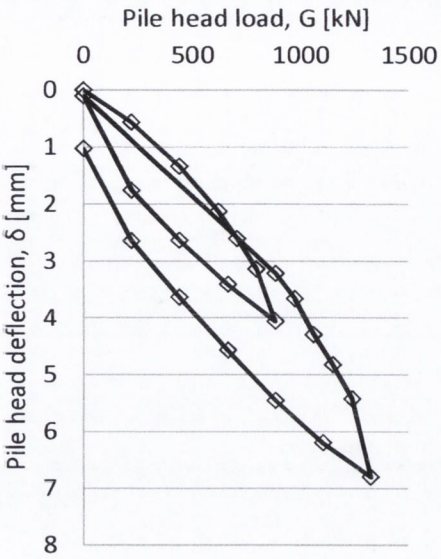


Figure B.111 – Pile 124

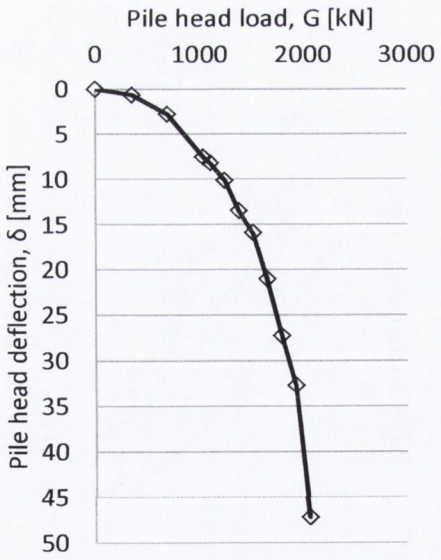


Figure B.110 – Pile 123

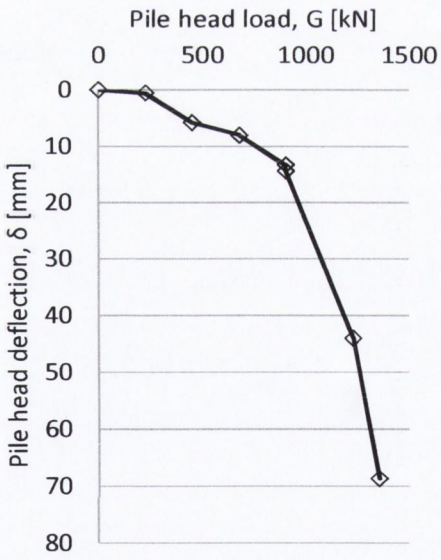


Figure B.112 – Pile 125

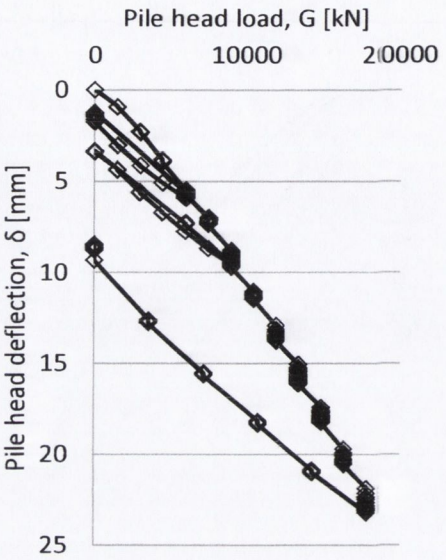


Figure B.113 – Pile 126

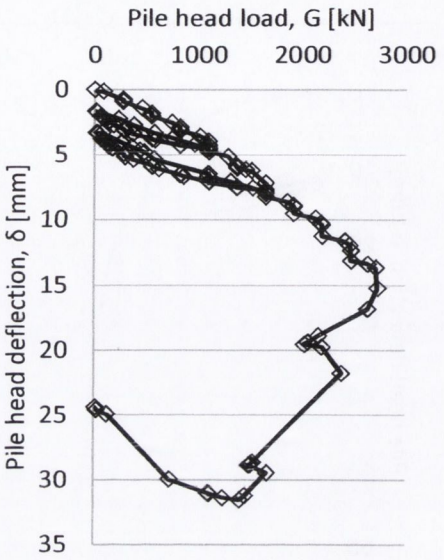


Figure B.115 – Pile 129

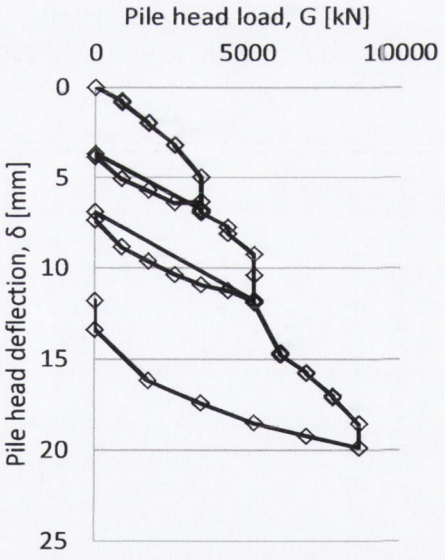


Figure B.114 – Pile 128

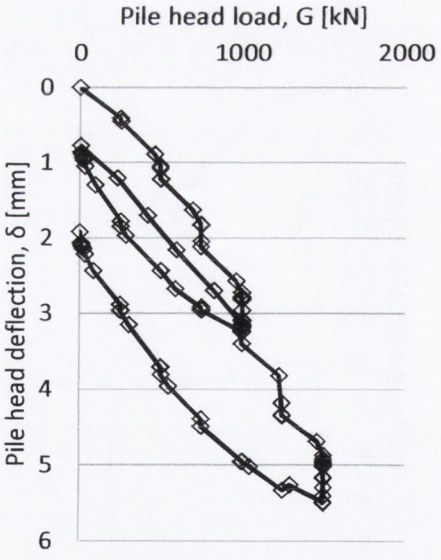


Figure B.116 – Pile 130

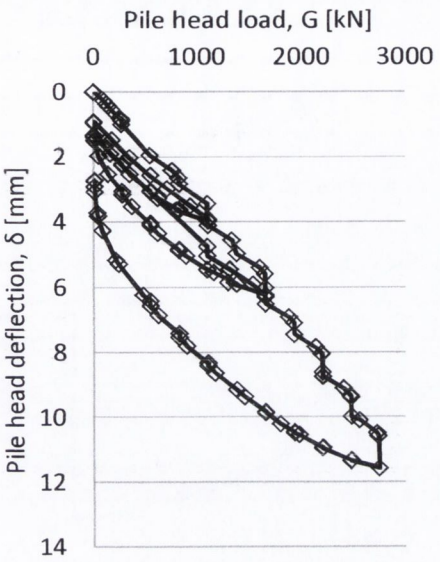


Figure B.117 – Pile 131

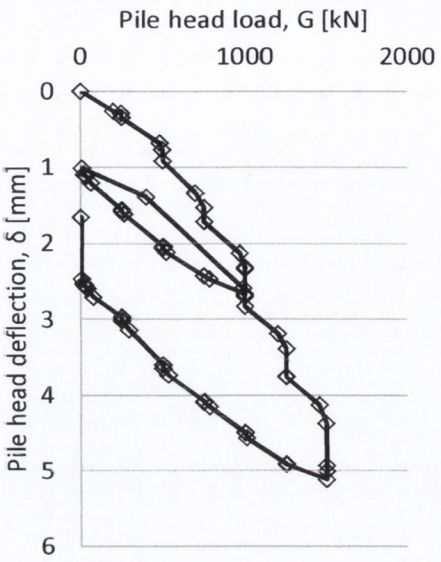


Figure B.119 – Pile 133

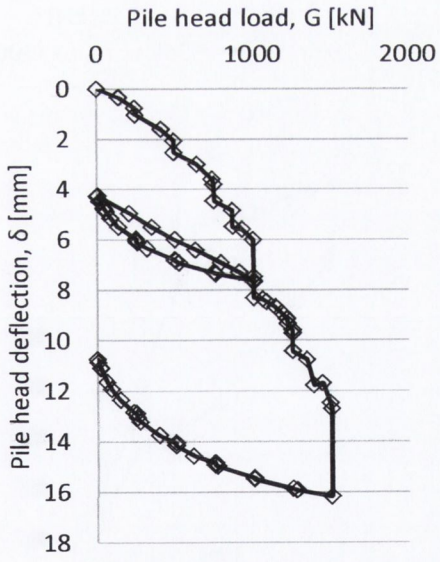


Figure B.118 – Pile 132

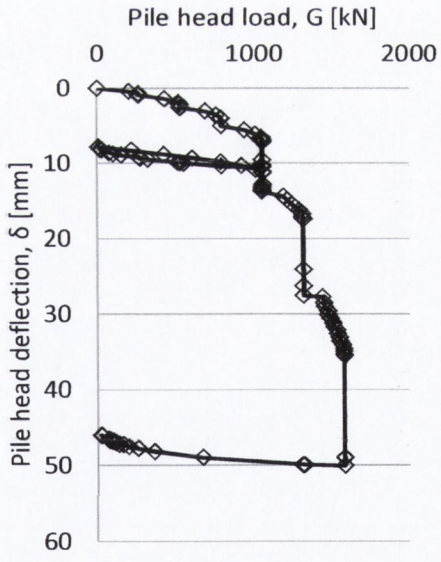


Figure B.120 - Pile 134

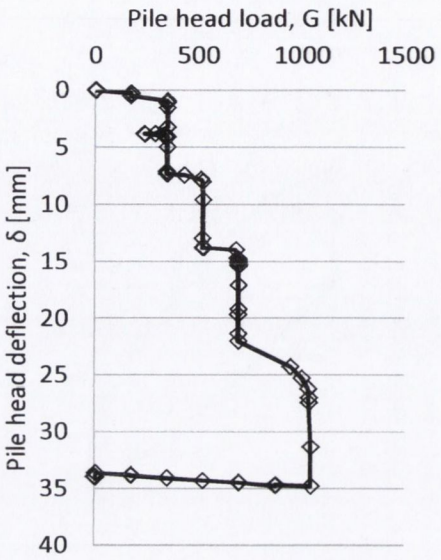


Figure B.121 – Pile 135

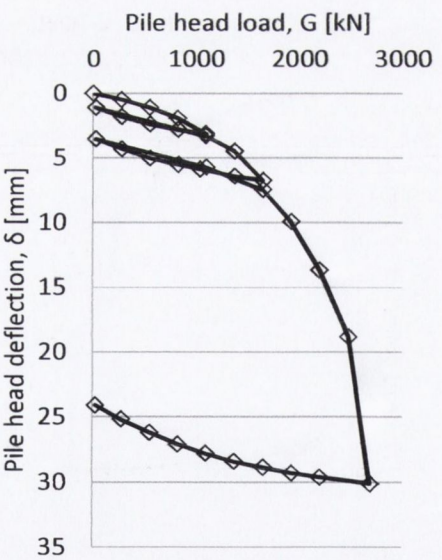


Figure B.122 – Pile 136

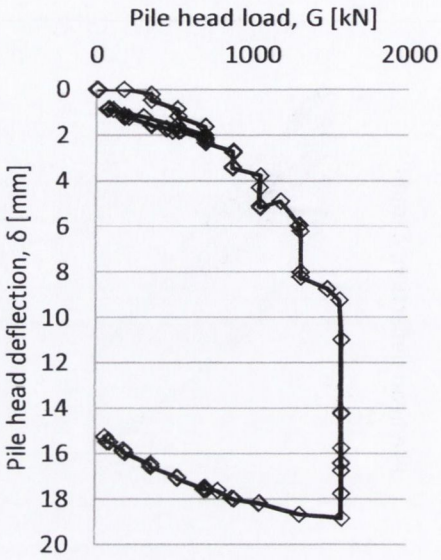


Figure B.123 – Pile 137

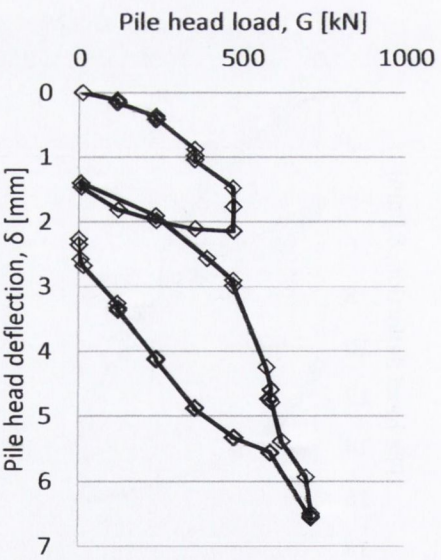


Figure B.124 – Pile 138 (Tension)

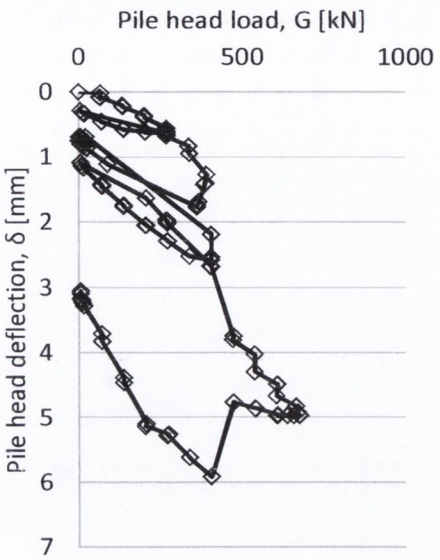


Figure B.125 – Pile 139 (Tension)

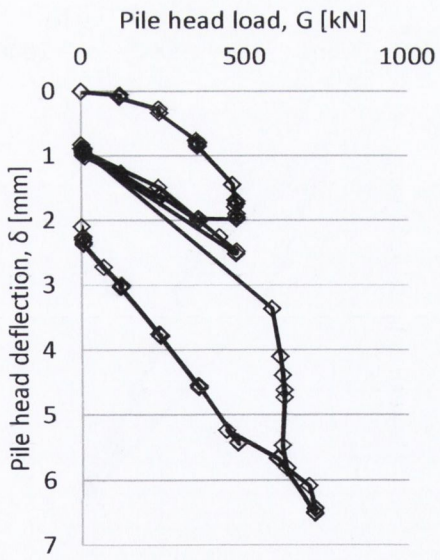


Figure B.126 – Pile 140 (Tension)

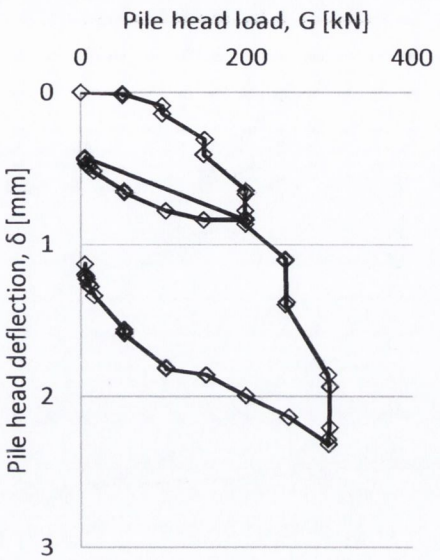


Figure B.127 – Pile 141 (Tension)

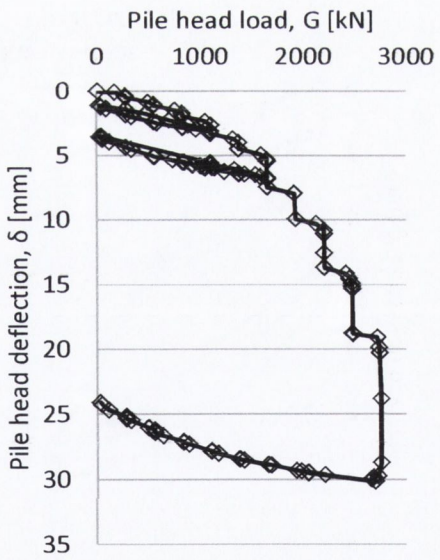


Figure B.128 – Pile 142

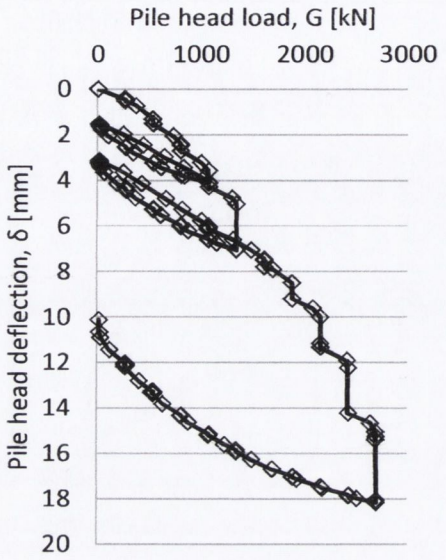


Figure B.129 – Pile 143

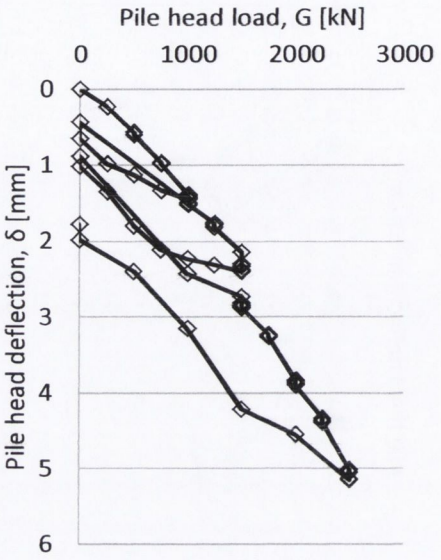


Figure B.131 – Pile 147

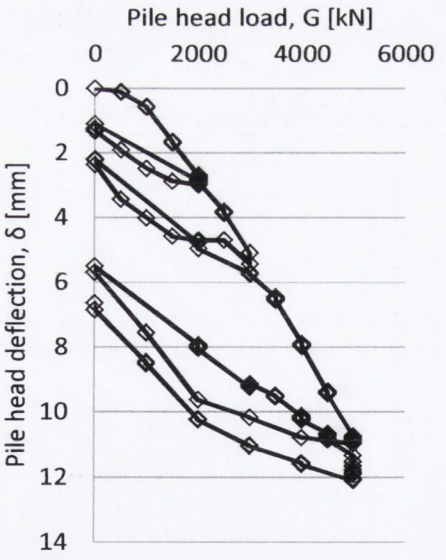


Figure B.130 – Pile 145

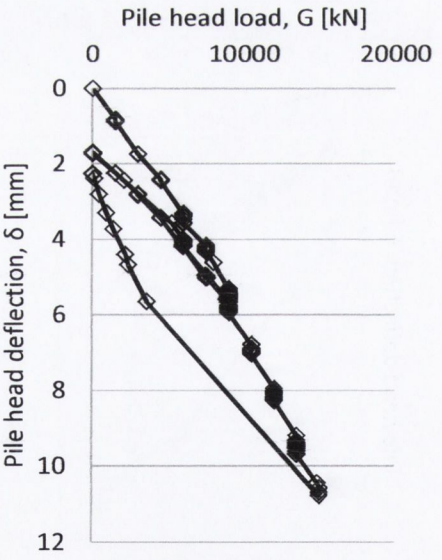


Figure B.132 – Pile 148

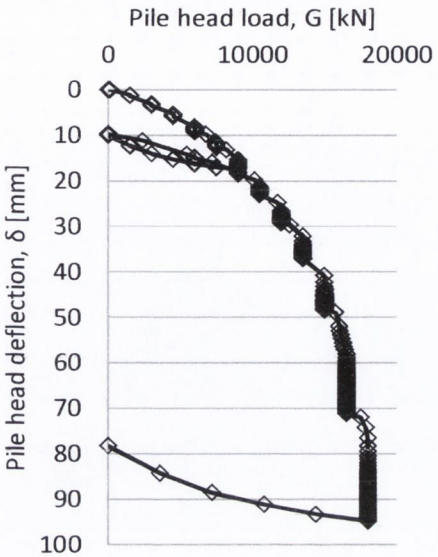


Figure B.133 – Pile 151

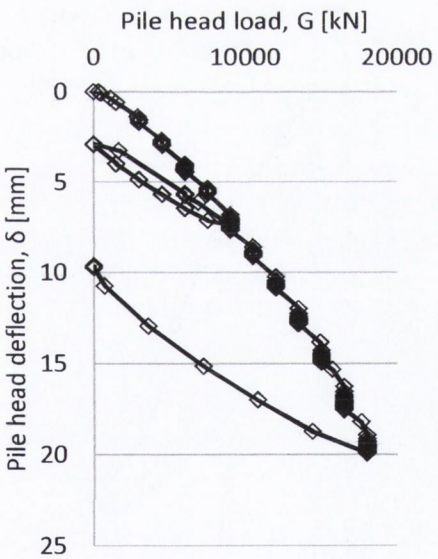


Figure B.134 - Pile 156

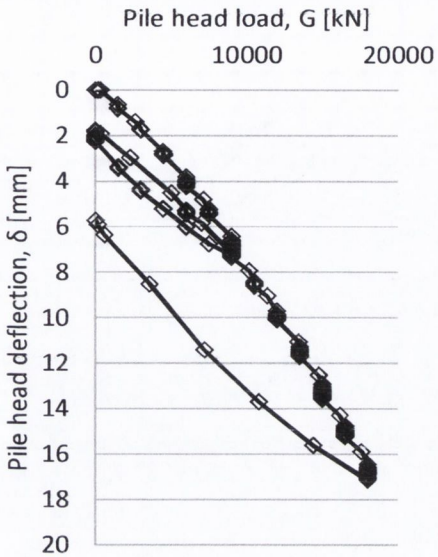


Figure B.135 – Pile 159

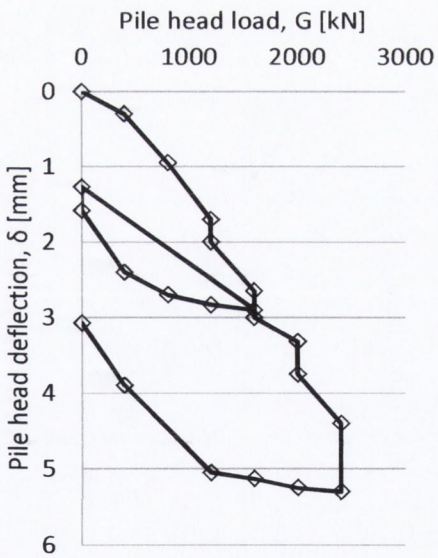


Figure B.136 – Pile 162

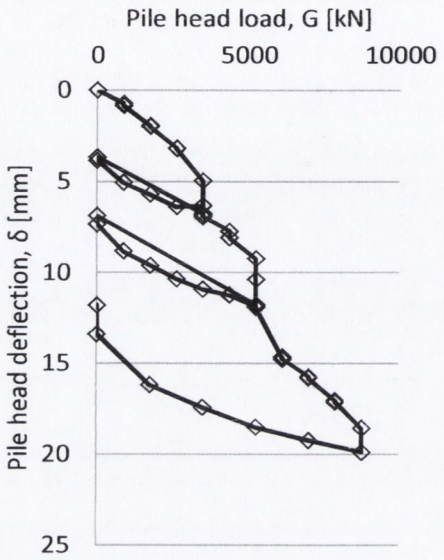


Figure B.137 – Pile 163

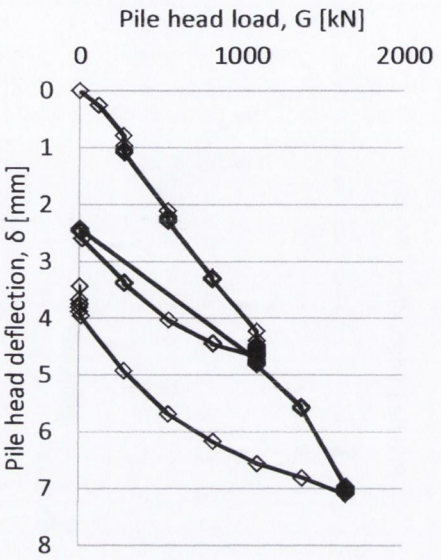


Figure B.139 – Pile 165

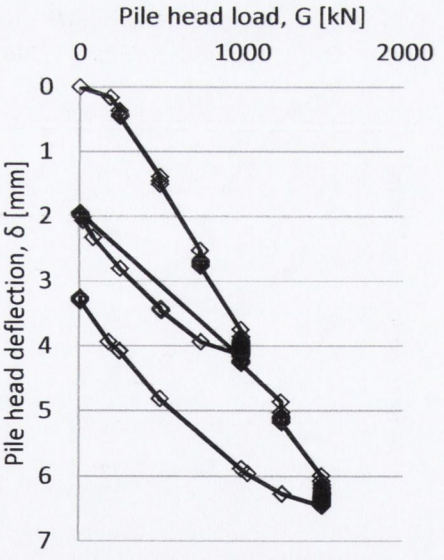


Figure B.138 – Pile 164

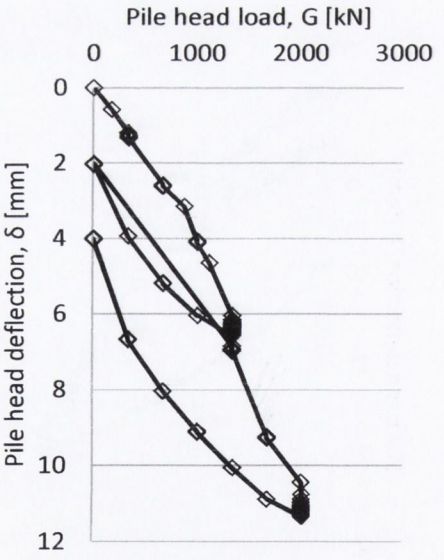


Figure B.140 – Pile 166

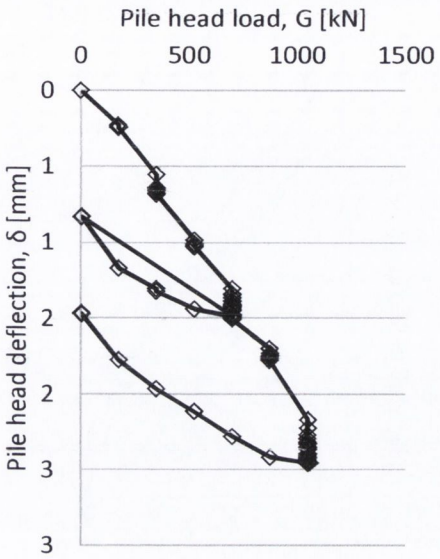


Figure B.141 – Pile 167

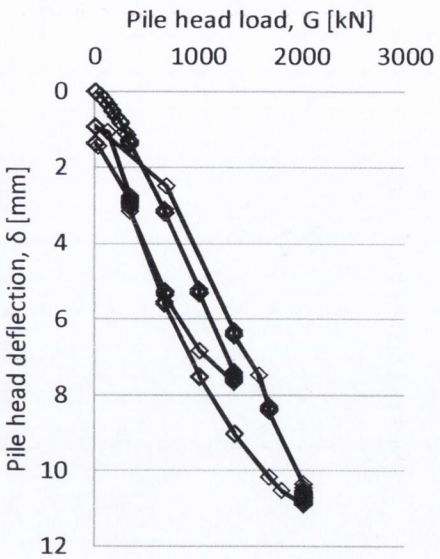


Figure B.143 – Pile 169

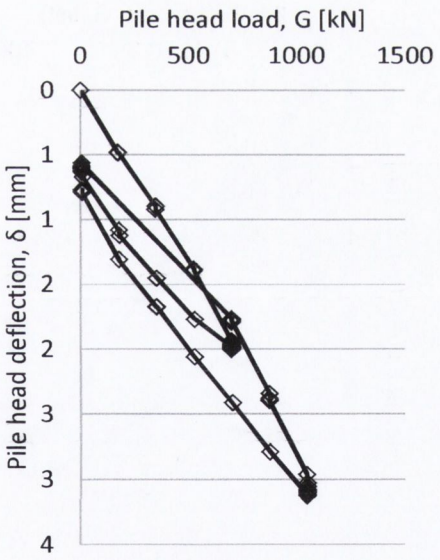


Figure B.142 – Pile 168

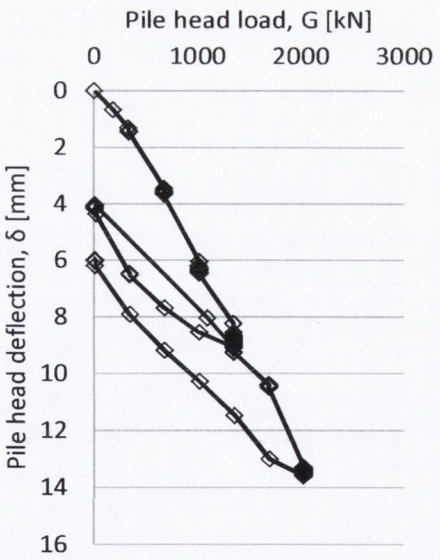


Figure B.144 – Pile 171

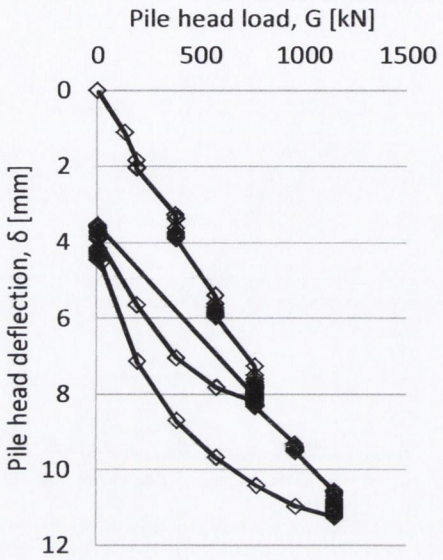


Figure B.145 – Pile 172

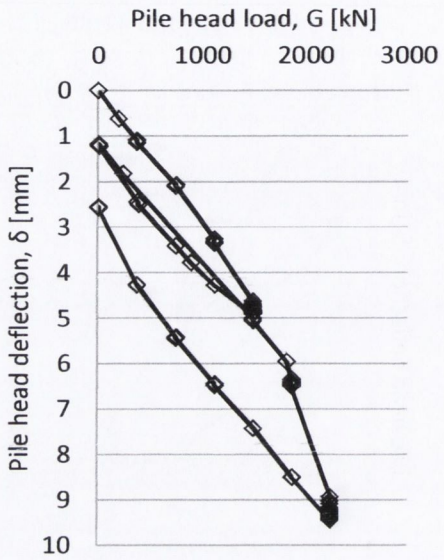


Figure B.147 – Pile 174

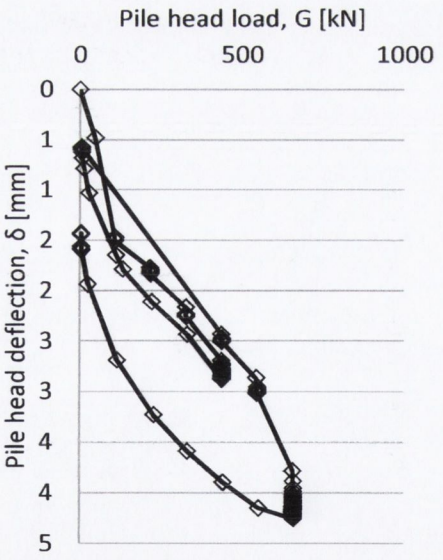


Figure B.146 – Pile 173

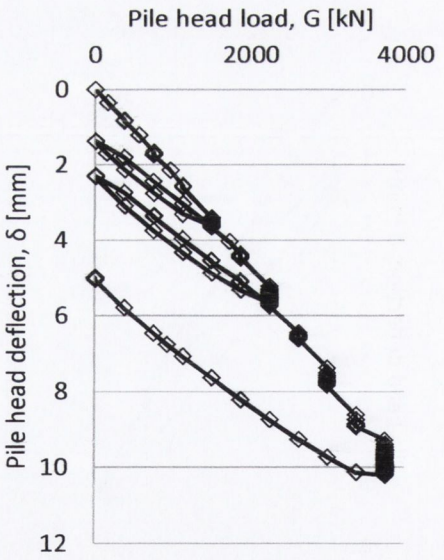


Figure B.148 – Pile 175

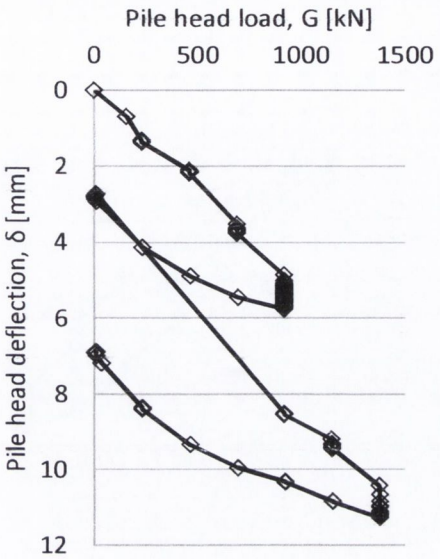


Figure B.149 – Pile 177

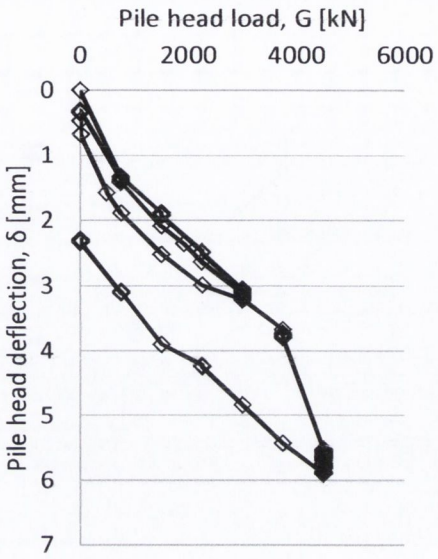


Figure B.151 – Pile 180

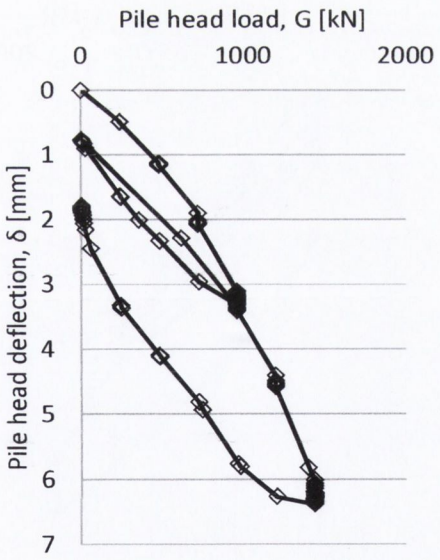


Figure B.150 – Pile 178

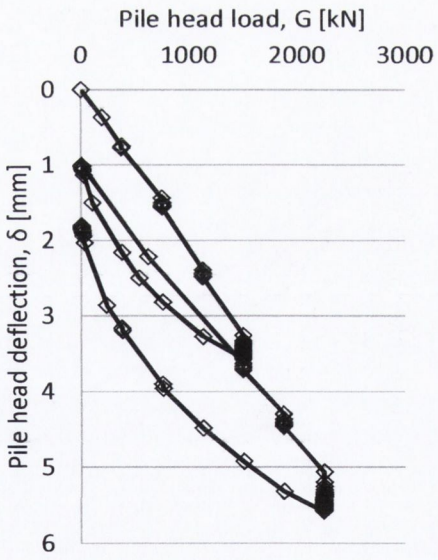


Figure B.152 – Pile 181

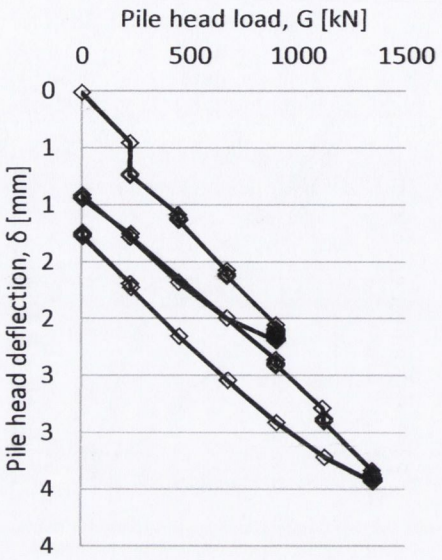


Figure B.153 – Pile 182

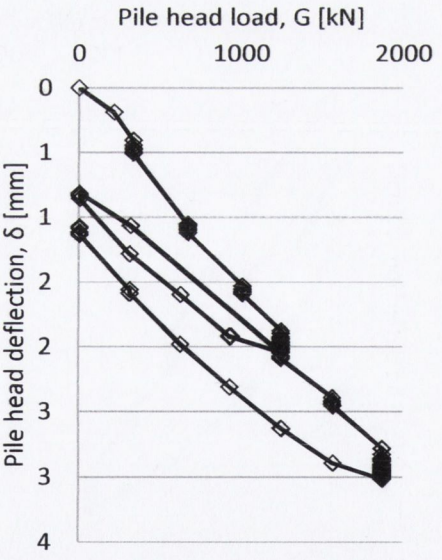


Figure B.154 – Pile 183

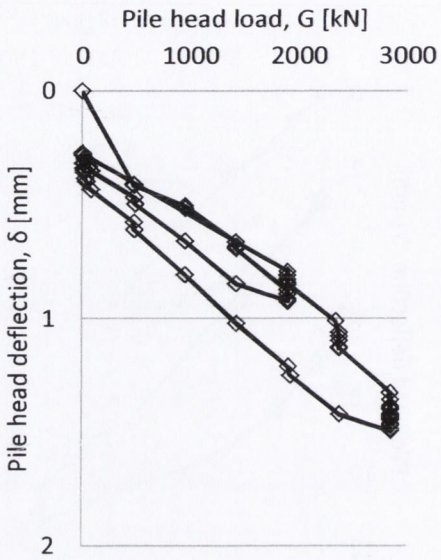


Figure B.155 – Pile 184

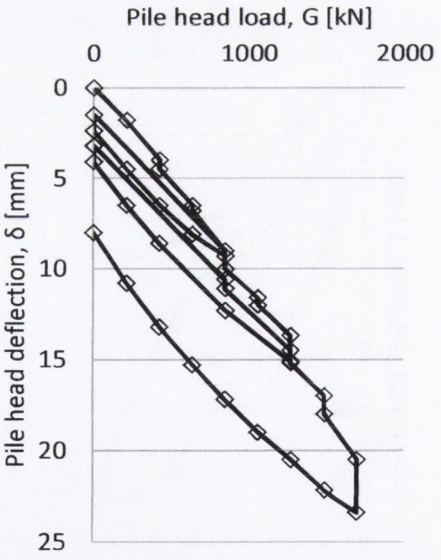


Figure B.156 – Pile 185

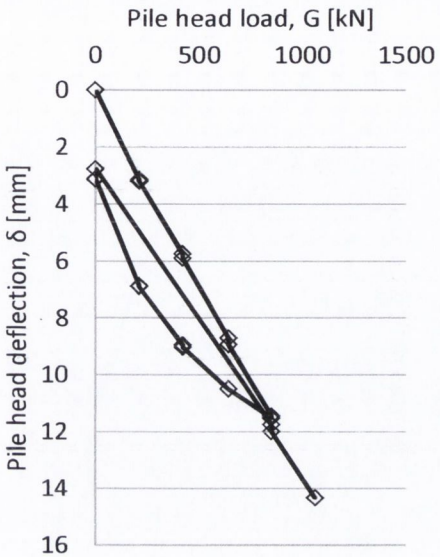


Figure B.157 – Pile 186

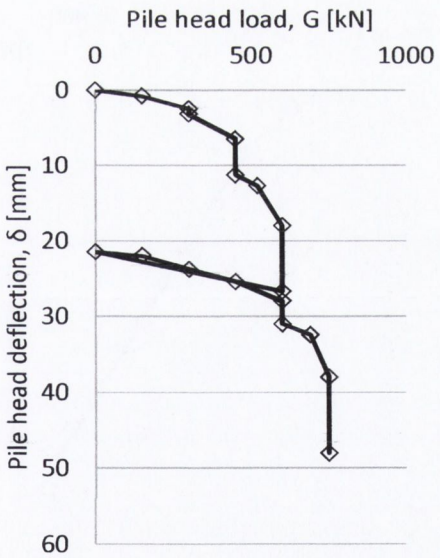


Figure B.158 – Pile 187

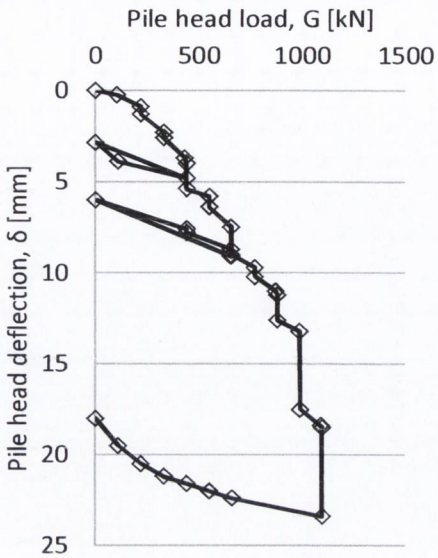


Figure B.159 – Pile 188

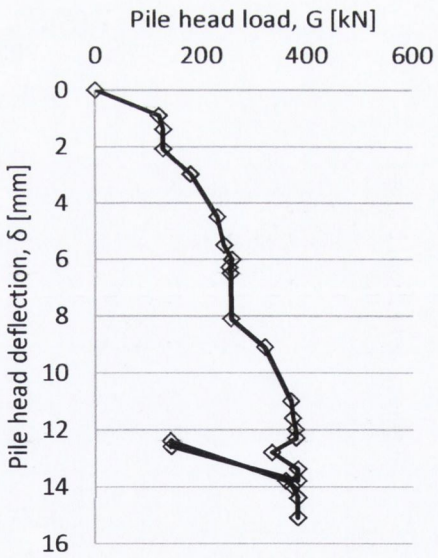


Figure B.160 – Pile 189

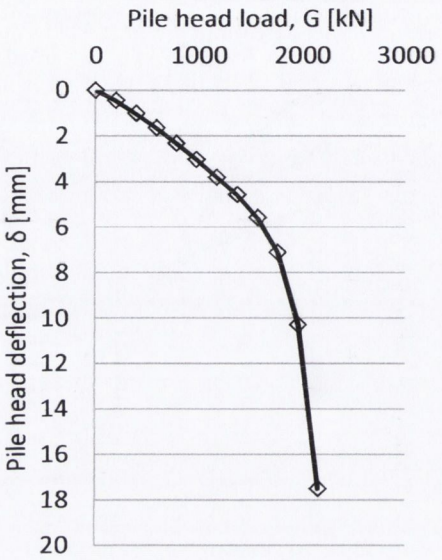


Figure B.161 – Pile 190

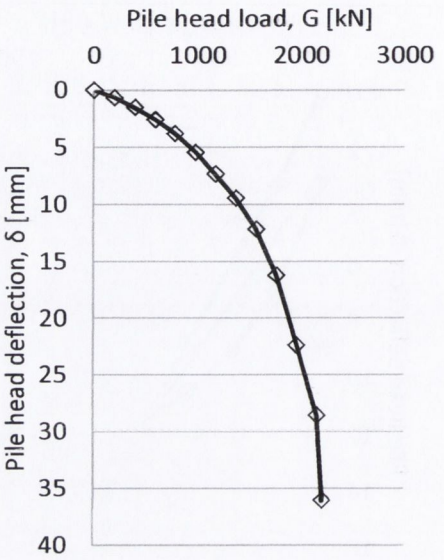


Figure B.163 – Pile 192

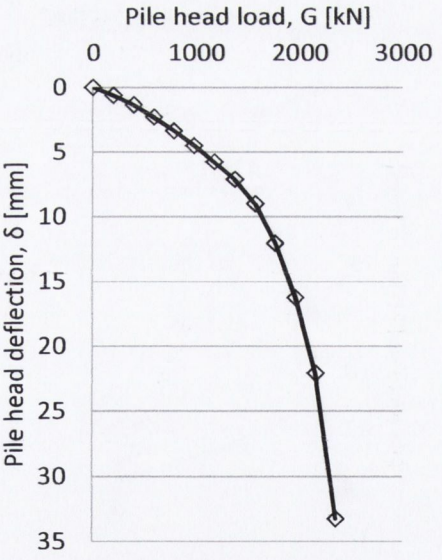


Figure B.162 – Pile 191

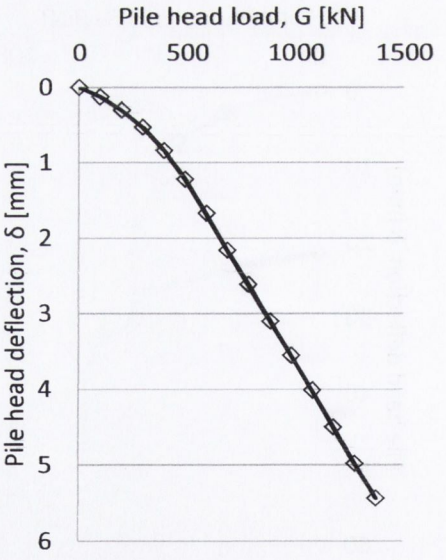


Figure B.164 – Pile 193

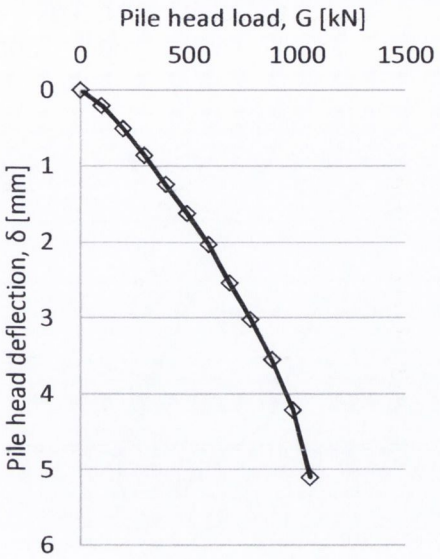


Figure B.165 – Pile 194

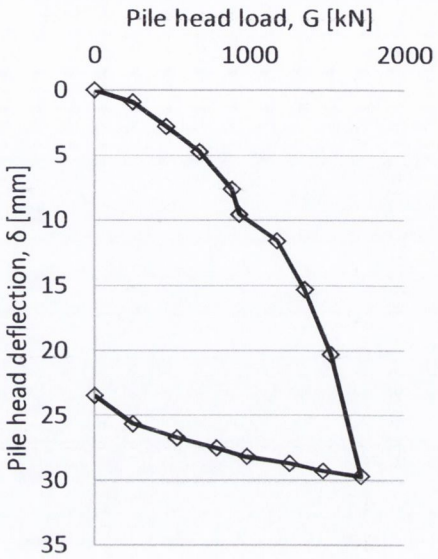


Figure B.167 – Pile 196

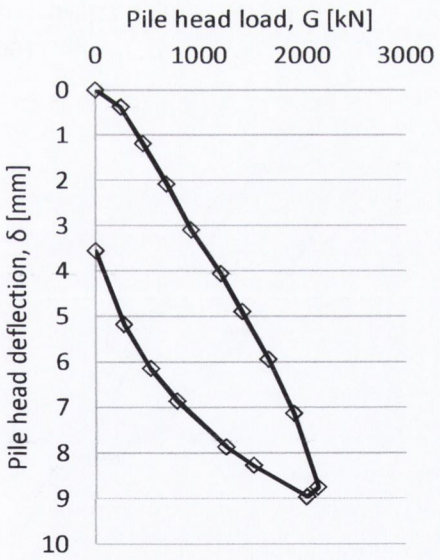


Figure B.166 – Pile 195

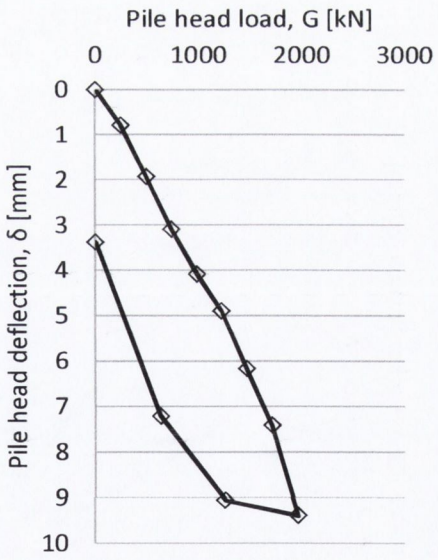


Figure B.168 – Pile 197

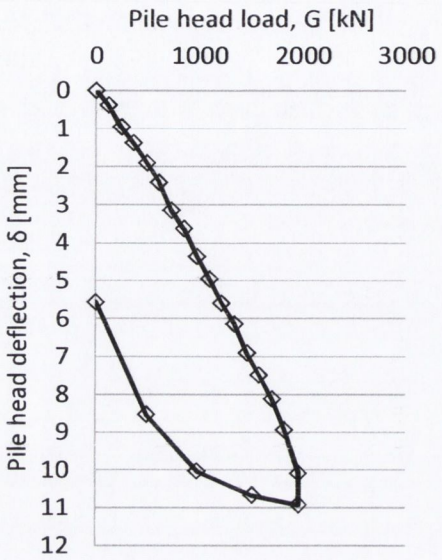


Figure B.169 – Pile 198

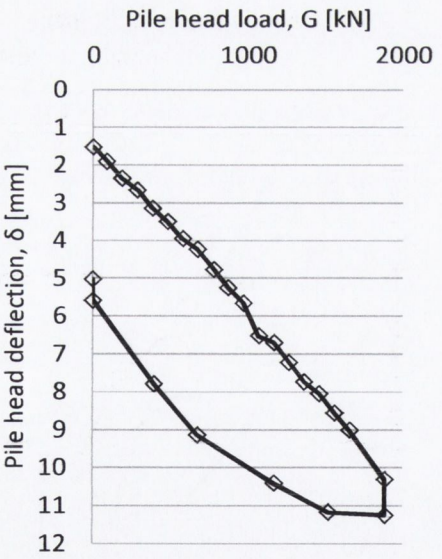


Figure B.170 – Pile 199

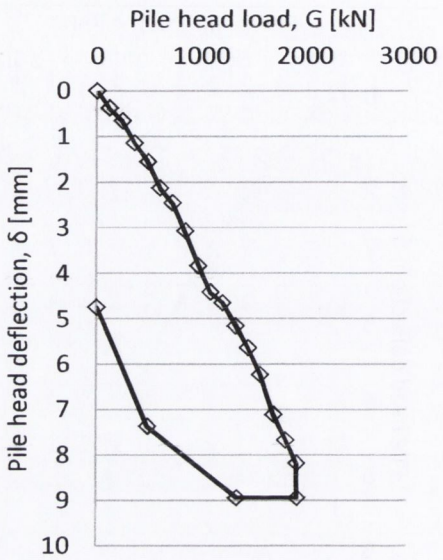


Figure B.171 – Pile 200

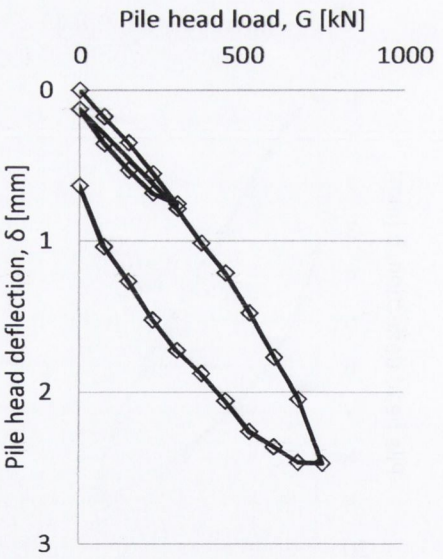


Figure B.172 – Pile 201

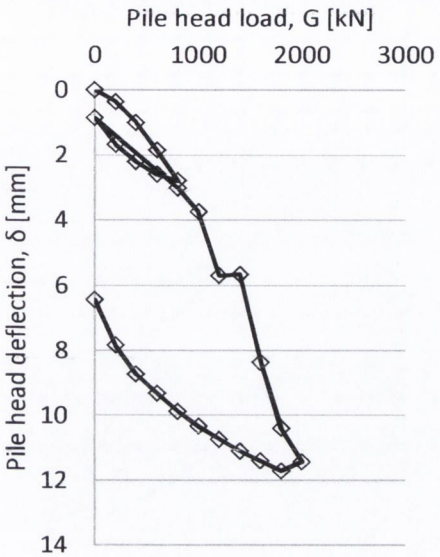


Figure B.173 – Pile 202

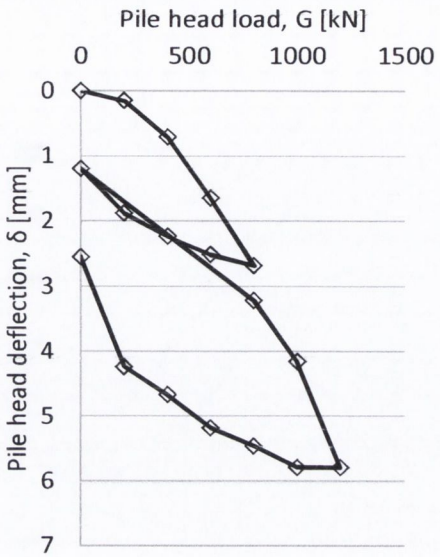


Figure B.175 – Pile 204

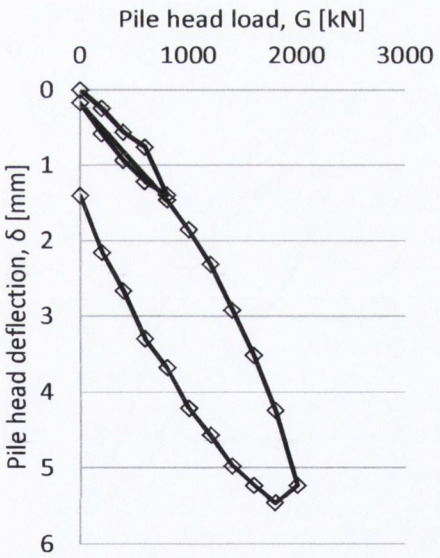


Figure B.174 – Pile 203

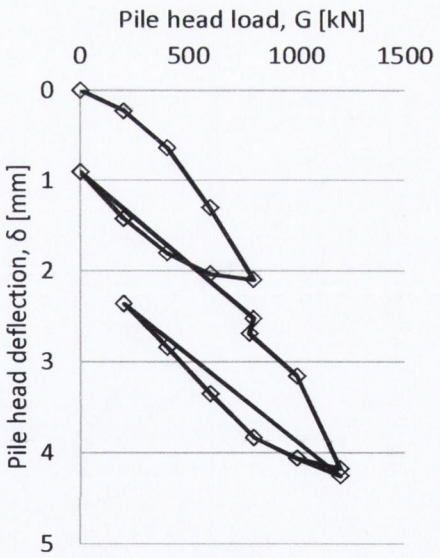


Figure B.176 – Pile 205

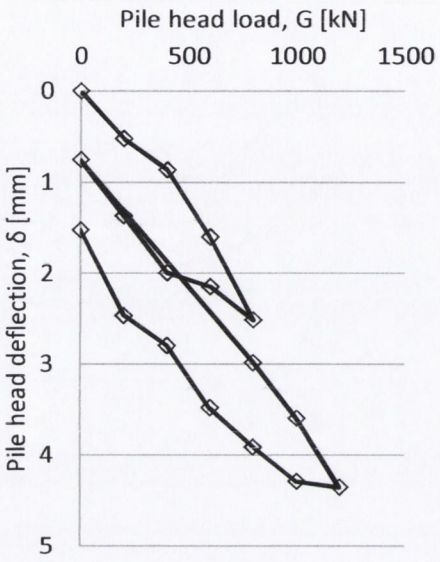


Figure B.177 – Pile 206

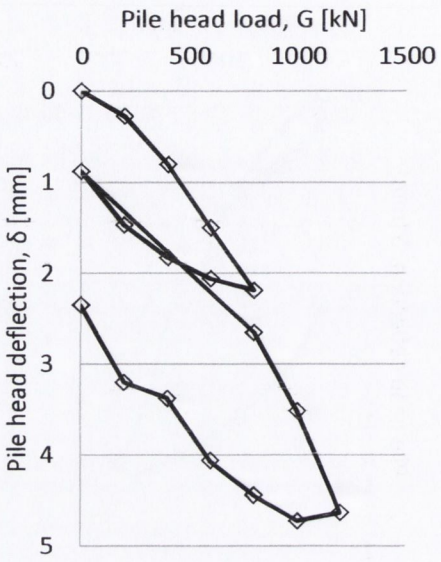


Figure B.179 – Pile 208

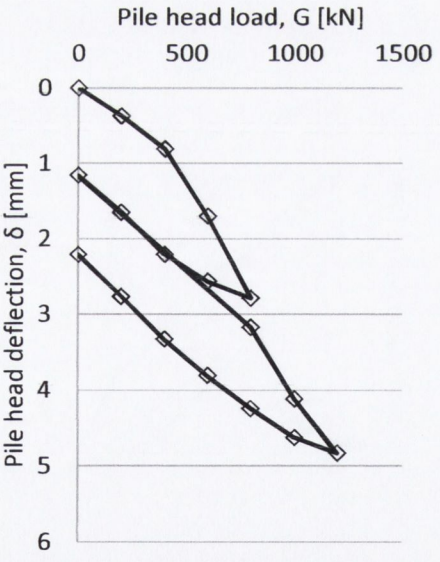


Figure B.178 – Pile 207

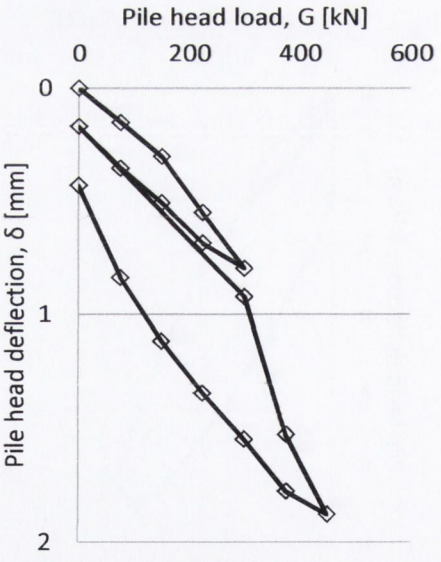
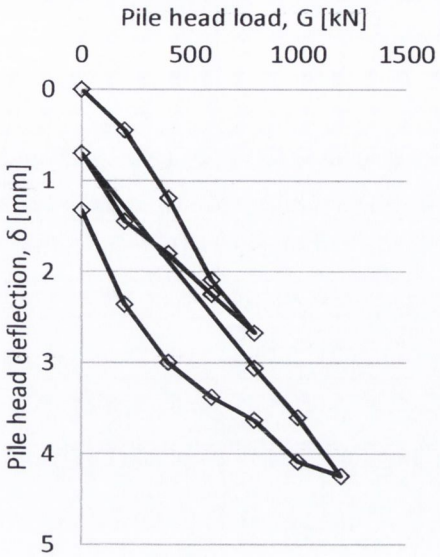


Figure B.180 – Pile 209

Figure B.181 – Pile 210



C. Details of additional tests relating to instrumented piles

C.1 Introduction

This Appendix outlines information pertaining to pile load testing presented in Chapter 6 of this thesis. The test pile logs, as recorded by the piling rig used to install the piles, are included alongside details of the instrumentation used to record strain in the pile during the pile load test. Installation of the instrumentation is outlined and the means by which data was acquired on interrogation of the instrumentation is also presented.

Further to this, the results of other testing carried out in support of the interpretation of the results of the pile load testing, including the determination of the stress-strain behaviour of concrete samples taken from the piles, are presented.

The details of another short length of pile, referred to in the main text of the thesis as a *dummy* pile, installed at the same time as the test piles and using the same methods of installation is also outlined in this Appendix. The *dummy* pile, which was also instrumented with strain gauges, was first allowed to cure on site for a period prior to extraction and transportation to the geotechnical laboratory in Trinity College Dublin where it was load tested. Details of how this load testing was carried out and of the results are outlined in this Appendix.

a. Test pile logs

The test pile logs, which are automatically recorded and compiled by the piling rig, are shown in Figure C.1 and in Figure C.2 for P450 and P640 respectively. These include details of penetration of the rig, the torque required, drill resistance encountered and an estimation of the volume of concrete provided to the pile bore.

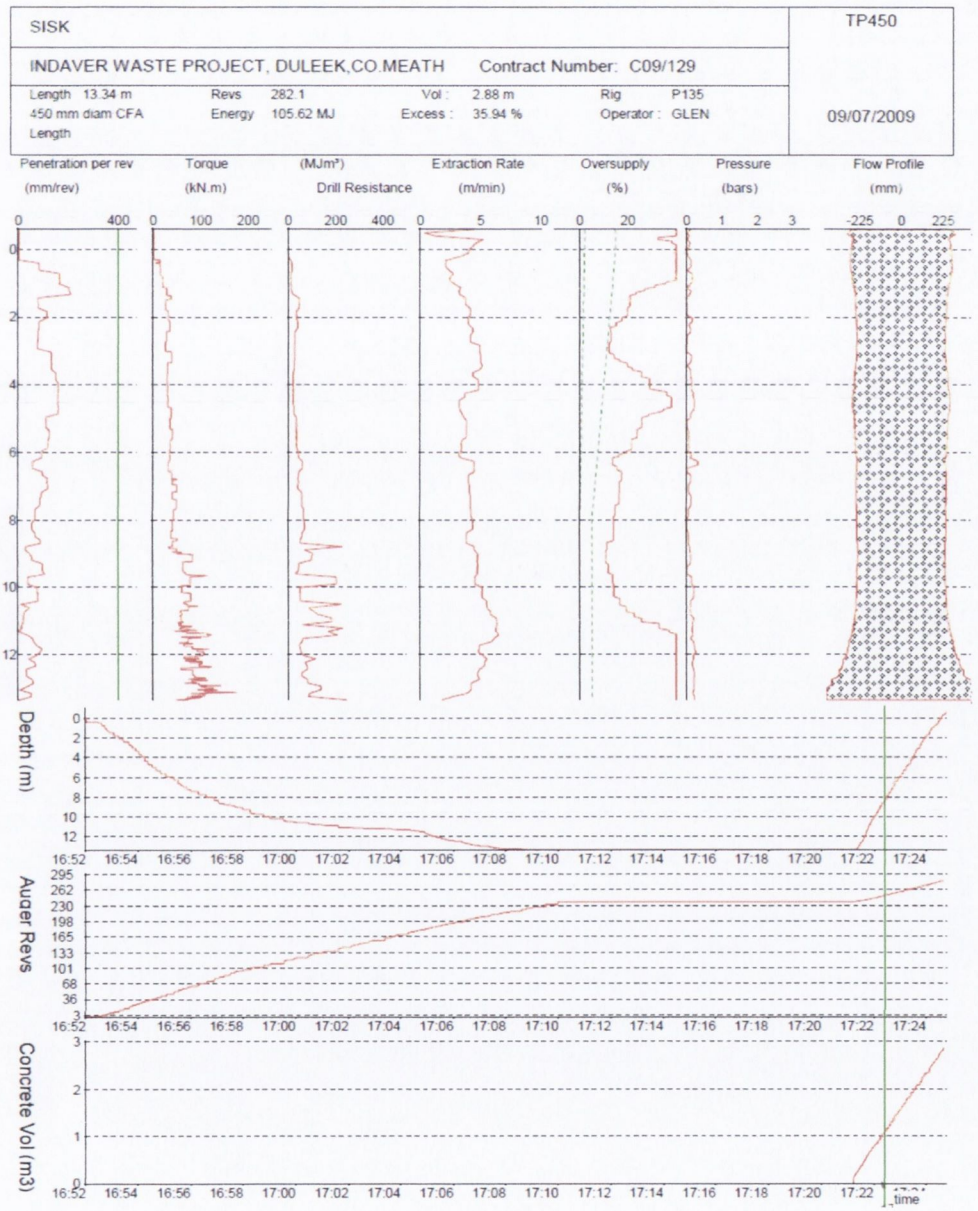


Figure C.1 - Pile log, Pile 450

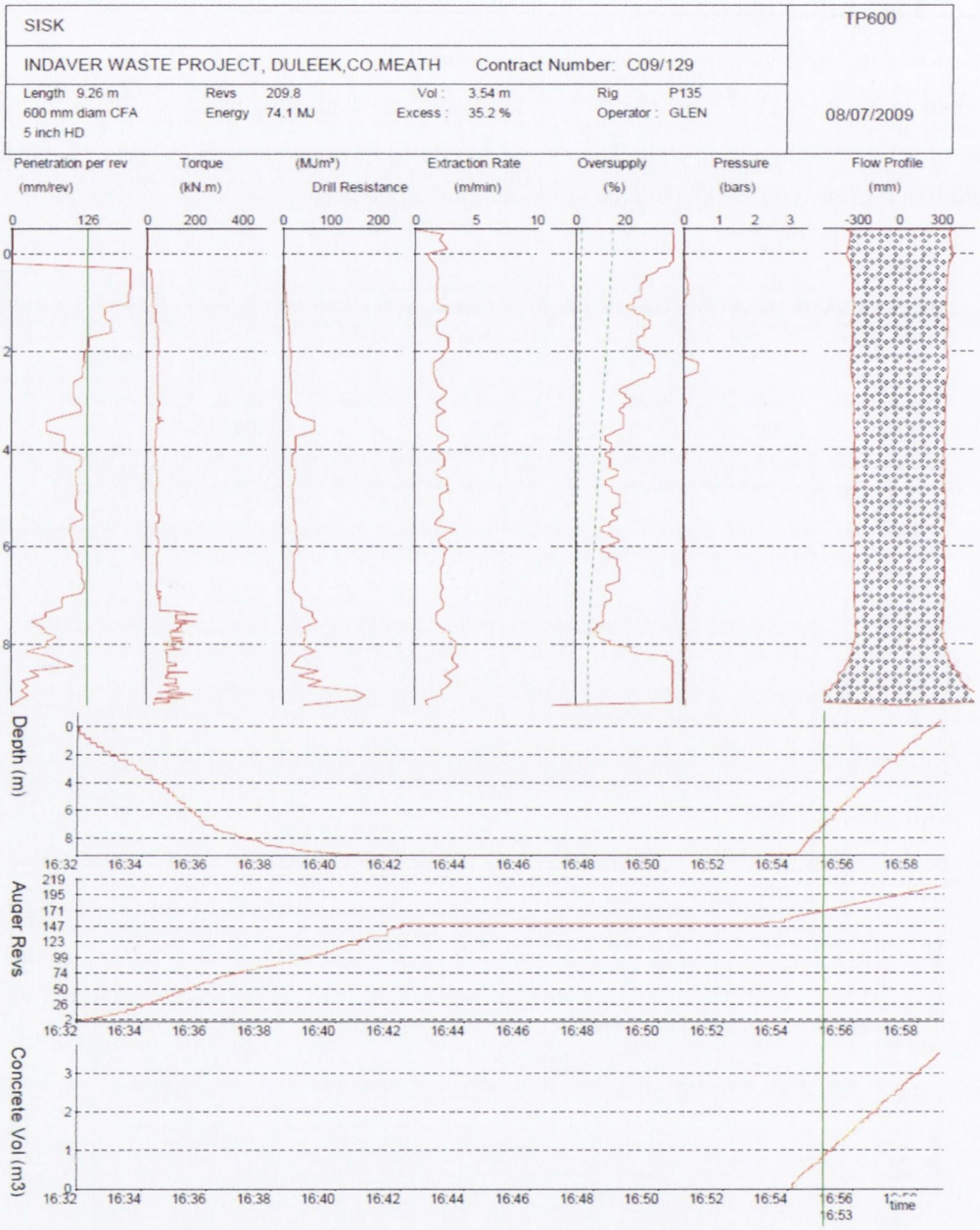


Figure C.2- Pile log, Pile 640

b. Instrumentation and data acquisition

i. Installation of strain gauges

A combination of electrical resistance (foil) and vibrating wire strain gauges were used in the instrumentation of the piles tested during this study and the installation of these is outlined in this section.

1. Foil Gauges

An area on the steel bars larger than the strain gauge was cleared of rust using an angle grinder before degreasing the cleared area using a solvent immediately prior to adhesion of the gauge. Pressure sensitive cyanoacrylate was used to bond the gauges to the steel, as recommended by the supplier (Radionics). A small amount of the adhesive was dispensed on the steel and the gauge placed by hand under a leaf of wax paper, then the fore finger was rolled back and forth gently over the wax paper to ensure that the gauge was properly fixed. After a few minutes, the wax paper was carefully removed and the alignment of each gauge checked. Solder pads were then adhered to the area behind the gauge with which to attach the cables for connection to the data acquisition equipment.

Multi-core cable was used to relay the gauge signals to the equipment and these cables were run from the gauges to the top end of the cage where they were colour coded to enable individual identification of the gauges (Figure C.3). Cables were firmly attached at points along the longitudinal reinforcement using tape and plastic cable ties and some strain relief was provided to each gauge by looping of the wires near the point of solder and lightly taping this loop to the steel bar. An excess of 10m was left on each cable to run from the pile head to the data acquisition system nearby.

Finally, the strain gauge and solder pad were completely encased in a two part epoxy adhesive aimed at waterproofing the gauges, this process was repeated at least twice to decrease the chance of water ingress subsequent to installation and also to decrease the chance of a strain gauge being damaged during installation of the steel cage. An installed foil strain gauge already waterproofed is shown in Figure C.4.

The thermal output of the strain gauges used is rated as $\pm 2\mu\varepsilon/^{o}C$ (Radionics 1997), therefore, temperature compensation was not considered necessary (the temperature of the ground is known to remain fairly constant over short periods of time and measurements of

strain were taken some time after concrete placement such that heat evolved during cement hydration should have dissipated).



Figure C.3 - Coiled and colour coded cables on instrumented rebar



Figure C.4 - Strain gauge attachment and protective coat

2. Vibrating wire strain gauges

Vibrating wire strain gauges (VWSG) consist of a tensioned wire, housed in a casing for protection. This tensioned wire is electronically agitated (by an electromagnet) and the frequency of its response recorded, the frequency varies as the length of the wire changes, thus strain may be measured.

VWSG have been used traditionally in pile testing as they are relatively robust and have the ability to withstand relatively high transient loads often inflicted during installation of

bored pile reinforcement and subsequent concreting. There are several types of VWSG and the embedment type was selected here. These gauges were installed to provide measurement of strain values but also to develop confidence in the readings from the foil gauges described previously.

The embedment type VWSG were very quickly and easily installed by tying to the reinforcement cage, here using four short wire ties and with two wooden spacers as shown in Figure C.5.



Figure C.5–Strain gauges installed

ii. Data acquisition

Static load tests are relatively slow to carry out, usually requiring at least three working days from start to finish as it is often required to subject the piles to three load-unload cycles and they must be carried out on site where the pile is installed. Data acquisition equipment (DAE) for the foil strain gauges is expensive, bulky, sensitive to the weather and requires 220V electricity supply, and therefore, should be suitably and safely housed for the duration of these lengthy tests.

At each of the three test sites a portable office was specified and this was located next to the pile load test arrangement with a generator to supply power to the DAE as shown in Figure C.6. The cables were passed through the window and attached to the DAE inside the portable office as shown in Figure C.7. This provided a safe and comfortable place in which to make the required connections and from which to monitor the strain readings during testing.

Two sets of DAE for the foil gauges were used during testing, System 5000 and System 7000, both Strainsmart systems. The Strainsmart software allows interrogation of the foil gauges at a specified rate, here the rate was 1 Hertz (1 recording per gauge per second).

A portable data-logger was to interrogate the VWSG's and these were connected and disconnected from the data-logger in turn and the reading recorded manually during testing.



Figure C.6 - Test arrangement with portable office

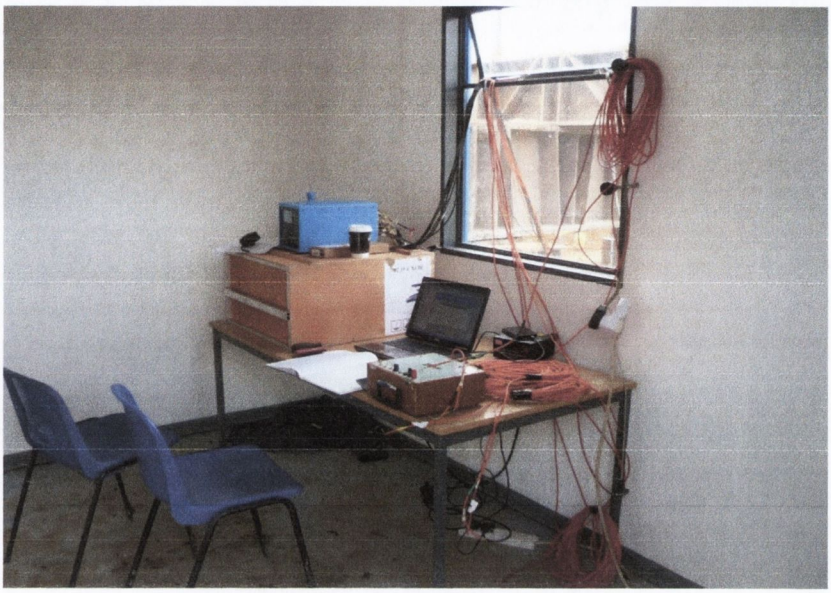


Figure C.7 - Inside portable office housing data acquisition equipment

c. Concrete cylinder tests

Concrete cylinders, comprising the concrete for Pile 450, were taken at the time of placement and transported to the laboratory and cured in a water bath in the usual way for 14 days prior to testing.

The aim of the load tests on the cylinders was to estimate the stress-strain response of the concrete and use this to estimate the stress-strain response of the pile under test. Pile stiffness is an important parameter in determining the load-depth profile throughout the pile load test.

i. Loading arrangement and experimental setup

The concrete cylinders were trimmed with a circular cutting blade at each end to ensure the ends were flat and perpendicular to the longitudinal axis of the cylinder. Each cylinder was instrumented with two strain gauges prior to loading, one aligned with the longitudinal axis and one circumferential strain gauge – placed to observe the effect of Poisson's ratio. The finished cylinder, instrumented with the strain gauges and placed in line with a digital load cell is shown in Figure C.8 and the typical mechanism of failure is shown in Figure C.10.

The cylinders were then loaded to failure over three load cycles with the rate of loading controlled by constant-rate-of-stress at around 1.5kN/s. The first two load cycles were to about a third of the total capacity (estimated by prior loading of two un-instrumented test cylinders from the same batch) and the third was to failure at the specified rate. The load-time graph for two of the cylinders, tested at 14 days is shown in Figure C.10.

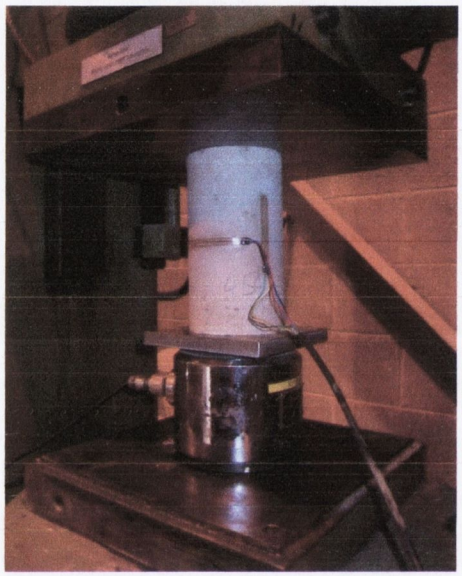


Figure C.8 – Load test arrangement and instrumentation of concrete cylinders

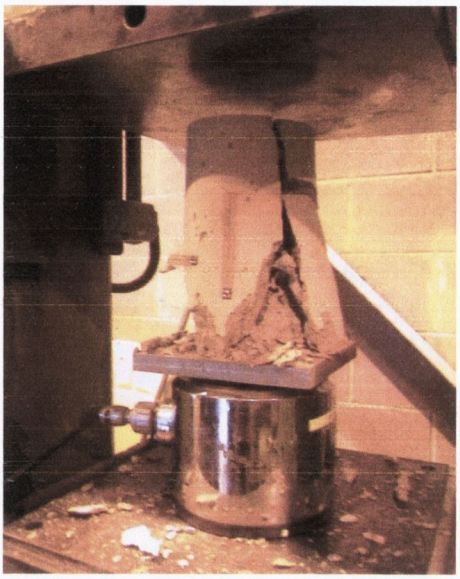


Figure C.9 – Typical failure mechanism of concrete cylinder

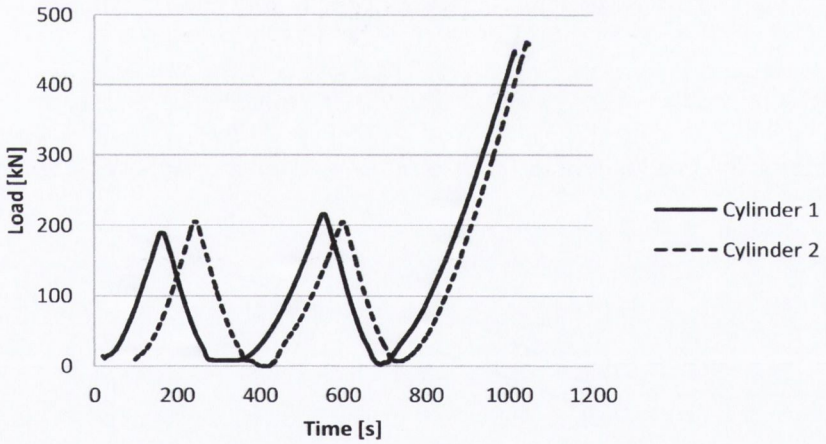


Figure C.10 - Load-time graph for concrete cylinders

ii. Stress-strain results

The measured stress-strain curves are shown for the two cylinders in Figure C.11 and are remarkably similar. The concrete achieved a failure stress of around 60MPa and a failure strain of about 3500με in the case of both cylinders. Figure C.12 shows a close up of the

stress-strain graphs of Figure C.11 over the range of strain observed during the pile load test on Pile 450.

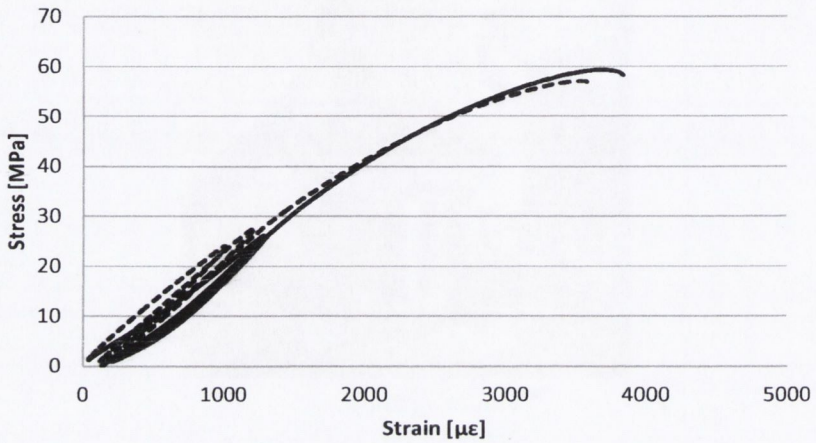


Figure C.11 – Measured stress-strain graphs for concrete cylinders

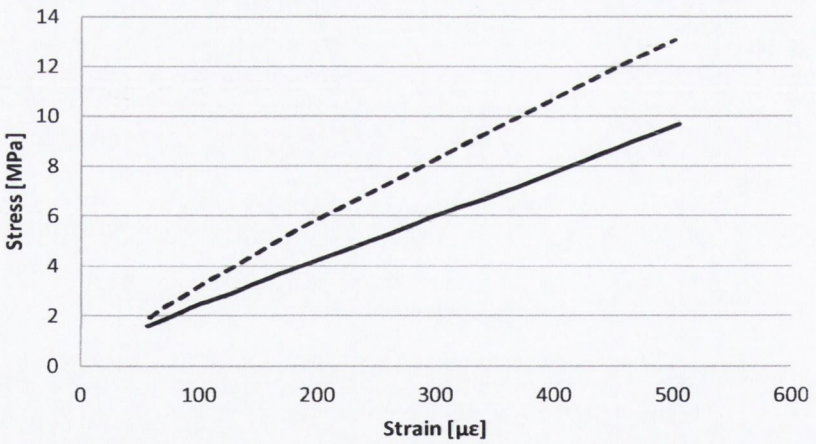


Figure C.12 – Measured stress-strain graphs for concrete cylinders for strain range observed in pile test

iii. Interpreted stiffness-strain

Dividing the stress by the corresponding strain to calculate the concrete stiffness, and plotting this against the strain, as shown in Figure C.13, indicates the level of reduction in concrete stiffness with increasing strain for the two cylinders. The value of E_c reduces from 35 and 30 to 16GPa for cylinder 1 and cylinder 2 respectively, over the range zero strain to the fracture strain of about 3500με, this shows that it is possible for the value of E_c to reduce by about half from zero strain to the failure strain.

Again the data is reduced for the range of strain observed during the load test on Pile 450 and this is shown in Figure C.14. The value of E_c interpreted from the concrete cylinders, reduces by about a third over the strain range measured in the pile load test.

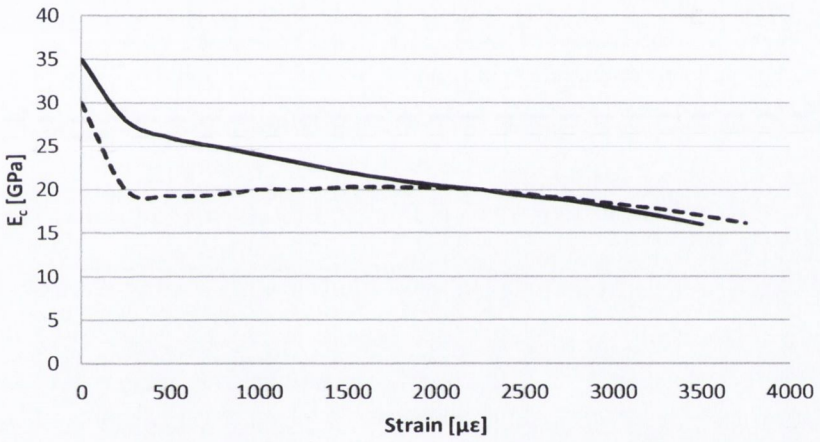


Figure C.13 – Stiffness degradation in concrete cylinders with increasing strain

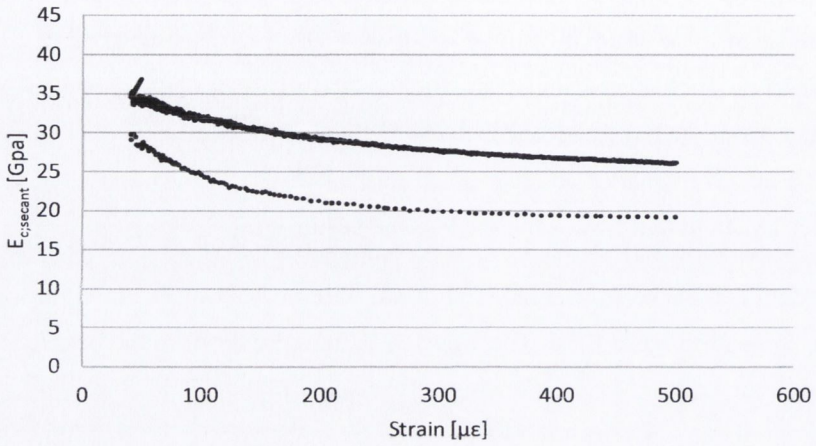


Figure C.14 – Stiffness degradation in concrete cylinders with increasing strain for strain range observed in pile test

d. Dummy pile test

A 1.8m length instrumented dummy pile was installed a few metres away from Pile 450 immediately after installation of Pile 450 using the same CFA piling rig and using the same concrete as that supplied to Pile 450. This instrumented dummy pile was allowed to cure on-site in the ground for several days before it was excavated and transported to the geotechnical laboratories of TCD for load testing.

This Section outlines the details of the loading arrangement for the dummy pile and the results recorded, interpretation of the measurements taken can be found in the main text.

i. Loading arrangement and experimental setup

The loading arrangement and experimental setup is best described by photographs taken prior to load testing of the dummy pile. The dummy pile was tested in uniaxial compression, in a horizontal position, between the two uprights of the smaller of two large testing frames in the structures laboratory at TCD, as shown in Figure C.15.

The dummy pile was loaded by means of a large hydraulic ram of maximum capacity 300 Tonnes (~3000kN) shown in Figure C.16. With a view to distributing the stress induced by

loading over the full cross-section of the dummy pile a wooden shim, in conjunction with a thick steel plate, was placed at both ends of the dummy pile. The contact between the surfaces can be seen in detail in Figure C.16 and in Figure C.17.

Additional gauges were attached to the outer surface of the dummy pile in three locations spaced evenly around the circumference at about half way along the pile. The location is shown in Figure C.18 and a detail of the attachment and type of gauge used is shown in Figure C.19 – these were the same type of gauge used in testing of the concrete cylinders described previously.



Figure C.15 – Dummy pile in test frame

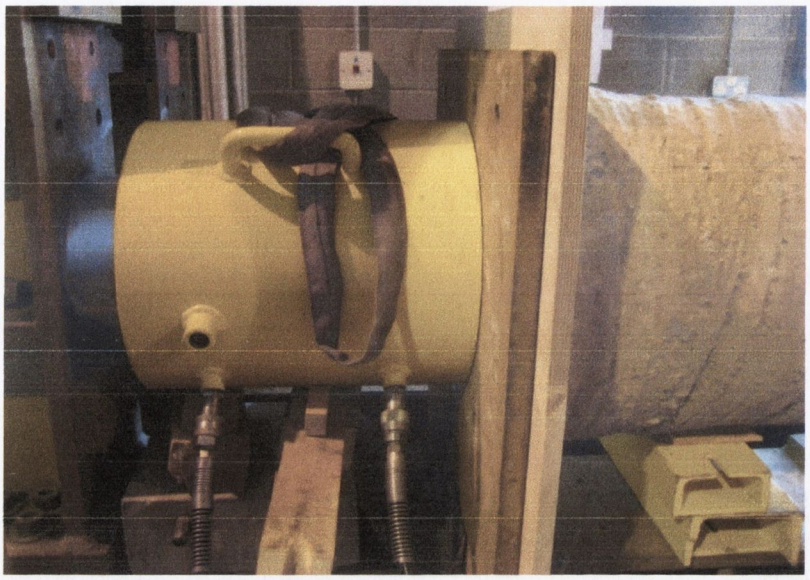


Figure C.16 – Hydraulic ram in position for *loading*



Figure C.17 – End detail: Dummy pile contacting wooden shim



Figure C.18 - Location of surface strain gauges



Figure C.19 - Detail of surface strain gauges

The dummy pile was subjected to three load cycles similar to those applied to Pile 450. It was intended that the dummy pile would be subjected to the same three load cycles as Pile 450 was in the field, however, on recalibration of the hydraulic jack used for loading,

subsequent to the test, the loads were adjusted upward as they were thought to be slightly underestimated. The approximated load-time schedule for the dummy pile is shown in Figure C.20 and is similar to that for Pile 450.

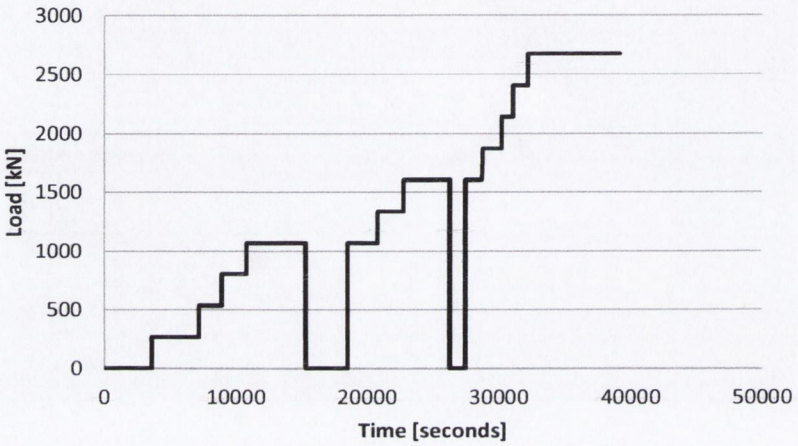


Figure C.20 – Load-time graph for dummy pile

ii. Stress-strain results

The stress-strain readings are plotted in Figure C.21. The dummy pile was loaded such that a maximum measured average strain of almost 1000με was calculated. The strain readings recorded at each of the three cross-sections are seen to be agreeable with the reading at one cross-section matching the average almost precisely. The three surface gauges gave readings much lower than those of the internal gauges, less than half, and the reason for this is not known, but perhaps it can be attributed to the method of attachment of the gauges – never-the-less the results from the surface gauges are were ignored in any analysis.

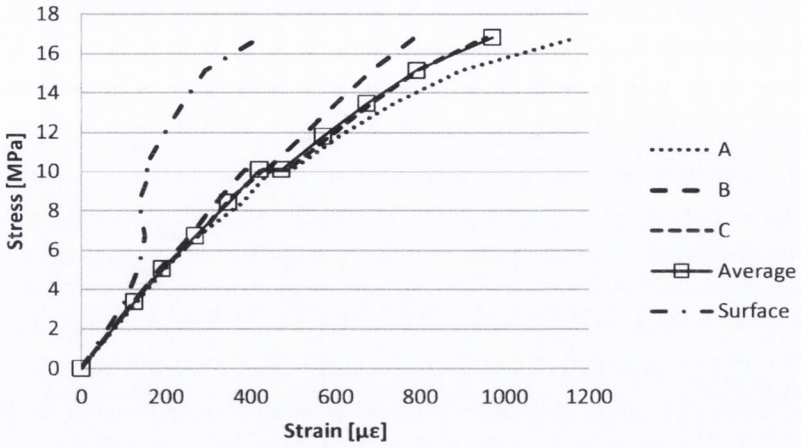


Figure C.21 – Average stress-strain curve for dummy pile

D. Reliability

D.1 Introduction

This Appendix contains the results of reliability analysis applied to each of the piles in the PTD. Figure D.1 to Figure D.6 show the results of the reliability analysis applied to single piles while Figure D.7 to Figure D.12 show the results of the reliability analysis including within site variability. Similar figures were presented in Chapter 7 of this thesis but these were produced on the assumption that the value of R_c fitted a log-normal distribution.

Figure D.1 to Figure D.12 are based on the assumption that the values of R_c fit the normal distribution. In reality it is difficult to assess which underlying distribution is most suited to the data available and thus the results of the analysis based on the assumption of data normality are presented here just for completeness.

The underlying normal assumption leads to lower reliability values than that assuming log-normality of the data. The log-normal assumption is thought to be more suited to the data as it results in a higher value of the reliability which corresponds to a lower probability of failure of the foundation which is more akin to that observed historically.

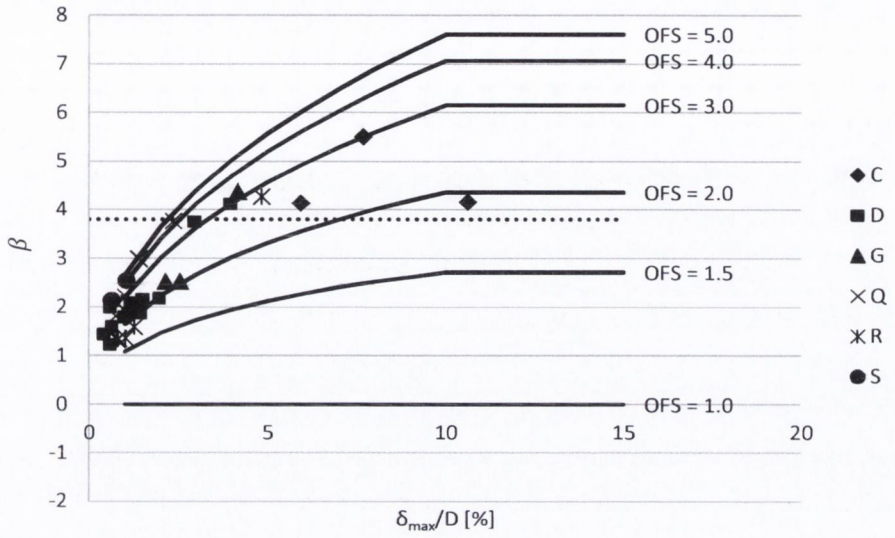


Figure D.1 – CFA piles in DBC: Calculated β for a single pile

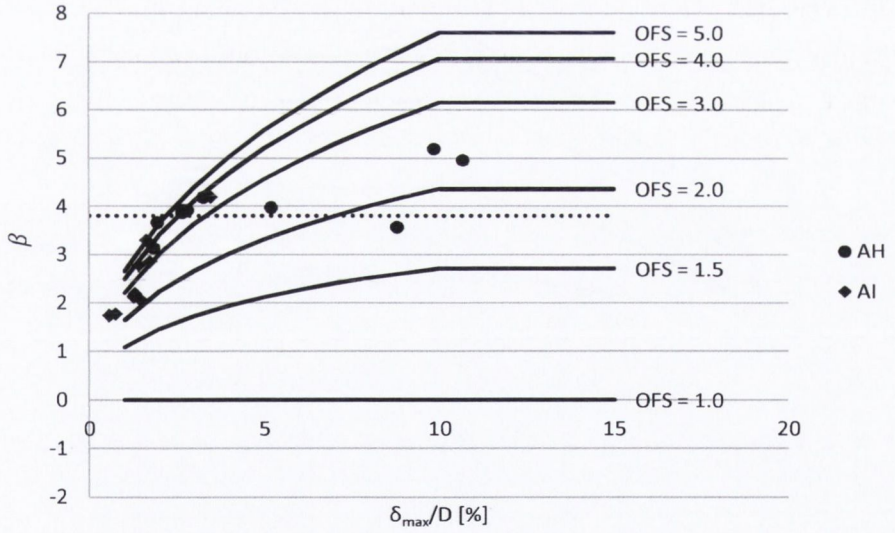


Figure D.2 – Driven piles in DBC: Calculated β for a single pile

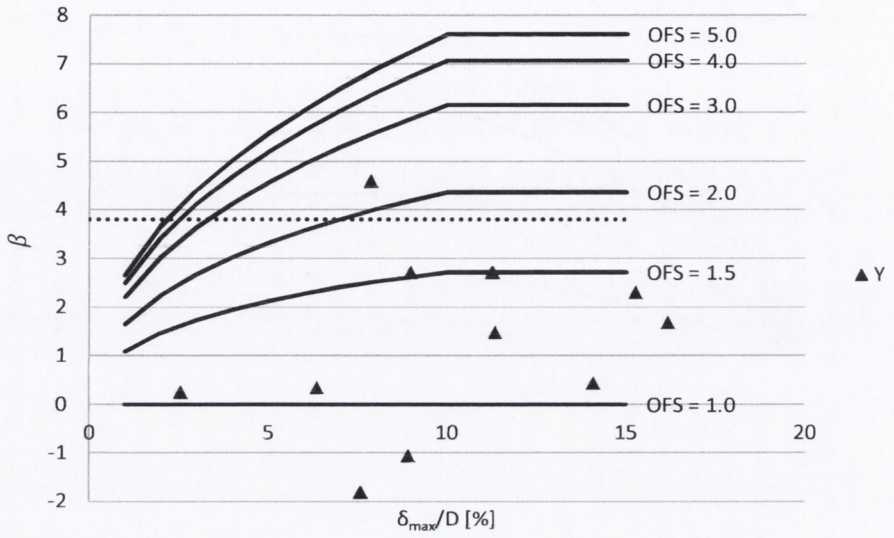


Figure D.3 – CFA piles in boulder clay: Calculated β for a single pile

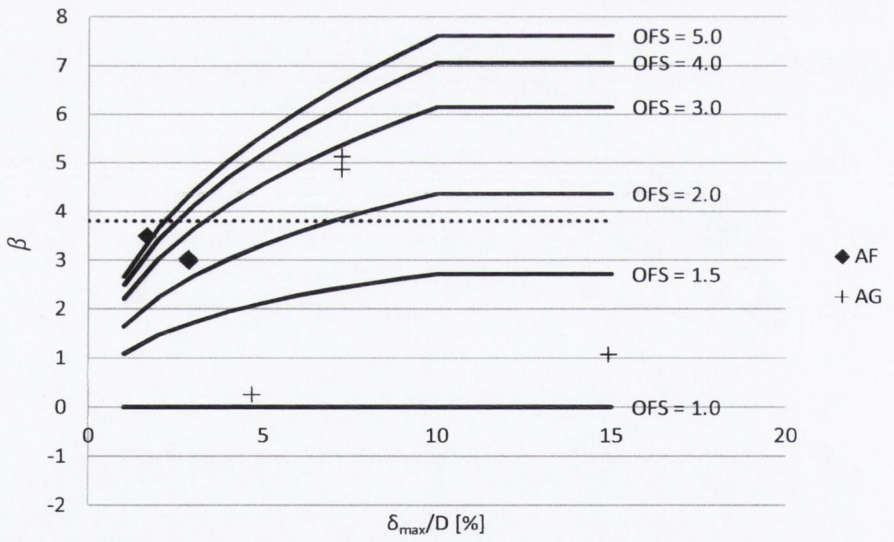


Figure D.4 – Driven piles in boulder clay: Calculated β for a single pile

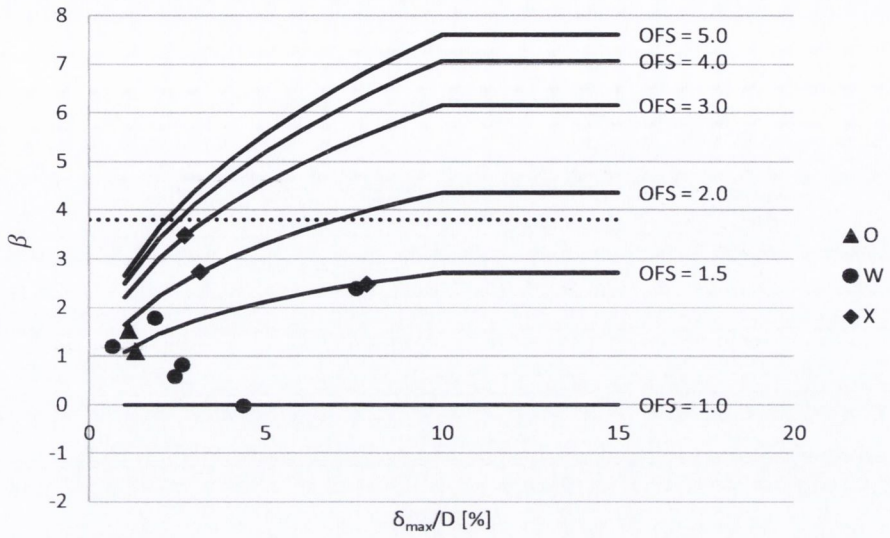


Figure D.5 – Bored and CFA piles in sand/gravel: Calculated β for a single pile

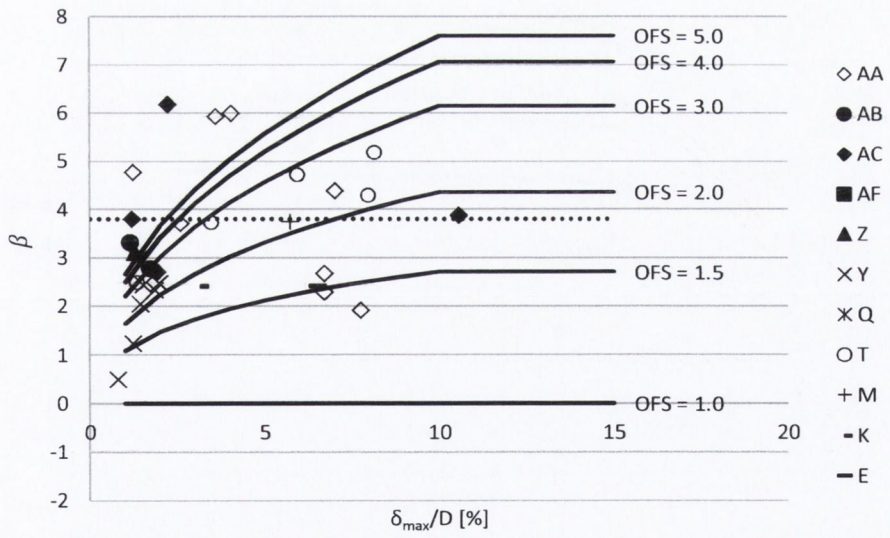


Figure D.6 – Bored and CFA piles in rock: Calculated β for a single pile

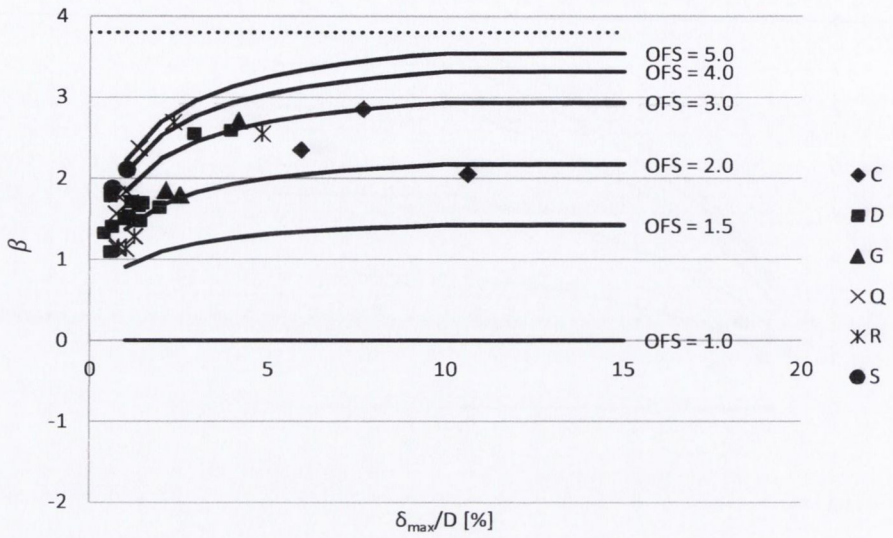


Figure D.7 – CFA piles in DBC: Calculated β for a pile design

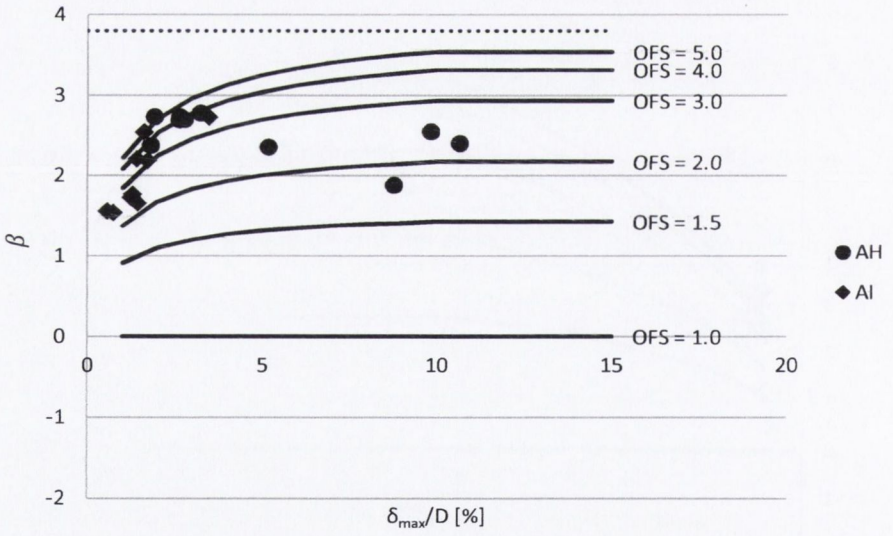


Figure D.8 – Driven piles in DBC: Calculated β for a pile design

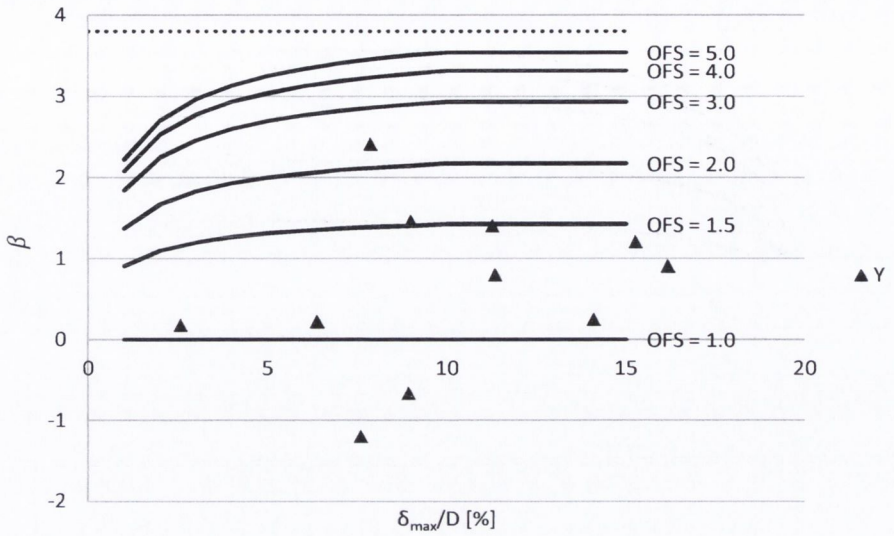


Figure D.9 – CFA piles in boulder clay: Calculated β for a pile design

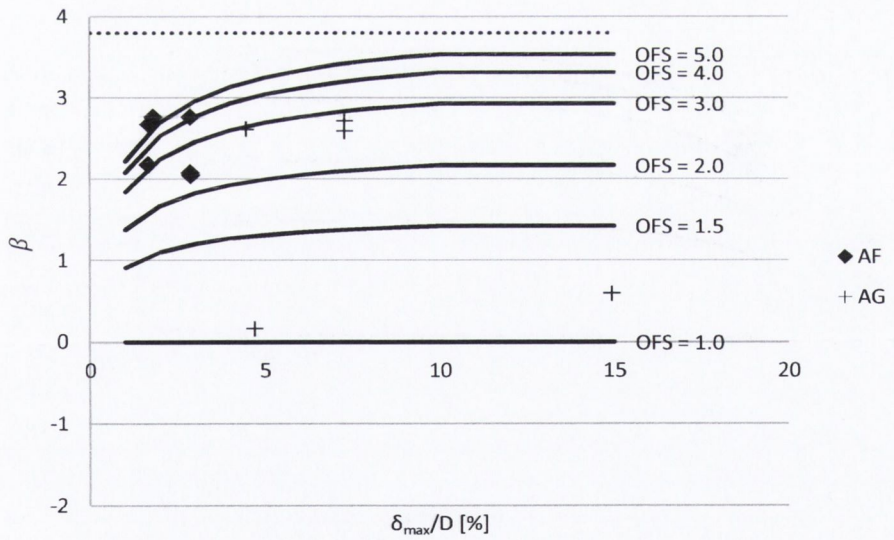


Figure D.10 – Driven piles in boulder clay: Calculated β for a pile design

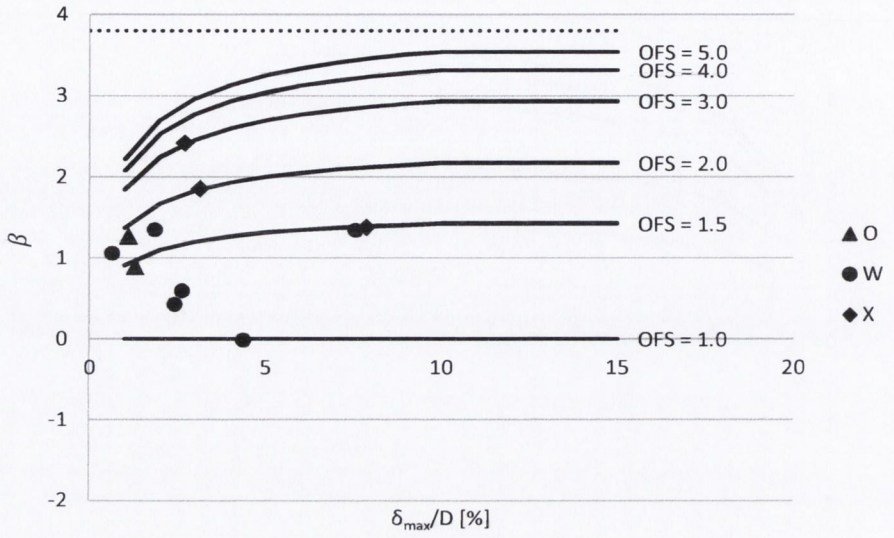


Figure D.11 – Bored and CFA piles in sand/gravel: Calculated β for a pile design

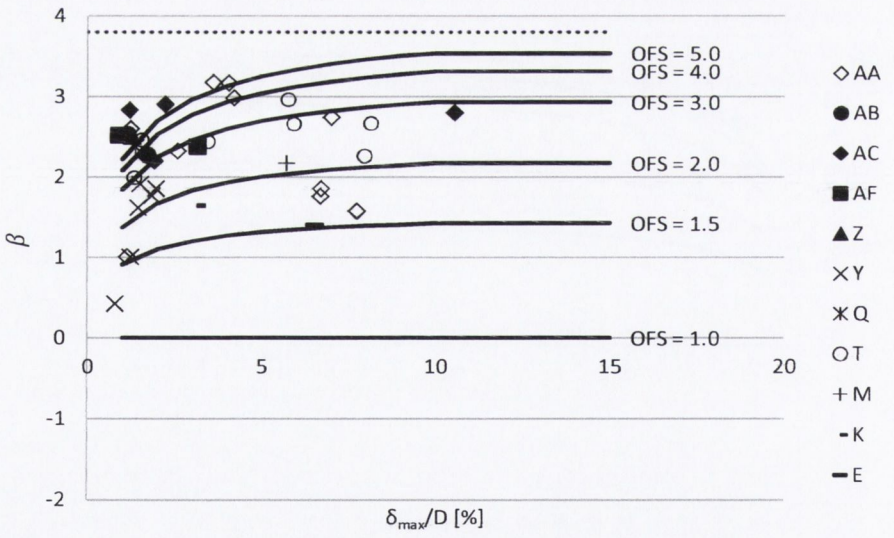


Figure D.12 – Bored and CFA piles in rock: Calculated β for a pile design